

---

Doctoral

Science

---

2016

## Anode Catalysts for the Direct Ethanol Fuel Cell

Daryl Fox

*Technological University Dublin*

Follow this and additional works at: <https://arrow.tudublin.ie/sciendoc>

 Part of the [Medicinal and Pharmaceutical Chemistry Commons](#)

---

### Recommended Citation

Fox, D. (2016) *Anode Catalysts for the Direct Ethanol Fuel Cell*. Doctoral thesis, DIT, 2016.

This Theses, Ph.D is brought to you for free and open access by the Science at ARROW@TU Dublin. It has been accepted for inclusion in Doctoral by an authorized administrator of ARROW@TU Dublin. For more information, please contact [arrow.admin@tudublin.ie](mailto:arrow.admin@tudublin.ie), [aisling.coyne@tudublin.ie](mailto:aisling.coyne@tudublin.ie), [vera.kilshaw@tudublin.ie](mailto:vera.kilshaw@tudublin.ie).

# Anode Catalysts for the Direct Ethanol Fuel Cell



Submitted for examination for the award of Doctor of Philosophy (PhD), School of Chemical and Pharmaceutical Sciences, Dublin Institute of Technology, Kevin Street, Dublin 8.

**Author:** Daryl Fox BSc. (Hons).

**Supervisors:** Dr. Anthony J. Betts.

Professor John F. Cassidy.

School of Chemical and Pharmaceutical Sciences,  
FOCAS Institute, DIT, Camden Row, Dublin 8.

January 2016.

## **Declaration**

I certify that this thesis which I now submit for examination for the award of \_\_\_\_\_, is entirely my own work and has not been taken from the work of others, save and to the extent that such work has been cited and acknowledged within the text of my work. This thesis was prepared according to the regulations for postgraduate study by research of the Dublin Institute of Technology and has not been submitted in whole or in part for another award in any other third level institution. The work reported on in this thesis conforms to the principles and requirements of the DIT's guidelines for ethics in research.

Signature \_\_\_\_\_ Date \_\_\_\_\_

Candidate

## Table of Contents:

<u>Section:</u>	<u>Page number:</u>
<b>Abstract</b> .....	7
<b>List of Abbreviations</b> .....	8
<b>1. The Fuel Cell</b> .....	10
1.1 Introduction.....	10
1.2 How the Direct Ethanol Fuel Cell works.....	13
1.3 Catalysis for the Direct Ethanol Fuel Cell.....	20
1.4 The Research Question.....	23
1.5 Aims of the Project.....	25
1.6 References.....	28
<b>2. Platinum/carbon and gold catalysts</b> .....	34
2.1 Introduction.....	34
2.2 Experimental.....	38
2.3 Carbon Ink Electrode Appearance.....	40
2.4 Electrolyte and Reference Electrode.....	44
2.4.1 Saturated Calomel Electrode.....	45
2.4.2 Perchloric acid, HClO <sub>4</sub> , as electrolyte.....	49
2.5 Background electrolyte behaviour at platinum in acidic pH.....	51
2.6 Methods of manufacturing catalysts.....	54
2.6.1 Metal Deposition Methods.....	60

2.7 Carbon Substrate.....	68
2.7.1 Carbon Ink Electrode.....	69
2.7.2 Carbon Paper Electrode/Gas Diffusion Electrode.....	71
2.7.3 Vulcan XC72 Powder.....	75
2.7.4 Carbon Ink Substrate effects.....	78
(i) Platinum Electrodeposition Carbon Ink Electrodes (Pt/CIE).....	78
(ii) Gold Electrodeposition Carbon Ink Electrodes (Au/CIE).....	80
2.8 Methanol Oxidation Reaction.....	81
2.9 Effect of ethanol on cyclic voltammetry.....	84
2.9.1 Ethanol Oxidation Reaction on platinum.....	84
2.9.2 Ethanol Oxidation Reaction behaviour on gold electrodes.....	91
2.10 Intermediates: Acetaldehyde and Acetate.....	96
2.11 Increasing platinum loading.....	101
2.12 Impact of concentration on EOR at platinum catalysts.....	105
2.13 Effect of increased temperature on EOR at platinum catalysts.....	108
2.14 Impact of scan rate and gold Rotating Disk Electrode on EOR.....	111
2.15 Effect of pH on EOR.....	113
2.16 Conclusions.....	119
2.17 References.....	123
<b>3. Palladium Ethanol Oxidation Reaction catalysts.....</b>	<b>138</b>
3.1 Introduction.....	138
3.2 Experimental.....	141

3.3 Morphological Features.....	143
3.4 Palladium electrodeposition.....	146
3.5 Ethanol Oxidation Reaction on palladium catalysts.....	149
3.6 Increasing pH for the EOR at palladium catalysts.....	154
3.7 Effect of temperature on palladium bimetallic catalysts.....	158
3.8 Chronocoulometry and potential step testing.....	161
3.9 Effect of scan rate on EOR at palladium catalysts.....	167
3.10 Conclusions.....	171
3.11 References.....	173
<b>4. Nickel electrocatalysts and Tafel analysis.....</b>	<b>179</b>
4.1 Introduction.....	179
4.2 Experimental.....	182
4.3 Ni/C Electrode Appearance.....	184
4.4 Electrooxidation of ethanol at nickel electrodes.....	187
4.5 Potential step and Chronocoulometry at nickel electrodes.....	197
4.6 Tafel Analysis.....	201
4.7 Conclusions.....	207
4.8 References.....	209
<b>5. Electrochemical Impedance Spectroscopy.....</b>	<b>213</b>
5.1 Introduction.....	213
5.2 Experimental.....	222

5.3 EIS plots – platinum sheet in ethanol.....	226
5.4 EIS plots – electrodeposited platinum/CIE.....	229
5.5 EIS data – electrodeposited Pd/CIE, Ni/CIE and Au/CIE.....	239
5.6 Conclusions.....	246
5.7 References.....	248
<b>6. Fuel Cell Power Curves.....</b>	<b>252</b>
6.1 Introduction.....	252
6.2 Experimental.....	258
6.3 Commercial Anode Test.....	261
6.4 Platinum Deposits on Carbon Ink and Carbon Paper.....	263
6.5 Power curves collected at selected bimetallic catalysts.....	269
6.6 Power curve data obtained from Vulcan XC72 electrodes.....	274
6.7 Conclusions.....	277
6.8 References.....	280
<b>7. Achievements, Conclusions and Future Work.....</b>	<b>283</b>
7.1 Achievements and Conclusions.....	283
7.2 Future Work.....	290
<i>Publications and Presentations.....</i>	<i>293</i>

## Abstract

The anodic reaction of the Direct Ethanol Fuel Cell has been studied with various catalysts such as electrodeposited platinum, palladium, nickel and gold electrodes. The mechanism of bimetallic catalysts was used to reduce the platinum content needed for ethanol oxidation. The effects of increased temperature, ethanol concentration, electrolyte pH and scan rate have been examined. The impact of different carbon surfaces such as carbon ink, carbon paper and commonly used Vulcan XC72 have also been analysed in order to determine the optimum conditions for the EOR in a fuel cell.

Electrochemical methods were used to analyse catalyst performance such as cyclic voltammetry, linear sweep voltammetry, current/time plots, chronocoulometry and Tafel analysis. Tafel slopes were calculated from 250 mV/decade up to 550 mV/decade. In addition, the best performing catalysts, Pt75%Pd25% and Pt90%Ni10% were used in a model fuel cell with an air cathode where power between 30 and 100  $\mu$ W was obtained. Moreover, selected catalysts were analysed by Electrochemical Impedance Spectroscopy, circuit modelling, Scanning Electron Microscopy and elemental mapping.

Electrodeposition was found to be a quick, reliable and reproducible method for catalyst deposition and 120 mC/cm<sup>2</sup> or 0.12 mg/cm<sup>2</sup> of precious metal was typically used for analysis. The carbon substrate was found to be a major limitation due to induction periods for charge collection measured by chronocoulometry and its high resistance of 800-1000  $\Omega$ .cm<sup>2</sup> measured by Impedance Spectroscopy.

## List of Abbreviations

**PEM** = Polymer Exchange Membrane

**AEM** = Anion Exchange Membrane

**PEMFC** = Polymer Exchange Membrane Fuel Cell

**AAEMFC** = Alkaline Anion Exchange Membrane Fuel Cell

**AAEM** = Alkaline Anion Exchange Membrane

**AFC** = Alkaline Fuel Cell

**SOFC** = Solid Oxide Fuel Cell

**DEFC** = Direct Ethanol Fuel Cell

**DMFC** = Direct Methanol Fuel Cell

**DAFC** = Direct Alcohol Fuel Cell

**MMS** = mercury/mercury sulphate

**RHE** = Reversible Hydrogen Electrode

**MEA** = Membrane Electrode Assembly

**HOPG** = Highly Oriented Pyrolytic Graphite

**CIE** = Carbon Ink Electrode

**CPE** = Carbon Paper Electrode

**CE** = Carbon Electrode

**DEMS** = Differential Electrochemical Mass Spectroscopy

**EOR** = Ethanol Oxidation Reaction

**MOR** = Methanol Oxidation Reaction

**SNIFTIRS** = Subtractively Normalised Interfacial Fourier Transform Infra Red Spectroscopy

**FTIR** = Fourier Transform Infra Red

**EIS** = Electrochemical Impedance Spectroscopy

**CPhE** = Constant Phase Element

**OCP/OCV** = Open Circuit Potential/Open Circuit Voltage

**PGM** = Platinum Group Metal(s)

**RDE** = Rotating Disk Electrode

**SEM** = Scanning Electron Microscopy

**EDX** = Energy Dispersive X-Ray

**CV** = Cyclic Voltammetry

**Pt** = platinum

**Pd** = Palladium

**Au** = gold

**Ni** = Nickel

**mA** = Current (milliamps)

**E** = Potential

**V** = Voltage

**W** = Power (watts)

**A, B, C** = ethanol oxidation peaks associated with neutral media

**X, Y** = ethanol oxidation peaks associated with high pH media

## Chapter 1: The Fuel Cell

### 1.1 Introduction:

The focus of this chapter is to outline the research questions of the project, as well as to describe the role of a fuel cell and compare it to a battery for its intended use in energy production. In addition, the aims and objectives of the project will be put forward.

Primarily, the hydrogen fuel cell has been intensively studied since the middle of the 20<sup>th</sup> Century with the Apollo 11 space mission, but especially with heavy investment in the late 1990s.<sup>1</sup> The use of a fuel cell is very much categorised by the fuel and the power required for the device intended.<sup>2</sup> A list of examples of intended applications and their power requirements is shown in Table 1(a).

The trends for the research topic have recently transformed with particular respect to electrolyte and fuel as well as the change in primary applications which continue to evolve. Furthermore, a description of carbon supports for an electrocatalyst will be included. The American department of energy has set targets for mobile applications which include power requirements, and technical challenges such as operation underwater and increased running time.<sup>2</sup> Even the most advanced lithium ion batteries suffer in terms of run-time due to ‘power hungry’ devices.<sup>2</sup> During the last 15 years in particular, high energy fuels such as hydrogen, methanol and ethanol have been considered to meet these requirements.

<b>Application</b>	<b>Power Range (W)</b>
<b>MP3 player</b>	0.1-1
<b>Mobile Phone</b>	2-5
<b>Laptop Computer</b>	15-30
<b>Military</b>	25-50
<b>Forklift</b>	500-1000

Table 1(a): Examples of portable power applications and the required energy requirements.<sup>2</sup>

There are several different types of fuel cells which exploit temperature, surface chemistry, fuel, electrolyte or the exchange membrane. These include the Phosphoric Acid Fuel Cell (PAFC); the Alkaline Fuel Cell (AFC), the Direct Methanol (DMFC) and Direct Ethanol fuel cell (DEFC) and the Solid Oxide Fuel Cell (SOFC). These will be discussed later in this chapter and the ethanol fuel cell will be discussed throughout this work. Typically, the fuel cell of choice consists of an exchange membrane – either proton exchange or anion exchange - for their application in most developmental research.<sup>3</sup> One of the main reasons for the move from hydrogen fuel cell research is the limitations of hydrogen storage;<sup>4</sup> indeed it has been described as the most challenging technical hurdle in the use of hydrogen fuel. The storage efficiency and net density values for hydrogen compared to methanol is shown in Table 1(b). The Net Energy Density is the energy

gained after the necessary energy inputs are taken into account, in particular the compression of the hydrogen gas along with its safe storage and transport.

<b>Fuel</b>	<b>Energy Density (MJ/kg)</b>	<b>Net Energy Density (MJ/kg)</b>	<b>Storage Efficiency (%)</b>
<b>Hydrogen</b>	119.9	0.72	0.65
<b>Methanol</b>	19.9	18.9	95

Table 1(b): Comparison for the hydrogen and methanol fuel cell with respect to energy output.<sup>5</sup>

The distribution network required for hydrogen as a fuel, along with storage issues, flammability and travel restrictions – such as use in tunnels and possible traffic accidents - cast doubt on the industrial adoption of hydrogen.<sup>6</sup> This is reflected by a recent trend towards alternative fuels, such as alcohols including methanol and later ethanol, as a suitable combustion material. Furthermore, these have been described as more promising fuels because the liquid alcohol is used directly in the cell, rather than being reformed into hydrogen gas and then used for the classic hydrogen fuel cell.<sup>7</sup>

The energy density for ethanol is slightly higher than methanol at 26.8 MJ/kg, but ethanol possesses a carbon to carbon double bond which can be difficult to break. In addition, methanol is considered as neurotoxic, and the availability of ethanol from biomass along

with its low toxicity,<sup>8</sup> makes it more attractive as a fuel. This shift from hydrogen reflects the progression towards the direct ethanol fuel cell and the development of the optimum conditions for its use in mobile and stationary applications.

## 1.2 How the Direct Ethanol Fuel Cell works

There are two increasingly common portable energy sources, the fuel cell and the battery. Crucially, a fuel cell involves a constant flow of the feedstock to the electrocatalytic surface which guarantees a continual reaction. A fuel cell can operate in two configurations to produce current, the Proton Exchange Membrane Fuel Cell (PEMFC) and Alkaline Anion Exchange Membrane (AAEMFC) shown in figure 1.2(a).

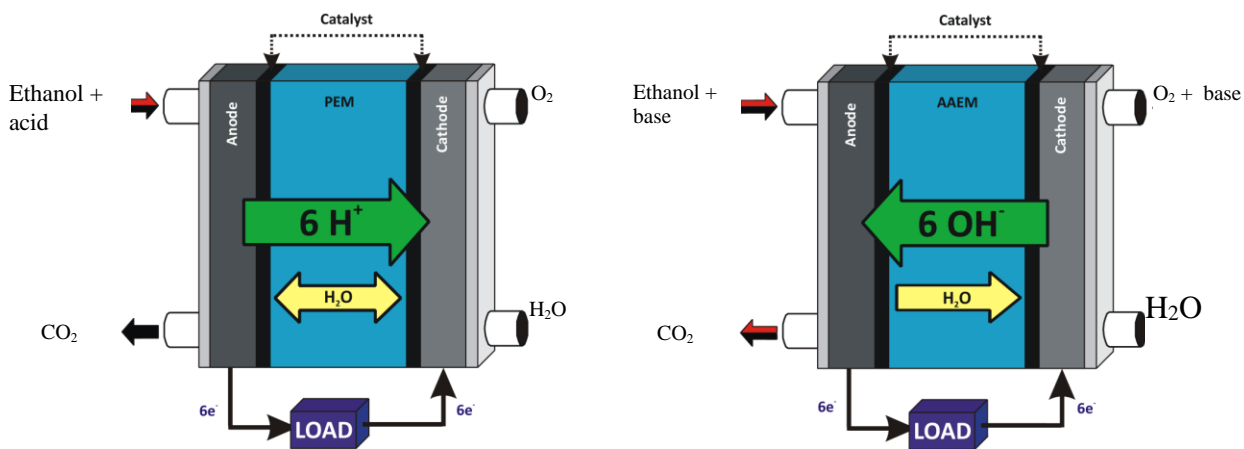


Figure 1.2(a): The Proton Exchange Membrane Fuel Cell (left) and Alkaline Anion Exchange Membrane Fuel Cell (right) adapted from Lamy.<sup>10</sup>

The primary application for fuel cells was as auxiliary power units in space flights and subsequently, power generation, transportation and finally portable applications.<sup>9</sup> These two configurations require different electrolytes and separate electrocatalysts for

optimum performance. As an example of the possibilities of an alcohol fuel cell, there is potential for methanol possessing the same driving range as the internal combustion engine.<sup>9</sup> An example of a practical, complete, ‘single-stack’ fuel cell station is shown in figure 1.2(b).

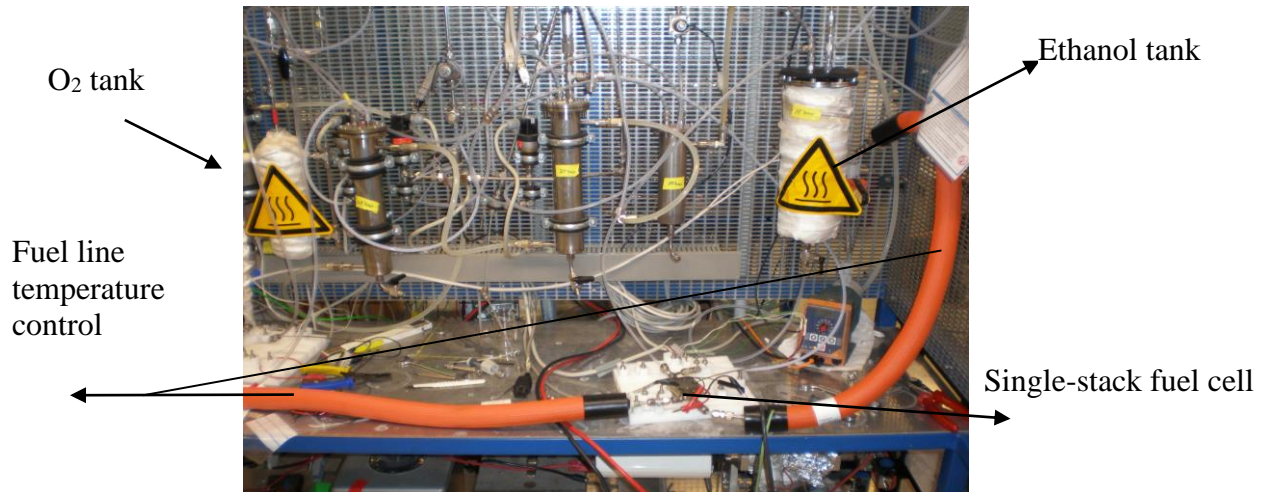
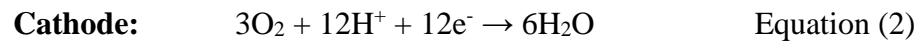


Figure 1.2(b): A single-stack fuel cell with fuel tank for the anode, oxygen tank supply to the cathode and bipolar plate-membrane-electrode apparatus (at the Technische Universität München).

A single stack fuel cell refers to the number of individual ‘units’ connected together. Each ‘stack’ or unit consists of one anode, one cathode and one membrane. The output of each individual unit can then be combined to maximise the power, current and potential from the device by attaching each unit together in series. The power requirement for a particular operation can be met by connecting several units stacked together into a multi-

stack cell. Typically, applications that demand large power such as automotive markets will require substantial numbers of fuel cells stacked together.

The reactions at the heart of the Direct Ethanol Fuel Cell (DEFC) occur at the anode and cathode of the cell for the overall combustion reaction and these equations (1 and 2) are shown for acidic media.



Manipulation of the electrolyte, membrane and catalytic surface greatly affects the role of each component part. The anions produced at the cathode cross the membrane in high pH electrolytes, thereby completing the circuit as shown in figure 1.2(b). Cations are produced at the anode, typically hydrogen ions in acidic media, therefore a selective membrane that does not suffer from alcohol crossover is important. This fuel crossover is a particular challenge for methanol fuel cells, but less so for ethanol fuels. The membrane is typically a flexible sheet such as Nafion<sup>®</sup>, made of up of long polymeric chains with SO<sub>3</sub>H and fluorine attached which allow ions to pass in channels through ion exchange. A quaternary ammonium polymer acts as an alkaline membrane for the exchange of anions in high pH. The polymer chains are bridged by nitrogen whereby the anions can pass across from the cathode to react at the anode.

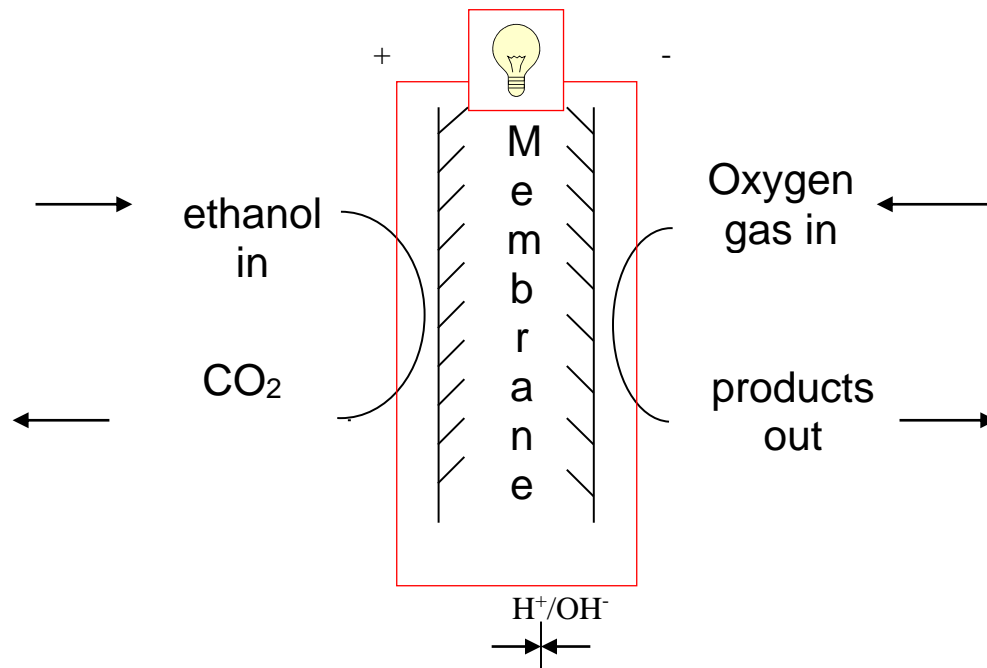


Figure 1.2(c): Diagram illustrating how an ethanol fuel cell operates with a load across a membrane. Hydrogen ions in acid cross from the anode to the cathode whereas  $\text{OH}^-$  ions in base cross from the cathode to the anode.

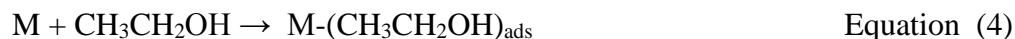
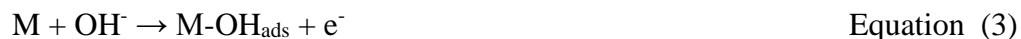
Crossover of the fuel results in oxidation of the alcohol at both the anode and cathode.

The consequence is no difference in potential on either side of the membrane. The membrane in this case needs to be selective enough to allow ions to cross but not the fuel itself.

A strongly basic electrolyte which contains hydroxide ions at the cathode can then cross through the Anion Exchange Membrane (AEM) and provide an extra source of oxygen.

This extra source of oxygen is required to complete oxidation from adsorbed intermediates that collect on the metal surface as shown in equations 3-6, where M describes the catalyst surface.<sup>11</sup> This process is the means by which the ethanol oxidation reaction (EOR) products are formed which include acetic acid, acetaldehyde and carbon

monoxide. Different metals help prevent poisoning of the catalyst surface to various extents and this will be discussed in greater detail in section 2.9.



The various products collected determine the power output from the fuel cell. The production of ethanoic acid in equation 6 is readily produced and releases four electrons. Since there are 12 electrons possible for complete ethanol oxidation to carbon dioxide, any product that is not carbon dioxide is referred to as incomplete or partial oxidation. The bifunctional mechanism describes the interaction of an adsorbed small organic molecule on a metallic surface. This is a popular explanation for the reactions shown in equations 3-6. The adsorbed poison, in this case carbon monoxide, can be removed to form  $\text{CO}_2$  by the adsorbed OH species at another catalyst site.

The ethanol is adsorbed onto the platinum sites of the catalyst and where carbon monoxide forms as a poison on the surface, the extra oxygen from the  $\text{MOH}_{\text{ads}}$  completes the oxidation to the final product such as carbon dioxide.<sup>12</sup> A Pt site is covered with adsorbed CO. This platinum site will be blocked from further ethanol adsorption unless there is a nearby source of oxygen, such as at another platinum site with adsorbed OH.

This adsorbed OH provides the necessary input to break the Pt-C bond and the CO desorbs as CO<sub>2</sub>.

This applies for all intermediates and it leaves a fresh Pt site for further oxidation. These reactions are commonly illustrated by equations by seven and eight for adsorbed CH<sub>3</sub>CO<sub>ads</sub> to form CH<sub>3</sub>COOH by the same, bifunctional, mechanism. The metal that forms OH<sub>ad</sub> most readily is the major factor in selecting a suitable catalyst.



Various temperatures are suited to a particular type of fuel cell, such as the Phosphoric Acid, various alcohols, Formic Acid, Borohydride, and Solid Oxide Fuel Cell, outlined in Table 1(c). In general, increasing the temperature increases the rate of the reaction. However, complex or specialised materials such as ceramics are required at very high temperature as carbon undergoes ‘coking’ or becomes coal-like, reducing performance.

<b>Fuel Cell</b>	<b>Electrolyte</b>	<b>Temperature</b>
<b>Phosphoric Acid</b>	H <sub>3</sub> PO <sub>4</sub>	>150°C
<b>Proton Exchange</b>	H <sub>2</sub> SO <sub>4</sub>	20-60°C
<b>Alkaline</b>	NaOH	20-70°C
<b>Solid Oxide</b>	Ceramic	>500-600°C
<b>Molten Carbonate</b>	Alumina	600°C

Table 1(c): Various types of fuel cell with fuels, operating temperature and electrolyte used respectively.

Alcohol as a fuel has attractive properties in comparison to hydrogen<sup>13</sup>; liquid at room temperature, easy to store, handle and transport while not requiring bulky equipment.<sup>13</sup> The high theoretical efficiency of a fuel cell is also an attractive power source.<sup>14-16</sup> There have been multiple approaches to increasing power and current from an ethanol fuel cell; changing the catalyst support, preparation of bimetallic components, membraneless cells, as well as the removal of adsorbed poisons on the surface.<sup>17-18</sup> It is generally agreed that electrocatalysis is improved by alloying or combining platinum or platinum oxides.<sup>18</sup> However, to-date, the power densities from DEFCs are still lower than required for commercial needs, primarily due to the performance of the anode.<sup>19</sup> As such, the anode performance is where the focus of DEFC research continues to be concentrated, particularly in a high pH electrolyte.<sup>20</sup> At very high pH, the use of strongly concentrated

potassium hydroxide can overcome the aforementioned ‘coking’, but also leads to degradation of the AAEM in such a harsh electrolyte.<sup>20</sup>

### 1.3 Catalysis for the Direct Ethanol Fuel Cell:

Historically, ethanol oxidation has largely been conducted in acid conditions. The principal reason for this was the availability of a commercially available proton exchange membrane, Nafion<sup>®</sup>. In comparison, anion exchange membranes are a recent development. In the early 1980s, Lamy and Kadirgan conducted work varying pH<sup>10</sup> and subsequently focused on low pH research with platinum based electrodes. In particular, work was carried out on PtSn bimetallic electrodes<sup>6,8</sup> to determine the optimum conditions for this catalyst in a DEFC with a critical comparison against their most suitable electrode for the Direct Methanol Fuel Cell (DMFC), a PtRu electrocatalyst.<sup>8</sup> Lamy *et al.*<sup>8,10</sup> found that the optimum ratio for tin was 20% whereby greater or lesser amounts of Sn resulted in a performance drop.

In contrast, Colmati *et al.*<sup>21</sup> and Zhou and co-workers<sup>22</sup> both used and found different proportions of Sn as their optimum conditions to that of Lamy as well as other work referencing PtSn in acid.<sup>23</sup> This difference highlights the contradiction in results<sup>6</sup> and that multiple electrode configurations can be used in various experimental arrangements such that this needs to be determined for each multimetallic electrode under a variety of conditions. For the EOR in acid conditions, platinum was considered a reference element for electrocatalysis<sup>6</sup> - its high activity and crucially high stability at low pH makes it a

suitable catalyst. At moderate temperature however, it is strongly poisoned by carbon monoxide adsorption.<sup>24</sup> At low pH – approximately 0 - the platinum oxides that exist could provide the extra oxygen species to complete the oxidation process.<sup>25, 26</sup>

Other potential catalysts were found to be less stable in very low pH such the adsorption of hydrogen by palladium. However, several mg/cm<sup>2</sup> of platinum was required as a suitable catalyst for the DEFC increasing the cost substantially.<sup>27</sup> One research group has suggested that, to compete with a current standard combustion engine, between 72-94 g of platinum are required in fuel cells<sup>28</sup> The cost of platinum alone in a PEMFC for a 100 kW passenger vehicle is substantially greater than the current cost of an entire 100 kW gasoline engine.<sup>29</sup> Various acidic electrolytes have been used including perchloric acid<sup>30-32</sup> and sulphuric acid.<sup>23, 27, 33-36</sup> The main reported products of the EOR in acidic media are intermediate substances, specifically, acetaldehyde and acetic acid.<sup>27, 37</sup> The complication with acetic acid production was the four electron process, or partial oxidation, to form the product resulting in decreased cell efficiency.<sup>6</sup> This was considered a final product for the reaction which could not be further oxidised to form CO<sub>2</sub>.

Substantial work has been conducted into the understanding of the EOR mechanism in acid conditions for a PtSn bimetallic electrode. as mentioned previously resulting from studies by Demirci into the location of the d-band centre of the catalyst.<sup>38</sup> Demirci suggests that there is a symbiotic relationship between metal hydroxides and the EOR. This EOR mechanism will be mentioned in greater detail in chapter 2.9. Over the past decade, there has been an increasing trend from low pH research to high pH as the demand increased for a less expensive solution to the catalyst. The cost of palladium and transition metals remained relatively static while rhodium, platinum and gold diverged

and increased.<sup>39</sup> In 2001, platinum and palladium prices were similar, while by 2006, platinum was now reaching three times the cost of the latter noble metal.<sup>39</sup>

Similarly rhodium, for example, was nearly ten times the cost of platinum. However it was still investigated by Gupta *et al.*<sup>27</sup> to determine its optimum conditions and activity towards the EOR. Rhodium prices have dramatically decreased in the past five years – almost tenfold – and as such, its suitability towards the EOR in terms of its surface chemistry and its products from the EOR becomes increasingly appropriate now.

Since 2004, there was an increasing demand for stable anion exchange membranes in DEFCs such as that developed by the University of Surrey<sup>40</sup> as the potential power densities achievable in high pH media began to gradually increase from almost 0 mW/cm<sup>2</sup> to above 200 mW/cm<sup>2</sup>. The increasing stability of the Alkaline Anion Exchange Membrane (AAEM) has resulted in the revisiting of past publications in base electrolyte such as carbonate<sup>31</sup> or hydroxides.<sup>13, 25, 42-49</sup> As a result, it was found that the platinum content required for the catalyst to be effective for the EOR could indeed be reduced when the electrolyte was at pH 14.<sup>25</sup> This correlated with the historical assumption of reduced platinum content at high pH. This sets the trend for the state of the art of the research topic. In the past five years, there has been considerable work in the EOR and the AAEM and alkaline fuel cell. As increasing analytical instrumentation and hyphenated techniques are attached in-situ for detection of intermediates, such as spectroelectrochemistry, significantly larger current efficiencies have been determined. Rao *et al.* used Differential Electrochemical Mass Spectrometry (DEMS)<sup>45</sup> to determine a

55% efficiency in alkaline media compared to 2% in acidic media. Rao indicated that the critical step in the EOR, the scission of the carbon-carbon double bond, is easier in high pH compared to acidic media.<sup>45</sup> The introduction of transition metals allows for extensive studies of metal hydroxides formed by these more inexpensive elements such as nickel which form NiOOH and NiOH.<sup>25</sup> These hydroxides are thought to be beneficial for promotion of the mechanism of the EOR and now provide the dynamic for future research irrespective of the medium. Cremers *et al.*<sup>50</sup> outline that, despite promising results in alkaline environments, the EOR does take place faster than methanol oxidation. This indicates that entirely new systems, electrolytes and membranes need to be continually developed and improved to maximise operation in alkaline or neutral pH.<sup>50</sup> This includes additives such as NaBH<sub>4</sub> to promote ethanol oxidation by PdO reduction thereby causing reproduction of a fresh catalyst surface for ethanol oxidation.

Furthermore, the commercial carbon support that was used in acidic media tests – Vulcan XC72 from De Nora Industries - is a very high surface area carbon powder that is currently no longer readily available. Consequently, alkaline research has invoked investigations into a suitable support for the electrocatalyst. For example, Toray carbon paper has been used by Hariyanto *et al.*<sup>24</sup> and Highly Oriented Pyrolytic Graphite (HOPG)<sup>51</sup> has been used in DAFCs as well as graphite particles by Gupta and co-workers<sup>27</sup> and others.<sup>52-61</sup>

#### **1.4 The Research Question:**

The development of the fuel cell depends upon several key components of the experimental set-up. For hydrogen, the predominant cost is for the construction and machining of the flow plates, but also includes the exchange membrane used, the electrode and the platinum electrocatalyst.<sup>1</sup> An example of a flow plate is included in figure 1.4(a). Reducing the cost is paramount to developing a cell for an individual application. For example, a hydrogen fuel cell fabrication costs approximately €1,400/kWh for the state of the art.<sup>1</sup> The desired level for industrial automotive adoption of a fuel cell has been quoted as low as €30/kWh.<sup>1</sup> The final choice of cell arrangement depends greatly on the field of application.<sup>8</sup>

Electrocatalysts are typically highly loaded with a noble metal to overcome sluggish electrode kinetics.<sup>9</sup> Transition metals, which catalyse alcohol oxidation,<sup>10</sup> can be used to increase the electrode surface area by reducing agglomerated particles which are associated with noble metal electrodes.<sup>9</sup> As a result, the performance, surface chemistry and mechanism of the ethanol oxidation reaction needs to be assessed for each electrode.

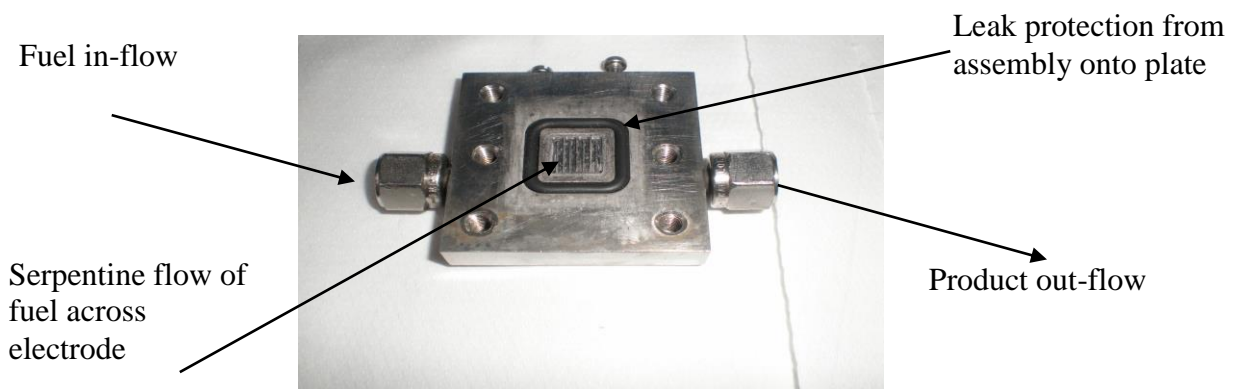


Fig 1.4(a): A serpentine flow (in centre) plate for a 1cm<sup>2</sup> fuel cell.

The effect caused by bimetallic electrodes and trimetallic electrodes with transition metals needs to be studied. The high cost of the electrocatalyst constitutes a major barrier to the industrial development of a fuel cell, requiring several  $\text{mg/cm}^2$  of platinum to date towards alcohol oxidation.<sup>21-28</sup> Furthermore, greater understanding of the mechanism and products from the EOR, in optimum conditions, acts as a driving force for developing fuel cells for energy production. Both of these elements remain the key questions in the research field.

### **1.5 Aims of the Project**

The principal aims for this project are as listed below. The fulfilment of these aims will be scrutinised on the basis of the achievements, conclusions made based on the results and where future work is required throughout chapter seven.

There are different methods to produce electrodes for ethanol fuel cells which can be complex. The ideal process for electrode production should be robust, reproducible and cost efficient. Similarly, the method should be fast without overnight treatment for immediate analysis. The electrodes themselves should be made of readily available or common materials. The electrodes should not impede the activity of the catalysts towards the EOR. The quickest and simplest method to manufacture electrodes for the study of the EOR should be determined and used throughout the project.

As with the manufacture of the electrodes, the catalysts should be simple, reproducible and prepared from common materials in a timely fashion. Highly specialised electrodes such as single crystals may be impractical outside of a laboratory setting. The composition of the electrodes should be well defined and reproducible. The most suitable elements are to be deposited for the EOR by a quick and simple method.

The platinum content in the electrocatalyst should be minimised in lieu of more inexpensive transition metals, ideally producing a platinum-free catalyst. Each catalyst needs to be characterised in terms of power and current density and assessed in terms of both in-situ and ex-situ methods such as Tafel Analysis, potential step and SEM-EDX analysis. Platinum is the most widely used catalyst but is prohibitively expensive to use for catalysis. The development of a platinum free catalyst would be a significant step in development of commercially viable ethanol fuel cells.

Further understanding of the ethanol fuel cell should be established and contribute to the knowledge already known. The alcohol fuel cell has been studied with methanol and ethanol, however, there are gaps in knowledge, especially with regard to the use of platinum free catalysts and the use of non-acidic media.

The use of pH should be exploited to develop an electrocatalyst in neutral media, moderately alkaline electrolyte and strongly basic conditions. The recent trend with the Direct Ethanol Fuel Cell is to increase the pH of the electrolyte. There are increasingly stable membranes in alkaline electrolytes. This allows further study into electrocatalysts

at high pH to gather pace. This is the major criterion for catalysts of the future. Meanwhile, neutral pH shows promising signs in terms of the voltammetric data compared in highly acidic electrolytes. The advantage of neutral or near neutral pH may be the ability to work within the current membranes widely available. In particular Nafion<sup>®</sup> membranes will be stable to operate a fuel cell in near neutral pH. The characterisation of catalysts at increased pH is the main goal of this project.

The catalysts will be tested to determine the other optimum operating conditions for ethanol oxidation. There are numerous conditions that may affect the performance of the catalyst. These include concentration of the fuel, loading of the catalyst, the scan rate, the deposition conditions, the carbon surface as well as the best operating temperature for any particular electrode. The activity of the catalyst towards other low molecular weight fuels such as methanol and any possible intermediates also needs to be considered.

An aim of the project is to investigate the catalysts and characteristic adsorption in the EOR using Electrochemical Impedance Spectroscopy. EIS provides potentially useful information on what is occurring at the electrode surface at a given potential. It can provide insight into the most suitable catalyst and contribute to an overall explanation of the carbon electrode and catalyst combination.

The aim is to gain mechanistic information from ethanol oxidation and the catalysts used. The typical features of ethanol oxidation by voltammetric methods can indicate the best performing catalyst and provide insight into the mechanism of oxidation.

## 1.6 References

1. Meyers, J.P; (2008), *Interface*, The Electrochemical Society, Winter Edition, 36-39.
2. Narayan, S.R.; Valdez, T.I; (2008), *Interface*, The Electrochemical Society, Winter Edition, 40-45.
3. Wilkinson, D.P; (2001), *Interface*, The Electrochemical Society, Spring Edition, 22-25.
4. Sandi, G.; (2004), *Interface*, The Electrochemical Society, Autumn Edition, 40-44.
5. Laminie and Hicks, (2003), *Fuel Cell Systems Explained - Direct Methanol Fuel Cells*, John Wiley & Sons. Ltd., Second Edition, **6**, ISBN: 0-470-84857-X.
6. Simoes, F.; dos Anjos, D.M.; Vigier, F.; Legér, J.-M. ; Hahn, F. ; Coutanceau, C. ; Gonzalez, E.R. ; Tremiliosi-Filho, G. ; de Andrade, A.R.; Olivi, P.; Kokoh, P.; (2007), *J. Power Sources*, **167**, 1-10.
7. Vigier, F; Coutanceau, C.; Perrard, C.; Belgsir, E.M.; Lamy, C.; (2004), *J. Appl. Electrochem.*, **34**, 439-446.

8. Lamy, C.; Rousseau, S.; Belgsir, E.M.; Coutanceau, C.; Léger, J.-M.; (2004) *Electrochim. Acta*, **49**, 3901-3908.
9. Lamy, C.; Léger, J.-M.; Srinivasan, S.; (2001), *Modern Aspects of Electrochemistry*, edited by Bockris, J.O'M.; **34**, Kluwer Academic/Plenum Publishers, New York.
10. Kadirgan, F.; Léger, J.-M.; Lamy, C.; (1981), *J. Electroanal. Chem.*, **125**, 89-103.
11. Yu, E.H.; Krewer, U.; Scott, K.; (2010), *Energies*, **3**, 1499-1528.
12. Baltruschat, Ernst and Bagolowski, (2011), "Catalysis in Electrochemistry: From Fundamentals to Strategies for Fuel Cell Development: Chapter 9: Electrocatalysis at Bimetallic Surfaces obtained by Surface Decoration", **9**, 297, edited by Santos, E, Schmickler, W.; John Wiley and Sons Ltd., New Jersey.
13. Zakaria, Z.; Kamarudin, S.K.; Timmiati, S.N.; (2016), *Appl. Energ.*, **163**, 334-342.
14. Majidi, P.; Pickup, P.G.; (2015), *Electrochim. Acta*, **182**, 856-860.
15. An, L.; Zhao, T.S.; Li, Y.S.; (2015), *Renew. Sust. Energ. Rev.*, **50**, 1462-1468.
16. Badwal, S.P.S.; Giddey, S.; Kulkarni, Goel, J.; Basu, S.; (2015), *Appl. Energ.*, **145**, 80-103.
17. Jablonski, A.; Lewera, A.; (2015), *Chinese J. Catal.*, **36**, 496-501.
18. Dutta, A.; Mondal, A.; Datta, J.; (2015), *J. Power Sources*, **283**, 104-114.

19. Figueiredo, M.C.; Sorsa, O.; Arán-Ais, R.M.; Doan, N.; Feliu, J.M.; Kallio, T.; (2015), *J. Catal.*, **329**, 69-77.
20. Jurzinsky, T.; Cremers, C.; Jung, F.; Pinkwart, K.; Tubke, J.; (2015), *Int. J. Hydrogen Energ.*, **40**, 11569-11576.
21. Colmati, F.; Antolini, E.; Gonzalez, E.R.; (2006), *J. Power Sources*, **157**, 98-103.
22. Zhou, W.J. ; Song, S.Q. ; Li, W.Z. ; Zhou, Z.H. ; Sun, G.Q. ; Xin, Q. ; Douvartzides, S. ; Tsiakaras, P. ; (2005), *J. Power Sources*, **140**, 50.
23. Jiang, L. ; Hsu, A. ; Chu, D. ; Chen, R. ; (2010), *Int. J. Hydrogen Energ.*, **35**, 365-372.
24. Hariyanto ; Purwanto, W.W. ; Soemantojo, R.W. ; Stimming, U. ; *J. Chem. Nat. Resources Eng*, **2**, 47-61.
25. Spendelow, J.S. ; Wieckowski, A. ; (2007), *Phys. Chem. Chem Phys*, **9**, 2654-2675.
26. Hansen, H.A.; Rossmeisl, J.; Nørskov, J.K.; (2008), *Phys. Chem. Chem Phys*, **25**, 3722.
27. Sen Gupta, S.; Datta, J.; (2006), *J. of Electroanal Chem.*, **594**, 65-72.
28. Kiros, Y. COST 543: Bioethanol Fuel Cells, Workshop Meeting Presentation, Helsinki, May 2009.
29. <http://www.sciencedaily.com/releases/2008/07/080731143916.htm>, published 2008, accessed January 2013.

30. Friedrich, K.A. ; Henglein, F. ; Stimming, U. ; Unkauf, W. ; (2000), *Electrochim. Acta*, **45**, 3283-3293.
31. Bergamaski, K. ; Gomes, J.F. ; Goi, B.E. ; Nart, F.C. ; *Eclét. Quím.*, (2003), **28**, 87-92.
32. Li, H. ; Sun, G. ; Cao, L. ; Jiang, L. ; Xin, Q. ; (2007), *Electrochim. Acta*, **52**, 6622-6629.
33. Bonilla, S.H. ; Carvalho, J.G.A. ; Almeida, C.M.V.B. ; Gianetti, B.F. ; Zinola, C.F. ; (2008), *J. Electroanal. Chem.*, **617**, 203-210.
34. Wang, Z-B. ; Yin, G-P ; Lin, Y-G ; (2007), *J. Power Sources*, **170**, 242-250.
35. Thompson, S.D. ; Jordan, L.R. ; Shukla, A.K. ; Forsyth, M. ; (2001), *J. Electroanal. Chem.*, **515**, 61-70.
36. El-Aziz, A.M. ; Kibler, L.A. ; (2002), *J. Electroanal. Chem.*, **534**, 107-114.
37. Camara, G. ; Iwasita, T. ; (2005), *J. Electroanal. Chem.*, **578**, 315-321.
38. Demirci, U.B, (2007), *J. Power Sources*, **173**, 11-18.
39. [www.kitco.com](http://www.kitco.com), Platinum and Palladium Prices, viewed March 2015.
40. Slade, R.; Varcoe, J.; (2011), symposium 4: Fuel Cells, 61<sup>st</sup> meeting of the International Society of Electrochemistry, Electrochemistry from Biology to Physics, Nice, France.

41. Park, S.-M. ; Chen, N.C. ; Doddapeneni, N. ; (1995), *J. Electrochem. Soc.*, **142**, 40-45.
42. Coutanceau, C. ; Demarconnay, L. ; Lamy, C. ; Léger, J.-M. ; (2006), *J. Power Sources*, **156**, 14-19.
43. Wang, L. ; Bambagioni, V. ; Bevilacqua, M. ; Bianchini, C. ; Filippi, J. ; Lavacchi, A. ; Marchionni, A. ; Vizza, F. ; Fang, X. ; Shen, P.K. ; *J. Power Sources*, (2010), 195, 8036-8043.
44. de Lima, R.B. ; Varela, H. ; *Gold Bullion*, 2008, 41/1.
45. Rao, V. ; Hariyanto ; Cremers, C. ; Stimming, U. ; (2007), *Fuel Cells*, WILEY-VCH Verlag GmbH, Weinheim, 7, 5, 417-423.
46. Wang, D. ; Liu, J. ; Wu, Z. ; Zhang, J. ; Su, Y. ; Liu, Z. ; Xu, C. ; (2009), *Int. J. Electrochem. Sci.*, **4**, 1672-1678.
47. Xu, C.W. ; Wang, H. ; Shen, P.K. ; Jiang, S.P. ; (2007), *Adv. Mater.*, **19**, 4256.
48. Xu, C.W. ; Liu, Y.L. ; Yuan, D.S. ; (2007), *Int. J. Electrochem. Sci.*, **2**, 674.
49. Liu, J.P. ; Ye, J.Q. ; Xu, C.W. ; Jiang, S.P. ; Tong, Y.X. ; (2008), *J. Power Sources*, **177**, 67.
50. Cremers, C. ; Bayer, D.; Jung, F. ; Kintzel. B. ; Joos, M. ; Tuebke, J. ; Krausa, M., (2008), *ECS Trans.*, **16**, 1263.
51. Kucernak, A. ; Chowdhury, P.B. ; Wilde, C.P. ; Kelsall, C.H. ; Zhu, Y.Y. ; Williams, D.E. ; (2000), *Electrochim. Acta*, **45**, 4483-4491.

52. Maillard, F.; Bonnefont, A.; Chatenet, M.; Guétaz, L.; Doisneau-Cottignes, B.; Roussel, H.; Stimming, U.; (2007), *Electrochim. Acta*, **53**, 811-822.
53. Cheung, K.-C.; Wong, W.-L.; Ma, D.-L.; Lai, T.-S.; Wong, K.-Y.; (2007), *Co-ordin. Chem. Rev.*, **251**, 2367-2385.
54. Singh, R.N.; Singh, A. ; Anindita; (2009), *Carbon*, **47**, 271-278.
55. Krewer, U.; Vidakovich-Koch, T.; Rihko-Struckmann, L.; (2011), *Chem. Phys. Chem.*, **12**, 2518-2544.
56. Wang, H.; Xu, C.; Cheng, F.; Jiang, S.; (2007), *Electrochem. Comm.*, **9**, 1212-1216.
57. Benseba, F.; Farah, A.A.; Wang, D.S.; Bock, C.; Du, X.M.; Kung, J.; Page, Y.L.; (2005), *J. Phys. Chem. B*, **109**, 15339.
58. Mu, S.C.; Tang, H.; Wan, Z.H.; Pan, M.; Yuan, R.Z.; (2005), *Electrochem. Comm.*, **7**, 1143.
59. Liu, J.; Ye, J.; Xu, C.; Jiang, S P; Tong, Y.; (2008), *J. Power Sources*, **177**, 67-70.
60. Sen Gupta, S.; Datta, J.; (2005), *J.Chem. Sci.*, **117**, 337-344.
61. Pournaghi-Azar, M.H.; Habibi-A, B.; (2005) *J. Electroanal. Chem.*, **580**, 23-34.

## Chapter 2: Platinum/Carbon and gold catalysts

### 2.1 Introduction:

The focus of this chapter is on platinum and gold samples with electrodeposits on carbon ink electrodes (CIEs) and carbon paper electrodes (CPEs). Platinum sheet electrodes will also be used as a working electrode to determine their suitability as catalysts. In addition the most suitable carbon substrate will be analysed. Platinum has been used historically as it was believed to be the best performing catalyst for the ethanol oxidation reaction, EOR, in acidic media.<sup>1-4</sup>

Platinum enables the breaking of carbon-hydrogen bonds and facilitates the initial adsorption of ethanol onto the surface.<sup>5</sup> It is impossible to circumvent its properties to initiate the C-H bond cleavage during the first adsorption steps.<sup>5</sup> Furthermore, the platinum oxides that are formed aid with continuous oxidation of adsorbed species.<sup>5</sup> In comparison, gold electrodes were found to be unsuitable for ethanol adsorption, but can have an anti-fouling effect to enhance the EOR at other metals, or may act as a conductive layer onto which other catalysts can be subsequently deposited.<sup>6-7</sup> As a result, a gold electrode can act as an electrode at which ethanol oxidation is not favoured. However gold has been used as a substrate to deposit other EOR active metallic species<sup>6-</sup>  
<sup>7</sup>. The voltammetry of a gold surface in an aqueous ethanol solution can be used to study the behaviour of a surface at which the ethanol oxidation kinetics are very slow but can

still be used in multimetallic catalysts. Multimetallic catalysts consist of different metals, each playing a role to aid efficient ethanol oxidation.

Various carbon supports have been used in the literature for alcohol oxidation such as Highly Oriented Pyrolytic Graphite<sup>8</sup> (HOPG) along with the industry standard, Vulcan XC72 powder<sup>9-11</sup> and graphite.<sup>12</sup> Ideally, a carbon support is a conducting surface that comprises finely dispersed catalyst species, is inexpensive, and promotes the EOR.<sup>13</sup> Electrodeposition at carbon materials overcomes problems experienced by the colloidal route, such as the heating or oxidative treatment required to clean the particles from surfactant contamination.<sup>13</sup> A critical analysis over the most suitable choice from a selection of methods by which catalysts are produced will be discussed later in this chapter. Recent economic developments have resulted in the Vulcan XC72 supplied by E-tek and De Nora Industries to be taken off the market. Therefore, alternatives are sought that do not affect the ethanol oxidation reaction itself, but are easily prepared, characterised and quickly analysed for activity towards the EOR. As Gupta and Mahaptra outline, there are a number of solutions to achieve more active anode catalysts for the DEFC, namely: (i) synthesis of finely dispersed catalysts on conducting surfaces, (ii) reduction of the relative loading of Platinum on the catalyst surface and (iii) the use of substrate.<sup>14</sup> This work examines an electrode that is very easy to produce, cost effective and allows an efficient EOR.

As mentioned previously, the best performing catalysts to-date are platinum-based in acidic media and thus, the cost of the electrodes are high. This is a barrier to the

implementation of a commercial fuel cell. Furthermore, electrodes are produced that are highly specific and may not be suitable for a fuel cell aimed at real world applications such as small scale energy alternatives, particularly laptop and mobile phone batteries. Work conducted by Baltruschat used single crystal platinum electrodes with a highly stepped crystal orientation of (3, 3, 2).<sup>15</sup> Although this is interesting for the purposes of ethanol oxidation due to the increased edges present, where the rate of the EOR is to be increased as outlined further in this work, it is impractical to scale up these crystals on a widespread level. Furthermore, platinum electrodes prepared by, for example, the Bönemann method,<sup>9,16</sup> use a constant supply of Argon gas overnight<sup>9</sup> which may be prohibitive in cost. Moreover, platinum has increased 2.5 times in cost in the previous ten years (2005) from \$500/oz to \$1,200/oz.<sup>17</sup> This is reportedly due to the introduction of increasingly stricter controls on emissions standard from catalytic converters in automobiles in the European Union, USA and Japan since the beginning of the 21<sup>st</sup> century thus increasing demand for platinum.

In addition, numerous conditions need to be investigated for an electrode to perform at its optimum, such as temperature (to a designated 'low temperature' limit of 333 K-373 K), reactant concentrations, catalyst loading and particle size. Agglomeration of the particles will reduce surface area and subsequently, the propensity for the metal surface to act towards the EOR. Most importantly, the pH of the solution can greatly affect the efficacy of platinum in the ethanol oxidation reaction.

Historically, as mentioned earlier, a strongly acidic electrolyte was used extensively due to the suitability of an acid medium to scale up to an operating fuel cell, stability of platinum in low pH as well as the availability of appropriate Proton Exchange Membranes (PEM) that will be discussed later. As shown previously in figure 1.2 (a) and outlined for hydroxyl ions in high pH in chapter one, an operating acidic fuel cell requires a flexible membrane for hydrogen ions to pass through and react at the cathode. In comparison, an alkaline fuel cell operates in reverse where hydroxide ions pass through to the anode, complete the circuit and assist in further oxidation of the ethanol at the surface. Recent developments in robust alkaline membranes allows for the investigation at increasing pH levels. This work both reflects and aims to investigate the impact of increasing the pH from acidic solution to neutral through to high pH. For this purpose, the ability of platinum to form oxides and hydroxides in solutions of increased pH, up to and including basic solutions, needs to be studied. This reflects the current trend in ethanol fuel cell research into the field of operation at high pH.

## 2.2 Experimental

Polycrystalline platinum disks (Metrohm), a platinum foil sheet from Johnson Matthey, electrodeposited platinum and electrodeposited gold on carbon supports were used as platinum and gold electrodes in a conventional three electrode system. A saturated (3 M KCl) calomel electrode, Hg/Hg<sub>2</sub>Cl<sub>2</sub> (SCE), +240 mV vs. SHE and an Hg/Hg<sub>2</sub>SO<sub>4</sub> (MMS), + 640 mV vs. SHE, were purchased from Radiometer Analytical Instruments (ref 640) and were used as the reference electrodes with a Pt sheet as an auxiliary electrode. CHI 600A and CHI 620A Series potentiostats were used to collect electrodeposition and cyclic voltammetric; chronocoulometric and chronoamperometric data.

Carbon ink electrodes were prepared by coating a non-porous plastic sheet (Xerox) with finely dispersed, particle-based graphite inside an ink binder solvent (Acheson Industries, Electrodag 423 SS). The ink coating was then allowed to dry overnight. The fabricated electrodes were then cut into 1 cm<sup>2</sup> samples used for further testing, acting as working electrodes. A solution of commercial nail polish, acting as insulation, was added to the stem of each electrode in order to guarantee its geometrical area. Electrodeposition was conducted from the respective salt, K<sub>2</sub>PtCl<sub>4</sub> or H<sub>2</sub>AuCl<sub>4</sub>, was used at a concentration of 0.01 M.

Vulcan XC72-R electrodes were prepared using 10 mg and 50 mg of a high surface area carbon powder with 57.5% pre-loaded platinum (DeNora Chemicals, USA), supplied by

the Technical University of Munich, TUM. The powder sample was added to a solution of ethanol and de-ionised water. The resultant solution was allowed to evaporate slowly where a pre-defined weight of carbon ink (Acheson Industries, Electrodag 423 SS) was added. This process incorporated the carbon powder into an ink mixture and was then spread onto a plastic non-porous support. The electrodes were allowed to dry and subsequently sectioned into 1 cm<sup>2</sup> electrodes.

The effect of scan rate on ethanol oxidation was tested using polycrystalline platinum disks (Metrohm), and rotation rates ranging between 500 rpm and 1500 rpm were used at a gold rotating disk electrode (RDE). In order to examine the carbon substrate effect of the platinum electrode, a solution of 0.01 M potassium ferricyanide was prepared in 0.1 M potassium chloride, both supplied by Sigma Aldrich. A range of electrolytes were used, specifically sulphuric acid, 0.1 M potassium nitrate and sodium hydroxide, NaOH at various concentrations all purchased from Sigma Aldrich. Typically, the concentration of sodium hydroxide was 1 M NaOH. The temperature study was carried out using an IKA C-MAG HP7 heating plate/stirrer. The temperature of the cell was kept between 293 K and 333 K and the cell was de-aerated with oxygen-free nitrogen (BOC gases). To study the effect of pH, the concentration of aqueous potassium hydroxide was varied between pH 11 and pH 14 (0.001 M NaOH and 1 M NaOH). Typically the scan rate was set to 10 mV/s, however a range of scan rates were also employed for some studies ranging between 1 mV/s to 200 mV/s. Solutions of pure ethanol and pure methanol were purchased from Sigma Aldrich. The concentration of ethanol varied from 0.1 M to 3.0 M in aqueous solution.

### 2.3 Carbon Ink Electrode Appearance:

Upon visual inspection, the Pt deposited metal appeared grey in comparison to the insulated section of the carbon ink electrode (CIE) as shown in figure 2.3(a).



Figure 2.3(a): Photograph of a platinum deposit on a 1 cm<sup>2</sup> carbon ink electrode before electrodeposition.

The colour of the stem of the electrode reflects the colour of the electrode before any deposition or other process used to prepare the catalyst. Under a Scanning Electron Microscope, the deposits appeared to be mushroom-shaped individual beads of platinum, as shown in figure 2.3(b), supported by the carbon substrate. The bare carbon surface gave a mottled appearance and will be shown in magnification further in this chapter. The surface is uneven in figure 2.3(b) with isolated 'islands' of metal deposited across the surface. The carbon paper electrodes (CPE) that were manufactured appeared identical in

terms of colour and size. The active surface of the CPE was made up of fibres or strands of carbon rather than particle/ink suspension of a CIE and will be presented later in this chapter.

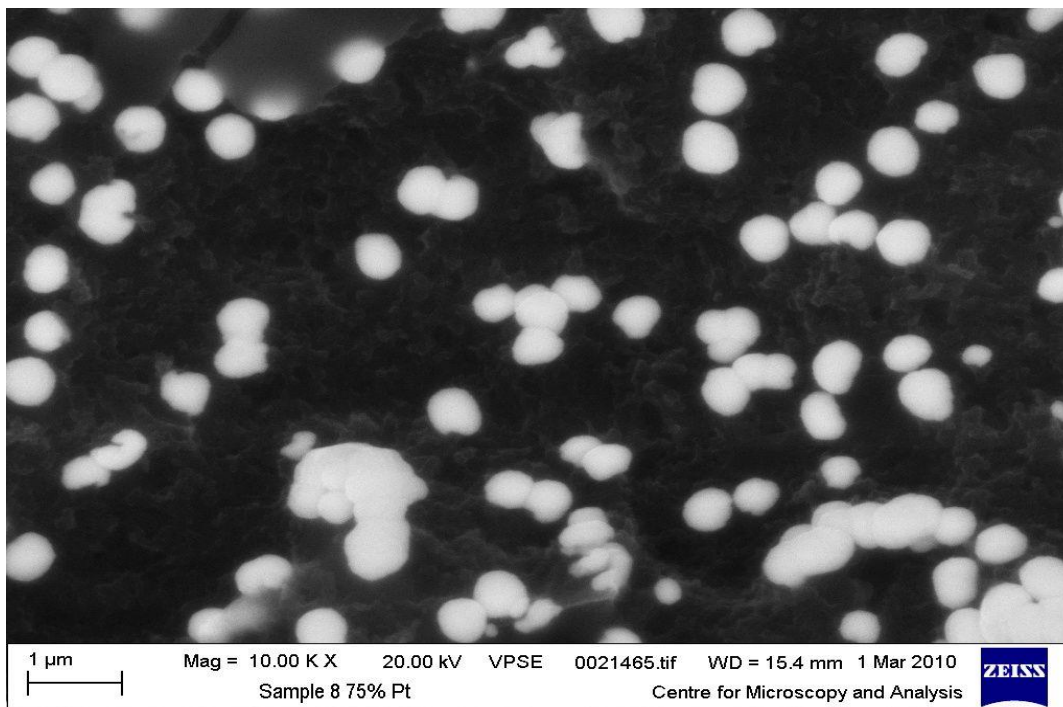


Figure 2.3(b): An SEM image of platinum electrodeposited onto a carbon ink electrode from a solution of 0.01 M  $\text{K}_2\text{PtCl}_4$  in de-aerated 0.1 M  $\text{KNO}_3$  from a two electrode system with an applied potential of -1.0 V and charge passed of  $120 \text{ mC/cm}^2$ .

Such an uneven surface at a CIE promotes the deposition of Pt clusters around the perimeter of ledges and steps. However as figure 2.3(c) shows, the metal can also accumulate over the face of the electrode surface. As the charge passed in the deposition process is increased, the particle geometry and progressive growth was observed by

SEM-EDX to remain consistent with individual ‘islands’ growing larger, but not spreading out across the carbon surface. Pletcher<sup>18</sup> describes the processes that take place for metal deposition in sequential steps as bulk diffusion of the ion to the surface, electron transfer, the formation of an ad-atom on the surface, surface diffusion to form a cluster of ions and growth either vertically or radially as deposition progresses.

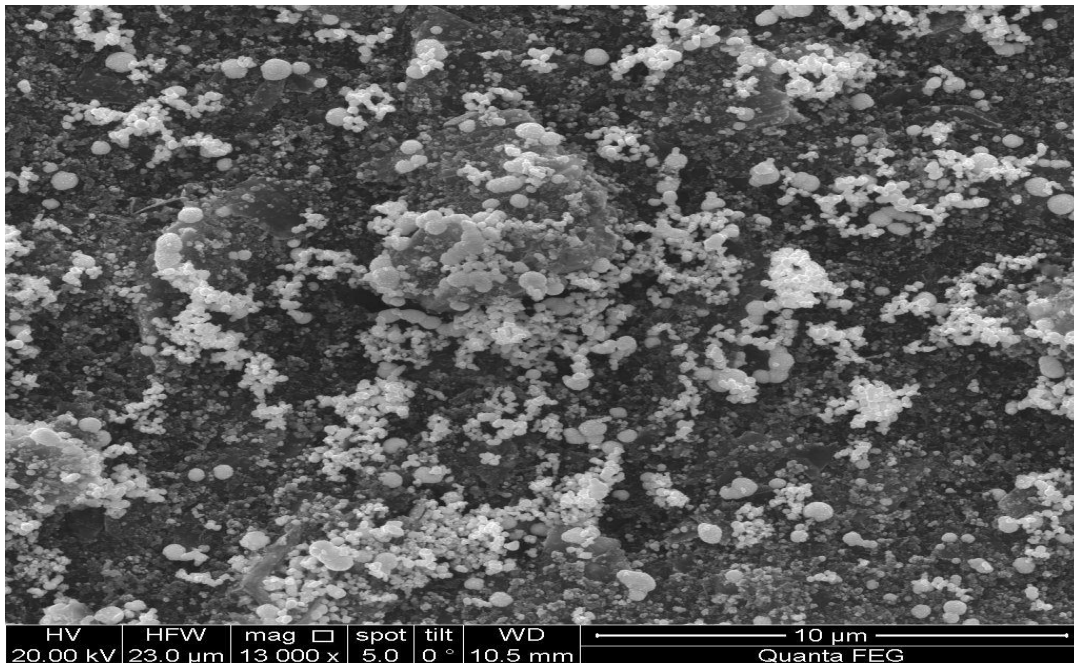


Figure 2.3(c): SEM image showing a platinum deposit across a carbon ink electrode when larger deposits are allowed to develop from an electrodeposition solution containing 0.01 M  $K_2PtCl_4$  and deaerated 0.1 M  $KNO_3$ , at an applied potential of -1.0 V in a two electrode system and with uncontrolled charge.

The particle sizes of the platinum deposits were measured to be between 50-500 nm dependant on deposition time and charge passed. Growth of the deposit was evident primarily at individual nucleation sites or ‘islands’, consistent with a 2D nucleation

mechanism. The island or bead configuration is surrounded by the carbon surface, which is inactive to the EOR, resulting in the creation of a substantial amount of individual active edges. Edge diffusion rather than linear diffusion allows for a greater quantity of fuel at the surface to react at the interface between deposit and insulated surface.<sup>18</sup> The bead configuration increases the surface area and edges in comparison to a simple planar electrode. Oxidation of ethanol occurs more readily at an electrode containing defects such as kinks, steps and edge and surface vacancies of the electrode compared to a planar electrode as illustrated by Del Colle *et al.*<sup>19</sup> and in figure 2.3(d) below.

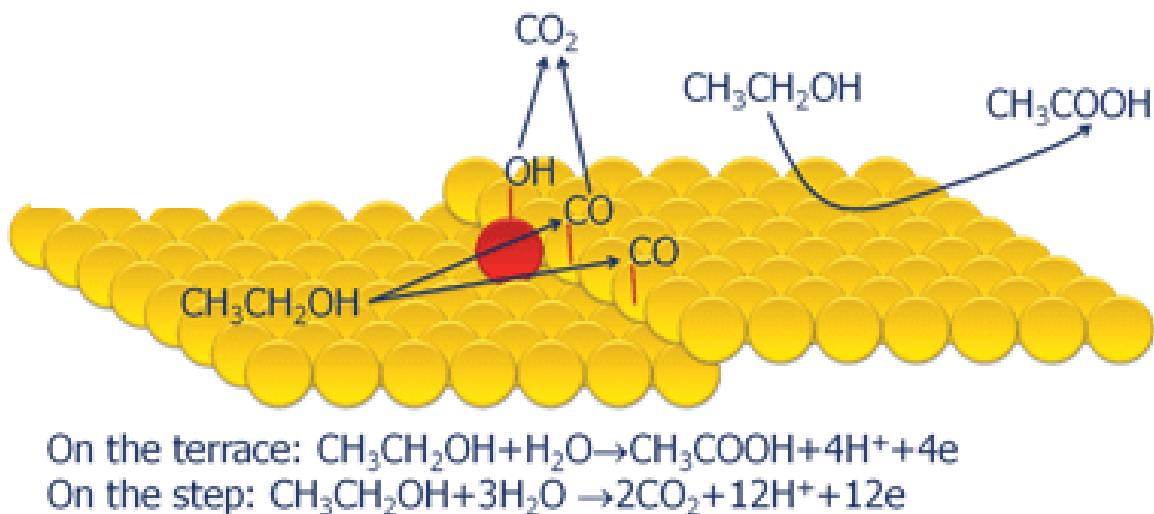


Figure 2.3(d): Illustration outlining the difference between ethanol oxidation at a step or an edge of a metal surface compared to the EOR at a metal planar surface or terrace, adapted from Del Colle *et al.*<sup>19</sup>

Electrodeposition allows for a direct electrical contact between the metal on the surface and the fuel in solution, ethanol. It has proved a simple and versatile method for alloy preparation where controllable parameters such as solvent, temperature, pH or additives

can alter particle morphology. At the edge or step of a metal surface, ethanol oxidation is enabled preferentially, as demonstrated by Baltruschat *et al.*<sup>14</sup> and Del Colle<sup>19</sup>, as four electrons are produced at a planar surface compared to a maximum of twelve electrons produced at an edge surface. In addition to this, on the terrace of an electrode surface, acetic acid (CH<sub>3</sub>COOH) which is an intermediate product, is accumulated over time and reduces the overall performance of the electrode.

Typically, electrodes with small particle size deposits are used (nanometre range), however as the layer builds up over reaction time, the difference due to the effect of particle size on the EOR can be negligible. Gonzalez *et al.*<sup>20-21</sup> have investigated larger particle size electrodes – approximately 50nm in size and found the EOR was active at a wide range of crystallite sizes, but that higher alcohol adsorption was more prominent with decreasing particle size.<sup>20</sup> Bianchini have prepared ethanol electrocatalysts ranging in sizes 3-25nm.<sup>22</sup> To this effect, electrodes with very high miller indices<sup>14</sup> and hence very highly stepped electrodes have shown an enhanced activity for ethanol oxidation.

## **2.4 Electrolyte and reference electrode**

The choice of reference electrode and electrolyte is important to allow the study of the surface reaction taking place. At platinum surfaces, surface adsorption of ionic contaminants from the metal salts used for electrodeposition may affect the availability of the precious metal to oxidise the ethanol at the surface by coating the platinum surface and thereby blocking ethanol adsorption. Chloride is a contributor to this contamination<sup>23</sup>

and frequently, by using elemental distribution analysis with SEM, chloride was found to be present on the surface of the electrode, most probably in the form of the chloride anion. Impurities and additives have been known to help the ethanol oxidation reaction<sup>24</sup> and potentially for this reason, the commercially available and popular catalytic powder, Vulcan XC72<sup>TM</sup>®, contains sulphur as an impurity (elemental mapping not shown). Similarly this work will use the reaction at a Vulcan-based electrode as a comparison to determine the impact of impurities, particularly chloride. The Bönemann method used by Coutanceau *et al.*<sup>9, 16</sup> aims to eliminate the presence of chloride by using a surfactant to ‘absorb’ the chloride ions.

#### **2.4.1 Saturated Calomel Electrode**

Figure 2.4(a) shows a cyclic voltammogram (CV) of a polycrystalline Pt disk in a solution of ethanol and sulphuric acid. Using a Saturated Calomel Electrode (SCE) as a reference in an air saturated solution, no oxidation or reduction peaks are visible in the voltammogram.

Possible reasons for this voltammetry include the presence of Cl<sup>-</sup> from the reference electrode and the presence of oxygen. Cl<sup>-</sup> adsorption may affect electrochemical processes such as the blocking of active sites and surface restructuring<sup>23</sup> and can thereby act as a poison on the surface, significantly reducing catalytic performance. This results in a competing process to the desired reactions such as ethanol oxidation. This reduces the number of available surface sites for the ethanol to adsorb onto the platinum surface.

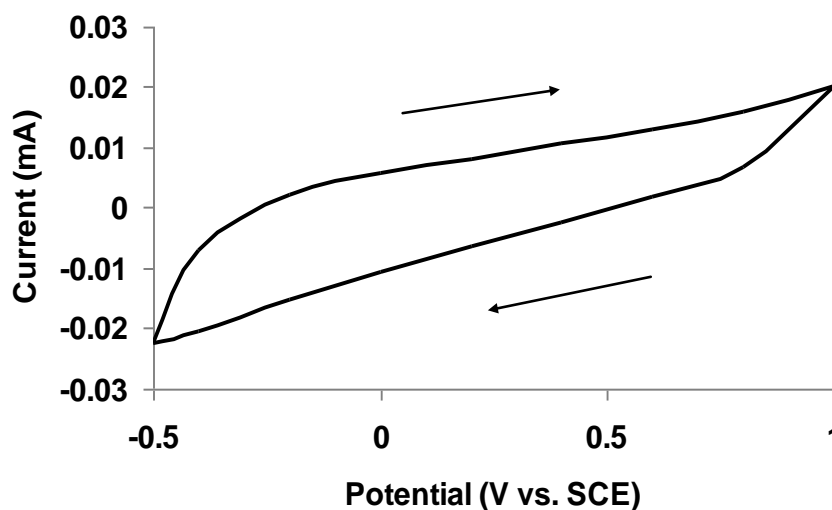


Figure 2.4(a): Cyclic Voltammogram showing oxidation of 0.5 M C<sub>2</sub>H<sub>5</sub>OH in air saturated 0.5 M H<sub>2</sub>SO<sub>4</sub> at a platinum polycrystalline disk, saturated calomel electrode as reference at a scan rate of 50 mV/s.

Similarly in the presence of oxygen, the oxidation is not observed. Subsequently, a two electrode system was used as a temporary measure instead of the saturated calomel electrode with a platinum disk as both auxiliary and reference electrode to overcome the presence and influence of Cl<sup>-</sup> on the working electrode. This chloride influence, and specifically, the effect of perchlorate will be discussed further in the next section 2.4.2. Furthermore other reference electrodes used in electrochemical analysis of ethanol oxidation include Hg/Hg<sub>2</sub>SO<sub>4</sub><sup>12</sup> and the reversible hydrogen electrode, RHE, as well as mercuric/mercuric oxide, Hg/HgO.<sup>14</sup> The RHE system however is an impractical approach due to the requirement of H<sub>2</sub> gas in H<sub>2</sub>SO<sub>4</sub>, however this reference electrode is commonly used in literature<sup>9,25-33</sup> The RHE changes potential with pH by 59 mV per unit of pH and in neutral solution the potential is unstable resulting in the voltage recorded not

necessarily being well defined. In acid solutions, a RHE reference electrode is suitable where the pH is driven to a low stable value and in strong acids, approximately 0-1. The use of hydrogen gas severely limits its use in this work. However, studies are increasingly carried out using alternatives such as the Hg/HgO reference electrode and Hg/Hg<sub>2</sub>SO<sub>4</sub> reference electrode, such as the work conducted by Gupta<sup>12,14</sup> and Dutta.<sup>34-35</sup> The Saturated Calomel Electrode uses the reaction the mercury/mercury chloride, Hg/Hg<sub>2</sub>Cl<sub>2</sub> in saturated KCl, however the chloride anion can leak through the glass frit over time. In contrast, a mercury/mercury sulphate electrode, Hg/Hg<sub>2</sub>SO<sub>4</sub>, was used to examine an identical reaction in ethanol and sulphuric acid at a platinum disk working electrode. Similarly to chloride, sulphate can be a contaminant as outlined by Tripkovic<sup>23</sup> and consequently the balance of reference electrode needs to be evaluated for specific systems.

The EOR at platinum using a platinum disk reference electrode (a two electrode system) is shown in figure 2.4(b). The oxidation which occurs is consistent with the literature at an RHE or Hg/HgO, particularly that of Gupta<sup>12, 14</sup> with peaks A, B and C occurring at similar potentials. Peaks A and B are on the forward sweep and peak C on the back sweep. In this body of work, these peaks are retained through the EOR oxidation below pH1 for each electrode to different extents, depending on the operating conditions. The peak current increases from 1<sup>st</sup> to 10<sup>th</sup> scan, attributed by Gupta<sup>14</sup> to an increased rate of adsorption of oxidative species during potential cycling, until steady state is obtained. Peak A is associated with the initial adsorption of ethanol and the hydrolysis of water to form OH<sub>ad</sub>. Peak B is associated with the oxidation of ethanol, typically adsorbed

acetaldehyde depending on the operating conditions and the catalyst used and peak C is the oxidation of an adsorbed intermediate from peak B, mostly reported as adsorbed carbon monoxide.

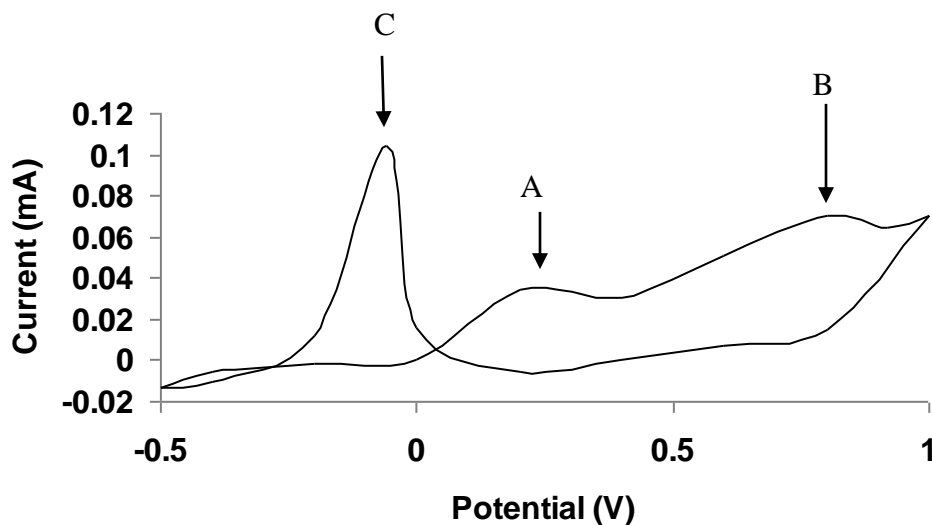


Figure 2.4(b): Cyclic Voltammogram illustrating oxidation of 0.5 M ethanol in deaerated 0.5 M H<sub>2</sub>SO<sub>4</sub> at a platinum sheet electrode (solid line: first scan; dashed line: scan 10), starting from Open Circuit Voltage (OCV): 0.1 V vs. platinum disk reference electrode (two electrode system), pH = 0.

The difference in potential between some of the reference electrodes used are relative to the SHE (Standard Hydrogen Electrode) and according to the stated potentials by Bard and Faulkner<sup>36</sup> in millivolts (mV). As a result, a mercury/mercury sulphate reference electrode was chosen throughout this work for a three electrode cell system.

## 2.4.2 Perchloric Acid, HClO<sub>4</sub>, as electrolyte

A voltammogram representing the oxidation of ethanol in perchloric acid at a platinum disk reference electrode is shown in figure 2.4(c). It is believed that hydrogen adsorption (“underpotential deposited hydrogen”) plays a key role, resulting in large currents at negative potentials through the initial sweep shown, but as noted in literature, also at potentials as high as 0 V vs. RHE.<sup>23</sup> A two electrode system was employed to remove the initial possibility of SO<sub>4</sub><sup>2-</sup> adsorption contributing to the voltammetry recorded.

Furthermore, in the presence of ethanol, this current is significantly enhanced compared to that of Pt in HClO<sub>4</sub> alone. Previously, perchlorate had been considered so inert that it could be used as an electrolyte, but this assumption has been found to be not generally valid.<sup>37</sup> Moreover, above 0.1 V, the voltammogram is featureless where the oxidation of ethanol has been found to be observed in literature. However, this voltammetry is reported to be indicative of the poisoning of the surface by Cl<sup>-</sup>.<sup>23</sup> All peaks observed in this region are diminished with the increasing presence of Cl<sup>-</sup> alone. This further indicates the impurities present in this electrolyte must be considered to have a detrimental effect. With the addition of ethanol producing increasing current in the hydrogen adsorption region, HClO<sub>4</sub> was not considered further as acidic electrolyte in deference to H<sub>2</sub>SO<sub>4</sub>. Ujvari *et al.* describes reduction of ClO<sub>4</sub><sup>-</sup> ions as forming very aggressive corrosion agents, at low concentrations, towards metals such as zinc, aluminium and nickel.<sup>38</sup> This is of particular interest in this work and Láng describes the reaction as being slower at nickel than at Fe or Co, but that ClO<sub>4</sub><sup>-</sup> decomposition cannot be neglected.<sup>39</sup>

Tripkovic describes that even in the most meticulously prepared  $\text{HClO}_4$ ,  $\text{Cl}^-$  is formed and present as an impurity.<sup>23</sup> Even the effect of trace levels can be significant, giving rise to  $\text{Cl}^-$  adsorbed species on the Pt surface, resulting in a blocked surface which inhibits ethanol adsorption and ethanol oxidation. Furthermore, the presence of metal oxide species has been found to favour the reduction of  $\text{ClO}_4^-$  to chloride<sup>40</sup> and Hassan suggests that  $\text{ClO}_4^-$  cannot be considered as a stable species even in neutral media.<sup>40</sup> The need for oxide species to aid the EOR further limits the desire to use  $\text{HClO}_4$  as an acidic electrolyte in this work, despite the use of perchloric acid by Barroso *et al.*<sup>41</sup> for ethanol oxidation. In addition to the corrosive agent on iron group metals, Láng mentions that chloride exhibits a strong adsorption onto noble metal surfaces.<sup>42</sup> Henderson *et al.*,<sup>43</sup> in agreement with Láng<sup>44</sup> have described aqueous  $\text{HClO}_4$  as thermodynamically unstable and, hence, decomposes in commonly chosen electrolyte concentrations.<sup>43</sup> In addition, from the work of Tripkovic *et al.*<sup>23</sup>, it can be concluded that a possible crystal orientation for the electrode used is similar to that of Pt (100).

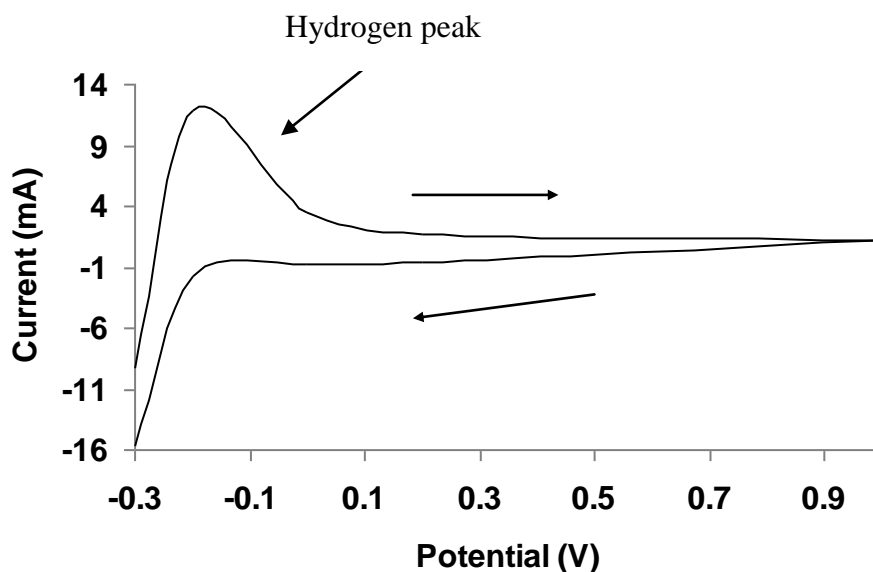


Figure 2.4(c) Cyclic voltammogram of ethanol oxidation at Pt disk in two electrode system, 0.5 M C<sub>2</sub>H<sub>5</sub>OH, deaerated 0.1 M HClO<sub>4</sub>, at a scan rate of 50 mV/s in a two electrode system.

Again as shown previously in this report, the voltammetry is notably different at a Pt (111) crystal orientation, reinforcing the concept that Pt crystal orientation plays a significant role in the voltammetry observed, but as the electrode used was a polycrystalline disk in this work, no specific crystal orientation was assigned to the results observed.

### 2.5 Background electrolyte behaviour at platinum in acidic pH

Figure 2.5(a) shows a cyclic voltammogram performed at a scan rate of 10 mV/s with a polycrystalline platinum electrode in 0.5 M sulphuric acid. The hydrogen adsorption region in deaerated sulphuric acid is well studied and was noted in figure 2.5(a) at low

potentials in the anodic sweep. There are typically two peaks associated with strongly bound and weakly bound Pt-H bonds,  $H_a$  and  $H_b$  respectively, with a third peak occurring between them in high purity aqueous solution. However, these peaks were not clearly observed at -0.8 V and -0.65 V, respectively, perhaps due to anion adsorption such as chloride or sulphate.

The two peaks associated with hydrogen reduction,  $H_r$ , were also poorly defined. In ethanol solution these peaks were not observed as ethanol preferentially adsorbs on the metallic surface. The current drops at -0.5 V reflecting the formation of a double layer at the electrode surface. Upon increasing the potential, the formation of platinum oxides,  $O_f$ , on the surface is a gradual and complex process with Pt-OH, Pt-OOH and ultimately Pt-O bonds forming at an approximate potential of +1.0 V. In the cathodic sweep this layer of oxygen on the surface remains until approximately 0 V. At this potential oxygen is reduced, and a reduction peak,  $O_r$ , is thus observed in the reverse sweep.

The metallic surface is 'refreshed' enabling hydrogen adsorption to occur towards approximately -1.0 V in the reverse sweep. The region where M-O and M-OH occurs is of particular interest to this work, in the quest of enhance ethanol oxidation. It will be seen later that the preferential adsorption of ethanol occurs at the surface in the hydrogen region.

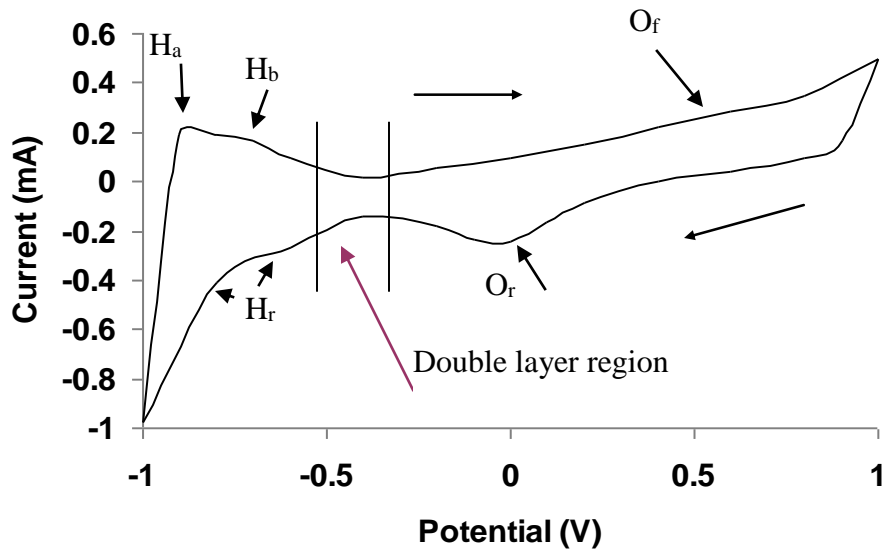


Figure 2.5(a): Cyclic voltammogram showing a polycrystalline platinum disk ( $0.07 \text{ cm}^2$ ) in de-aerated  $0.5 \text{ M H}_2\text{SO}_4$ , at a scan rate of  $50 \text{ mV/s}$ , purple arrow indicating the double layer region, two electrode system.

This metal oxide reduction peak,  $\text{O}_r$ , is reproducible and was well defined. Hence it is often used in calculations of electrode area along with the adsorption of carbon monoxide, CO on the anodic sweep which occurs at  $0 \text{ V}$  vs. MMS (not shown) on the forward sweep. This indicates a strong propensity for CO adsorption onto platinum. Similarly the hydrogen adsorption peaks disappear in the presence of CO at the surface. The oxide reduction peak observed at approximately  $0 \text{ V}$  is of interest for the performance of a fuel cell catalyst as upon removal of the oxide layer, the underlying metallic surface becomes available to allow the continued oxidation of the fuel such as ethanol.

## 2.6 Methods of manufacturing catalysts

The oxidation of ethanol is sensitive to catalyst structure.<sup>9</sup> For this reason, the technique used to form the catalyst particles is very important when preparing an electrocatalyst. Methods of catalyst synthesis should be adaptable in terms of scale up for the fabrication of fuel cell electrode applications.<sup>9</sup> They should primarily allow for easily varying the metal structure, the atomic ratio and the microstructure of the catalysts.<sup>9</sup> There are various methods of manufacturing catalysts, the most popular of which is the widely used impregnation method.<sup>33</sup> A selection of methods were scrutinized by Coutanceau *et al.*<sup>9</sup> Electrochemical deposition, outlined below as an overall general cathode reaction equation below (equation 1) for metal reduction where M relates to the metallic species and z the number of electrons, enables a direct metal contact between the surface and the solution. For platinum in this work,  $z = 2$ .



Furthermore, control over the size and shape of the deposits can be achieved by altering the deposition conditions.<sup>33, 45-46</sup> Rao and Trivedi<sup>46</sup> state that electrodeposits have fine structure, valuable physical properties, such as high hardness, as well as it is the only technique by which metals with high melting points such as platinum and rhodium can be deposited. Rao also supplies a useful scheme to show the mechanism of how the metal ion exists in solution.<sup>46</sup> Thompson *et al.* suggest a platinum particle diameter of

1.5-1.8 nm is possible by removing chloride and forming hexasodium platinumtetrasulphite,  $\text{Na}_6\text{Pt}(\text{SO}_3)_4$  which is subsequently reduced.<sup>47</sup> Thompson concludes that electrodeposition offers an alternative for preparing active Pt/C catalysts, but that size remains the main issue.<sup>47</sup> Platinum particles of less than 20 nm have been electrodeposited from platinum chloride salts along with the preparation of 1.5 nm sized particles and Choi *et al.* by a pulsed electrodeposition method.<sup>48</sup> The amount of metal deposited can be managed by the relationship between charge and weight (in mg) for any metal such as platinum. By applying a pre-determined charge, the weight of metal can be calculated using Faraday's Constant; 96,485 C/mol. Conversion between charge and the number of moles can be used to determine the quantity of platinum on the electrode. The synthesis can be allowed to proceed or stop at the suitable predetermined charge deposited as shown in figure 2.6(a).

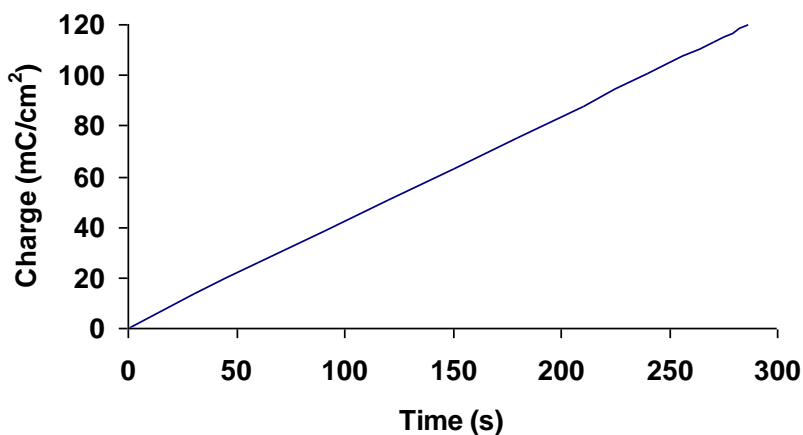


Figure 2.6(a): Charge vs. time plot for platinum deposition to a charge of 120 mC/cm<sup>2</sup> upon a carbon ink electrode, controlled using an applied potential of passed at -1.0 V (vs. MMS), in an unstirred, deaerated (oxygen-free nitrogen) solution of 0.01 M potassium tetrachloroplatinate and 0.1 M  $\text{KNO}_3$ .

In aerated solutions, there were, however, possible competing processes to the metal deposition at most negative potentials which can be observed in results shown for oxygen in figure 2.6(b). The two deposition processes shown are in the presence and absence of oxygen. For deaerated solutions, nitrogen was passed for 30 minutes through the deposition solution of 0.1 M potassium nitrate and 0.01 M potassium tetrachloroplatinate.

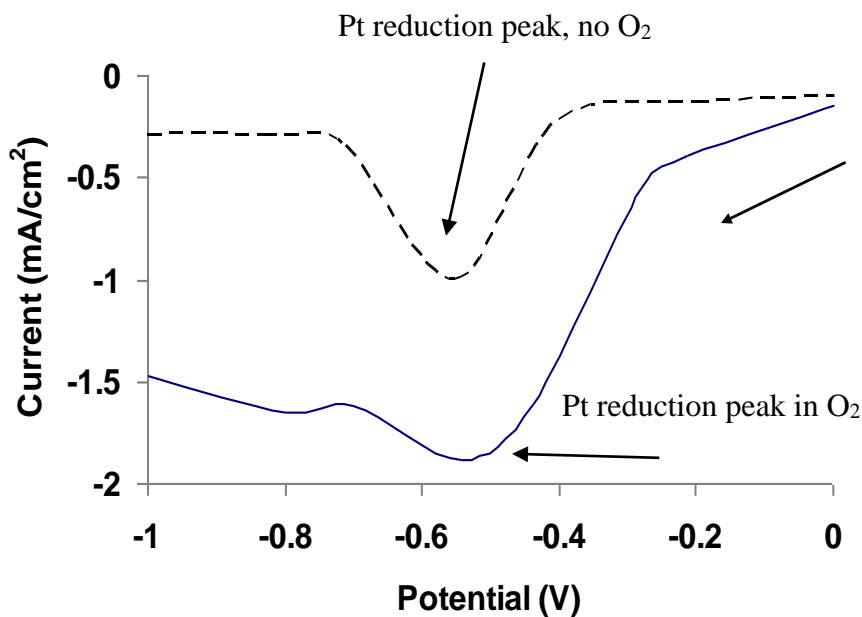
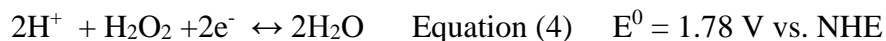
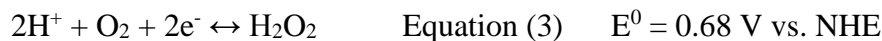
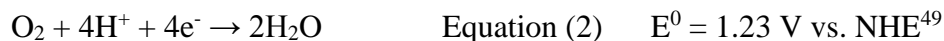


Figure 2.6(b): Linear Sweep Voltammetry of the deposition of 0.01 M  $K_2PtCl_4$  at a CIE, with 0.1 M  $KNO_3$  supporting electrolyte in the presence of (solid line) and absence (dashed line) of oxygen at a scan rate of 50 mV/s.

In the presence of oxygen, the current is higher in comparison to that without oxygen present. Clearly there is a significant reduction in the level of cathodic current in the absence of oxygen. Similarly when charge is monitored in the solution containing oxygen, the charge passed will not solely be due to the metal ion reduction. The reduction

of oxygen shown below in equation 2, competes together with the reduction of hydrogen forming hydrogen peroxide in equation 3<sup>49</sup> which can be reduced under deaerated conditions to water in equation 4.



When deposition potential and electrolyte were changed, the morphological features of the platinum particles were also altered. An extensive list of platinum salt nanostructures is reported by Peng *et al.*<sup>33</sup>, using a variety of reductants, surfactants, under various conditions of synthesis. A wide range of shapes was deduced to be possible, from cuboids to tripoid and numerous other geometric shapes such as tetrahedrons and octahedrons. The nodular shape of the typical particles in this work is comparable to that on graphite found by Gupta.<sup>12</sup> In strongly acidic pH, hydrogen evolution may be of influence where clear peaks are not observed on the voltammogram collected as shown in figure 2.6(c).

At low pH conditions, the platinum particles deposited in this work, observed under SEM-EDX analysis, were found to be dendritic and loosely adhered to the surface which will be shown later in this chapter. This result agrees with published work on ruthenium deposition on platinum in sulphuric acid media.<sup>50</sup>



The lack of discernible peaks shown in figure 2.6(c) suggests the occurrence of hydrogen evolution, as described by equation 5, and casts a doubt on the true quantity of the Pt deposited onto the electrode alone.

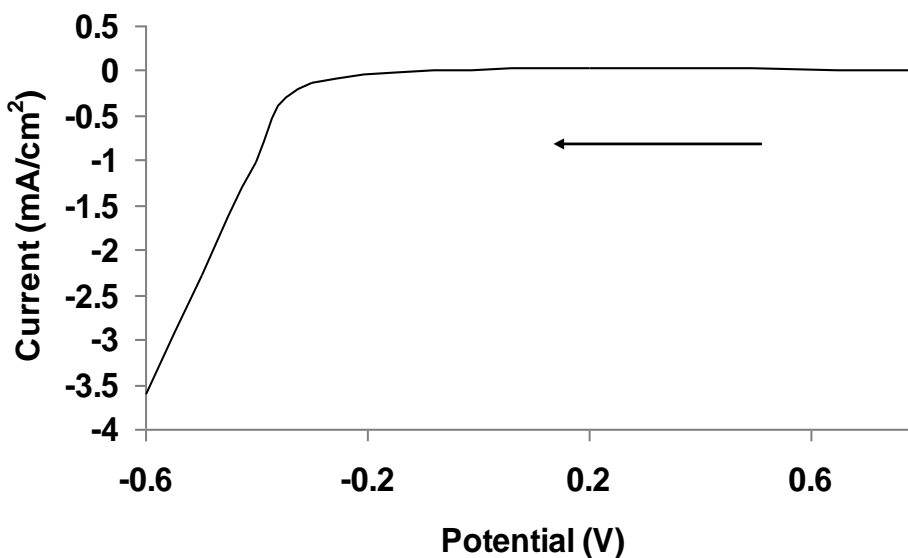


Figure 2.6(c): Voltammogram obtained at a carbon ink working electrode, in a deposition solution of 0.01 M  $\text{K}_2\text{PtCl}_4$  and 0.5 M  $\text{H}_2\text{SO}_4$ , at a scan rate of 50 mV/s in a two electrode system with a Pt sheet reference, pH~0.

When deposition is carried out in neutral media, this issue is circumvented, and results do not show the same characteristics to those obtained in acidic media, as shown previously in figure 2.6(b). However, with aggressive deposition at more negative potentials, hydrogen adsorption from any aqueous solution, even neutral media will remain an issue. To completely remove the hydrogen adsorption from the electrolyte, room temperature ionic liquids (RTILs) or deep eutectic solvents could be used because they are free from water. Non-aqueous solutions such as ethaline comprised of ethylene glycol and choline

chloride in a ratio of 1:2. Deposition in this deep eutectic solvent (DES) was carried out for platinum and the results are shown in figure 2.6(d). One individual clear peak is observed which was attributed to platinum salt reduction. When tested for the EOR, oxidation of ethanol was observed similar to that at regular electrodes in neutral and acidic pH, shown in figure 2.4(b). There are a wide range of RTILs and DES as salts that are liquids below 100°C.<sup>51</sup> Reviews by Gasparotto<sup>52</sup> and Ohno<sup>53</sup> outline electrodeposition and electrochemical characteristics from such substances, though limitations with regard to toxicity will limit their use for large scale application. In particular, aluminium can be electrodeposited from ionic liquids.<sup>51</sup> Developing suitable RTILs or an appropriate DES for ultimate use in the DEFC requires more extensive investigation.

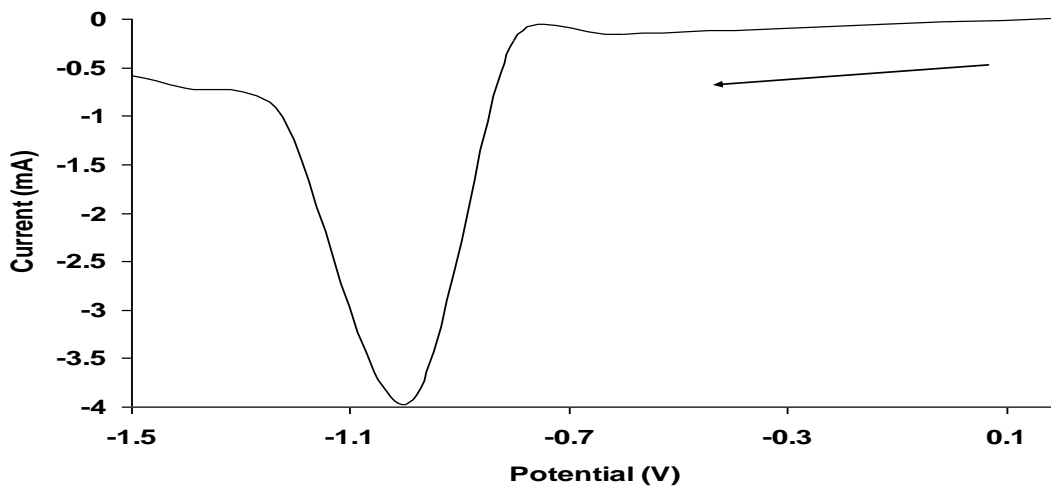


Figure 2.6(d): Linear Sweep Voltammogram of the electrodeposition of platinum onto a carbon ink electrode from a solution of 0.01 M  $K_2PtCl_4$  in a 20 cm<sup>3</sup> ethaline (a mix of ethylene glycol and choline chloride, 2:1)/water mix (50:50) and oxygen free nitrogen at a scan rate of 50 mV/s.

Electrodeposition of platinum has been conducted by Coutanceau<sup>9</sup> and by Kadirgan *et al.*<sup>54</sup> amongst others.<sup>12, 46-48, 55-57</sup> Coutanceau and Kadirgan also found that the ratio of metal determined on the surface of the electrode (from chloride salts) reflected the proportional composition of the deposition solution when a large relative quantity of one metal over another was present in the deposition solution. This indicates that electrodeposition is a useful technique to produce bimetallic catalysts containing platinum. EDX analysis was found to be not possible on some smaller size deposits due to the corresponding small and isolated islands of metal. Consequently, for intermediate bimetallic solutions, the compositional ratios of metals deposited were less useful.

There are many ways to reduce metal salts to fabricate electrodes ready for the EOR<sup>9</sup> such as a chemical reduction process like electroplating<sup>58</sup> and the microemulsion method.<sup>59</sup> Three methods were further tested and compared by Coutanceau *et al.*,<sup>9</sup> namely, the impregnation reduction method, colloidal routes such as the Bönemann Method<sup>16</sup> and the water-in-oil microemulsion method.

### **2.6.1 Metal Deposition Methods**

*(i). The impregnation reduction method:*<sup>9</sup>

This technique uses aqua regia - a solution of hydrochloric acid and nitric acid - to oxidise a carbon powder (commercially available Vulcan XC72) generating OH (hydroxyl) groups on the carbon surface. A given amount of the activated carbon – with

OH groups - is then added to a solution of hexachloroplatinic acid in ultrapure water and adjusting the pH to approximately 1. The process was completed after 24 hours by drying at 70° C overnight, calcined at 300 °C for four hours in air to remove moisture and a further four hours at 300 °C in a pure hydrogen, reducing atmosphere. This method was consequently determined to be slow and impractical for fuel cell work. Coutanceau<sup>9</sup> also found that Pt/C catalysts show a good dispersion on the support, but that the loading of metal is limited and too low for DEFC applications. Therefore, on two counts, the process is not viable.

(ii). *The modified Bönemann Method:*<sup>9, 16</sup>

The original Bönemann method was first described in 1991.<sup>16</sup> This was slightly modified by Coutanceau<sup>9</sup> for the preparation of monometallic catalysts which was carried out in an argon atmosphere free from water and oxygen. Initially, tetraalkylammonium triethylborohydride is prepared,  $(C_nH_{2n+1})_4N[B(C_2H_5)_3H]$ , and used as a surfactant which ensures control of the particle size, in retarding agglomeration. Equations 6 and 7<sup>9</sup> show that the tetraalkylammonium portion of the surfactant [in red] attaches to the chloride ions in solution.



The solutions are then dried at 300 °C in air to remove the organic surfactant. The use of an argon atmosphere was judged in this work to be disadvantageous from both cost and

time perspectives and not suitable for further fabrication as an appropriate to scale up for catalyst preparation.

(iii). *The water-in-oil microemulsion method:*<sup>9, 59</sup>

Coutanceau used the method primarily developed by Boutonnet *et al.*<sup>59</sup> Two emulsions were prepared, one containing the metal salts in water and the other containing sodium borohydride and a surfactant in oil. These two emulsions were mixed and the catalyst is formed within a micelle. The micelle is then dried and calcined in H<sub>2</sub> atmosphere, upon which the metal particles are formed.<sup>59</sup> Coutanceau<sup>9</sup> concluded that the latter two methods showed promising results but that all methods tested had advantages and limitations. The advantage to this method over the Bönemann method is that the argon gas atmosphere is not required.<sup>9</sup> As Coutanceau reported the possibility that small perturbations to this third method destabilized the emulsion when already mixed, means that it is perhaps unreliable or not robust enough for large scale preparation.

The work conducted by Coutanceau *et al.* found that platinum could be reproducibly deposited with particle sizes aggregating in terms of tens of nanometers.<sup>9</sup> This work found similar results for platinum deposition since particles were obtained by charge control and gold (Au) deposition in 0.1 M KNO<sub>3</sub>. With increased charge deposited, beads aggregated into larger, less useful micrometre scale particles. SEM images obtained at Tyndall National Institute, figure 2.6(f), confirmed that particle size increases with increasing charge. The activity of the particle sizes towards the EOR will be looked at in

section 2.11. For a gold electrode of charge equating to  $120 \text{ mC/cm}^2$ , large aggregated particles in excess of 100 nm were observed. For lower deposition charge values (as low as  $20 \text{ mC/cm}^2$ ), smaller particles were observed in the range of 30-48 nm.

Similarly for platinum, the particle size increases as the deposition proceeded. For an uncontrolled deposition, i.e. over longer periods of time, the platinum deposits appeared as very large, round, beads with approximate size in excess of 400 nm. It is notable that the 'islands' of platinum remain in the areas where deposition continued to take place, rather than a continuous layer covering the entire electrode over time as in electroplating.

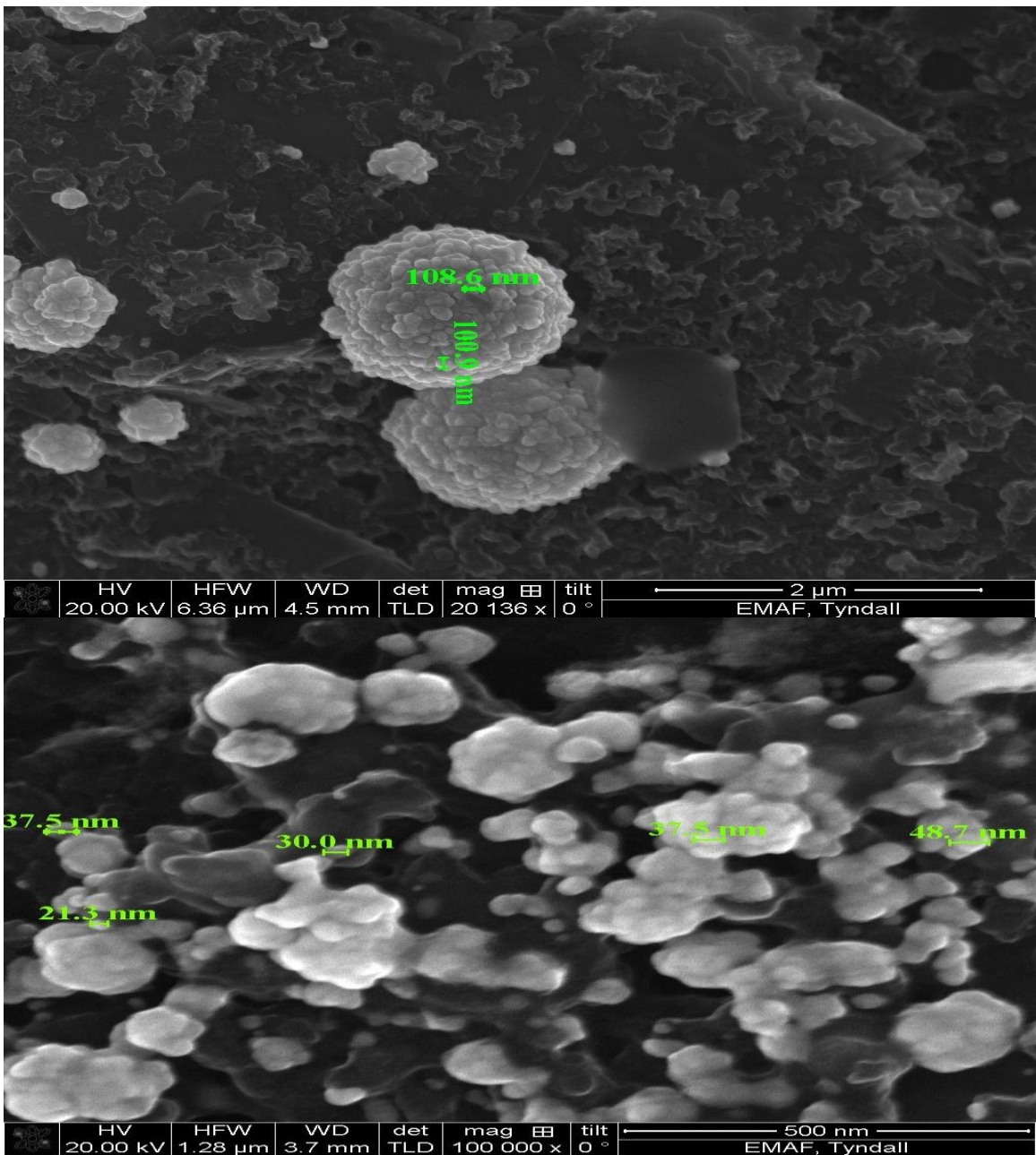


Figure 2.6(f): SEM images (100,000x and 20,136x respectively) of gold particles size with a charge passed of (i) 20 mC/cm<sup>2</sup> [30-48 nm] and (ii) 120 mC/cm<sup>2</sup> [100 nm] electrodeposited from 0.01 M HAuCl<sub>4</sub> and deaerated 0.1 M KNO<sub>3</sub> deposition solution.

This confirms instantaneous the growth of the particles which has also been differentiated by a potential step method from the initial ad-atom on the surface of the electrode.

Nucleation kinetics, and how the first metallic nuclei form on a substrate, is a critical step in understanding their deposition.<sup>60</sup> The nature of platinum particles deposited in neutral solution is shown by SEM image comparison to that in acidic medium. In neutral solution, particles are bead like, while in acid, particles are dendritic or snowflake in appearance. These results are similar to those found by Coutanceau<sup>9</sup> and also that of Gupta *et al.*<sup>12</sup> In an acidic medium, the platinum electrodeposits shown in figure 2.6(g) were found in a valley. Furthermore, the particles agglomerated together to form larger particles.

Electrodeposition was found to be the best suitable or most practical technique for this work to prepare catalysts in the study of the oxidation of ethanol. Neutral pH was used as outlined previously in section 2.4 to aid elimination of hydrogen adsorption and oxygen free nitrogen was used to remove the contribution of oxygen in the deposition solution. A suitable ionic liquid was not found to show clear advantages in the oxidation of ethanol to warrant its use (EOR voltammetry not shown) and requires further investigation to find suitable and usable mixtures for the deposition process.

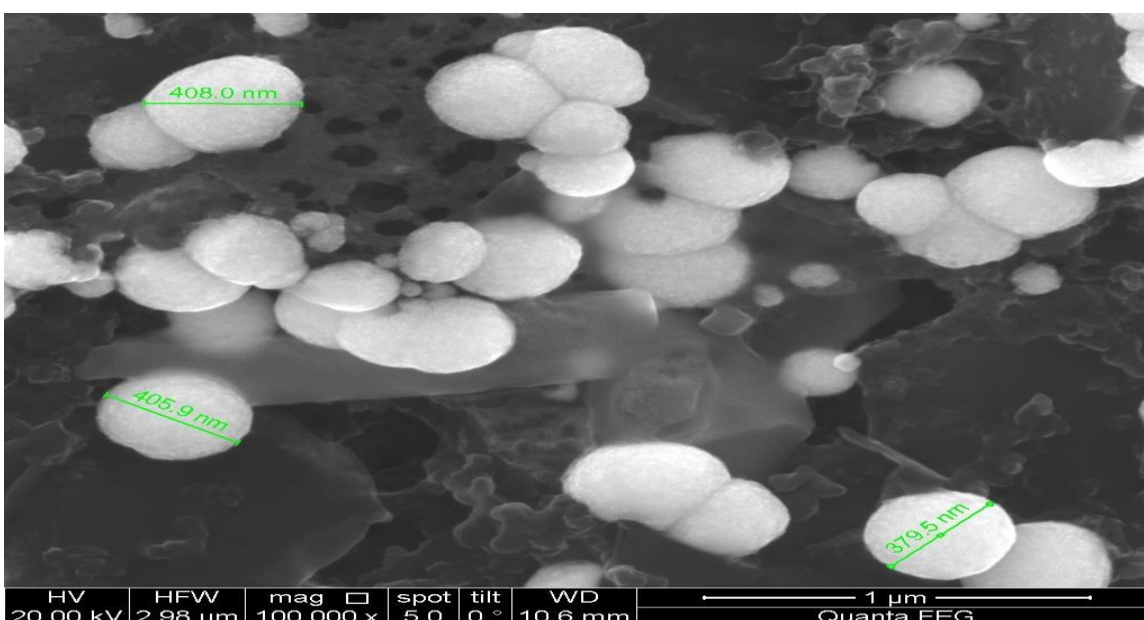
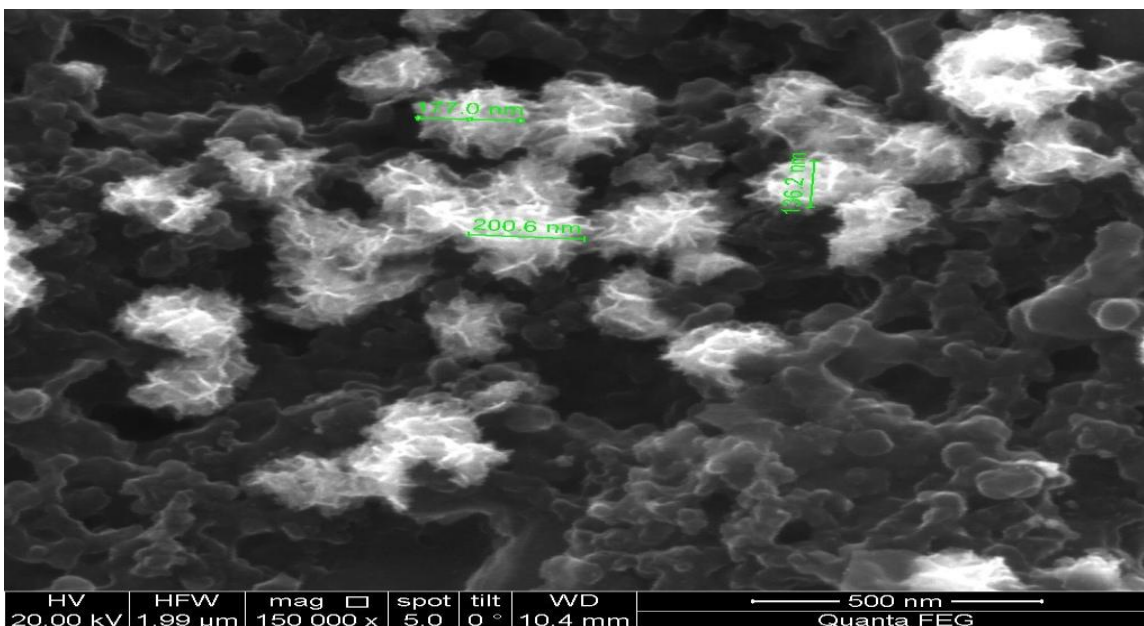


Figure 2.6(g): SEM image (150,000x and 100,000x respectively) of 120 mC/cm<sup>2</sup> platinum electrodeposit/CIE from a deaerated solution of 0.01 M K<sub>2</sub>PtCl<sub>4</sub> in (i) 0.5 M sulphuric acid [dendritic], pH = 0, or in (ii) 0.1 M KNO<sub>3</sub> [beads], pH = 6, respectively.

Considerations such as environmental factors and competing process such as presence of chloride and sulphate need to be examined in great detail. However as previously outlined, there is a myriad of possible ionic liquids so this work requires extensive investigation for the production of a catalyst.

For smaller amounts deposited, there is a clear delineation between areas of the carbon electrode backbone that contain metallic platinum or gold on them and those that do not. This supports the notion of 3D growth after an initial deposition from initial ad-atoms. There are uneven edges and protrusions in the deposit surfaces which may have a beneficial effect in terms of developing nucleation from the initial deposition. The carbon-based electrodes used in this work display edges, ledges and valleys. Such uneven structures appear to aid initial deposition shown later. The exchange current density is an indication of the current flowing when the net current is zero and it can be found from the y-axis intercept from Tafel slope.<sup>61</sup> The greatest current that is obtained for the least potential input means that the best electrocatalysts possess high  $j^0$  values such as the platinum group metals which possess high  $j^0$  values, while metals such as lead typically have low  $j^0$  values. The Volcano Curve has been used to categorise the best hydrogen fuel cell catalyst by exchange current density, but to the knowledge of this author, no such table exists for the DEFC.

## **2.7 The carbon substrate**

A common approach in the literature is the use of a carbon substrate with which to support the deposits and precious metals acting as catalysts.<sup>9,12</sup> These are ideally inexpensive, easily prepared, show good conductivity and a high chemical stability in alkaline or acidic pH.<sup>62</sup> Such materials include finely divided graphite particles,<sup>12</sup> HOPG,<sup>8</sup> carbon felt,<sup>63</sup> carbon nanotubes,<sup>64-65</sup> Toray ® carbon paper,<sup>66</sup> the commercially available carbon black Vulcan XC72,<sup>9-11, 25-33, 67</sup> carbon microspheres<sup>68</sup> and glassy carbon.<sup>69-71</sup> Among the carbon materials, different types of graphite have long been used as anodes in electrochemical processes.<sup>62</sup> HOPG however is an expensive material and obtained by high temperature decomposition (3,500 °C) of organic compounds<sup>62</sup> and hence was discounted from this work. In addition, Vulcan XC72 powder is no longer readily available for commercial use from its suppliers (E-tek, De Nora Chemicals). In this work, Vulcan XC72 was mixed into the carbon ink to use as a comparison to an electrode with no electrodeposited metals present. A highly desirable property of the backbone is a high surface area with a large proportion of edges in the surface rather than a planar surface.<sup>62</sup> This inactivity on a planar surface is a problem for one of the newest forms of carbon, graphene, as reported by Banks *et al.* recently.<sup>72-73</sup> A carbon ink electrode and a Toray 60% carbon paper were manufactured into electrodes that appeared upon visual inspection like the image shown in figure 2.3(a).

### **2.7.1 Carbon ink electrode**

The SEM image shown in figure 2.7(a), was obtained from a blank CIE after fabrication of the electrode. No contamination appears to have occurred during the manufacturing

process, as carbon is the dominant species (EDX analysis) with no metallic particles or other impurities present on its surface. It appears to possess a mottled surface with depth to the image with ledges and edges present where ad-atoms tend to form similar to those in figure 2.6(f) and figure 2.6(g). This surface may be suitable for metal deposition enabling growth from an initial ad-atom which can then agglomerate in clusters as shown in previous images in section 2.6. A crucial element of a suitable electrode is its porosity.

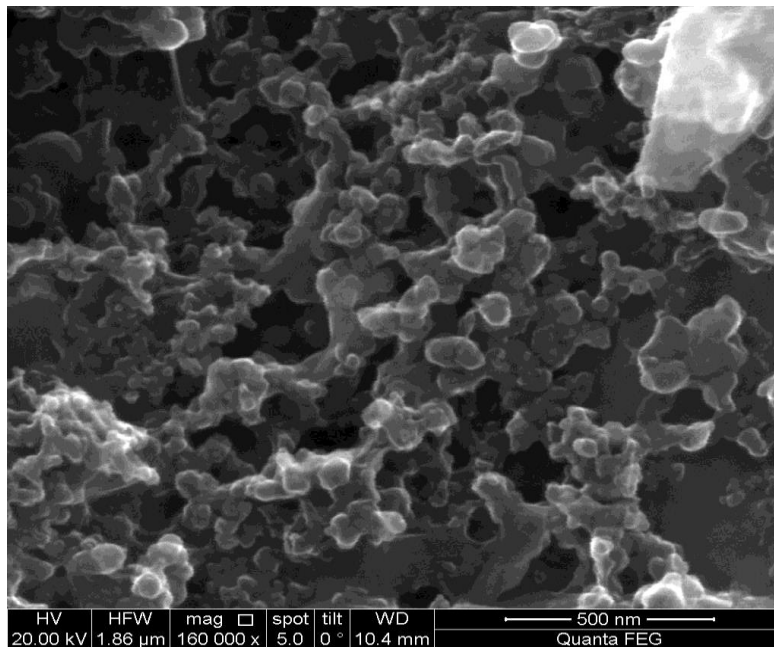


Figure 2.7(a): An SEM image (160,000x) of an bare carbon ink electrode (1cm<sup>2</sup>) on a plastic support.

An example of a Membrane Electrode Assembly (MEA) with the catalyst either side is shown in section 1.2(b). The ethanol fuel cell will be discussed in greater detail throughout chapter 6 with a photograph of an MEA. This allows its use in fuel cells such as DEFC for the ethanol to work its way through the electrode, react with the metallic

surface via the carbon surface, and on through to the membrane that the electrode sits upon when used in an MEA. However, in this chapter, and in figure 2.7(a), the electrode was sitting on a plastic sheet to test the activity of the electrodeposits towards the EOR.

### **2.7.2 Carbon Paper Electrode/Gas Diffusion Electrode**

In figure 2.7(b), an SEM image of the commercially available blank carbon paper electrode used in this work is shown. This material is used as a gas diffusion electrode in a fuel cell set-up and is expected to be extremely porous for this purpose. Such porosity is an highly desirable characteristic for a DEFC anode. To the human eye, the electrode appears as identical in shape to that shown in section 2.3, yet more fibrous in character. Under SEM imaging, these fibres appear to be similar in width, woven across each other in a mesh-like fashion. The blurriness present in the image is a characteristic of a highly porous electrode where the SEM instrument causes charging when the sample is not electrically connected to the stub. The use of carbon paper as a desirable gas diffusion electrode in an MEA is possible due to its porosity.

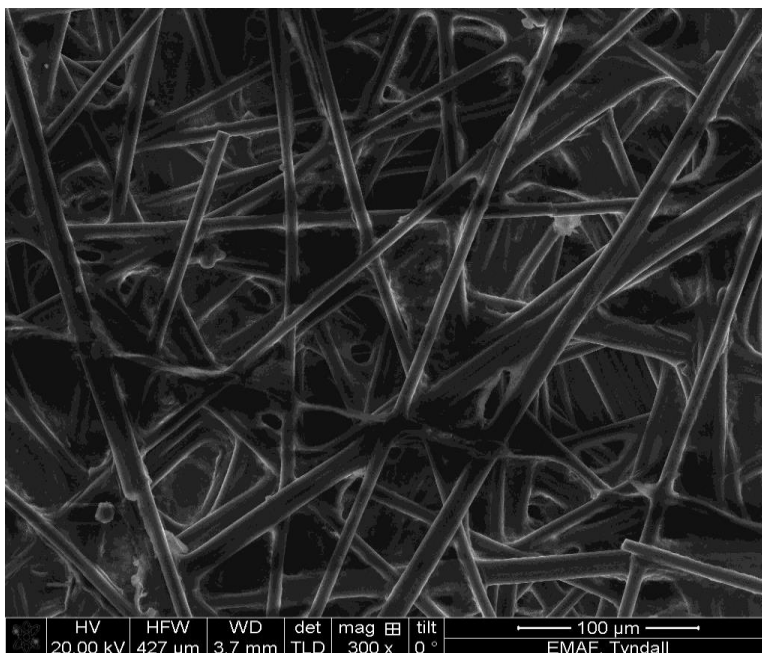


Figure 2.7(b) SEM image (300x) of a bare carbon paper electrode (60% Toray carbon paper).

In addition, the top image in figure 2.7(c) shows an SEM image of a platinum electrodeposit on a carbon paper substrate taken at a low magnification. The characteristic deposits shown in the previous images are present on the individual fibres. Furthermore, the lower image in figure 2.7(c) shows elemental mapping distribution of platinum deposited on a carbon paper electrode. The metallic deposit is revealed and is distributed along the fibre with the carbon background appearing as the darker areas of the image. The lower image shows the elemental mapping of a cross-section of one of the fibres in the upper image.

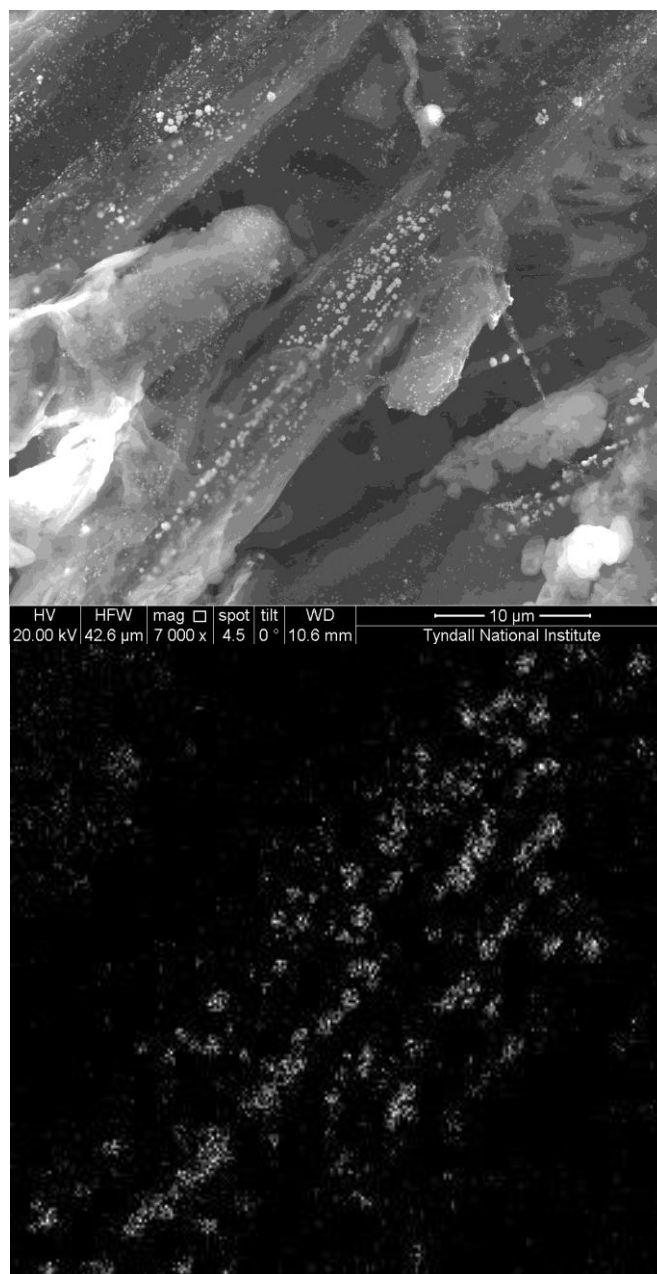


Figure 2.7(c): **[Top]** An SEM image (7000x) of platinum electrodeposited ( $120 \text{ mC/cm}^2$ ) onto a Toray carbon paper electrode from a deposition solution of  $0.01 \text{ M K}_2\text{PtCl}_4$  and deaerated  $0.1 \text{ M KNO}_3$  at  $-1.0 \text{ V vs. MMS}$ . **[Bottom]** Elemental mapping of distribution of platinum electrodeposited ( $120 \text{ mC/cm}^2$ ) onto a Toray carbon paper electrode from a deposition solution of  $0.01 \text{ M K}_2\text{PtCl}_4$  and deaerated  $0.1 \text{ M KNO}_3$  at  $-1.0 \text{ V vs. MMS}$ .

At a deposit of  $120 \text{ mC/cm}^2$ , the particles were shown to range from 100-300 nm. This pattern of deposition appears similar to other carbon materials such as carbon cloth. The porosity of the electrode means that ethanol can filter through and around the circumference of the fibre, possibly enhancing activity towards the EOR.

### **2.7.3. Vulcan XC72 powder**

Vulcan XC72 (57.5% platinum) was obtained from Technische Universitat Munchen and deliberately added into a sample of carbon ink to immobilise the powder onto an electrode to be examined. This cumbersome immobilisation method limits the use of such types of high surface area of carbon as well as carbon black which is also a powder.<sup>62</sup> Figure 2.7(d) shows an SEM image taken of this electrode. While no individual particles were observed, the EDX spectrum taken of the sample identified platinum and carbon to be present, along with small quantities of sulphur, silicon and chloride.

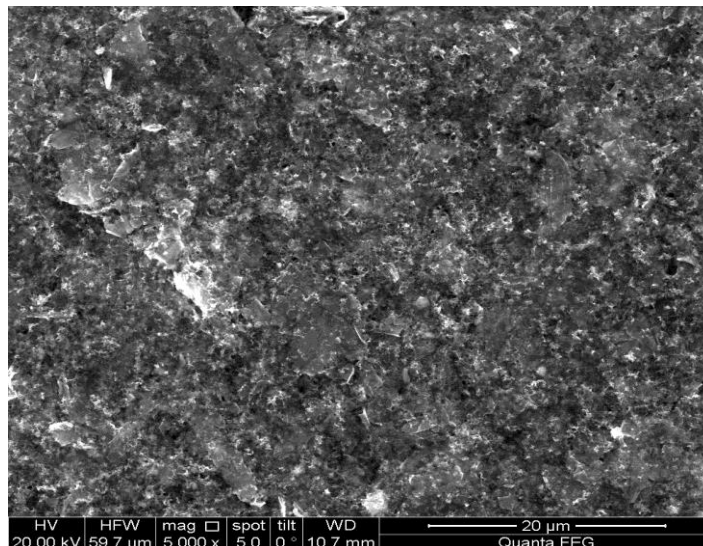


Figure 2.7(d): An SEM image (5000x) of Vulcan XC72 powder deliberately added into the ink coated into a carbon ink electrode.

The purpose of the Vulcan powder in this work is to clarify the impact of the presence of chloride present in the metal salts used in deposition solutions. Each Vulcan XC72 based electrode was manufactured identically and exposed to a 0.5 M ethanol solution in various electrolytes. The voltammetric behaviour of the electrode in neutral electrolyte ( $\text{KNO}_3$ ) is shown below in figure 2.7(e).

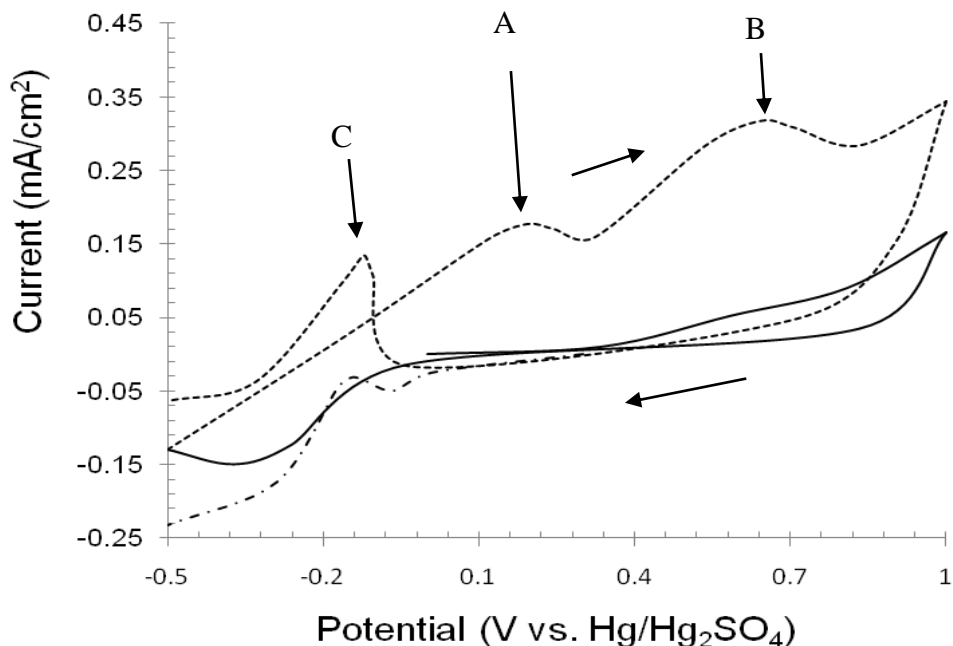


Figure 2.7(e): Cyclic Voltammogram showing a Vulcan XC72/CIE activity over time, 0.5 M C<sub>2</sub>H<sub>5</sub>OH in deaerated 0.1 M KNO<sub>3</sub>, MMS reference, in a deaerated solution at a scan rate of 10 mV/s, sweep 1 (solid line), sweep 10 (dashed line).

Two forward peaks, 'A' and 'B', are observed on the positive sweep with increasing sweep number and an increasing oxidation peak, 'C', on the negative sweep. These peaks represent the initial metal oxide formation and oxidation of ethanol at peak A; an adsorbed intermediate with a carbon-carbon bond, typically acetaldehyde, at peak B and reoxidation of the fuel or adsorbed poisons such as CO at peak C. This voltammetry is characteristic for the typical oxidation of ethanol at platinum in acid media<sup>12, 14</sup> and similar features to that of the voltammogram of the platinum electrode deposited in a deep eutectic solvent/water mix (deposition shown previously). These features agree with published articles discussing the reaction mechanism in acid media.<sup>11, 12, 14</sup> The initial peak corresponding to the formation of adsorbed OH and ethoxi species on the surface

before ethanol oxidation at the platinum/platinum oxide surface on the anodic sweep and sharp desorption peak after the platinum oxide is reduced on the sweep in the negative direction. This will be discussed in detail later in section 2.9.

The presence of similar EOR peaks in electrodes where platinum was electrodeposited would suggest that any chloride present on the surface, detected by SEM-EDX analysis, from the deposition process, did not impede ethanol oxidation. The current associated with PtO formation, beyond peak B at +1.0 V vs. MMS, appears to be increasing steadily with scan number. This indicates that less energy is required for peak B to appear at a Vulcan XC72R electrode, due to the high surface area available at the surface. When peak B is present at higher potentials with different electrodes (shown further in this chapter), there is a contributing effect by this PtO peak on the current measured. The lack of porosity of the carbon ink dictates that the Vulcan XC72R must be at the surface of the electrode. This is another limitation based on immobilizing the carbon powder onto the electrode. The EOR may be impacted by the poor reproducibility of the platinum surface on the face of the electrode.

#### **2.7.4: Carbon Ink Substrate effects**

##### **(i) Platinum Electrodeposition Carbon Ink Electrodes (Pt/CIE)**

There are various published methods by which the real surface area of the electrode can be determined.<sup>74-77</sup> It has been reported that the real surface area is different to the geometric surface area for any polished electrode by a factor of two<sup>76</sup> and typically at least three times greater.<sup>76</sup> Commonly, the electrochemical or real surface area of a platinum fuel cell catalyst is determined using CO stripping voltammetry. This is a technique that uses platinum in sulphuric acid as outlined in section 2.5 with adsorbed carbon monoxide being stripped off the electrode surface at 0 V vs. MMS. The benefit is the reliable two electron transfer process in CO stripping. At the potential where CO is oxidised, there is no competing process (at 0 V vs. MMS) and the peak can be used to determine the area based on the electrons transferred.

The geometric area has been used by some groups<sup>78</sup> and is adopted for all work in this thesis. All electrodes used are manufactured to 1 cm<sup>2</sup> for this reason. One of the methods used above<sup>77</sup> can be used to demonstrate the slow kinetics of the carbon electrode compared to the electrodeposits, namely the one electron transfer process in the Fe<sup>3+</sup>/Fe<sup>2+</sup> redox couple. The results for a carbon ink electrode and a platinum deposit/CIE (120 mC/cm<sup>2</sup> in deaerated 0.1 M KNO<sub>3</sub>) in a solution of 0.01 M ferricyanide, [Fe(CN)<sub>6</sub>]<sup>3-</sup>, are shown in figure 2.7(f), starting from the measured Open Circuit Potential (OCP) of 0 V vs. MMS. The solid line shows the reaction at a bare carbon ink surface. The redox reaction spans approximately 800 mV, compared to the ideal separation is 57 mV for a reversible one electron transfer process.

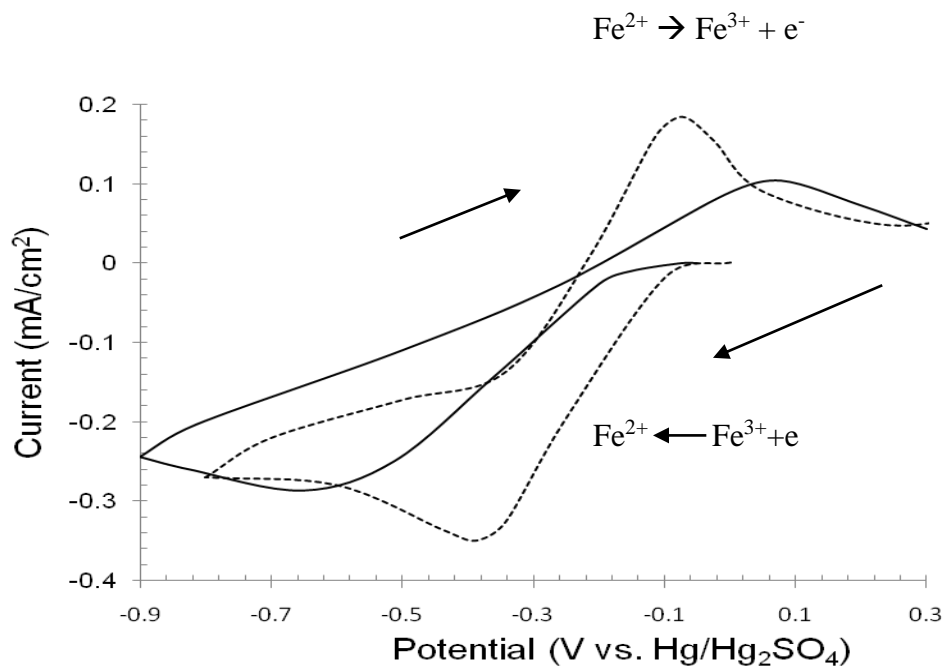


Figure 2.7(f): Cyclic Voltammogram showing a carbon ink electrode (Solid line), and platinum (dashed line) electrodeposit (120 mC/cm<sup>2</sup> in deaerated 0.1 M KNO<sub>3</sub>) on a CIE passed at -1.0 V vs. MMS in a solution of 0.01 M [Fe(CN)<sub>6</sub>]<sup>3-</sup> in 0.1 M KNO<sub>3</sub> at a scan rate of 100 mV/s, pH = 6.

This indicates the reaction is very slow at a carbon surface which agrees with the overall inactivity observed at a carbon surface for alcohol oxidation. Similar slow or poor kinetics at the inactive basal plane of graphene was reported by Hallam and Banks.<sup>79</sup> For the platinum electrode, this separation between the reduction and oxidation peak decreases substantially to 225 mV.

A possible explanation for this may be that the reaction at both the platinum deposit and the underlying carbon contribute to the overall current. From SEM images in figure 2.6(e) and figure 2.6(f), it can be seen that the electrodeposits are areas of metallic beads that grow further with longer times. Consequently, at low metal composition of

120 mC/cm<sup>2</sup> (equivalent to 0.12 mg/cm<sup>2</sup> platinum), there will be both a conductive carbon surface and a platinum or gold surface on the electrode. The graphite particles suspended in the ink need to be at the surface for any reaction to occur and electrons may have to travel through the ink to get to the surface and the stem of the electrode, illustrated in figure 2.7(g)

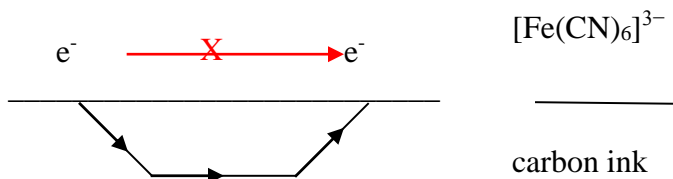


Figure 2.7(g): Scheme illustrating the path of an electron through a carbon ink electrode via a series of adjacent graphite particles embedded in the ink and not across the polymer film in which they were dispersed.

### (ii) Gold Electrodeposition Carbon Ink Electrodes (Au/CIE)

Figure 2.7(h) below shows a CV of a gold electrode in the same solution as that in figure 2.7(f). The gold/CIE electrode, in comparison to a Pt/CIE electrode, exhibits peak to peak separation of 500 mV which is an intermediate distance compared to platinum and carbon. The gold surface shows broader oxidation and reduction peaks for the  $\text{Fe}^{3+}/\text{Fe}^{2+}$  couple than at a platinum surface. Both gold and platinum, when used as a layer or conductive surface, which can decrease the separation of the two peaks. The underlying carbon surface still affected the reaction kinetics at a simple one electron transfer in

solution due to the island nature of the deposits. The impact may be even larger on the EOR as ethanol oxidation is a multi-step complex surface reaction.

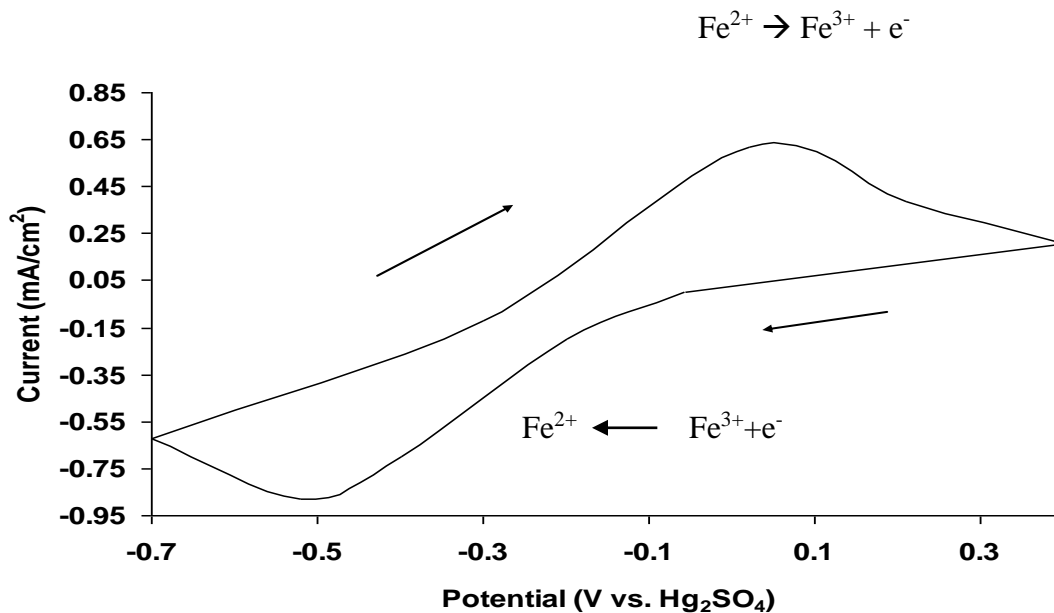
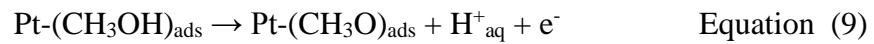


Figure 2.7(h): CV showing a gold electrodeposit ( $120 \text{ mC/cm}^2$  in deaerated  $0.1 \text{ M KNO}_3$ ) on a carbon ink electrode passed at  $-1.0 \text{ V}$  vs. MMS in a solution of  $0.01 \text{ M } [\text{Fe}(\text{CN})_6]^{3-}$  in  $0.1 \text{ M KNO}_3$  at a scan rate of  $100 \text{ mV/s}$ ,  $\text{pH} = 6$ .

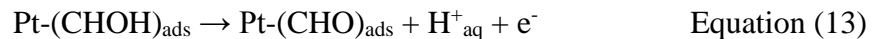
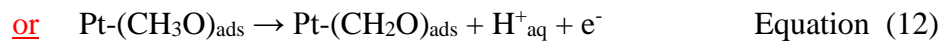
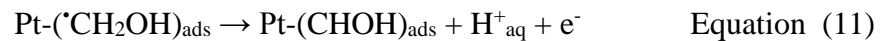
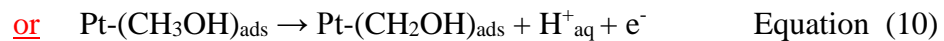
## 2.8 Methanol Oxidation Reaction

Methanol as mentioned previously is a well studied (up to 71 years) direct alcohol fuel cell feedstock before ethanol.<sup>80-93</sup> The main development in DMFCs is the stability of the PEM fuel cell in acid electrolyte.<sup>93</sup> Platinum is able to catalyse methanol oxidation more easily than ethanol due to the lack of a carbon to carbon bond in methanol. The characteristic voltammetry observed in figure 2.8(a) demonstrates the oxidation of methanol at a polycrystalline Pt disk. One peak is observed in the anodic sweep, assigned

peak 'A', and describes methanol oxidation at approximately 0.5 V vs. MMS. It is suspected that peak A is the oxidation of methanol, typically CH<sub>3</sub>O through multiple intermediates and pathways in equations 8-13<sup>93</sup>. On the reverse scan, the small oxidation peak observed on the reverse scan, peak 'C', is that of adsorbed CO oxidation. The mechanism for methanol oxidation according to Lamy is outlined by equations 8-13.<sup>93</sup>



It is believed that the third oxidation peak, peak B in ethanol systems, which is not present in methanol oxidation, may be a mixture of CO<sub>ads</sub> and acetaldehyde or similar C-C bond substances. The lack of a C-C bond in methanol explains the lack of this peak, previously ascribed as peak B in ethanol. However, it is apparent that the current densities obtained for methanol are in excess of those for ethanol as expected at a platinum disk electrode in acid solution.



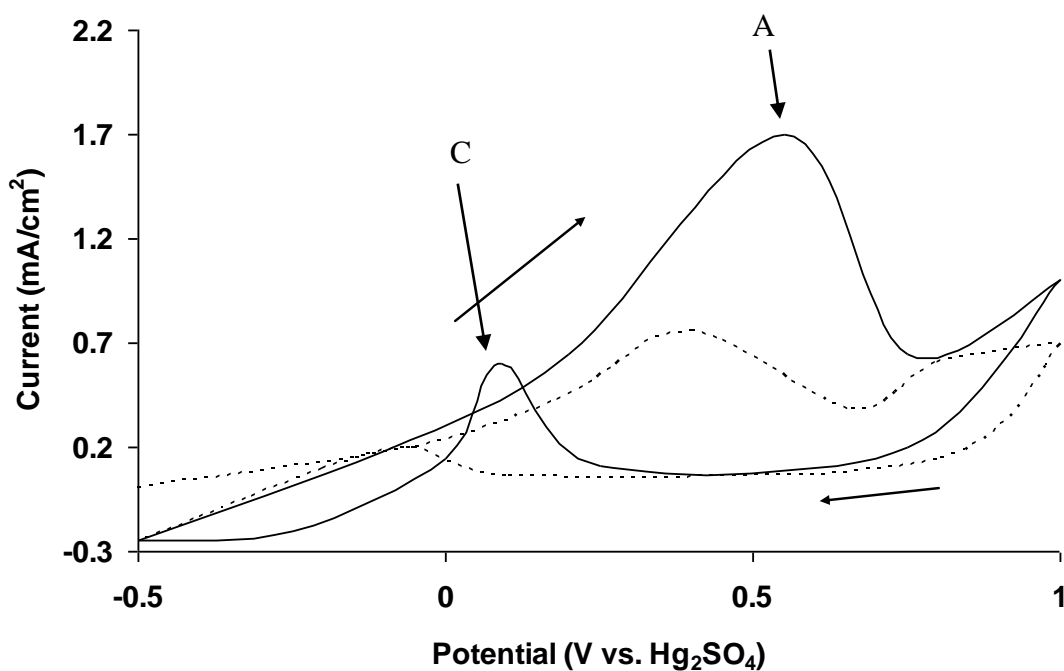
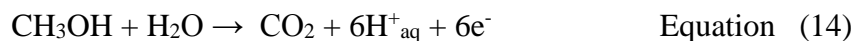


Figure 2.8(a): CV illustrating the Methanol Oxidation Reaction (MOR) at a Pt disk working electrode ( $0.07 \text{ cm}^2$ ) vs. MMS reference, with peaks A and C in  $0.5 \text{ M CH}_3\text{OH}$  and deaerated  $0.5 \text{ M H}_2\text{SO}_4$ , at a scan rate of  $50 \text{ mV/s}$ .

Lamy reports that the different species formed by equations 9-12 have been detected by infrared spectroscopy are widely accepted as dissociative steps if the exact nature of the species is unclear. The  $\text{Pt}-(\text{CHO})_{\text{ads}}$  formed in equation 13 spontaneously dissociates on platinum to form  $\text{Pt}-(\text{CO})_{\text{ads}}$ . Lamy reports the rate determining step is the production of  $\text{Pt}-(\text{CHO})_{\text{ads}}$  and can then be further oxidized with  $\text{OH}_{\text{ads}}$  to form  $\text{CO}_2$  either directly or through the formation of an intermediate species,  $\text{Pt}-(\text{COOH})_{\text{ads}}$  and subsequently to carbon dioxide. The overall anode reaction equation is shown in equation 14 below producing six electrons, half that of ethanol oxidation.<sup>93</sup>

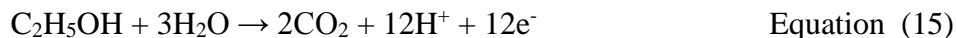


Pournaghi-Azar suggests that  $\text{CO}_{\text{ads}}$  reacts with an oxygen donor, such as  $\text{OH}_{\text{ads}}$ , following a Langmuir-Hinshelwood mechanism.<sup>89</sup> It has been reported that formic acid,  $\text{HCOOH}$ , not found by Lamy in the mechanism in equations 8-13, has been determined by Differential Electrochemical Mass Spectroscopy (DEMS).<sup>94</sup>

## 2.9 Effect of ethanol on cyclic voltammetry

### 2.9.1 Ethanol Oxidation Reaction on platinum

A DEFC operates with an anode and a cathode as shown in equations 15 and 16, respectively. Complete ethanol oxidation results, in theory, to  $\text{CO}_2$  being formed and 12 electrons being produced. This work concentrates on the half cell reaction at the anode. Adding ethanol to sulphuric acid with a Pt electrode considerably modifies the voltammetry observed.



The onset of ethanol oxidation begins at approximately 0.2V and the two peaks observed are initial ethanol adsorption as well as  $\text{OH}_{\text{ads}}$  formation at peak A and 'C<sub>2</sub>' adsorbates for

peak B.<sup>14</sup> The possible equations relating to peak A are shown in Equations 17, 18 and 19.

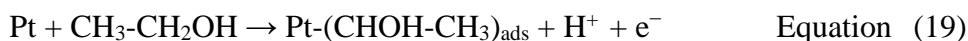
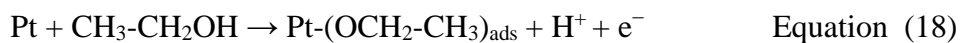


Figure 2.9(a) shows the typical voltammogram obtained with a polycrystalline Pt disk in a two electrode system. The characteristic oxidation of ethanol is observed with two peaks, 'A' and 'B', evident on the positive sweep and one large peak, 'C', on the reverse scan that increases in magnitude on each successive scan.

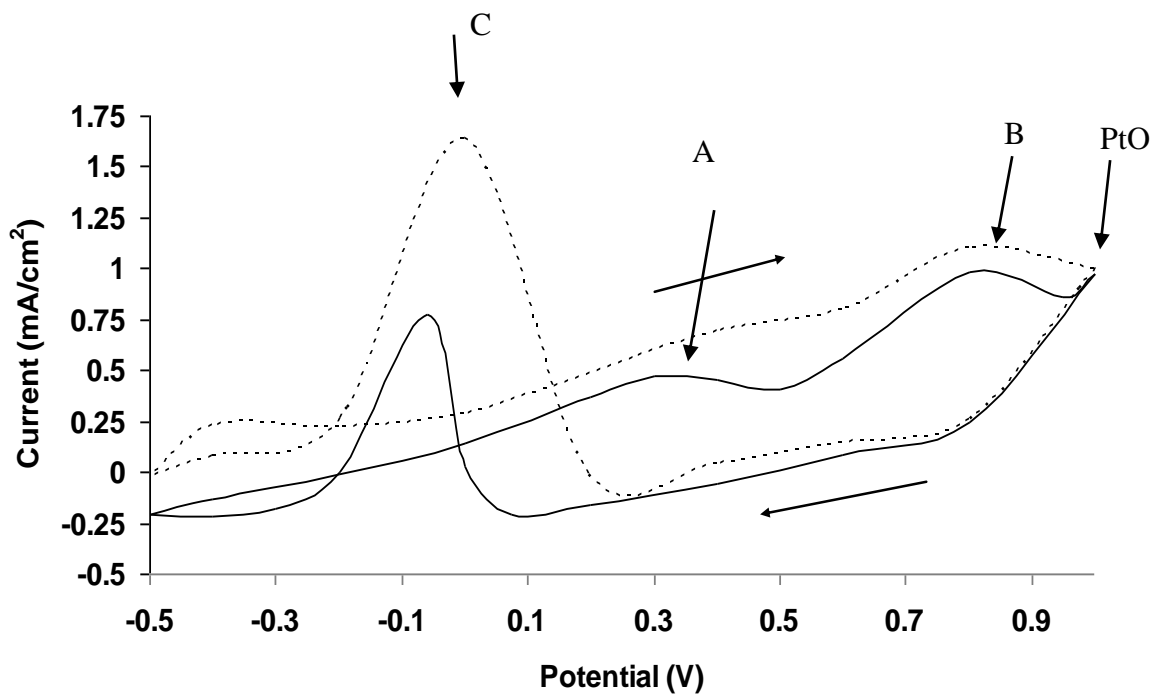
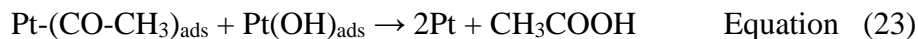
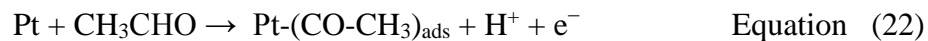


Figure 2.9(a): Cyclic voltammogram showing peaks A, B and C, the oxidation of ethanol at a platinum disk in a two electrode system in 0.5 M C<sub>2</sub>H<sub>5</sub>OH and deaerated 0.5 M H<sub>2</sub>SO<sub>4</sub> at a scan rate of 50 mV/s. Sweep 1 (solid line), sweep 10 (dashed line).

Furthermore, the hydrogen peaks present at negative potentials i.e. in the hydrogen region of Pt and sulphuric acid are diminished. The term 'C<sub>2</sub>' refers to a compound that contains two carbons, typically a carbon-carbon double bond such as acetaldehyde. Logically a 'C<sub>1</sub>' material is a term for compounds containing only one carbon, often CO. The second peak, peak B attributed to acetaldehyde and formation of a Pt oxide at approximately 1.0V.<sup>9, 10, 31</sup> The equations for possible routes from the adsorbed intermediates associated with peak A, Pt-(OCH<sub>2</sub>-CH<sub>3</sub>)<sub>ads</sub> or Pt-(CHOH-CH<sub>3</sub>)<sub>ads</sub>, for peak B to then occur for a C<sub>2</sub> intermediate to form acetic acid are outlined in equations 20-23.



On the reverse sweep, an adsorbed intermediate that has formed can be oxidised from the system, as peak C, once the platinum oxide is removed at approximately -0.1 V vs. MMS. In HClO<sub>4</sub>, no significant activity was found beyond 0V on the forward scan and consequently sulphuric acid was chosen as oxidation electrolyte for the initial phase of this work.

One common mechanism to form acetic acid describing the observed ethanol voltammetry is shown in equations 17-23.<sup>25, 95</sup> This is incomplete or partial oxidation, yielding four electrons. Platinum, as with all common metal catalysts, forms initially

Pt(OH)<sub>ads</sub> through the dissociation of water in acidic medium (equation 17). Equation 18 represents adsorption of ethanol at a platinum site. This initial adsorption can be an O-adsorption process or a C-adsorption process<sup>95</sup> and ethanol can either dissociate to form Pt-(OCH<sub>2</sub>-CH<sub>3</sub>)<sub>ads</sub> or Pt-(CHOH-CH<sub>3</sub>)<sub>ads</sub>. Cantane and Gonzalez refer to both of these substances as strongly adsorbed, intermediate organic residues.<sup>25</sup> Once acetaldehyde is formed from equation 20 or 21, it can adsorb on platinum to form Pt-(CO-CH<sub>3</sub>)<sub>ads</sub>. This adsorbed intermediate can be then further oxidised by oxygen species such as PtOH to form CH<sub>3</sub>COOH in equation 23. It was found by Rousseau *et al.*<sup>95</sup> that CH<sub>3</sub>CHO, CH<sub>3</sub>COOH and CO<sub>2</sub> were the only products which were detected by DEMS. The 12 electrons in equation 15 is based on complete oxidation to CO<sub>2</sub>.

Gonzalez states that CH<sub>3</sub>CHO can desorb and then diffuse into the bulk solution.<sup>25</sup> For this reason, depending on conditions such as electrolyte or ethanol concentration, parallel pathways are possible and this is summarised in figure 2.9(b). The partial oxidation pathway to CH<sub>3</sub>COOH returns four electrons and acetic acid cannot be further oxidized to CO<sub>2</sub>. Acetic acid is a final product when produced.

The production of CH<sub>3</sub>COOH gives a third of the possible power of a DEFC. The presence of intermediate products and adsorbates results in a pathway that can be attempted to engineer towards CO<sub>2</sub> production for certain catalysts. This pathway can be manipulated for different catalysts, but Rousseau found the maximum CO<sub>2</sub> is produced at a platinum electrode.<sup>95</sup> As a base result for platinum is shown, it acts as a benchmark for modified electrodes in future work.

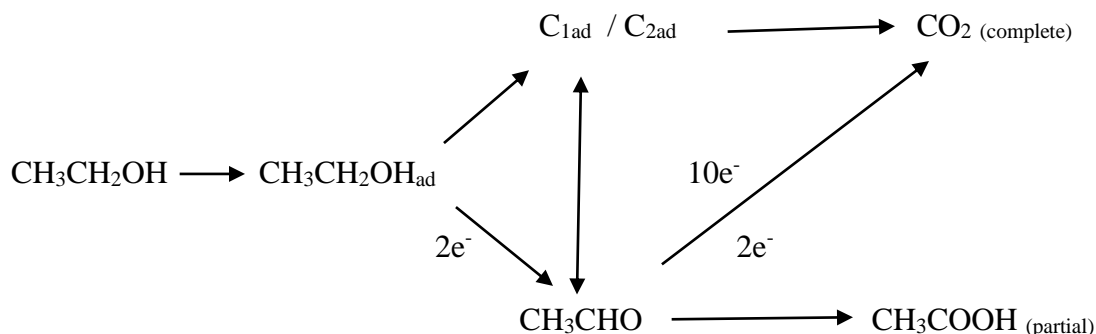


Figure 2.9(b): Schematic diagram summarising possible pathways for the ethanol oxidation reaction in low pH to complete oxidation and partial oxidation.

A major historic advantage of using acidic media is its use with acidic Nafion membranes in the Proton Exchange Membrane Fuel Cell (PEMFC).<sup>96</sup> To improve upon platinum, this typically involves the requirement of extra oxygen species through metal oxides or hydroxyl groups to force the reaction to further completion. However, platinum performs best as an electrocatalyst due to its inherent stability at low pH. No other metal is resilient enough to survive in the highly corrosive environment to produce more adsorbed hydroxides or oxides. The final step in equation 23 is an example of the bifunctional mechanism where Pt(OH) reacts and promotes further ethanol oxidation and while also removing a fouling ethanol adsorbate from a platinum site.

Figure 2.9(c) shows the increasing current of peak C,  $I_c$ , with increasing scan number, N, for a polycrystalline platinum electrode. The result illustrates an excellent linear correlation between  $I_c$  and N ( $R^2 = 0.9946$ ). With continuing scans, the amount of compound relating to peak C increases. This indicates that there is an increasing amount of adsorbed and poisoning intermediates, such as CO formed or that the cyclic

voltammogram reflects the cleaning of the electrode upon each completed forward and return sweep, activating the electrode surface for the consequent runs.<sup>14</sup>

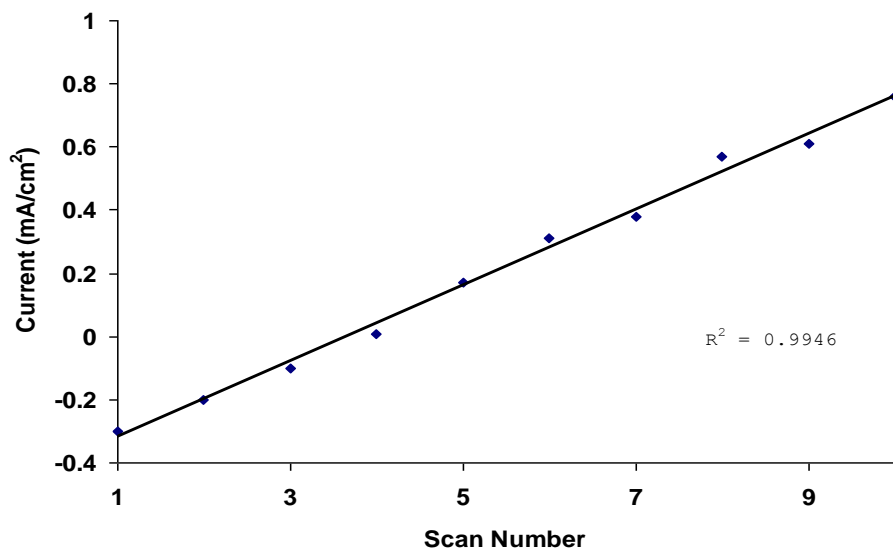


Figure 2.9(c): Plot showing increasing growth of peak C at a Pt disk such as in figure 2.9a – a two electrode system (Pt reference) containing 0.5 M C<sub>2</sub>H<sub>5</sub>OH in 0.5 M H<sub>2</sub>SO<sub>4</sub>, in deaerated at a scan rate of 50 mV/s as a function of scan number, N., pH = 0.

Figure 2.9(d) shows a cyclic voltammogram at the 10<sup>th</sup> sweep of ethanol oxidation at a platinum electrodeposit/CIE at a scan rate of 10 mV/s from a measured OCV of -0.1 V vs. MMS. The three characteristic ethanol oxidation peaks observed at a platinum disk are also evident in near neutral pH at the Pt electrodeposit/CIE. Notably the current magnitude remained similar for both the Pt electrodeposit/CIE and polycrystalline disk. Furthermore, the Pt electrodeposit/CIE, when controlled by charge, produced excellent reproducibility in terms of current on each sweep. The platinum disk electrode was poor, in terms of repeatability, despite identical rigorous polishing conducted between runs. For

this reason, Pt electrodeposits/CIE were used from this point. Peaks A and B are broad, shallow peaks, consistent with edge diffusion at the electrode surface where the oxidation occurs at the edge more prevalently than a flat surface. Peak C reflects a sharp, sudden increase in current at 0.1 V which will be discussed further later. It may be an indication of the presence of an adsorbed species, likely that of carbon monoxide.

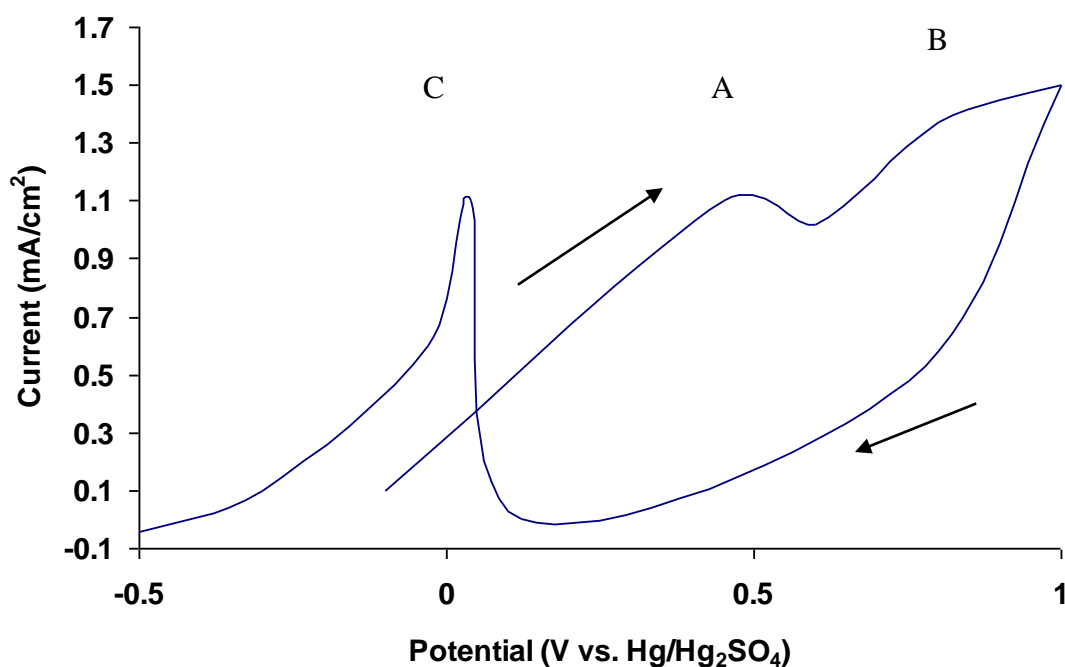


Figure 2.9(d): Cyclic voltammogram with peaks A, B and C, the oxidation of ethanol at a platinum electrodeposit/CIE (vs. MMS) in 0.5 M C<sub>2</sub>H<sub>5</sub>OH and deaerated 0.5 M H<sub>2</sub>SO<sub>4</sub> at a scan rate of 10 mV/s, 10<sup>th</sup> sweep.

A slow scan rate is required to clearly observe and distinguish separate peaks, ideally at scan rates of below 50mV/s, which will be discussed further later in the chapter. This is however immediately significant, reinforcing the theory that slow oxidation kinetics

require a slower scan rate to enable the EOR enough time to occur at the electrode surface.

### **2.9.2 Ethanol Oxidation Reaction behaviour on gold electrodes**

Figure 2.9(e) shows a cyclic voltammogram obtained on a gold electrodeposit/CIE electrode both in the presence of ethanol in deaerated 0.1 M  $\text{KNO}_3$  [top] and absence of ethanol (0.5 M methanol) in deaerated 0.1 M  $\text{KNO}_3$  [bottom] solutions. In the presence of ethanol, an initial adsorption peak is recorded at 0.42 V but not observed in subsequent cycles. After this immediate peak, the electrode appears to settle into a rhythm of AuO formation at high potentials and the metal oxide reduction peak observed on the return sweep. As gold appears to be a poor catalyst for ethanol oxidation in this work, ethanol adsorption may not affect the formation of metal oxide and reduction experienced at the electrode. As both voltammograms exhibit the same features, it is thought that neither methanol nor ethanol undergo oxidation at Au deposit/CIE surfaces.

Notably, in ethanol, an initial oxidation peak – the sweep starting at a measured Open Circuit Potential of 0 V vs. MMS – appears before being reduced instantly in further sweeps and remains diminished, in direct contrast to that at a platinum electrode where the current at this potential increases. This peak may be due to ethanol adsorption on a fresh surface, but there is no further evidence of the peak on subsequent scans or the associated peaks B or C compared to the platinum surface. This suggests that gold alone is unsuitable as a catalyst in this work. The underlying reactions at a gold electrode

exhibit similar features to the characteristics of the platinum electrode in sulphuric acid seen in figure 2.9(b). The current of the assigned oxide reduction peak,  $\text{AuO}_r$ , recorded at approximately 0.4V increases in magnitude with increasing charge as in figure 2.9(e). Similarly the peak is reproducible over a number of increasing scan rates.

The behaviour of a gold RDE in ethanol was tested but is not presented here. Rotating Disk Electrodes operate best for diffusion-controlled reactions, but as ethanol oxidation is adsorption controlled rather than diffusion controlled, increasing mass transport to the electrode surface from 500 rpm to 1500 rpm would have less impact. This was reflected in the disordered currents achieved with increasing rotation. However in high pH solution which will be discussed further later in the chapter, gold has been reported to play a role in the oxidation of ethanol. Typically gold is used as a substrate onto which metals are deposited or as a metallic substrate to provide active sites.

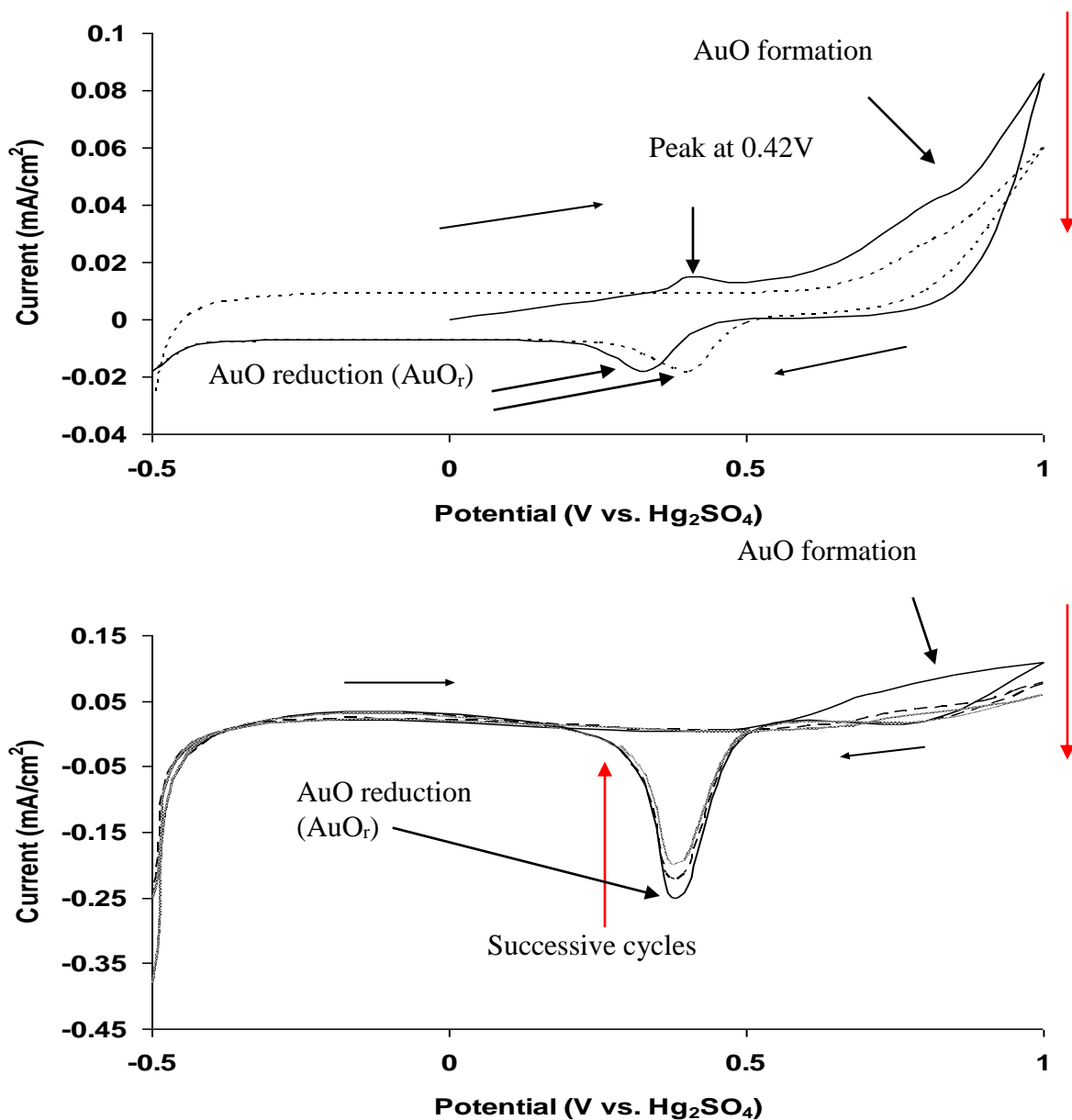
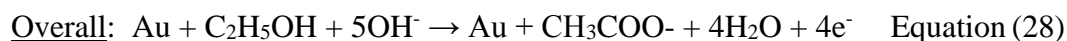
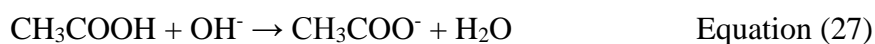


Figure 2.9(e): Cyclic voltammogram of a gold electrodeposit/CIE electrode (120 mC/cm<sup>2</sup> in deaerated 0.1 M KNO<sub>3</sub>) electrodeposited from a charge passed at -1.0 V vs.MMS, [top] 0.5 M C<sub>2</sub>H<sub>5</sub>OH and deaerated 0.1 M KNO<sub>3</sub> 1<sup>st</sup> sweep (solid line), 10<sup>th</sup> sweep (dashed line), and [bottom] 0.5 M methanol in deaerated 0.1 M KNO<sub>3</sub>, 1<sup>st</sup> sweep (solid line) 5<sup>th</sup> sweep and 10<sup>th</sup> sweep (dashed lines).

Dutta<sup>98</sup> found mixed results for various catalysts with gold, platinum and palladium electrocatalysts compared to binary compositions of those metals. Other groups have looked at gold for electrocatalysis, primarily in high pH environments.<sup>99-106</sup> De Lima and Varela<sup>105</sup> outlines a ‘tentative’ mechanism in agreement with Tremiliosi-Filho<sup>107</sup> in high pH as follows in equations 24-27 and the overall equation 28:



Similar to that of platinum in methanol reported by Pournaghi-Azar<sup>89</sup>, Varela describes gold oxidation in high pH being active towards the EOR by a Langmuir Hinshelwood step which assumes uniform surface coverage ( $\theta=1$ ) with all sites equal.<sup>105</sup> For a Langmuir mechanism, the reaction rate decreases as the concentration of an adsorbed species increases beyond a particular level.<sup>108</sup> Further, equation 25 involves an interaction between adsorbed ethoxy and non-adsorbed OH<sup>-</sup> ions which is best described by the Eley-Rideal mechanism. Another difference found by Varela<sup>105</sup> between platinum and gold is the orientation of the initial adsorption, a Pt-C bond was formed predominantly for platinum and since AuO is much more stable compared to Au-C. AuO blocks the electrode, limiting ethanol absorption. This may be more evidence to suggest the AuO is formed at high potentials (+1.0 V vs. MMS), seen in figure 2.9(e), instead of adsorbed

hydroxyl groups on gold. This may be more useful in near neutral or low pH towards the bifunctional mechanism by separating the Pt-C bonds described for platinum in section 2.9.1. The bifunctional mechanism illustrates the different roles that metals have in ethanol oxidation and it will be important in later chapters 3 and 4. Though gold appears to be inactive to the oxidation, Au sites deposited on CIE may play a role in the EOR by separating the platinum sites in a bimetallic catalyst. This reduces neighbouring interactions between two adjacent platinum sites with ethanol adsorbed, which affect the EOR.

There has however been recent interest in a gold plated, platinum electrode that has reported 100% conversion to CO<sub>2</sub> from ethanol in acid media.<sup>97</sup> Loukrakpam *et al.* states that the mechanism by which their electrode works is through a large upshift of the d-band centre of platinum.<sup>97</sup> This is an alternative mechanism to the bifunctional mechanism outlined previously and shown in figure 1.2(d). By raising this d-band centre towards the Fermi level, enhanced reactivity and bond breaking ability should be seen compared to similarly sized nanoparticles of the individual metal.<sup>97</sup> This has been also mentioned as a possible mechanism for platinum catalysts by Maillard<sup>109</sup> and Demirci<sup>110</sup> and used in density functional theory (DFT) to outline potential catalysts by Nørskov.<sup>111</sup> Loukrakpam comments that even this technique is a delicate balance as a large upshift will hinder C-C bond breaking due to increased strength of adsorption of ethanol.

It also is apparent their electrode contains a layer of gold upon which platinum is present, but the coverage of the gold layer by platinum is incomplete. As a result, there may also

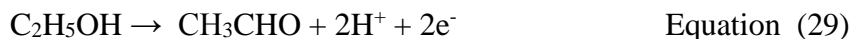
be a benefit towards the bifunctional mechanism where the neighbouring platinum atoms are further apart, possibly reducing the effect of fouling compared to a homogenous platinum surface. In addition, the incomplete coverage of platinum will result in highly stepped and highly conductive electrodes compared to glassy carbon. As the trend in ethanol oxidation moves from low pH to high pH, such work conducted in sulphuric acid proves an interesting development.

## **2.10 Intermediates: Acetaldehyde and Acetate**

Complete oxidation of ethanol produces carbon dioxide and 12 electrons, as mentioned in equation 15. However, as discussed in section 2.9, the mechanism is complex and alternative or intermediate products can be formed, as per the scheme in figure 2.9(b).<sup>112</sup> In concentrated ethanol solutions, acetaldehyde formation may be governed by an Eley-Rideal mechanism from the dehydrogenation of ethanol on the catalyst surface,<sup>113</sup> whereas at moderate concentrations, acetic acid is produced.<sup>113</sup> For this reason, the ethanol mechanism has not been definitively elucidated.<sup>113</sup> Prieto reports that acetate formed can block the active sites of a platinum electrode<sup>112</sup> while Antolini states ethanol reacts on pure platinum to produce only CO, CH<sub>4</sub> and C<sub>2</sub>H<sub>6</sub>.<sup>114</sup> As soon as acetaldehyde is formed it can then adsorb on a platinum surface to form a Pt-CH<sub>3</sub>CO species and is subsequently oxidized further by any available hydroxyl groups.<sup>114</sup> Consequently, some groups use this partial oxidation for selective oxidation of ethanol to acetic acid<sup>115</sup> and to potassium acetate.<sup>116</sup> Lamy and Demirci reported that ethanol did not “ideally” oxidise to CO<sub>2</sub> and the final products were acetaldehyde and acetic acid.<sup>5, 30, 117</sup> Krewer has pointed

out that partial oxidation of ethanol can be marketed as a fuel cell with zero CO<sub>2</sub> emissions, though proceeds to note that research is in its primary stage and it needs detailed analysis to assess the economic potential.

Cyclic voltammograms for the oxidation of acetaldehyde in solution were recorded at a Vulcan XC72 coated electrode and a platinum electrodeposit/CIE and are displayed in figure 2.10(a) and figure 2.10(b). The oxidation of acetaldehyde in solution at both platinum electrodes is observed at an onset potential of 0 V, peak A. The oxidation of ethanol to acetaldehyde produces two electrons according to equation 29.<sup>118</sup>



Park found that, in potassium carbonate electrolyte, the first anodic product is acetaldehyde and it leads to passivation of the platinum surface.<sup>119</sup> There is no apparent peak observed on the reverse sweep compared to that of the alcohol oxidation mechanisms shown previously from any adsorbed by-products of the oxidation of CH<sub>3</sub>CHO in solution. The peak current associated with PtO reduction is recorded at -0.4V is consistent with all platinum electrodes. However in figure 2.9(c), the platinum oxide reduction begins at potentials more cathodic than 0 V vs. MMS and instantaneously, ethanol re-oxidation or peak C commences as the surface oxide film is removed.

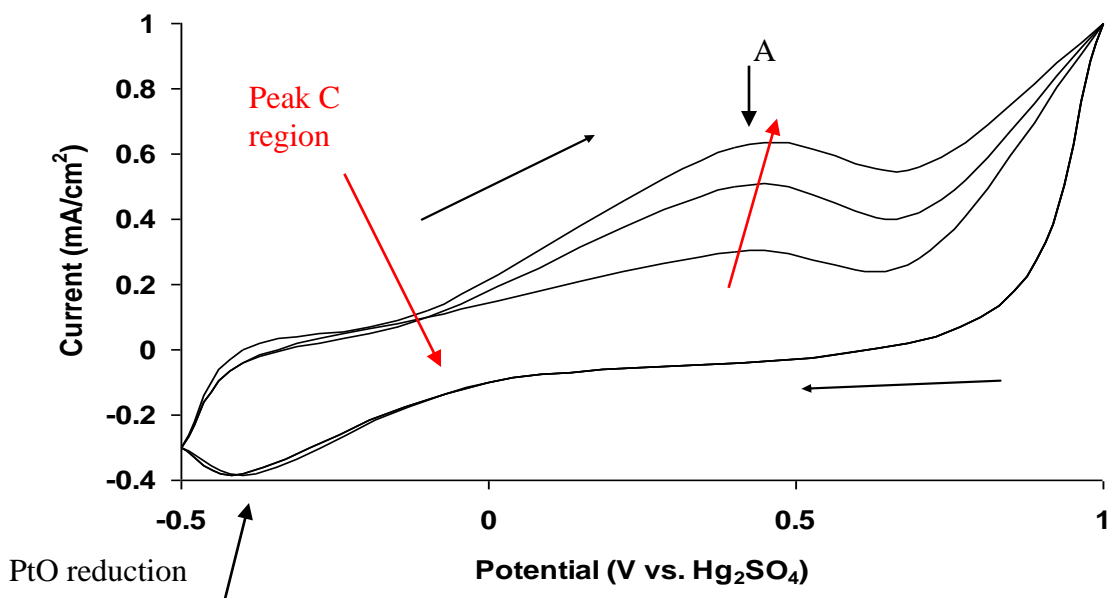


Figure 2.10(a): Cyclic Voltammetry of a Vulcan XC72/CIE (deliberately added to ink) in 0.5 M  $\text{CH}_3\text{CHO}$  in 0.1 M  $\text{KNO}_3$ , with MMS reference at a scan rate of 10 mV/s, pH = 6.

In acetaldehyde, this would occur at 0 V as PtO starts to be reduced beyond 0 V vs. MMS if there were adsorbed intermediates present such as CO or re-oxidation of the fuel.

Previous authors<sup>14</sup> have mentioned that this peak is due to the renewed oxidation of the fuel as opposed to the oxidation of an adsorbed species, particularly that of carbon monoxide.

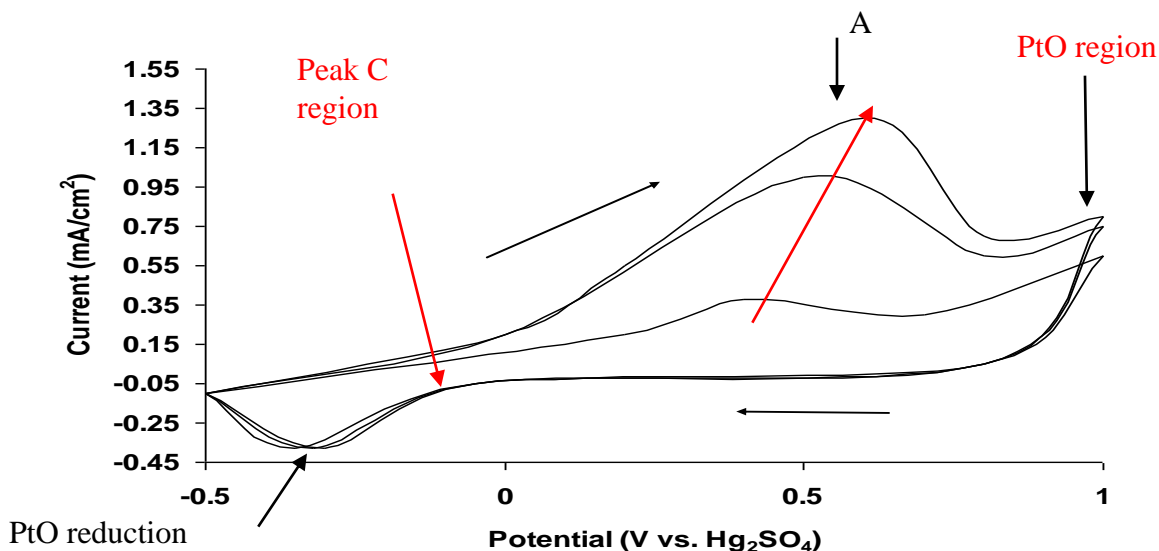


Figure 2.10(b): Cyclic Voltammetry of a platinum electrodeposit/CIE ( $120 \text{ mC/cm}^2$  in deaerated solution of  $0.1 \text{ M KNO}_3$ ) in  $0.5 \text{ M CH}_3\text{CHO}$  in  $0.1 \text{ M KNO}_3$ , with MMS reference at a scan rate of  $10 \text{ mV/s}$ ,  $\text{pH} = 6$ .

If the re-oxidation peak observed on the reverse sweep was as a direct result of a C-C compound, it should be present upon oxidation of the C-C compounds from the mechanism mentioned previously. Peak C is found when alcohols are oxidized, due to adsorbed CO or in ethanol with the possible adsorbed intermediates outlined in equations 18, 19 and 22. It can be seen that there is no peak C in oxidation of  $\text{CH}_3\text{CHO}$  or  $\text{CH}_3\text{COO}^-$  in solution, eliminating the possibility of adsorbed  $\text{CH}_3\text{CO}$ . The voltammetry in figure 2.10(a) and figure 2.10 (b) should record this adsorbed intermediate if it was present. This intermediate also plays a role with adsorbed hydroxyl groups (equation 23) to form acetic acid as postulated by Rousseau<sup>95</sup> and Antolini.<sup>114</sup>

Figure 2.10(c) shows a voltammogram of the oxidation of potassium acetate,  $\text{CH}_3\text{COOK}$ , at a platinum electrodeposit. The production of acetic acid produces four electrons as shown in equation 30.<sup>118</sup> A small current increase is observed on the forward run on the first sweep from open circuit potential, but no peak is apparent on the cathodic sweep except an increasing reduction current, again consistent with the PtO reduction peak.

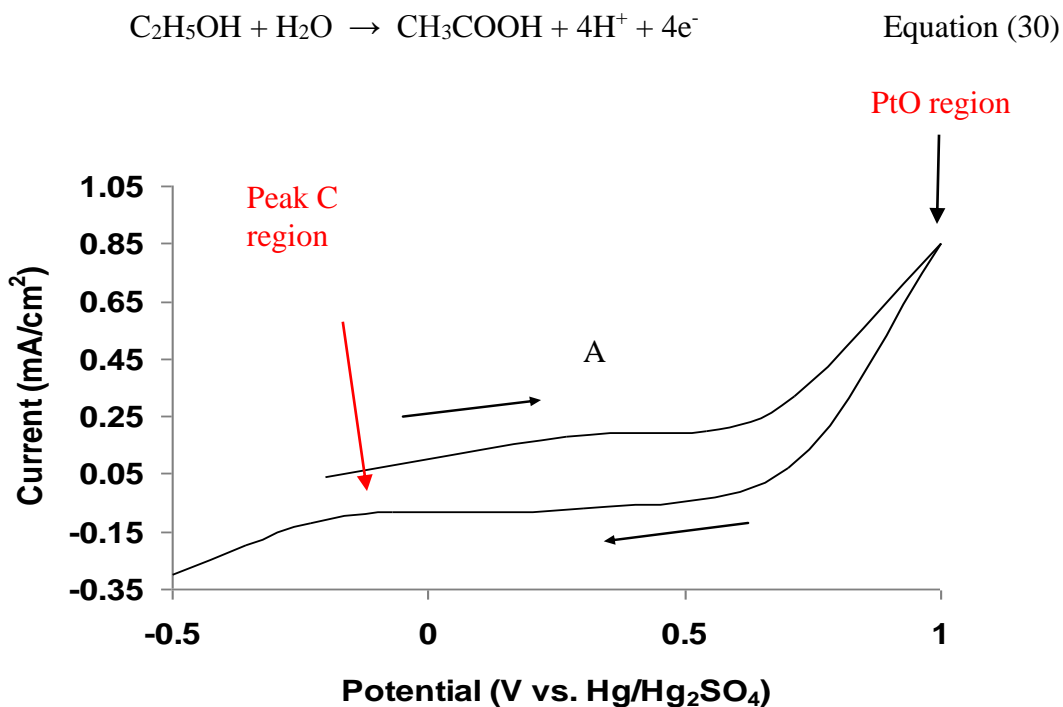


Figure 2.10(c): Cyclic Voltammetry of a platinum electrodeposit/CIE ( $120 \text{ mC/cm}^2$  in deaerated solution of  $0.1 \text{ M KNO}_3$ ) in  $0.5 \text{ M CH}_3\text{COOK}$  in  $0.1 \text{ M KNO}_3$ , with MMS reference and at a scan rate of  $10 \text{ mV/s}$ ,  $\text{pH} = 6$ .

In the voltammetry of these compounds, that there is a lack of a visible peak C indicating that that peak observed in ethanol is not strictly due to the oxidation of acetaldehyde or acetate or acetic acid. The increase in current for the actual peak observed in ethanol

solutions is often assigned to an adsorbed species on the surface, especially that of CO which has been noted to oxidise at 0V vs. MMS (not shown). At positive potentials, a platinum surface has been reported to be highly covered in oxygen containing species which become an inhibiting factor as mentioned by Tripkovic and Jiang.<sup>120-121</sup> Upon scan reversal, reduction occurs. Hence upon removal of the adsorbed PtO at the surface - an increased reduction current is observed - the ethanol<sup>12</sup> or adsorbed intermediate<sup>121</sup> can then be reoxidised at the surface.

This work is in agreement with Liang *et al.*<sup>122</sup> for the oxidation of various compounds containing a carbon-carbon bond. Liang reported a similar major difference in magnitude between the current observed in a solution of CH<sub>3</sub>COOK and a smaller difference recorded in a solution of CH<sub>3</sub>CHO to that of either ethanol or methanol, in agreement with the results found in this section for ethanol.

## **2.11 Increased platinum loading**

A study of platinum loading onto the carbon substrate was conducted to identify the optimum loading for the precious metal catalyst. Typically, as mentioned in chapter one, a current fuel cell contains 7-8 mg/cm<sup>2</sup> of platinum at its anode.<sup>123</sup> Decreasing this quantity is one of the strongest driving forces for research into electrocatalysts as well as the maximisation of current observed for a given metal loading.<sup>14</sup> Figure 2.11(a) shows the oxidation of ethanol in 0.1 M potassium nitrate at an electrocatalyst on a CIE with the mass of platinum corresponding to 5 mg/cm<sup>2</sup> according to Faraday's Law.

The first sweep in figure 2.11(a) overleaf shows that peak A exhibits almost thirteen times the current that is observed from the first sweep, from  $0.1 \text{ mA/cm}^2$  at  $0.12 \text{ mg/cm}^2$  loading up to  $1.55 \text{ mA/cm}^2$  at  $5 \text{ mg/cm}^2$  loading. This is a fifty-fold difference in weight of platinum for a multiple of thirteen in recorded current. At  $+1.0 \text{ V}$ , this current difference decreases again, up to 2.5 times the current observed at  $0.12 \text{ mg/cm}^2$  platinum electrode, to  $2.30 \text{ mA/cm}^2$ .

A characteristic of a high loading of platinum – above  $1 \text{ mg}$  - onto the CE observed in this work was the increased potential required of peak B in particular. In addition, all peaks at a high loading noticeably tended to move towards a more positive potential with increasing sweep number. By increasing potential, an increasing energy input is required to observe the reaction and that consequently, means that the reaction becomes more difficult to achieve over time. This phenomenon occurs to the extent that, at  $1.5 \text{ V}$  on a carbon ink electrode, peak B remains incomplete whereas at lower loading, for example  $0.12 \text{ mg/cm}^2$ , both peaks are clearly observed at  $+1.0 \text{ V}$  vs. MMS. There still remained a slight increase in potential as the sweep number was increased.

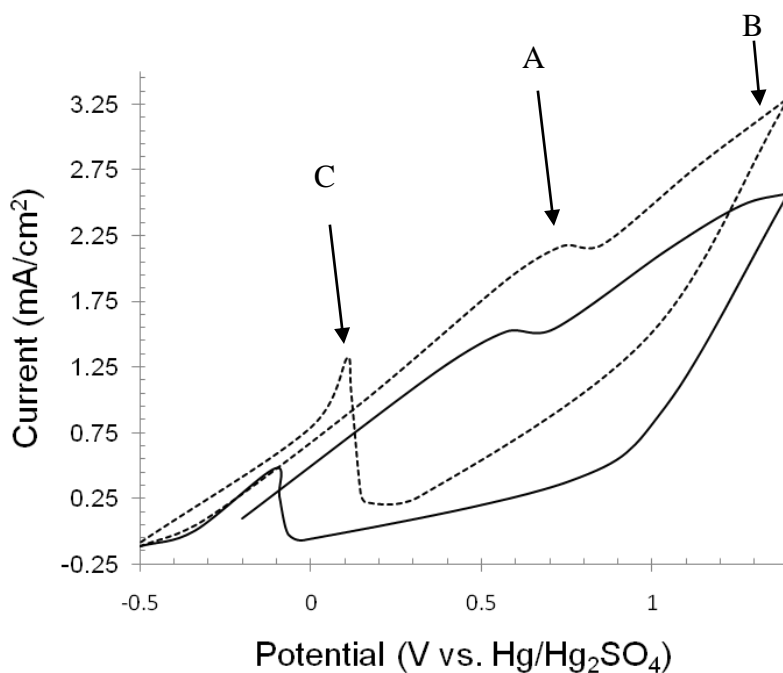


Figure 2.11(a): Cyclic voltammogram with peaks A, B and C, the oxidation of ethanol at a 5 mg platinum electrodeposit/CIE (5000 mC/cm<sup>2</sup> in deaerated 0.1M KNO<sub>3</sub>) on a carbon ink electrode in 0.5 M C<sub>2</sub>H<sub>5</sub>OH and deaerated 0.1M KNO<sub>3</sub> at a scan rate of 10 mV/s, 1<sup>st</sup> (solid line) and 2<sup>nd</sup> sweep (dashed line), MMS reference electrode.

In general, it has been found in this work that increasing the loading or sweep number has increased the current for all peaks, but also increased the potential at which the reactions or peaks occur. In particular peak B becomes less apparent without increasing the potential window. Above +1.0 V vs. MMS, PtO formation dominates and current increases considerably where no useful EOR an occur. The same effect of loading and sweep number on a carbon paper electrode was slightly improved in terms of the potential shift, but this trend was still observed. Furthermore, at a Toray carbon paper electrode, all peaks – A, B and C – are observed as consecutive peaks with increasing sweep number. There is no noticeable increase in potential for each peak over time which

may indicate that the carbon substrate plays an important role in facilitating deposition as a conductive surface and electron conductor in ethanol, but does not act as a catalyst.

Figure 2.11(b) shows a sample of electrodes and the maximum current, observed at 0.8 V (vs. MMS). Electrodes tested include loadings relating to a charge passed of 20 mC/cm<sup>2</sup>, 55 mA/cm<sup>2</sup>, 75 mC/cm<sup>2</sup>, 120 mC/cm<sup>2</sup>, 150 mC/cm<sup>2</sup>, 180 mC/cm<sup>2</sup>, 220 mC/cm<sup>2</sup> and 240 mC/cm<sup>2</sup>. Above 120 mC/cm<sup>2</sup>, the current observed appears to plateau with only a slight increase with increasing loading.

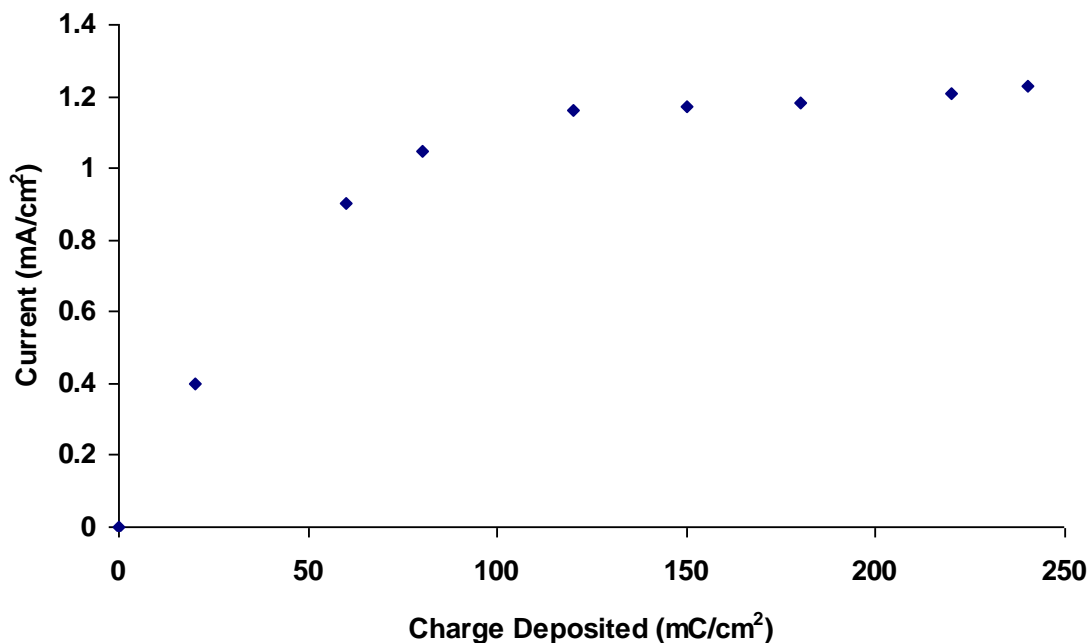


Figure 2.11(b): Graph plotting the effect of loading and current observed at 0.8V for the 10<sup>th</sup> scan. All eight platinum electrodeposits/CIE, controlled by charge (20 mC/cm<sup>2</sup>, 55 mA/cm<sup>2</sup>, 70 mC/cm<sup>2</sup>, 120 mC/cm<sup>2</sup>, 150 mC/cm<sup>2</sup>, 180 mC/cm<sup>2</sup>, 220 mC/cm<sup>2</sup> and 240 mC/cm<sup>2</sup> and deaerated 0.1 M KNO<sub>3</sub>), 0.5 M ethanol and deaerated 0.1 M KNO<sub>3</sub> with an MMS reference electrode at a scan rate of 10 mV/s, pH = 6.

There is a slight increase, but in terms of current added for each increased loading of platinum, the lower loadings of platinum prove to be the most productive in terms of the EOR. This may be linked to the method of electrodeposition and a limit towards a useful quantity of electrocatalyst. As the charge increases, the size of the metal particle is increased as shown in section 2.6, out to a micrometre scale. The smaller the particle results in the greater surface area which are most active towards EOR for the corresponding mass of platinum. As a consequence, an electrode reflecting 120 mC/cm<sup>2</sup> of charge passed in the deposition solution was used to investigate the catalyst and reaction mechanism from this point onwards in this work.

### **2.12 Impact of concentration on Ethanol Oxidation Reaction at platinum catalysts**

Ethanol concentration plays an important role in the mechanism of oxidation. From the literature, the concentration of ethanol affects each electrode separately ranging from 3 M<sup>124</sup> to 4.5 M<sup>125</sup> for various catalysts, although on both occasions palladium in high pH, not platinum was used as their catalyst. Bergamaski<sup>126</sup> and Chetty<sup>127</sup> have looked at platinum in lower pH media. Figure 2.12(a) shows a plot of the current observed at 3 M ethanol in neutral media.

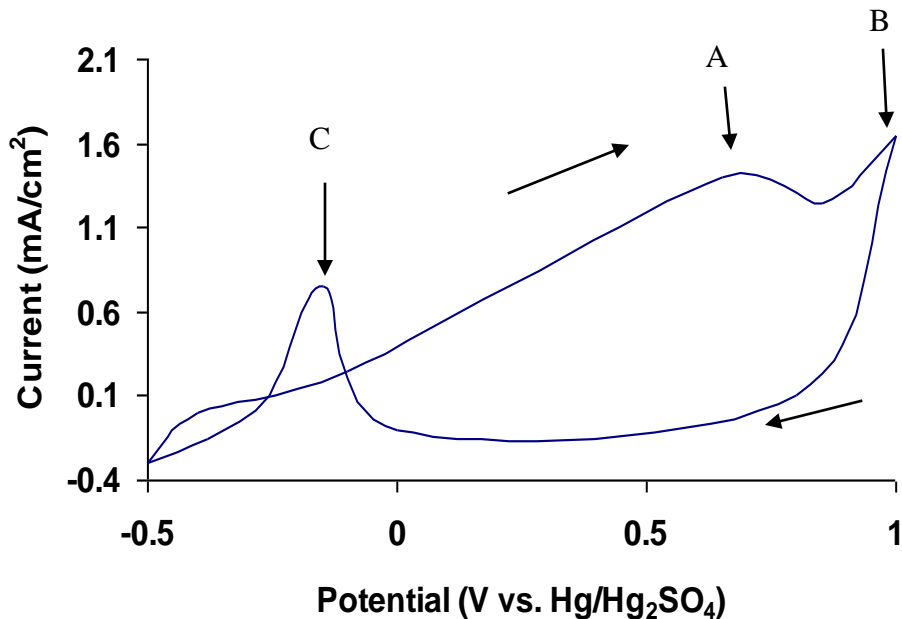


Figure 2.12(a): Cyclic Voltammetry showing the increase of current observed in deaerated 0.1 M KNO<sub>3</sub> with 3 M ethanol, for an electrodeposited platinum/CIE electrode (120 mC/cm<sup>2</sup> in deaerated 0.1 M KNO<sub>3</sub>), with MMS reference electrode and at a scan rate of 10 mV/s.

Once the maximum current is observed, increasing the ethanol concentration further results in a decrease in the current recorded. For example, Liang *et al.*<sup>122</sup> found that concentrations above 3 M ethanol caused this decrease. However it appears to be specific to each electrode and environment with various ethanol concentrations used by each group. Generally, 1 M ethanol<sup>127</sup> or 0.5 M ethanol is favoured. Table 2(b) below show the maximum current and peak potential for peak regions A and B shown in figure 2.12(a). Typically in electroanalytical work, such as the solution of ferricyanide in section 2.7.4, the concentration of analyte solutions are much lower, in the order of 0.01 M. Giz and Camara<sup>113</sup> analysed the effect of ethanol concentration on a platinum single crystal using

0.01 M, 0.1 M and 1.0 M ethanol. There was a factor of sixteen increase in current observed moving from 0.01 M ethanol to 0.1 M ethanol in perchloric acid from 95  $\mu\text{A}$  to almost 1600  $\mu\text{A}$ . In addition, Giz reports that the potential at which the peak current is observed is shifted to more positive potentials as the ethanol concentration is increased<sup>113</sup>.

<b>Ethanol Concentration (moles/dm<sup>3</sup>)</b>	<b>Peak Region A Potential (V vs. Hg/Hg<sub>2</sub>SO<sub>4</sub>)</b>	<b>Peak Region A Current (mA/cm<sup>2</sup>)</b>	<b>Peak Region B Potential (V vs. Hg/Hg<sub>2</sub>SO<sub>4</sub>)</b>	<b>Peak Region B Current (mA/cm<sup>2</sup>)</b>
0.01	0.24	0.09	0.75	0.39
0.05	0.27	0.21	0.82	0.63
0.1	0.34	0.35	0.85	0.95
1.0	0.45	0.79	0.9	1.26
2.0	0.57	1.13	1	1.48
3.0	0.68	1.48	1	1.65

Table 2(b): Table of potential position and current of peak regions A and B showing the increase of current and progression of potential observed in deaerated 0.1 M KNO<sub>3</sub> in various ethanol concentrations, electrodeposited platinum/CIE (120 mC/cm<sup>2</sup> in deaerated 0.1 M KNO<sub>3</sub>), with MMS reference electrode at a scan rate of 10 mV/s, 10<sup>th</sup> sweep.

For this purpose, this work looked at determining this maximum concentration for the Pt deposit/CIE. However, as noted when the loading of platinum was increased, it is increasingly difficult to oxidize the ethanol with increasing sweep number as each peak gradually shifts to a higher potential which agrees with Giz.<sup>113</sup> Above 3 M ethanol, this current is observed to decrease by comparison due to saturation of the surface.

This phenomenon has been reported to be due to the balance between adsorption of  $\text{OH}_{\text{ad}}$  Pt-O and ethoxy species at sites on the metallic surface<sup>120</sup>. The platinum oxides formed at +1.0 V vs. MMS are also an inhibitor to the EOR even on highly stepped crystals as Pt (755) and Pt (332) as Tripkovic<sup>120</sup> outlined. Using higher concentrations, the adsorbed ethoxy species dominate the surface and they significantly limit the ability of the OH species required to further oxidise the adsorbed organic compounds. This hydrogen region is diminished upon any surface adsorption and is particularly noted and utilised in carbon monoxide (CO) oxidation as mentioned previously.

### **2.13 Effect of increased temperature at platinum catalysts**

In DEFCs, ethanol oxidation occurs at a wide range of temperatures to different extents: from low temperatures (below 373 K), medium (373 K to 573 K) and high temperature (above 573 K) as tabulated in section 1.2. For this reason, particular fuel cells suit particular temperatures, such as the Solid Oxide Fuel Cell which operates at high temperatures, carbon electrodes may not be suitable due to 'coking' of the carbon surface

at such high temperatures. At low temperatures, the DEFC can operate between 313 K and 493 K with a liquid feed. Above 353 K in this work, the ethanol solution was unstable due to bubbling. Consequently, figure 2.13(a) shows the EOR at different temperatures up to a maximum of 333 K.

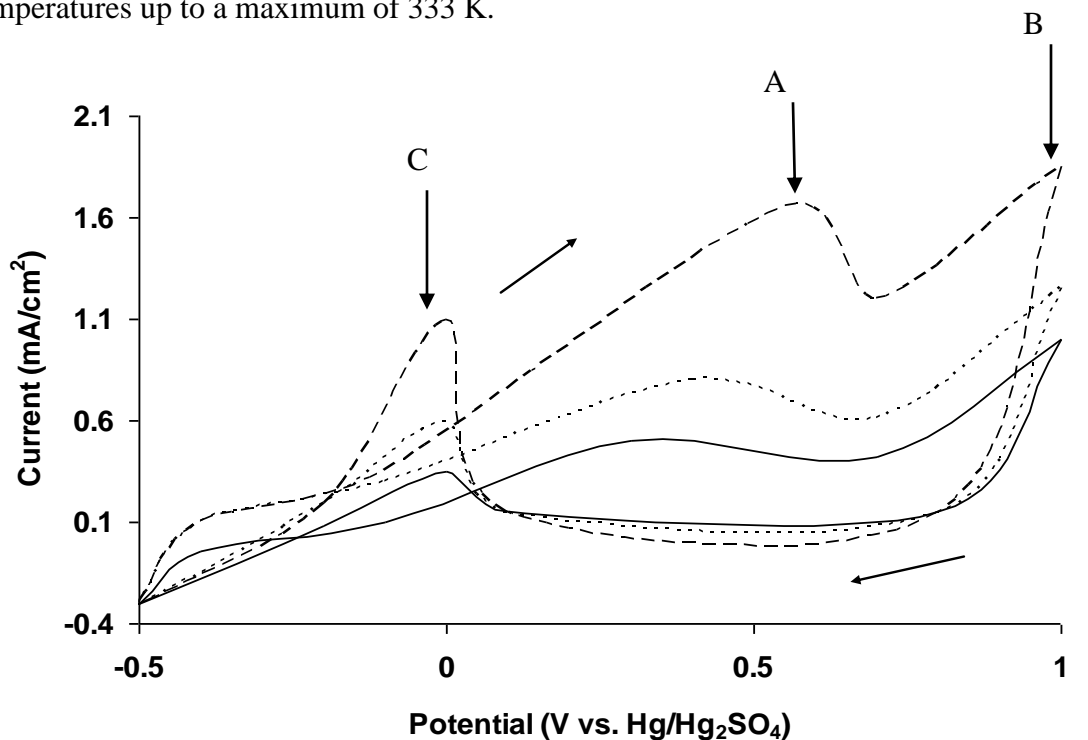


Figure 2.13(a): Cyclic Voltammetry highlighting the EOR with increasing temperature up to 308 K(solid line), 318 K (dashed line) and 333 K (broken line) observed in 0.5 M ethanol and deaerated 0.1 M KNO<sub>3</sub>, platinum electrodeposit/CIE (120 mC/cm<sup>2</sup> in deaerated 0.1 M KNO<sub>3</sub>), with a MMS reference at a scan rate of 10 mV/s, first sweep, pH = 6.

Increasing temperature from room temperature should increase the current observed though the onset potential of oxidation should remain similar.<sup>121</sup> Also, it is reported that this increase observed in high pH is due to an increased yield of CO<sub>2</sub>. There is an increase

in current observed, but the electrochemical CV profile exhibits the same characteristic redox peaks, A, B and C observed at room temperature. The onset potential of the reaction is not affected by the increase in temperature, but it facilitates an increase in rate once initialised. Figure 2.13(b) shows the Arrhenius plot from room temperature (295 K) up to 333 K in near neutral pH at +1.0 V vs. MMS. Below +1.0 V vs. MMS, the ethanol peaks shift potential as seen with the ethanol concentration and the effect of catalyst loading.

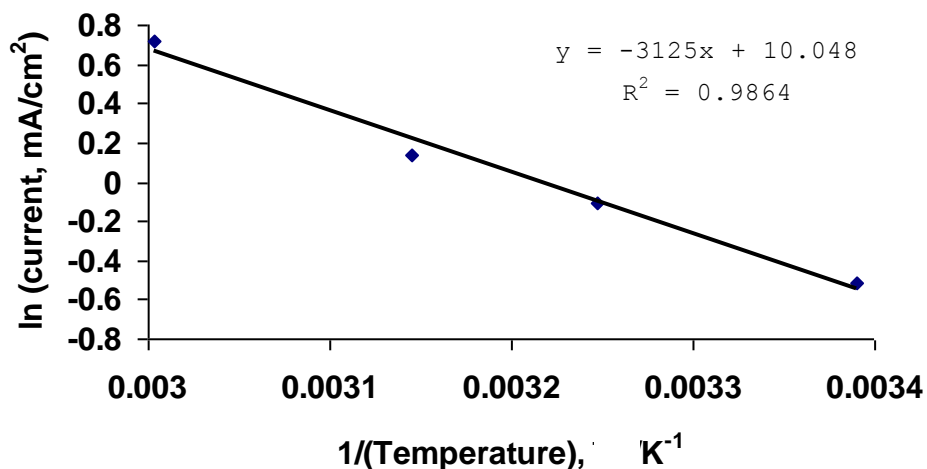


Figure 2.13(b): Arrhenius plot for ethanol oxidation at +1.0 V vs. MMS observed in 0.5 M ethanol and deaerated 0.1 M KNO<sub>3</sub> at temperatures of 295 K, 308 K, 318 K, 333 K, platinum electrodeposit/CIE (120 mC/cm<sup>2</sup> in deaerated 0.1M KNO<sub>3</sub>), with an MMS reference at a scan rate of 10 mV/s, first sweep, pH = 6.

Colmati and other groups<sup>98, 101, 128</sup> use the same method to determine the E<sub>a</sub> as shown in the Arrhenius equation in equation 31 and the slope of this plot is calculated according to equation 32, where k is the rate or current of reaction (mA/cm<sup>2</sup>), A is a pre-exponential factor and related to the number of collisions, E<sub>a</sub> (kJ/mol), R is the gas constant,

8.314 J/K/mol and temperature is T, in Kelvin. As such, the activation energy was calculated to be 27.71 kJ/mol and ln A calculated to be 10.048.

$$\ln k = \ln A - E_a/R (1/T) \quad \text{Equation (31)}$$

$$\text{slope} = -E_a/R \quad \text{Equation (32)}$$

The lower the activation energy the better kinetics as Gupta outlines.<sup>129</sup> The typical range of activation energies for the ethanol oxidation in the literature is between 24 kJ/mol and 30 kJ/mol.<sup>98, 101, 128-129</sup> The value collected from figure 2.13(b) falls into the middle of this range. As the  $E_a$  increases, it reflects the lack of platinum sites free for ethanol adsorption. As the platinum surface oxides increase, the energy with which it is required for ethanol adsorption grows. Bimetallic catalysts may aid this process by producing greater quantities of  $\text{OH}_{\text{ads}}$  to allow for better catalytic activity at lower potentials by keeping the platinum sites free for dehydrogenation and adsorption of ethanol as shown in the scheme in section 1.2. Li *et al.*<sup>130</sup> indicate that low temperature fuel cells need to be pushed to above 150°C to enable large scale applications, but development continues to be conducted for the DEFC between 60°C to 100°C in prominent research groups such as Colmati<sup>128</sup> and Camargo *et al.*<sup>131</sup>

## **2.14 Impact of scan rate and gold Rotating Disk Electrode on Ethanol Oxidation Reaction**

The scan rate used to conduct the CV is important, as it can affect the observed features and it has a significant effect on the amount of current produced at all values of potential.<sup>132-133</sup> If not chosen properly, the scan rate can cause a misinterpretation of the CV data, especially at faster rates.<sup>132</sup> Figure 2.14(a) shows a collection of CVs completed at a various scan rates for a platinum electrodeposited electrode and in 0.5 M ethanol in high pH medium. It is one of the parameters where variation is predicted to result in a current change.

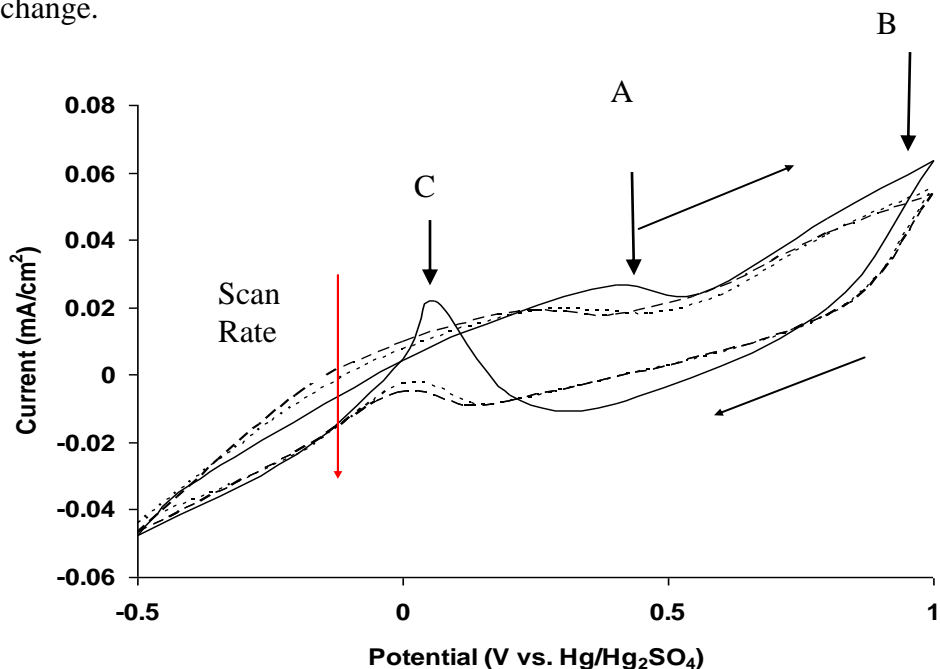


Figure 2.14(a): Cyclic Voltammetry showing decreasing current at peak C with increasing scan rates 1 mV/s (solid line), 100 mV/s (dashed line) and 200 mV/s (broken line) in deaerated 0.1 M KNO<sub>3</sub>, 0.5 M ethanol, electrodeposited platinum (120 mC/cm<sup>2</sup> in deaerated 0.1 M KNO<sub>3</sub>), with an MMS reference, 1<sup>st</sup> sweep.

Other such parameters include temperature or ethanol concentration, revolutions per minute at an RDE<sup>134</sup> or even use of an additive<sup>135</sup> to alter the surface chemistry or react

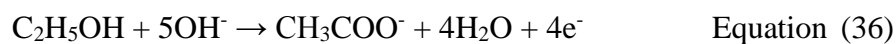
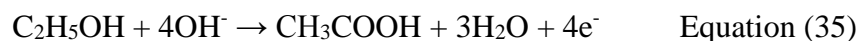
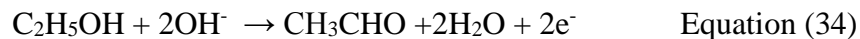
with intermediate species. Typically, in acidic electrolytes, 50 mV/s is used for the EOR.<sup>26, 31</sup> Teng *et al.*<sup>134</sup> observed a 33% increase in the current seen two different sweep rates, 5 mV/s to 10 mV/s. For scan rates between 100 mV/s and 200 mV/s, two broad peaks are observed on the positive sweep and one slight, broad peak observed on the return sweep. It is noticeable that as the scan rate is decreased from 200 mV/s, that all peaks become increasingly discernible. For scan rates below 100mV/s, it is becoming more evident that peak C is becoming more evident with an ever decreasing scan rate. At 1mV/s, there also appears to be a very broad peak C on the positive sweep in comparison to that at higher scan rates. However, the scan rate chosen in this work was 10 mV/s because of the slower reaction kinetics at the carbon ink electrode and carbon paper electrode as shown in section 2.7.4. In order to increase the current observed for the EOR, faster scan rates can be employed.

### 2.15 Effect of pH on the EOR

An important experimental parameter for ethanol oxidation on platinum and other electrocatalysts is pH. A neutral or slightly alkaline environment plays a crucial role in platinum dispersion for some methods of catalyst synthesis.<sup>135</sup> Both the stability of the platinum surface as well as issues concerning the products formed are affected by the pH. As an example, the progressive carbonation of the electrolyte solution from the complete EOR in equation 33 below.<sup>136</sup>



Evident from equation 33, production of carbon dioxide reduces the pH of the alkaline solution.<sup>135</sup> Furthermore, the production of acetaldehyde and acetic acid in acid conditions can be achieved according to equations 34 and 35, from Fujiwara *et al.*<sup>137</sup> To form acetate, Bianchini<sup>116</sup> gives the anode equation in full as equation 36:



As mentioned previously, research on DAFCs has been well developed for low pH or acidic fuel cells. Nafion® cation exchange membranes have been used since the 1960s<sup>136</sup> and work has traditionally focused on platinum electrodes in acid electrolyte.<sup>138</sup> Increasingly, there are developments in the field of alkaline anion exchange membranes and platinum based catalysts in alkaline medium.<sup>139</sup> Though the EOR is much less studied due to impracticalities such as carbonation of the fuel and dissolved CO<sub>2</sub> as shown in equation 33, there is a need for improved solid alkaline electrolytes (AEMs).<sup>141</sup> Slade and Varcoe<sup>142</sup> have shown the recent upward trend in the state of the art alkaline based membranes measured by the number of papers published with an Alkaline Anion Exchange Membrane (AAEM) being employed, practically zero W/cm<sup>2</sup> being recorded up to 2004 to in excess of mW/cm<sup>2</sup> in 2015. Lai and Koper add that very little research has been conducted in pH solutions greater than pH 2 and less than pH 12<sup>138</sup>. Notably, Lai<sup>138</sup> uses an Hg/Hg<sub>2</sub>SO<sub>4</sub> reference electrode similar to this work. As mentioned in this thesis in section 2.4, Lai states numerous advantages of non-acidic electrolytes.<sup>138</sup> The

role of adsorption of ions from supporting electrolyte or surface reactions is strongly dependent on electrolyte pH.<sup>138</sup> Figure 2.15(a) shows the CV for the EOR collected at pH 11 and pH 14 respectively. By changing the electrolyte the stability of intermediates, and thereby the reaction mechanism, in neutral and alkaline media is impacted.

Panagiotapoulou<sup>143</sup> has also stated that there are potential benefits to balancing the strongly alkaline pH environment with suitable materials, i.e. reducing the harsh pH environment. Both pH environments showed increased current larger than in acidic and near neutral media reported up to that point. At very high pH, the current dramatically increased up to  $9\text{mA/cm}^2$  for the initial EOR peak X on the forward sweep which is ten times larger than near neutral pH and 5 times larger than in pH 11. This is similar to that observed by Koper<sup>138, 141</sup> with a large increase in current from pH 2 and pH 8 of close to  $3\text{mA/cm}^2$  up to  $16\text{mA/cm}^2$  in pH 12. In pH 14, peak Y is typically observed as a broad, shoulder-like peak at  $0.8\text{V}$  vs. MMS and is similar in nature to that for peak C in neutral media.

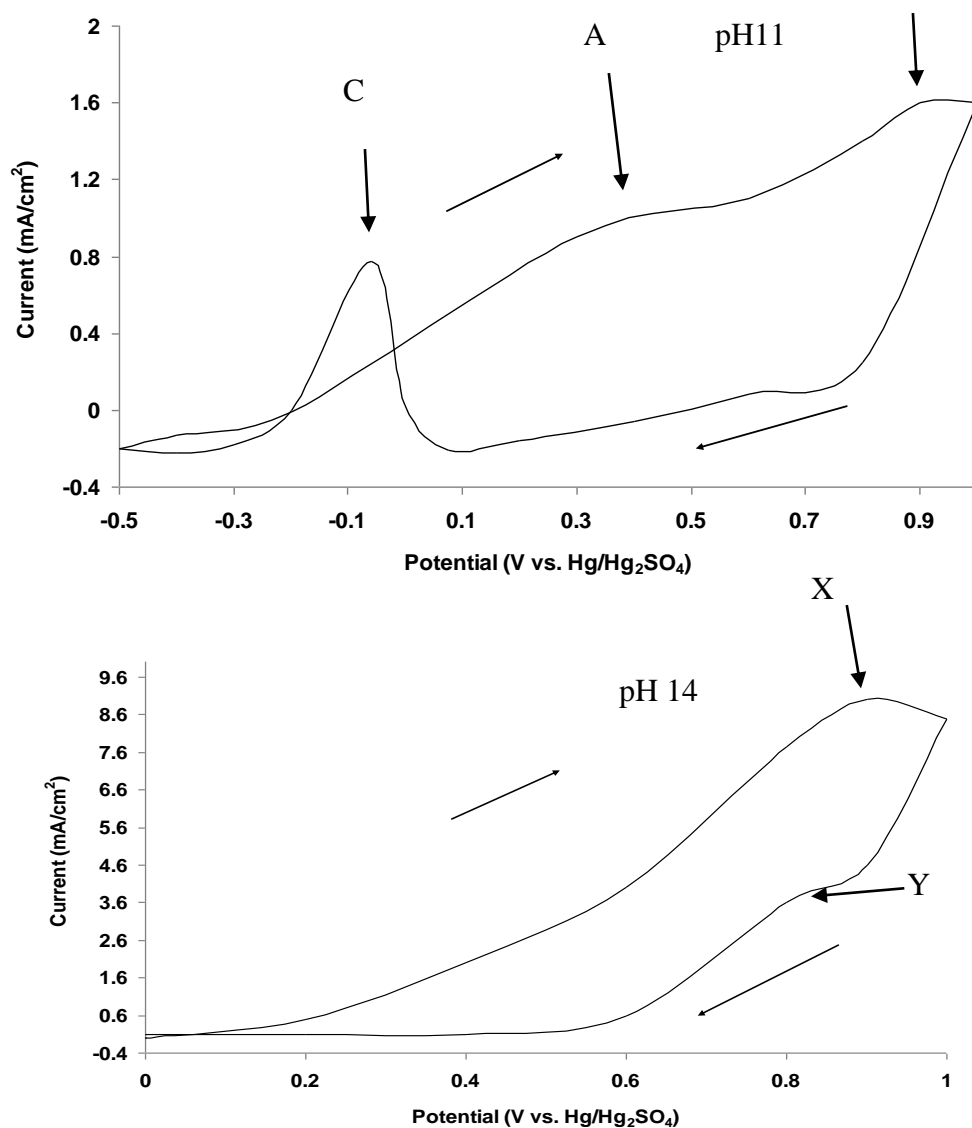


Figure 2.15(a): Cyclic voltammetry showing the EOR, 0.5 M C<sub>2</sub>H<sub>5</sub>OH in (i) pH 11, (deaerated 0.001 M NaOH) and (ii) pH 14 media (deaerated 1 M NaOH) on a platinum electrodeposit [120 mC/cm<sup>2</sup> in deaerated 0.1 M KNO<sub>3</sub>], with an MMS reference electrode, and at a scan rate of 10 mV/s.

As shown previously by CV in section 2.9, in acid media the EOR is characterized by two peaks on the positive scan, peaks A and B and one peak, labelled C, assigned to

C<sub>1</sub>/C<sub>2</sub> adsorbed species on the reverse sweep. One peak, peak A, is typically ascribed to the dissociation of water and dehydrogenation of ethanol adsorption on the surface. In high pH, the availability of OH<sub>ads</sub> should potentially increase the current substantially. It will be seen in further chapters using Anson plots that the reaction rate increases very fast in NaOH compared to the same reaction in near neutral pH which exhibits a more staggered progression of reaction, dependent on the dissociation of water. Koper finds a two peak oxidation arrangement on the positive sweep, assigned peaks A and B in this chapter, at a pH 1.5 up to pH 12 and in 0.1 M HClO<sub>4</sub><sup>138</sup> whereas Barroso<sup>41</sup> and Li<sup>130</sup> find one oxidation peak on the positive sweep in perchloric acid. As a result, the features in voltammetry can differ in the same electrolyte based on conditions and the electrocatalyst used in any individual work. Koper found that as the pH is increased, the current does not drop significantly from pH 1.5 up to pH 8.<sup>138</sup> This agrees largely with the EOR seen in this chapter from acid to near neutral pH in 0.1 M KNO<sub>3</sub> where the current is similar in both environments. However, work conducted by Jiang *et al.*<sup>121</sup> has displayed two peaks on the positive sweep for acid and base medium. Koper finds two peaks on the positive sweep, even up to pH 12, though peak I, as Lai labels it, is dominant and peak II is diminishing with increasing pH.<sup>138</sup> In figure 2.15(a) for pH 11, two peaks can also be observed, similar to neutral and acidic pH, though the current increases from 1 mA/cm<sup>2</sup> to 1.9 mA/cm<sup>2</sup> from pH 6 to pH 11.

It has been speculated that a major issue with neutral media would be the lack of ionic strength in the electrolyte, but these results seem to be in contrast to this view. The ionic strength can be accounted for by increasing the concentration of the electrolyte. Similarly

Kadirgan *et al.*<sup>54</sup> has investigated similar ethanol oxidation voltammetry in both acid and base. Kadirgan found that the onset potential of the EOR oxidation at platinum in high pH occurred at much lower onset potentials than in neutral or acidic media.<sup>54</sup> This was not reported by Koper<sup>138</sup> nor observed in this section. At pH 11, the oxidation rate appears to be similar to that in acidic and neutral media, with two peaks in the forward sweep and one peak found, probably due to adsorbed species, on the reverse sweep. The current is considerably lower to that seen in a high pH medium, however the ionic strength of the solution may have impacted on the current observed. At pH 14, the current observed is increased, but one peak is observed on both anodic and cathodic sweeps. At pH 14, there is a reported issue with carbonate formation, should the reaction go to completion to form CO<sub>2</sub>, so complete oxidation may not be desirable, limiting the use of pH to the production of CH<sub>3</sub>COO<sup>-</sup>.

In high pH, typically one peak is observed for EOR in the literature on the anodic sweep and one peak on the cathodic sweep.<sup>120, 141</sup> This is often assigned to the greater quantities of OH<sub>ad</sub> availability from OH<sup>-</sup> in solution compared to the dissociation of water to form OH<sub>ad</sub> in low pH solutions. The production of acetic acid would not be possible in strongly basic solution, and formation of the acetate ion, CH<sub>3</sub>COO<sup>-</sup> is likely to occur as per equation 36. In higher pH, the availability of OH<sup>-</sup> to form OH<sub>ad</sub> from solution should facilitate oxidation of ethanol rapidly and the current trend in the field is to investigate the most suitable catalyst for the ethanol fuel cell in high pH electrolytes.<sup>144-151</sup> Yu, Krewer and Scott<sup>146</sup> outlined a general multi-step mechanism resulting in formation of acetate for ethanol oxidation in alkaline media as in equations 37-41:



Yu, Krewer and Scott<sup>146</sup> added that the rate determining step is the reaction of  $CH_3CHO_{ad}$  with  $OH_{ad}$  in equation 40 and in terms of electron transfer, equations 37 and 39 are important. This mechanism appears to be much more likely than that described in section 2.9.2 whereby equation 38 and 39 are separate rather than being combined in equation 24. They also reported that the main product in concentrations in excess of 0.5 M NaOH is sodium acetate, while the greatest activity to the EOR was found in 1 M NaOH electrolyte. Some groups use different concentrations, such as 2 M KOH. This work continues with this trend by looking to move away from acidic pH and introduce bimetallic and trimetallic catalysts such as PtPdAu electrodes and PdNi electrodes and this will be examined in the next chapters.

## 2.16 Conclusions

The electrochemical apparatus must be carefully selected to minimise adsorption of undesirable adsorbates that block ethanol adsorption onto a fresh catalyst surface. This involves selection of the most suitable reference electrode. The most suitable reference electrode was the mercury/mercury oxide or the mercury/mercury sulphate where

chloride interference is minimised compared to the saturated calomel electrode or silver/silver chloride reference electrode. In addition, the electrolyte used needs to be evaluated. In low pH, there are several options and the most suitable was determined to be sulphuric acid. Perchloric acid has been found to dissociate into chloride ions at weak concentrations and this was observed with large currents at low potentials associated with hydrogen.

The carbon electrode needs to be carefully selected as porosity was a key element to an anode for the DEFC. In addition, the more porous carbon paper electrodes were found to exhibit much improved voltammetric behaviour. The electrode that possesses the most surface edges and defects was most suitable for a fuel cell. The carbon ink electrode possessed valleys where the metal will deposit preferentially over a smooth or planar electrode. It was found that electrodeposition was the most suitable method of electrode manufacture, for reasons of cost and time. It was found that platinum electrodeposits were active towards the EOR, exhibiting three oxidation peaks and most importantly, a peak in the cathodic sweep, commonly associated with the oxidation of an adsorbed intermediate, carbon monoxide. By comparison, gold surfaces were a poor catalysts for ethanol oxidation where repetitive cycling resulted in the formation and reduction of AuO.

Temperature, loading, increased pH, concentration, and scan rate were used to analyse the EOR at platinum electrodeposits and all parameters had an effect. Increasing the temperature up to 333 K increased the current observed indicating an optimum

temperature. Above 343 K, the results are unreliable. When loading of platinum was increased, the current also increased, but it was not a linear relationship with the corresponding weight of catalyst. For this reason 120 mC/cm<sup>2</sup> was found to be a suitable mass of platinum to work with and maximise the current per gramme of platinum. This corresponds with the extra loading causing larger particles to form, as seen by SEM images which reduced the surface area.

When the concentration of fuel was increased up to 3 M ethanol, the current increased to a maximum, but the potential at which oxidation peaks A, B and C. At higher concentrations, the current recorded began to drop as ethanol adsorption dominates the metal surface. This is in agreement with similar values of Liu<sup>124</sup>, Li<sup>125</sup> and Liang.<sup>122</sup>

When the scan rate was changed, the voltammetry observed began to change. As the scan rate increased, the three peaks associated with ethanol oxidation became ill defined. Due to the slow kinetics noted at a carbon ink electrode, 10 mV/s was decided upon as the most advantageous. Faster scan rates up to 200 mV/s caused an increase in the current observed, but the features of ethanol oxidation were difficult to define clearly and as such the higher scan rate is not useful in determining other optimum operating conditions.

Most notably, the pH played a critical role in the current recorded. When the pH was moved from zero in sulphuric acid to pH 6 in potassium nitrate and further to pH 14 in 1 M NaOH, the voltammetry dramatically changed from three peaks to two oxidation peaks. In particular, the current observed in near neutral media was similar to that

recorded in low pH. When membranes become more stable in high pH, the current will increase dramatically to that currently in Nafion<sup>®</sup> based membranes.

## 2.17 References:

1. Vielstich, W.; Lamm, A.; Gasteiger, A.H.; (2003), "Handbook of fuel cells. Fundamentals, Technology and Applications", John Wiley and Sons Ltd, 1, ISBN: 0-471-49926-9.
2. Zurowski, A.; Kolary-Zurowska, A.; Marassi, Kulesza, P.J.; (2010), *ECS Trans.*, **25** (35), 147-154.
3. Shen, P.K.; Xu, C.; (2006), *Electrochem. Comm.*, **8**, 184-188.
4. Hariyanto, Purwanto, W.W.; W-Soemantojo, R.; Stimming, U.; (2009), *J. Chem. Nat. Resources Eng.*, **2**, 47-61.
5. Leger, J-M. ; Rousseau, S. ; Coutanceau, C. ; Hahn, F. ; Lamy, C. ; (2005), *Electrochim. Acta*, **50**, 5118-5125.
6. Sai Siddhardha, R.S.; Anupam Kumar, M. ; Lakshminarayanan, V. ; Sathish Ramamurthy, S. ; (2014), *J. Power Sources*, **271**, 305-311.
7. Jusys, E.; Massong, H.; Baltruschat, H.; (1999), *J. Electrochem. Soc.*, **146**, 1093.
8. Rodríguez-Nieto, F.J.; Morante-Catacora, T.Y. ; Cabrera, C.R.; (2004), *J. Electroanal. Chem.*, **571**, 15-26.
9. Coutanceau, C.; Brimaud, S.; Lamy, C.; Léger, J-M. ; Dubau, L. ; Rousseau, S. ; Vigier, F. ; (2008), *Electrochim. Acta*, **53**, 6865-6880.

10. Vigier, F.; Coutanceau, C.; Perrard, A.; Blegisir, E.M. ; Lamy, C. ; (2004), *J. Appl. Electrochem.*, **34**, 439-446.
11. Liu, Z.; Hong, L.; (2007), *J. Appl. Electrochem.*, **37**, 505-510.
12. Gupta, S.S.; Datta, J.; (2005), *J. Chem. Sci.*, **117**, 337-344.
13. Coutanceau, C.; Rakotondrainibé, A.F.; Lima, A.; Garnier, E. ; Pronier, S. ; Léger, J-M. ; Lamy, C. ; (2004), *J. Appl. Electrochem.*, **34**, 61-66.
14. Gupta, S.S.; Mahaptra, S.S.; Datta, J.; (2004), *J. Power Sources*, **131**, 169-174.
15. Abd-El-Latif, A.A. ; Mostafa, E. ; Huxter, S. Huttard, G.; Baltruschat, H.; (2010), *Electrochim. Acta*, **55**, 7951-7960.
16. Bönemann, H.; Brijoux, W.; Brinkmann, R.; Fretzen, R.; Jousen, T.; Köppler, R.; Korall, B.; Neiteiler, P.; Richter, J.; (1994), *J. of Mol. Cat.*, **30**, 1312.
17. <http://www.kitco.com/historical/charts/platinum>, viewed May 2015.
18. Pletcher, D.; Steady, State and potential Step Techniques, Instrumental Methods in Electrochemistry, Horwood Publishing, 9, 284, ISBN:1-898563-80-2.
19. Del Colle, V., Berna, A., Tremiliosi, G., Herrero, E., Feliu, J.M, (2008) *Phys. Chem. Chem. Phys*, **10**, 3766.

20. Lima, F.H.B.; Profeti, D.; Lizcano-Valbuena, W.H.; Ticianelli, E.A.;  
Gonzalez, E.R.; (2008), *J. Electroanal. Chem.*, **617**, 121-129.
21. Gonzalez, E.R. (2010), 61<sup>st</sup> meeting of the International Society of  
Electrochemistry, Electrochemistry from Biology to Physics, Nice, France.
22. Bianchini, C.; Shen, P.K.; (2009), *Chem. Rev.*, **109**, 4181-4204.
23. Tripkovic, D.V.; Strmcnik, D.; van der Vliet, D.; Stamenkovic, V.;  
Markovic, N.; (2008), *Faraday Discuss*, **140**, 25-40.
24. Wang, L.; Bambagioni, V.; Bevilacqua, M.; Bianchini, C.; Filippi, J.;  
Lavacchi, A.; Marchionni, A. ; Vizza, F.; Fang, X.; Shen, P.K. (2010), *J.*  
*Power Sources*, **195**, 8036-8043.
25. Cantane, D.A.; Gonzalez, E.R.; (2009), *ECS Trans.*, **25** (1), 1161-1168.
26. Lamy, C. ; Rousseau, S. ; Belgsir, E.M. ; Coutanceau, C. ; Léger, J-M. ;  
(2004), *Electrochim. Acta*, **49**, 3901-3908.
27. Vigier, F. ; Gloaugen, F. ; Léger, J-M. ; Lamy, C.; (2001), *Electrochim.*  
*Acta*, **46**, 4331-4337.
28. Delime, F.; Léger, J-M. ; Lamy, C. ; (1999), *J. Appl. Electrochem.*, **29**,  
1249-1254.
29. Coutanceau, C. ; Demarconnay, L. ; Lamy, Léger, J-M. ; (2006), *J. Power*  
*Sources*, **156**, 14-19.

30. Lamy, C. ; Lima, A. ; LeRhun, V. ; Delime, F.; Coutanceau, C.; Léger, J-M. ; (2002), *J. Power Sources*, **105**, 283-296.
31. Simoes, F.C.; dos Anjos, D.M. ; Vigier, F. ; Léger J-M. ; Hahn, F. ; Coutanceau, C.; Gonzalez, E.R. ; Tremiliosi-Filho, G. ; de Andrade, A.R.; Olivi, P.; Kokoh, K.B.; (2007), *J. Power Sources*, **167**, 1-10.
32. Garcia,-Rodriguez, S.; Rojas, S.; Pena, M.A. ; Fierro, J.L.G. ; Baranton, S. ; Léger, J-M. ; (2011), *Appl. Catal. B : Environ.*, **106**, 520-528.
33. Peng, Z. ; Yang, H. ; (2009), *Nano Today*, **4**, 143-164.
34. Dutta, A.; Datta, J.; (2013), *Int. J. Hydrogen Energ.*, **38**, 7789-7800.
35. Datta, J.; Dutta, A.; Biswas, M.; (2012), *Electrochem. Comm.*, **20**, 56-59.
36. Bard, A.J.; Faulkner, L.R.; (1980), “Electrochemical Methods, Fundamentals and Applications”, John Wiley and Sons Ltd., New York.
37. Rusanova, M.Y.; Ploaskov, P.; Muzikar, M.; Ronald Fawcett, W.; (2006), *Electrochim. Acta*, **51**, 3097-3101.
38. Ujvári, M.; Láng, G.; Horányi, G.; (2002), *J. Appl. Electrochem.*, **32**, 581-582.
39. Láng, G.; Inzelt, G.; Vrabcz, A.; Horányi, G.; (2005), *J. Electroanal. Chem.*, **582**, 249-257.
40. Hassan, H.H.; (2006), *Electrochim. Acta*, 1-7.

41. Barroso, J.; Pierna, A.R.; Blanco, T.C.; Morallón, E.; Huerta, F.; (2011), *J. Power Sources*, **196**, 4193-4199.
42. Láng, G.G; Horányi, G.; (2003), *J. Electroanal. Chem.*, **552**, 197-211.
43. Henderson, M.P.; Miasek, V.I.; Swaddle, T.W.; (1971), *Can. J. Chemistry*, **49**, 317-324.
44. Láng, G.; Ujvari, M.; Horányi, G.; (2003), *Corros. Sci.*, **45**, 1-5.
45. Russell, A.; Hayden, B.; “Electrochemistry, Electrochemical Engineering and Electrochemical Technology”, Southampton Summer School, University of Southampton, July 2010.
46. Rao, C.R.K. ; Trivedi, D.C.; (2005), *Coordin. Chem. Rev.*, **249**, 613-631.
47. Thompson, S.D.; Jordan, L.R.; Shukla, A.K.; Forsyth, M.; (2001), *J. Electroanal Chem.*, **515**, 61-70.
48. Choi, K.H.; Kim, H.S.; Lee, T.H.; (1998), *J. Power Sources*, **75**, 230.
49. Bockris, J.O’M.; Reddy, A.K.N.; Gamboa-Aldeco, M.E.; Electrodicts, “Modern Electrochemistry 2A: Fundamentals of Electrodicts”, 7, 1269.
50. Zhu, A.L.; Teo, M.Y.; Kulinich, S.A.; (2009), *Appl. Catal. A: Gen.*, **352**, 17-26.
51. Abbott, A.P.; Capper, G.; McKenzie, K.J.; Ryder, K.S.; (2007), *J. Electroanal Chem*, **599**, 288-294.

52. Gasparotto, L.H.S. ; Prowald, A. ; Borisenko, N.; Zein El Abedin, S.; Garsuch, A.; Endres, F.; (2011), *J. Power Sources*, **196**, 2879-2883.
53. Ohno, H.; (2005) “Electrochemical Aspects of Ionic Liquids”, John Wiley & Sons Ltd., New York.
54. Kadirgan, F.; Léger, J.-M.; Lamy, C.; (1981), *J. Electroanal. Chem.*, **125**, 89-103.
55. Mahaptra, S.S.; Dutta, A. ; Datta, J. ; (2010), *Electrochim. Acta*, **55**, 9097-9104.
56. Lu, J. ; Lu, S. ; Wang, D. ; Yang, M.; Liu, Z.; Xu, C.; Jiang, S.P.; (2009), *Electrochim. Acta*, doi: 10.1016/j.electacta.2009.04.048.
57. Katikawong, P.; Ratana, T.; Veerasai, W.; (2009), *J. Chem. Sci.*, **121**, 329-337.
58. Jiang, J. ; Kucernak A. ; (2009), *Electrochem. Comm.*, **11**, 1005-1008.
59. Boutonnet, M.; Logdberg, S.; Svensson, E.E.; (2008), *Curr. Opin. Colloid In.*, **13**, 270-286.
60. Danaee, I. ; (2013), *J. Ind. Eng. Chem.*, **19**, 1008-1013.
61. Pletcher, D. ; “Steady, State and Potential Step Techniques, Instrumental Methods in Electrochemistry”, Horwood Publishing, 1, 23, ISBN:1-898563-80-2.

62. Bagotsky, V.S.; "Fundamentals of Electrochemistry", 2<sup>nd</sup> Edition, John Wiley and Sons Ltd, 28, 539.
63. Bagotsky, V.S.; "Fundamentals of Electrochemistry", 2<sup>nd</sup> Edition, John Wiley and Sons Ltd, 28, 542-545.
64. Chatterjee, M.; Chatterjee, A.; Ghosh, S.; Basumallick, I.; (2009), *Electrochim. Acta*, **54**, 7300-7304.
65. Bambagioni, V.; Bianchini, C.; Marchionni, A.; Filippi, J. ; Vizza, F. ; Teddy, J. ; Serp, P.; Zhiani, M.; (2009), *J. Power Sources*, **190**, 241-251.
66. Otomo, J.; Nishida, S.; Takahashi, H.; Nagamoto, H.; (2008), *J. Electroanal. Chem.*, **615**, 84-90.
67. Xu, C.; Cheng, L.; Shen, P.; Liu, Y.; (2007), *Electrochem. Comm.*, **9**, 997-1001.
68. Mohanty, U.S.; (2010), *J. Appl. Electrochem.*, doi: 10.1007/s10800-010-0234-3.
69. Stoychev, D.; Papoutsis, A.; Keladiopoulou, A.; Kokkinidis, G.; Milchev, A.; (2001), *Mater. Chem. Phys*, **72**, 360-365.
70. Duarte, M.M.E.; Pilla, A.S.; Sieben, J.M.; Mayer, C.E.; (2006), *Electrochem. Comm.*, **8**, 159-164.
71. Wang, Z-B.; Yin, G-P. Lin, Y-G.; (2007), *J. Power Sources*, **170**, 242-250.

72. Brownson, D.A.C.; Kampouris, D.K.; Banks C.E.; (2011), *J. Power Sources*, **196**, 4873-4885.
73. Randviir, E.P.; Brownson, D.A.C.; Banks, C.E.; (2014), *Mater. Today*, **17**, 426-432.
74. Motheo, A.J.; Machado, S.A.S.; Van Kampen, M.H.; Santos Jr, J.R.; (1993), *J. Brazilian Chem. Soc.*, **4**, 122-127.
75. Watt-Smith, M.J.; Friedrich, J.M.; Rigby, S.P.; Ralph, T.R.; Walsh, F.C.; (2008), *J. Phys. D: App. Phys.*, **41**, 1-8.
76. Trasatti, S.; Petrii, O.A.; (1991), *Pure Appl. Chem.*, **63**, 711-734.
77. <http://www.people.clarkson.edu/surfacearea0.htm>, viewed January 2015.
78. Xu, C. ; Zeng, R. ; Shen, P.K.; Wei, Z.; (2005), *Electrochim. Acta*, **51**, 1031-1035.
79. Hallam, P.M.; Banks, C.E.; (2011), *Electrochem. Comm.*, **13**, 8-11.
80. Wu, G.; Li, L.; Xu, B-Q.; (2004), *Electrochim. Acta*, **50**, 1-10.
81. Santos, A.L.; Profeti, D.; Olivi, P.; (2005), *Electrochim. Acta*, **50**, 2615-2621.
82. He, P.; Liu, H.; Li, Z.; Li, J.; (2005), *J. Electrochem. Soc.*, **152**, E146-E153.
83. Yi, Q. ; Zhang, J.; Chen, A.; Liu, X.; Xu, G.; Zhou, Z.; (2008), *J. Appl. Electrochem.*, **38**, 695-701.

84. Guo, Y.; Zheng, D.; Liu, H.; Friedrich, A.; Garche, J.; (2006), *J. New Mat. Electrochem. Sys.*, **9**, 33-39.
85. Salazar-Banda, G.R.; Suffredini, H.B.; Calegari, M.L.; Tanimoto, S.T.; Avaca, L.A.; (2006), *J. Power Sources*, **162**, 9-20.
86. Seiler, T.; Savinova E.R.; Friedrich, K.A.; Stimming, U.; (2004), *Electrochim. Acta*, **49**, 3927-3936.
87. Wei, Z.D. ; Chan, S.H. ; (2004), *J. Electroanal. Chem.*, **569**, 23-33.
88. Schulz, T.; Weinmuller, C.; Nabavi, M.; Pouliakos, D.; (2010), *J. Power Sources*, **195**, 7548-7558.
89. Pournaghi-Azar, M.H.; Habibi-A, B.; (2005), *J. Electroanal. Chem.*, **580**, 23-34.
90. Kucernak, A.; Jiang, J.; (2003), *Chem. Eng. Journal*, **93**, 81-90.
91. Chen, R.; Zhao, T.S.; (2007), *Electrochem. Comm.*, **9**, 718-724.
92. Lamy, Léger, J-M. ; Srinivasan, S. ; (2001), *Modern Aspects of Electrochemistry*, 34, Kluwer Academic/Plenum Publishers, New York.
93. Gileadi, E.; “Physical Electrochemistry, Fundamentals, Techniques and Applications”, Wiley-VCH Verlag, GmbH, Weinheim, 20.4.3, 348-352.
94. Hamann, C.H. ; Hamnett, A. ; Vielstich, W.; “Electrochemistry“, Wiley-VCH Verlag, GmbH, Weinheim.

95. Rousseau, S.; Coutanceau, C.; Lamy, C.; Léger, J-M. ; (2006), *J. Power Sources*, **158**, 18-24.
96. Robinson, R.A., Stokes, R.H., *Electrolyte Solutions*, (1968), Butterworths, Appendix 6.1, 463.
97. Loukrakpam, R.; Yuan, Q.; Petkov, V.; Gan, L.; Rudi, S.; Yang, R.; Huang, Y.; Brankovic, S.R.; Strasser, P.; (2014), *Phys. Chem. Chem. Phys.*; **16**, 18866-18876.
98. Dutta, A.; Mahaptra, S.S.; Datta, J.; (2011), *Int. J. Hydrogen Energ.*, 1-9.
99. Choi, S.; Seo, B.; Kim, J.; (2010), *B. Kor. Chem. Soc.*, **31**, 104-111.
100. El-Aziz, A.M.; Kibler, L.A.; (2002), *J. of Electroanal. Chem.*, **534**, 107-114.
101. Datta, J.; Dutta, A.; Mukherjee, S.; (2011), *J. Phys. Chem.*, **115**, 15324-15334.
102. Kwon, Y.; Lai, S.C.S.; Rodriguez, P.; Koper, M.T.M. ; (2011), *J. American Chem. Soc.*, **133**, 6914-6917.
103. Ye, J.; Liu, Y.; Xu, C.; Jiang, S.P. ; Tong, Y. ; (2007), *Electrochem. Comm.*, **9**, 2760-2763.
104. Moller, H.; Pistorius, P.C.; (2004), *J. Electroanal. Chem.*, **570**, 243-255.
105. de Lima, R.B.; Varela, H. ; (2008), *Gold Bull.*, **41**, 15-22.

106. Qian, Q-Y. ; Yang, C. ; Zhou, Y-G. ; Yang, S. ; Xia, X-H. ; (2011), *J. Electroanal. Chem.*, **660**, 57-63.
107. Tremiliosi-Filho, G.; Gonzalez, E.R.; Motheo, A.J.; Belgsir, E.M.; Léger, J-M.; Lamy, C.; (1998), *J. Electroanal. Chem.*, **444**, 31.
108. Laidler, K.J.; (1987), “Chemical Kinetics”, Harper and Row Publishers, New York, third edition.
109. Maillard, F.; Bonfont, A.; Chatenet, M.; Guétaz, L.; Doisneau-Cottignies, B.; Roussel, H. ; Stimming, U. ; (2007), *Electrochim. Acta*, **53**, 811-822.
110. Demirci, U.B.; (2007), *J. Power Sources*, **173**, 11-18.
111. Hammer, B.; Nørskov, J.K.; (2000), *Adv. Catal.*, **45**, 71.
112. Prieto, M.J. ; Tremiliosi-Filho, G. ; (2011), *Electrochem. Comm.*, **13**, 527-529.
113. Giz, M.J. ; Camara, G.A. ; (2009), *J. Eletroanal. Chem.*, **625**, 117-122.
114. Antolini, E.; (2007), *J. Power Sources*, **170**, 1-12.
115. Krewer, U.; Vidakovic-Koch, T.; Rihko-Struckmann, L.; (2011), *ChemPhysChem*, **12**, 2518-2544.
116. Bianchini, C.; Bambagioni, V.; Filippi, J.; Marchionni, A. ; Vizza, F.; Bert, P. ; Tampucci, A. ; (2009), *Electrochem. Comm.*, **11**, 1077-1080.
117. Demirci, U.B. ; (2007), *J. Power Sources*, **169**, 239-246.

118. Chia, Z.W.; Lee, J.Y., Crabtree, R.H.(Ed) ; “Energy Production and Storage: Direct Ethanol Fuel Cells”, John Wiley and Sons Ltd.; ISBN: 978-0-470-74986-9, (230), 229-246.
119. Park, S-M.; Chen, N.C.; Doddapaneni, N.; (1995), *J. Electrochem. Soc.*, **142**, 40-45.
120. Tripkovic, A.V.; Popovic, K.Dj.; Lovic, J.D.; (2001), *Electrochim. Acta*, **46**, 3163-3173.
121. Jiang, L.; Hsu, A.; Chu, D.; Chen, R.; (2010), *Int. J. Hydrogen Energ.*, **35**, 365-372.
122. Liang, J.; Scott, K.; (2010), *Electrochim. Acta*, **6**, 224-241.
123. Kluy, N.; Stimming, U.; (2011), COST 543 Action: Concluding Meeting, Faculty of Science Building, (TTK), May 2011, Eötvös Loránd University, Budapest, Hungary.
124. Li, Y.S.; Zhao, Z.X.; Liang, J.; (2009), *J. Power Sources*, **187**, 387-392.
125. Liu, J., Ye, J., Xu, C., Jiang, S.P.; Tong, Y., (2007), *Electrochem. Comm.*, **9**, 2334-2339.
126. Bergamaski, K. ; Gomes, J.F. ; Goi, B.E. ; Nart, F.C. ; (2003), *Eclét. Quim.*, **28**, 87-92.
127. Chetty, R.; Scott, K.; (2007), *Electrochim. Acta*, **52**, 4073-4081.

128. Colmati, F.; Antolini, E.; Gonzalez, E.R.; (2006), *J. Power Sources*, **157**, 98-103.
129. Gupta, S.S. ; Singh, S. ; Datta, J. ; (2010), *Mater. Chem. Phys.*, **120**, 682-690.
130. Li, H.; Sun, G.; Cao, L.; Jiang, L. ; Xin, Q. ; (2007), *Electrochim. Acta*, **52**, 6622-6629.
131. Camargo, A.P.M.; Previdello, B.A.F.; Varela, H.; Gonzalez, E.R.; (2010), *Quím. Nova*, **33**, 1-10.
132. Roberge, P.; “Handbook of Corrosion Engineering”, McGraw Hill, 7, 529-530.
133. Teng, Z-H.; Wang, Y-J; Wu, B.; Tang, Y-W.; Lu, T-H. ; Gao, Y. ; (2008), *Appl. Cat. B : Environ.*, **84**, 400-407.
134. Tian, T.; Liu, C.; Liao, J.; Xing, W. ; Lu, T. ; (2007), *J. Power Sources*, **174**, 176-179.
135. Hui, C.L.; Li, X.G.; Hsing I-M.; (2005), *Electrochim. Acta*, **51**, 711-719.
136. Matsuoka, K.; Iriyama, Y.; Abe, T.; Matsuoka, M.; Ogami, Z.; (2005), *J. Power Sources*, **150**, 20, 7-31.
137. Fujiwara, N.; Siroma, Z.; Yamazaki, S-i.; Ioroi, T.; Senoh, H.; Yasuda, K.; (2008), *J. Power Sources*, **185**, 621-626.

138. Lai, S.C.S.; Kleijn, S.E.F.; Oeztuerk, F.T.Z.; van Rees, V.C.; Vellinga; Koning, J.; Rodriguez, P.; Koper, M.T.M.; (2010), *Catal. Today*, **154**, 92-104.
139. Xie, S-W.; Chen, S.; Liu, Z-Q.; Xu, C-W.; (2011), *Int. J. Electrochem. Sci.*, **6**, 882-888.
140. Koper, M.T.M.; (2008), *Faraday Discuss.*, **140**, 11-24.
141. Lai, S.C.S.; Koper, M.T.M.; (2009), *Phys. Chem. Chem. Phys.*, **11**, 10446-10456.
142. Slade, R.; Varcoe, J.; (2011), symposium 4: Fuel Cells, 61<sup>st</sup> meeting of the International Society of Electrochemistry, Electrochemistry from Biology to Physics, Nice, France.
143. Panagiotapoulou, P.; Antoniadou, M.; Kondarides, D.I.; Lianos, P. ; (2010), *Appl. Cat. B: Environ.*, **100**, 124-132.
144. Rao, V.; Hariyanto; Cremers, C.; Stimming, U.; (2007), *Fuel Cells*, **7**, 417-423.
145. Yu, E.H.; Scott, K.; (2004), *J. Power Sources*, **137**, 248-256.
146. Yu, E.H.; Krewer, U.; Scott, K.; (2010), *Energies*, **3**, 1499-1528.
147. Liu, J.P.; Ye, J.Q.; Xu, C.W.; Jiang, S.P.; Tong, Y.X.; (2008), *J. Power Sources*, **177**, 67-70.
148. Xu, C.; Shen, P.K.; Liu, Y.; (2007), *J. Power Sources*, **164**, 527-531.

149. Spendelow, J.S.; Wieckowski, A.; (2007), *Phys. Chem. Chem. Phys.*, **9**, 2654-2675.
150. Ksar, F.; Ramos, L.; Keita, B.; Nadjo, L.; Beaunier, P.; Remita, H.; (2009), *Chem. Mater.*, **21**, 3677-3683.
151. Xu, C.W.; Liu, Y.L.; Yuan, D.S.; (2007), *Int. J. Electrochem. Sci.*, **2**, 674.

## Chapter 3: Palladium catalysts

### 3.1 Introduction

In this chapter, results are reported on palladium (Pd) as an electrocatalyst in the anode of a DEFC. Samples of palladium were electrodeposited onto different carbon supports and a variety of electrochemical techniques were used to investigate its role in the EOR.

Palladium is a transition metal with numerous oxidation states. It is commercially available as Pd(II) and Pd(IV) salts. These are finding increased use as part of bimetallic electrodes for the ethanol oxidation reaction, particularly in high pH media.<sup>1</sup>

The role of palladium in electrocatalysis is generally reported as part of the bifunctional mechanism mentioned previously in sections 1.2, 2.9 and 2.15. The readiness with which it produces adsorbed OH species is exploited to complete the oxidation process. At low pH, the use of palladium is affected by the preferential adsorption of hydrogen onto the metal surface. However, by increasing electrolyte pH, the ready formation of  $\text{OH}_{\text{ad}}$  enables further oxidation of ethanol through the bifunctional mechanism. It has been reported that palladium is active for ethanol oxidation in pH of approximately fourteen.<sup>2-8</sup>

The chapter will describe the morphology of palladium deposits and highlight the beneficial and sometimes detrimental role of palladium in bimetallic electrocatalysts in neutral and basic media. In addition, the effects of temperature and the scan rate will be demonstrated and will be discussed in order to identify the optimum conditions for the

EOR with palladium. With multimetallic electrodes, there can be a beneficial effect for the oxidation reaction based on the ability of a metal to produce  $\text{OH}_{\text{ad}}$  according to the equation 1 in neutral media and basic electrolytes in equation 2:



It has been reported that an increase of the percentage content of rhodium greatly affects the oxidation reaction at a platinum bimetallic electrode.<sup>9</sup> Gupta presented voltammetric results greatly influenced by a rhodium content of 65% compared to that of 10% rhodium due to the limited source of oxygen.<sup>9</sup> Until recently, rhodium was more expensive than platinum – however a recent decrease from \$350/g in 2008 has seen its value plummet to a cost equal to that of platinum, about \$45/g.<sup>10</sup> For each multimetallic electrodes, this ideal catalytic ratio can be significantly different, altering the cost of the catalyst and subsequently the fuel cell itself. Furthermore, palladium is 50 times more abundant than Pt<sup>11</sup> making it more likely to remain more cost effective in the short to medium term. For Ruthenium electrodes, the ideal ratio is widely reported as 40% ruthenium at a platinum electrode<sup>12-13, 15</sup> and for tin, this value reduces to 20% Sn at a platinum electrode.<sup>12-13</sup> Density Functional Theory (DFT) has been employed to predict the ideal ratio. Catalysts whose composition alters from this ratio for the given metal result in decreased activity.<sup>14</sup> Determining this ratio is critical to the performance of any multimetallic electrode.<sup>14</sup>

It can be noted that the expense of both Pt and Pd follow peaks and troughs over time, with platinum remaining the more expensive substance up to the turn of the 21<sup>st</sup> century<sup>17-18</sup>. After a short period of palladium becoming more expensive, the introduction of European legislation pertaining to the composition of automotive catalytic converters requiring the forced use of platinum, the cost of platinum has increased substantially to the current value of \$45/g<sup>17</sup>. Usage has increased in recent years, whereas palladium has decreased by up to 66%.<sup>19</sup> This platinum price compares unfavourably with palladium which is \$25/g. The cost incentive is a powerful driving force in developing Pd catalysts and consequently has seen an increase in the use of Pd in conjunction with the increased level of interest in high pH. Interest in high pH fuel cell research is due in part to the ever-increasing stability of alkaline membranes, the less corrosive alkaline conditions and enhancement of the ORR in alkaline electrolytes. The aims of this chapter are to investigate the use of palladium in the EOR, to characterise and optimise Pd deposits used in an attempt to replace partially or completely the Pt content of the EOR catalyst.

### 3.2 Experimental

Electrodeposited palladium on carbon supports – CIE, CPE mentioned previously - were used as electrodes in a conventional three electrode system. A mercury/mercury sulphate (MMS or Hg/Hg<sub>2</sub>SO<sub>4</sub>), +640 mV vs. SHE, purchased from Radiometer Analytical Instruments (ref 640) was used as a reference electrode with a Pt sheet as the auxiliary electrode. The CHI 600A and CHI 620A series potentiostats were used to perform the electrodeposition, cyclic voltammetric; chronoamperometric and chronocoulometric data.

Palladium was deposited from a 0.01 M solution of its salt, palladium (II) chloride, PdCl<sub>2</sub> purchased from Sigma Aldrich. Carbon ink electrodes were prepared by coating a non-porous plastic sheet (Xerox) with a finely dispersed particle-based graphite inside an ink binder solvent (Acheson Industries, Electrodag 423 SS). The ink coating was then allowed to dry. The fabricated electrodes were then sectioned into 1 cm<sup>2</sup> samples, acting as working electrodes. An insulating layer of varnish was added to the stem of each electrode in order to guarantee its geometrical area.

The effect of scan rate on ethanol oxidation was assessed using palladium electrodeposit electrodes. The temperature of the cell was kept at room temperature and it was de-aerated with oxygen-free nitrogen (BOC gases). A range of electrolytes were used, specifically 0.1 M potassium nitrate and 1 M sodium hydroxide, purchased from Sigma Aldrich. To change pH, the concentration of aqueous sodium hydroxide was varied to pH 14 (1 M NaOH). Typically the scan rate was set to 10 mV/s, however a range of other

scan rates were also employed for some studies ranging between 1 mV/s up to 200 mV/s. Solutions of pure ethanol were purchased from Sigma Aldrich and the concentration of ethanol was maintained as 0.5 M made up with electrolyte.

### 3.3 Morphological Features:

The appearance of Pd was examined under SEM-EDX for particle size and shape. Figure 3.3(a) shows a typical particle distribution at a deposit formed from a charge passed of  $120 \text{ mC/cm}^2$ . The particle size was found to range between 24 nm and 27 nm with the particles in a nodular shape. This particle size range is within the nanometre scale which may enhance the oxidation of ethanol at the surface. Literature reports that the ideal behaviour for ethanol oxidation is at particle sizes below 10 nm. However, work conducted by Gonzalez and Tremiliosi-Filho have reported that agglomerations of larger particle sizes show encouraging signs for alcohol oxidation.<sup>20</sup>

Figure 3.3(b) shows an electrode where the charge passed is substantially increased to  $1.6 \text{ C/cm}^2$ , so that the deposit is allowed to grow significantly larger. The appearance of the electrode shows florets of a Pd substance with the carbon substrate evident running through the centre of the image. Elemental mapping highlights the distribution of palladium for this image using elemental mapping. This confirmed that the florets in figure 3.3(b) are indeed palladium.

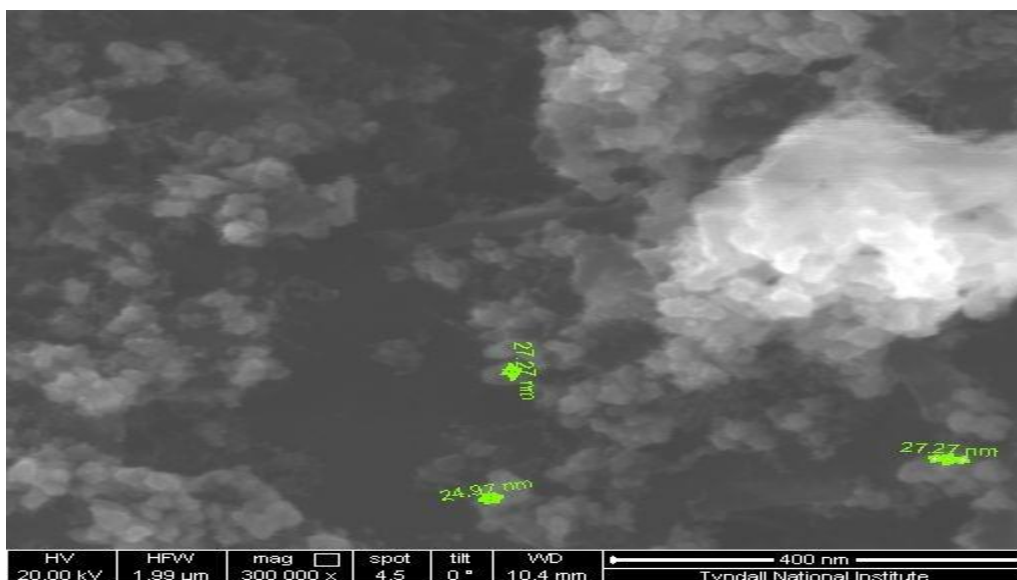


Figure 3.3(a): An SEM image of palladium electrodeposited from a deaerated 0.01 M PdCl<sub>2</sub> deposition solution in 0.1 M KNO<sub>3</sub>, charge passed of 120 mC/cm<sup>2</sup> with particle size measured range from 24-27 nm, at -1.0 V vs. MMS reference electrode.

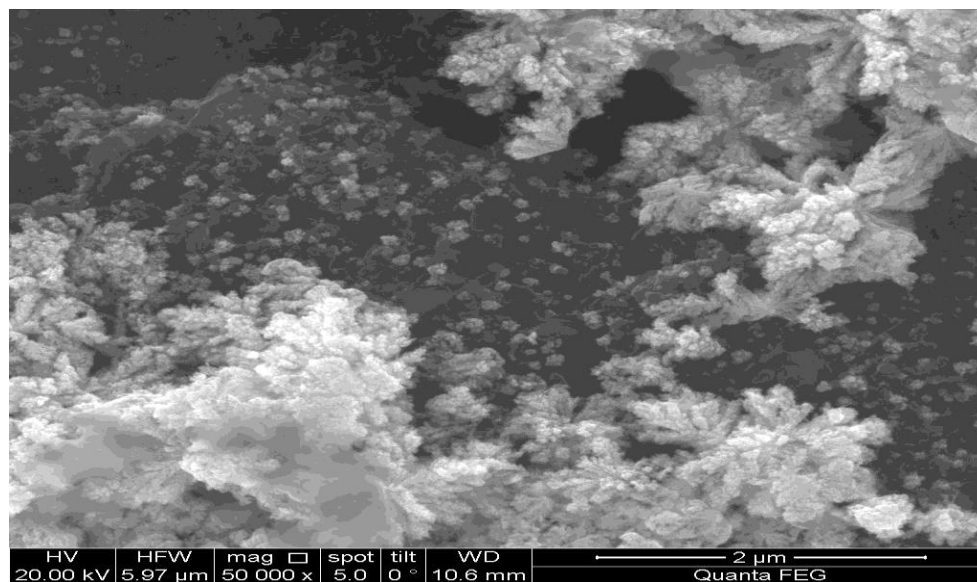


Figure 3.3(b): SEM image of palladium electrodeposited from a deaerated 0.01 M PdCl<sub>2</sub> deposition solution in 0.1 M KNO<sub>3</sub> charge passed of 1600 mC/cm<sup>2</sup> at -1.0 V with an MMS reference electrode.

Figure 3.3(c) shows an SEM-EDX image of the distribution of a platinum/palladium bimetallic electrode, with platinum appearing as green and palladium as red. The metallic surfaces appear to be deposited in separate ‘islands’ on the carbon surface. Both metals seem to be present on these islands. This would be beneficial for the operation of the bifunctional mechanism as the adsorbed species at both metals for ethanol oxidation could interact. Adjacent platinum and palladium islands are beneficial and desirable for the EOR for the bifunctional mechanism to be favoured. In contrast to separate and distinct areas of each metal on the electrode surface.

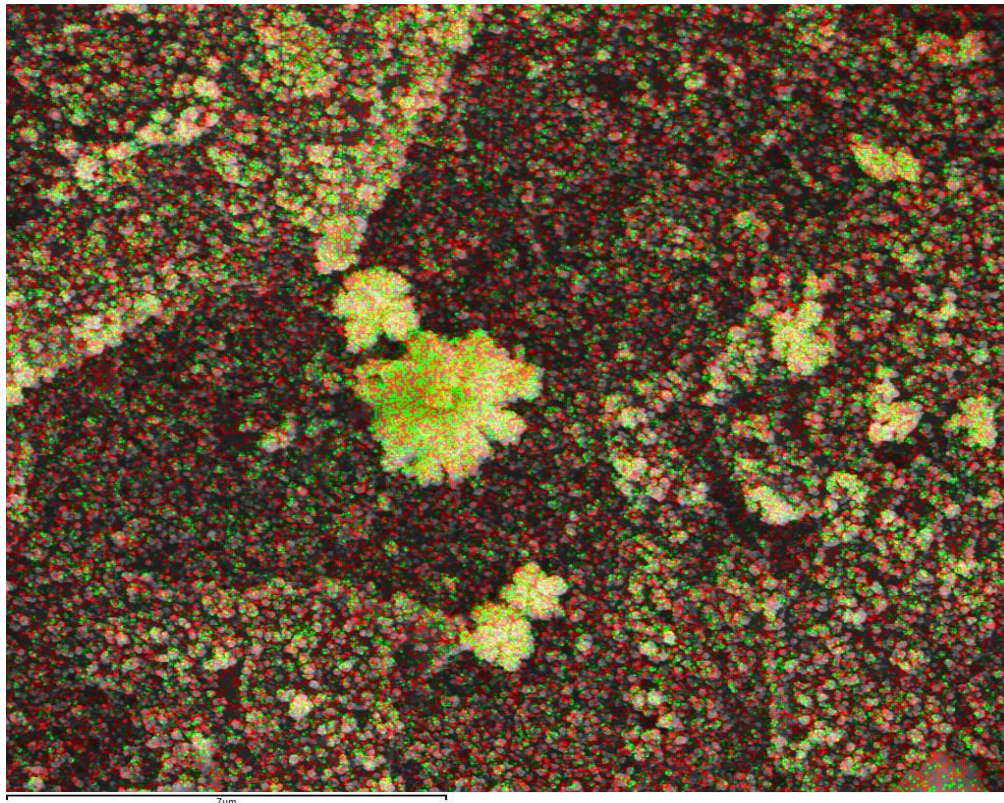
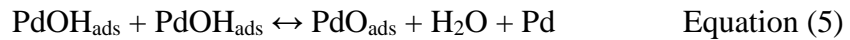


Figure 3.3(c): An SEM image and overlaid elemental mapping image of the distribution of platinum (green) and palladium (red) electrodeposited from a deaerated solution of 75%  $\text{K}_2\text{PtCl}_4$  and 25%  $\text{PdCl}_2$  deposition solution in 0.1 M  $\text{KNO}_3$  corresponding to a charge passed of  $240 \text{ mC/cm}^2$ .

### 3.4 Palladium electrodeposition:

Figure 3.4(a) overleaf shows a cyclic voltammogram obtained from a palladium electrode in 0.5 M ethanol in 0.1 M KNO<sub>3</sub> solution. A peak consistent with metal oxide reduction is evident at approximately -0.4 V vs. MMS on the return sweep according to equations 3, 4 and 5. Equation 5 was widely published without palladium metal as a product in error. By contrast, the cyclic voltammogram for a blank carbon electrode shows very little activity for ethanol oxidation in figure 3.4(b). Furthermore, the reduction peak at -0.35 V is not observed on the blank carbon surface. This suggests that in near-neutral conditions, palladium remains inactive for ethanol oxidation similar to its inactivity in low pH due to the adsorption and absorption of hydrogen.



The reduction peak observed in figure 3.4(a) indicated the successful deposition of palladium on the surface. In addition, the current observed on the forward sweep towards +1.0 V is similar to that observed at a blank carbon electrode. This may be caused by the oxidation of carbon at a high potential, approximately +1.0 V vs. MMS whereas in the Pd-CIE, the formation of a Pd-O bond on the surface which is reduced in the reverse sweep at -0.4 V vs. MMS. Figure 3.4(b) illustrates very little oxidation of ethanol by the

carbon substrate and, thus, the influence of the carbon substrate in terms of ethanol oxidation and adsorption can largely be discounted.

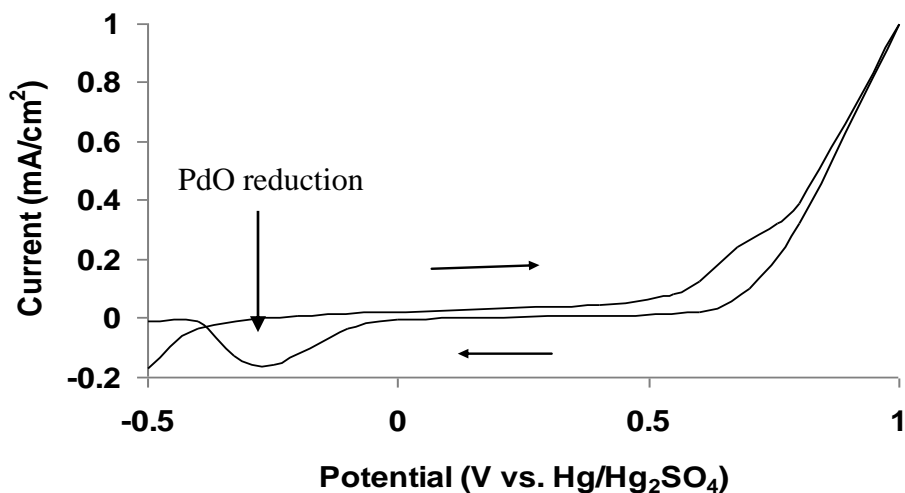


Figure 3.4(a): Cyclic voltammogram at a palladium electrodeposit/CIE (120 mC/cm<sup>2</sup> in deaerated 0.1 M KNO<sub>3</sub>) in 0.5 M ethanol in 0.1 M KNO<sub>3</sub> with an MMS reference electrode at a scan rate of 10 mV/s.

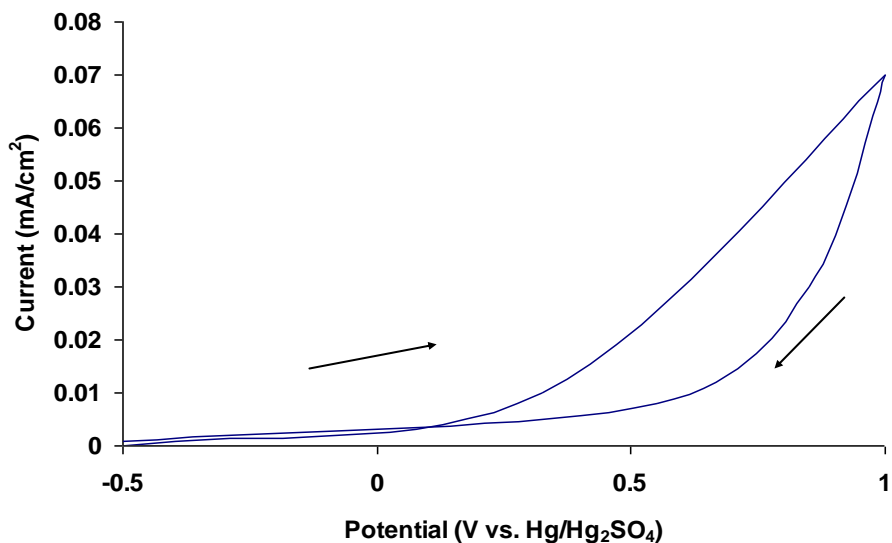


Figure 3.4(b): Cyclic voltammogram for a blank carbon ink electrode in 0.5 M C<sub>2</sub>H<sub>5</sub>OH and deaerated 0.1M KNO<sub>3</sub> with an MMS reference electrode, at a scan rate of 10 mV/s.

However, as mentioned in section 2.7, the nature of the carbon surface – such as the graphite ink or porous carbon, may limit the current and the immediacy of the reaction observed which will be highlighted in sections 4.6 and throughout chapter five.

Figure 3.4(c) illustrates the deposition of palladium compared to platinum by linear sweep voltammetry.

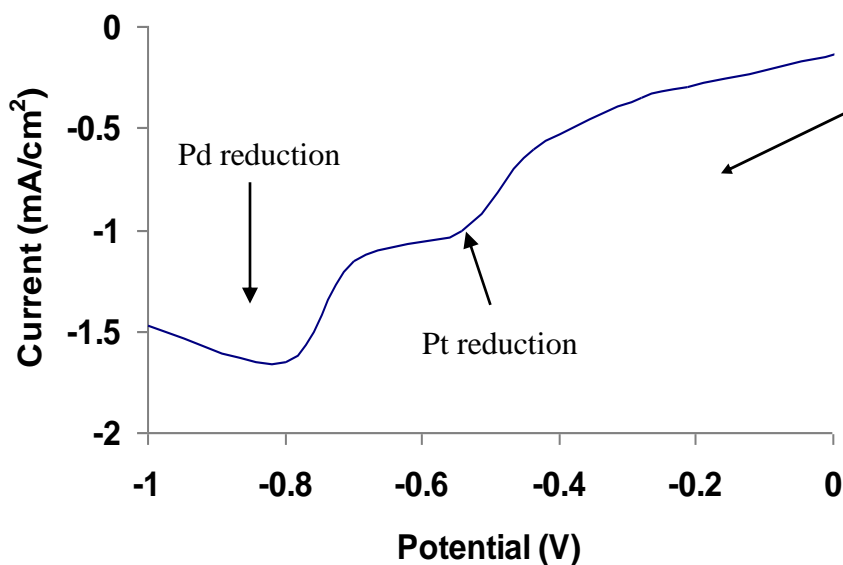


Figure 3.4(c): LSV illustrating Pt and Pd deposition (salt solution of aqueous 0.001 M  $K_2PtCl_4$  and 0.009 M  $PdCl_2$ ), Platinum10:90Palladium in deaerated 0.1 M  $KNO_3$ .

On this basis and the oxidation/reduction characteristics shown in figure 3.4(a), further palladium catalysts were deposited by the equivalent charge passed as outlined in section 2.6, for platinum electrodes. In the case of the electrode in figure 3.4(c), the deposition was allowed to progress uncontrolled by charge passed such as 120 mC/cm<sup>2</sup>. The Pd appears to be present at approximately -0.75 V vs. MMS in the PtPd deposition solution.

### 3.5 Ethanol Oxidation Reaction on palladium catalysts

Figure 3.5(a) shows an overlaid plot highlighting the difference in ethanol oxidation between various electrodes from different  $M^{2+}$  deposition solutions. The total  $M^{2+}$  concentration was kept constant to 10 mM for each CIE. As mentioned previously, the composition of the electrodes appears to greatly affect the EOR.

In agreement with the findings of Gupta with rhodium<sup>9</sup>, the initial EOR, peak A, on the forward scan becomes more prevalent with increasing palladium content in the deposition solution. However at a ratio of Pt50%Pd50%, the current observed is substantially lower than that of the three other compositions examined in this near neutral electrolyte. This agrees with the suggestion that there exists a symbiotic relationship. The EOR takes place due to the bifunctional mechanism outlined in figure 1(d) between the metals on each isolated island on the CE surface, until a particular amount of the secondary metal, in this case palladium, causes the blocking of the reaction from taking place, effectively inhibiting the EOR. Notably, since peak A becomes increasingly apparent at lower potentials as the palladium content increases, supporting a theory that the palladium is aiding the oxidation to take place with less energy input than at a platinum deposit. By elemental mapping, the catalysts at either extreme of the deposition solution accurately represent the catalyst present on the electrode and moreover, the surface island composition.

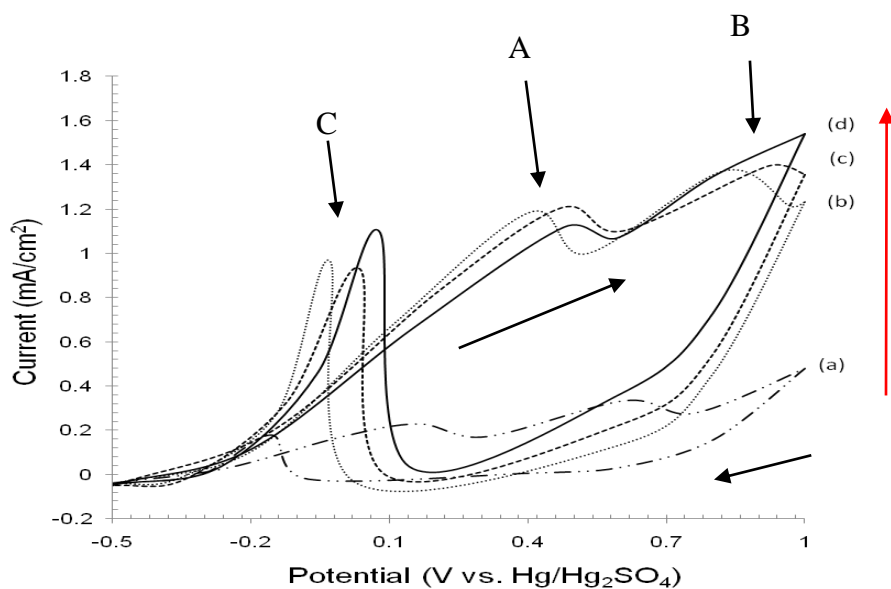


Figure 3.5(a): Cyclic voltammogram for the oxidation of ethanol at a platinum:palladium multimetallic electrodes in 0.5 M  $C_2H_5OH$  and deaerated 0.1 M  $KNO_3$  at a scan rate of 10 mV/s, 10<sup>th</sup> sweep corresponding to a charge passed of 120 mC/cm<sup>2</sup> through the following deposition solutions (a) 50%:50% (b) 75%:25% (c) 90%:10% (d) 100%:0%, pH = 6. The arrow indicates decreasing Pd content.

Interestingly, this work shows that the EOR is still prevalent in near neutral solution, rather than the common use of extreme pH. The current is comparable to that seen in acid previously on a platinum/CIE in section 2.9. It has been suggested previously that a detrimental aspect of neutral electrolyte is the weaker ionic strength, but the less corrosive conditions than extreme pH is beneficial in a real DEFC. Furthermore, Nafion<sup>®</sup> membranes are stated to be able to operate in a pH range that includes near neutral pH. For this reason, the already established Nafion<sup>®</sup> and acid conditions can be built upon for neutral pH. The onset potential is also lower with Pd electrodes than the 100% platinum electrode, indicating that the initial water dissociation step to form  $OH_{ads}$  takes place

quicker at palladium than at platinum.<sup>21</sup> Peak A is comprised of the water dissociation step as well as the adsorption and oxidation of ethanol for all metals<sup>22</sup> and the product formed has been reported by Subtractively Normalised Interfacial Fourier Transform Infra Red Spectroscopy (SNIFTIRS) as correlating to the presence of adsorbed acetate. SNIFTIRS uses laser beams to reflect off the catalyst surface to determine the products detected by Fourier Transform Infra Red (FTIR) spectroscopy. Other techniques used to identify EOR products include Mass Spectrometry where the mass is used to discern between different products. Again however, a range of substances have been claimed including methane. A wide range of products have been determined from the same catalyst. The initial onset potential of peak A is outlined for the first sweep in figure 3.5(b). The initial oxidation on a fresh surface occurs to a greater extent at the 25% palladium electrode.

The onset potential is reportedly that the  $\text{OH}_{\text{ads}}$  species on the palladium electrode is enables the reaction to take place more rapidly. In neutral media, the dissociation of water is required to produce  $\text{OH}^-$  to form  $\text{OH}_{\text{ads}}$  as outlined in equation 3 previously.<sup>23</sup>

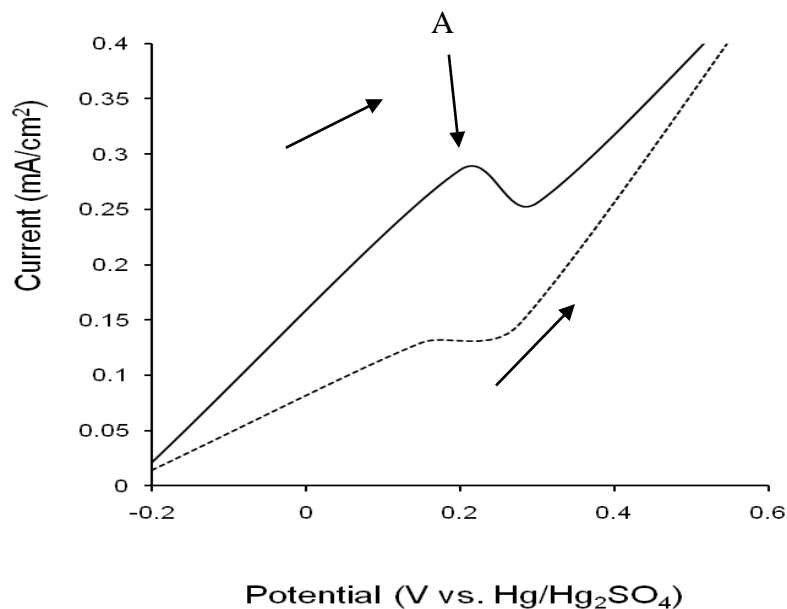


Figure 3.5(b): Cyclic voltammogram for the initial oxidation of ethanol at a Pt75%:Pd25% ( $120 \text{ mC/cm}^2$  in deaerated  $0.1 \text{ M KNO}_3$ ) bimetallic electrodes in  $0.5 \text{ M C}_2\text{H}_5\text{OH}$  and deaerated  $0.1 \text{ M KNO}_3$  at a scan rate of  $10 \text{ mV/s}$ , 75%:25% solid line, Pt100%:Pd0% dashed line,  $\text{pH} = 6$ .

The formation of hydroxyl groups provides the necessary oxygen to complete oxidation or initiate oxidation with less applied potential. When a catalyst originates from a deposition solution comprising of a high percentage  $\text{Pd}^{2+}$  in solution (in excess of 75%Pd), the voltammetry observed is noticeably different as shown in figure 3.5(c).

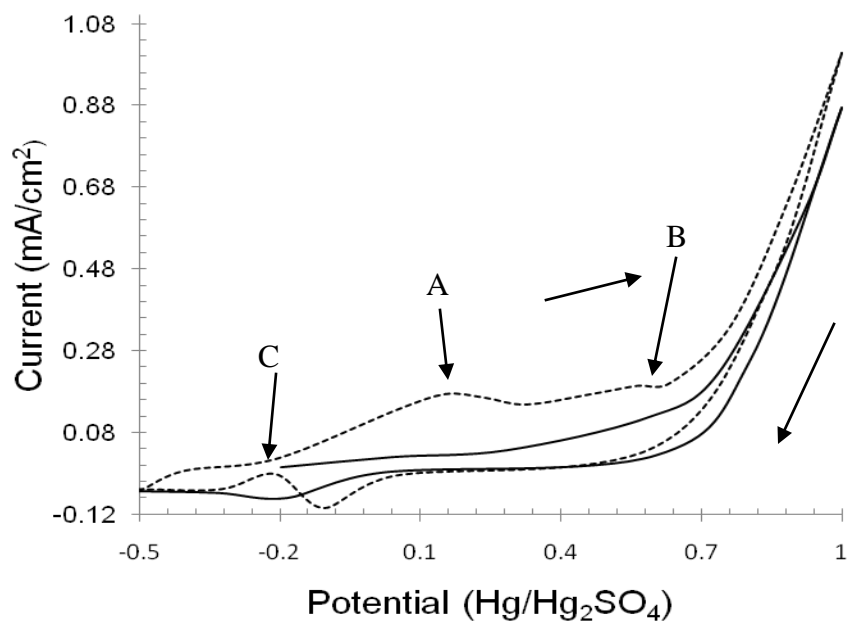


Figure 3.5(c): Cyclic voltammogram showing the oxidation of ethanol at a Pt10%Pd90% (120 mC/cm<sup>2</sup> in deaerated 0.1 M KNO<sub>3</sub>) electrode in 0.5 M C<sub>2</sub>H<sub>5</sub>OH and deaerated 0.1 M KNO<sub>3</sub> with MMS reference electrode, at a scan rate of 10 mV/s, 1<sup>st</sup> sweep (solid line), 2<sup>nd</sup> sweep (dashed line), pH = 6.

The current measured is considerably diminished from that of the electrodes with deposition solutions with higher Pt content, highlighting the importance of platinum in the oxidation of the ethanol. However peak A was observed to be more prevalent than that of peak B in high Pd catalysts. This indicates that peak B is more reliant on the adsorption of ethanol or the oxidation of an adsorbed species. When there is a deficiency of Pt, the Pd atoms do not act as a substitute. This helps elucidate some information on the mechanism from the CVs collected. Similar data has been found for other multimetallic electrodes in research conducted by Gupta and Datta.<sup>9</sup> With decreasing platinum content, the lower potential peak is the single peak observed for ethanol

oxidation. This was reported as a function of the deactivation of the electrode by strong metal oxide bonding where significant oxygen was found to be adsorbed at the surface, inhibiting ethanol oxidation. From the current observed and voltammetric characteristics, a Pt 75%: Pd25% electrode was chosen for further work in this chapter. The stated goals of decreasing the precious metal content for equal or improved behaviour is best matched by this selection.

### **3.6 Increasing pH for the Ethanol Oxidation Reaction at palladium catalysts**

Lai and Koper *et al.* suggest studies on the effect of electrolyte pH on the EOR have been significantly less for a pH range between pH 2 - pH 10.<sup>28</sup> This is despite advantages of employing electrolytes that are not strongly acidic.<sup>28</sup> Figure 3.6(a) shows a cyclic voltammogram of a palladium deposited electrode at high pH in ethanol solution, with one large peak on the forward sweep with a very sharp 'cut-off' or potential where the catalyst is deactivated at 0.85 V vs. MMS.

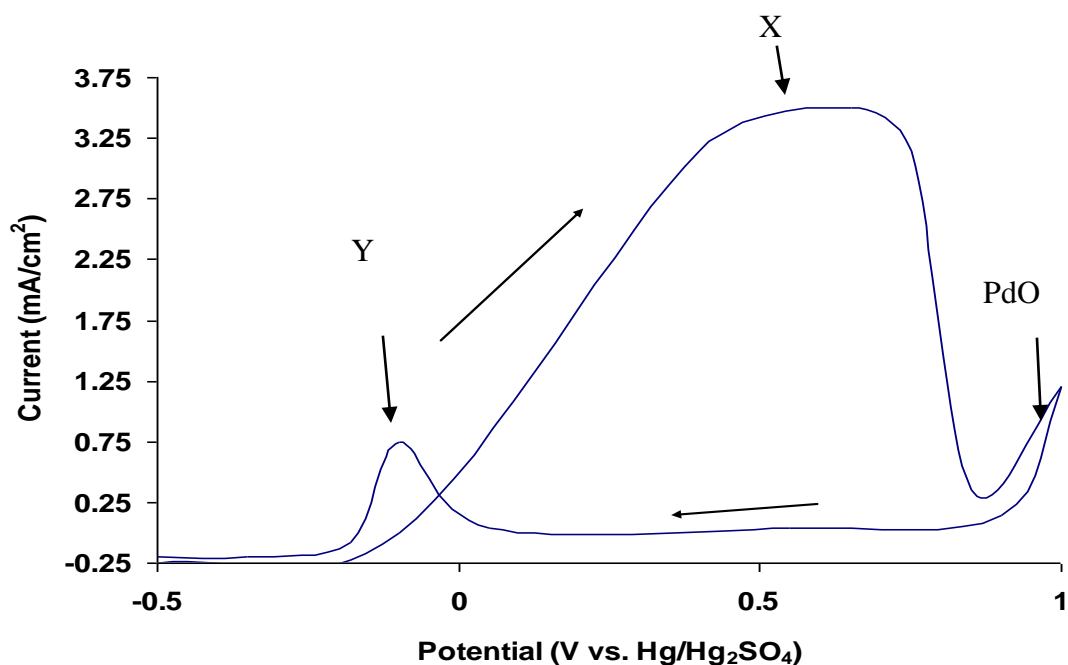


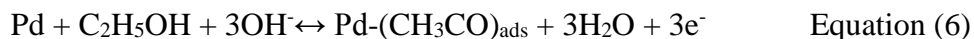
Figure 3.6(a): Cyclic voltammogram of a 100% Pd electrode ( $120 \text{ mC/cm}^2$  in deaerated  $0.1 \text{ M KNO}_3$ ), 1<sup>st</sup> sweep in  $0.5 \text{ M C}_2\text{H}_5\text{OH}$  and deaerated  $1 \text{ M NaOH}$  with an MMS reference electrode at a scan rate of  $10 \text{ mV/s}$ ,  $\text{pH} = 14$ .

Work conducted by Gupta and Datta<sup>9</sup> on platinum group metals indicates that the strength of the M-O bond formed at high potentials could cause electrodes to become deactivated. On the reverse scan, one oxidation peak of substantially less magnitude is observed, in line with the observations for alcohol oxidation at platinum and bimetallic electrodes previously.

Above  $0.85 \text{ V vs. MMS}$ , the collapse in current is clear, supporting the argument that Pd-O acts as an inhibitor to the EOR at high potentials. The signature return of oxidation peak C at  $0 \text{ V vs. MMS}$  is indicative that the peak on the positive sweep is associated with the EOR. For electrodes not active to ethanol oxidation, this peak is not present. The

one peak on the forward sweep (peak X) and one single oxidation peak (peak Y) is often a characteristic of ethanol oxidation in high pH environments. However, the current observed is still a little lower than that observed at a Pt75%Pd25% electrode in figure 3.6(b), hinting that the bifunctional mechanism still applies in terms of optimum conditions at these electrodes. Platinum can act on the carbon-hydrogen bonds of ethanol and palladium facilitates oxidation as well as perhaps contributing considerably more than that in near neutral pH conditions.

The current at Pd in high pH is considerably larger than that of the featureless voltammetry – with respect to ethanol oxidation - observed in acidic or neutral conditions. This is in agreement with the unsuitable Pd chemistry, as stated in section 3.1, which in strongly acidic conditions, suffers from the preferential adsorption of hydrogen onto its surface. As a result, near neutral media and alkaline media allows for a wider spectrum of supporting material and for non-platinum based catalysts.<sup>29, 30, 31</sup> To summarise, palladium is active in high pH towards the EOR to acetate production via formation of PdOH<sub>ads</sub>. This then reacts with the adsorbed intermediate (COCH<sub>3</sub>)<sub>ads</sub>, according to the equation 6<sup>31</sup>, 7<sup>32</sup> and overall equation 8 below:



This has been exploited throughout the field of palladium research on a variety of supports, co-catalysts and conditions, often with gold and platinum in alkaline media.<sup>33-65</sup> With growing attention on alkaline reactions for their increased current and non-platinum catalysts, alkaline exchange membranes are becoming more desirable.<sup>66</sup>

Figure 3.6(b) shows a cyclic voltammogram of a bimetallic electrode from a deposition solution of Pt75%Pd25% with platinum in ethanol at different pH. The magnitude of the current is also in agreement with work completed at near neutral pH,<sup>28</sup> in comparison to that at pH 14 where the electrocatalytic current is three to four times larger. This difference agrees with work conducted by Koper *et al.*<sup>28</sup>

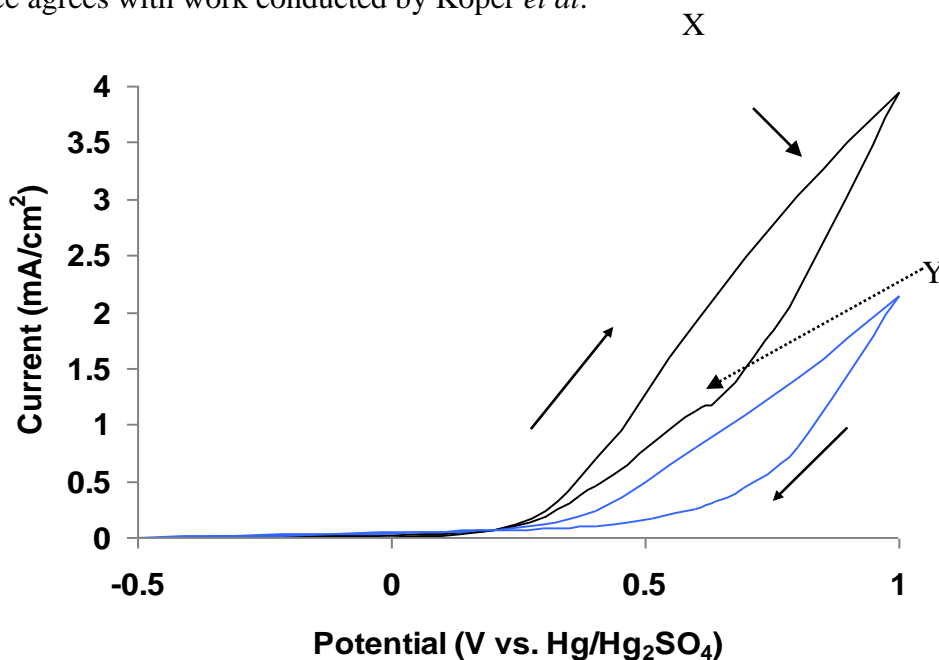


Figure 3.6(b): Cyclic voltammogram of Pt:Pd electrode 75%:25% deposition solution (120 mC/cm<sup>2</sup> in deaerated 0.1 M KNO<sub>3</sub>), 1<sup>st</sup> sweep (black line) and 10<sup>th</sup> sweep (blue line) in 0.5 M C<sub>2</sub>H<sub>5</sub>OH and deaerated 1 M NaOH with MMS reference electrode and at a scan rate of 10 mV/s, pH = 14.

Figure 3.6(b) shows more detail to that of platinum and that peak C is not observed, indicating more complete oxidation, as peak C represents an adsorbed intermediate or a poison, such as CO. With greater amounts of OH<sup>-</sup> available, the EOR can proceed faster without requiring the dissociation of water required at lower pH values. Carbon monoxide oxidation has been observed at 0 V vs. MMS on a platinum surface as outlined in section 2.5.

### **3.7 Effect of temperature on palladium bimetallic catalysts**

Temperature has been studied in order to increase the rate of the EOR. Figure 3.7(a) shows a plot of a Pt:Pd electrode, from a deposition solution containing 75%Pt and 25%Pd in ethanol at 303, 318 and 333 K respectively in near neutral pH. The increase in current observed is found to be at a maximum at 333 K. Above 343 K it was found the plot was more unstable as the bubbles and evaporation of ethanol were affecting the voracity of the data. In general, this agrees with similar operation of the DEFC at temperatures below 373 K. An *et al.*<sup>25</sup> demonstrated a theoretical fuel cell operating at a maximum temperature of 333 K. Li has similarly recorded a fuel cell operating at 313 K.<sup>26</sup> Increasing the temperature lowers the energy barrier required to increase the reaction rate and this is observed in increased current in figure 3.7(a). The reaction mechanism occurs with the same characteristics as in KNO<sub>3</sub> at room temperature, with peaks A, B and C present at elevated temperature.

Typically fuel cells operate at higher than room or ambient temperature to exploit this increased current with increased temperature. It can be seen that despite the increase in temperature, the voltage where peaks A and B occur shift to ever increasing potential values, highlighted in figure 3.7(a) with a red arrow. This indicates that increasing energy is required to catalyse the EOR for peaks A and B. Peak C upon reduction of the M-O bond formed at higher potentials remains consistent indicating that this is a defined potential for the oxidation of an adsorbed poison – potentially CO.

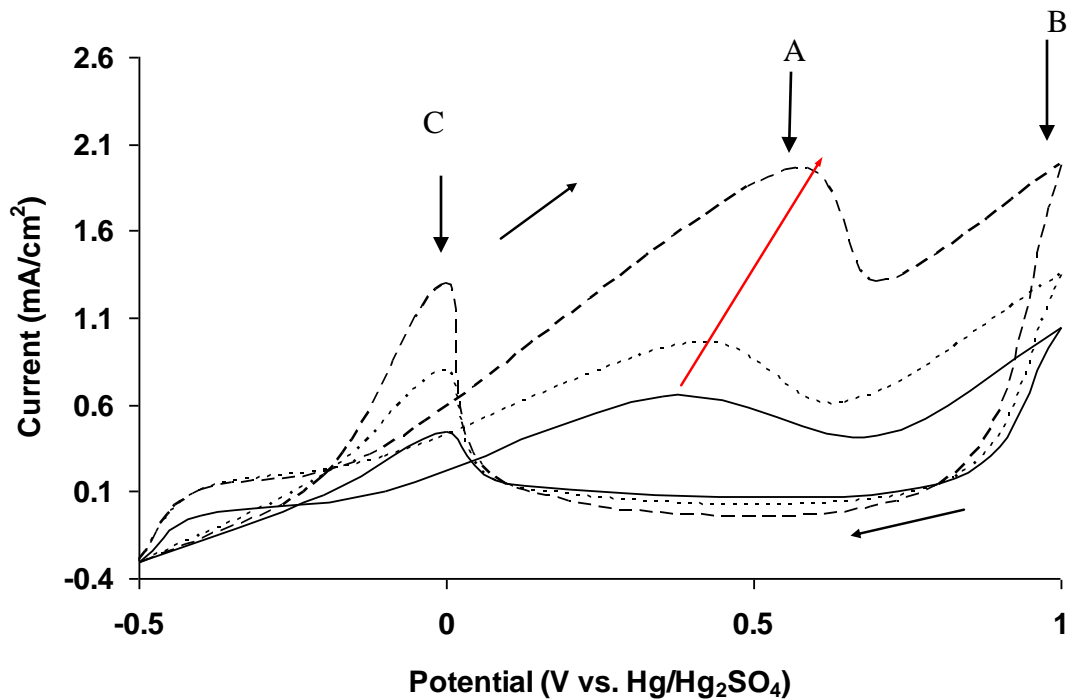


Figure 3.7(a): Overlaid cyclic voltammograms illustrating a Pt:Pd electrode 75%:25% ( $120 \text{ mC/cm}^2$  in deaerated  $0.1 \text{ M KNO}_3$ ),  $303 \text{ K}$  (solid line),  $318 \text{ K}$  (dashed line),  $333 \text{ K}$  (broken line) in deaerated  $0.1 \text{ M KNO}_3$  and  $0.5 \text{ M C}_2\text{H}_5\text{OH}$  with an MMS reference electrode at a scan rate of  $10 \text{ mV/s}$ ,  $\text{pH} = 6$ .

Furthermore, the backward sweep is featureless until the metal oxide reduction region is reached, despite simultaneous oxidation is still in progress at +1.0 V vs. MMS as a competing reaction. This compares to two peaks observed at low current and then substantially increased current at previous electrodes associated with M-O formation at +1.0 V vs. MMS, such as the Pt25%:Pd75% catalyst in section 3.5. As mentioned previously in Chapter 1, particular fuel cells use high temperatures to operate, such as the Solid Oxide Fuel Cell (SOFC), in excess of 973 K. At lower temperatures, fuel cells have been found operating at 333 K.<sup>25</sup> The increase in the use of alkaline media and alkaline membranes in fuel cells has been dictated by the thermal stability of the alkaline exchange membranes which limits the cell performance.<sup>25</sup>

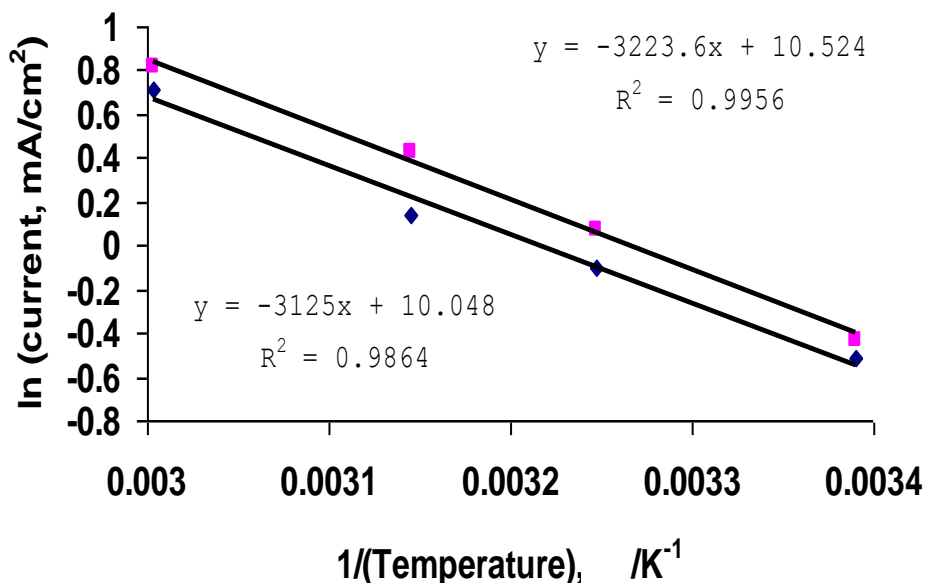


Figure 3.7(b) Arrhenius plot for ethanol oxidation at +1.0 V vs. MMS observed in 0.5 M ethanol and deaerated 0.1 M KNO<sub>3</sub> at a scan rate of 10 mV/s at temperatures of 295 K, 308 K, 318 K, 333 K, electrodeposit/CIE (120 mC/cm<sup>2</sup> in deaerated 0.1 M KNO<sub>3</sub>), with an MMS reference, first sweep (blue = Pt, pink = Pt75%Pd25%).

The increase in current observed for the EOR at increased temperature means that a major criterion for the ethanol fuel cell is the physical properties of the Anion Exchange Membrane, AEM.<sup>27, 68</sup> Using the equations shown in section 2.13 in equations 9 and 10 below, the Arrhenius plot was constructed in figure 3.7(b).

$$\ln k = \ln A - E_a/R (1/T) \quad \text{Equation (9)}$$

$$\text{slope} = -E_a/R \quad \text{Equation (10)}$$

Using the slope of the Arrhenius plot, the activation energy barrier on the palladium catalyst at +1.0 V is lower than that of platinum. The value of the activation energy,  $E_a$ , for the palladium electrode was 26.801 kJ/mol compared to 27.710 kJ/mol at a platinum electrode (section 2.13) with an error of 10% over the set of readings. The activation energy is mid-range with values in literature between 24 and 60 kJ/mol as described in chapter 2. This decrease highlights very slightly improved catalysis in the energy required to start the reaction.

### **3.8 Chronocoulometry and potential step testing**

Figure 3.8(a), figure 3.8(b) and figure 3.8(c) illustrate the chronocoulometric data integrated from the current time plots collected from the open circuit potential, (OCP), to 0.4 V vs. MMS, at both near neutral pH and at high pH electrolyte. At OCP, there is no current and after applying the step to 0.4 V vs. MMS, the data applies to the reaction taking place, i.e. for the peak corresponding to the initial adsorption/oxidation step in

near neutral media observed in previous sections. The advantage of using chronocoulometry is the possibility to determine the charge associated with adsorbed species on the surface of the electrode from the intercept on the charge axis.<sup>67</sup> However complex relationships are noted from the data presented and published by Pletcher.<sup>68</sup> There is a period of inactivity or lag time where  $t^{1/2} < 0.2$ . Pletcher assigns this lag time to a complex relationship for a specific unrelated system to the EOR surrounding the rate of the back reaction where it is negligible.<sup>68</sup>

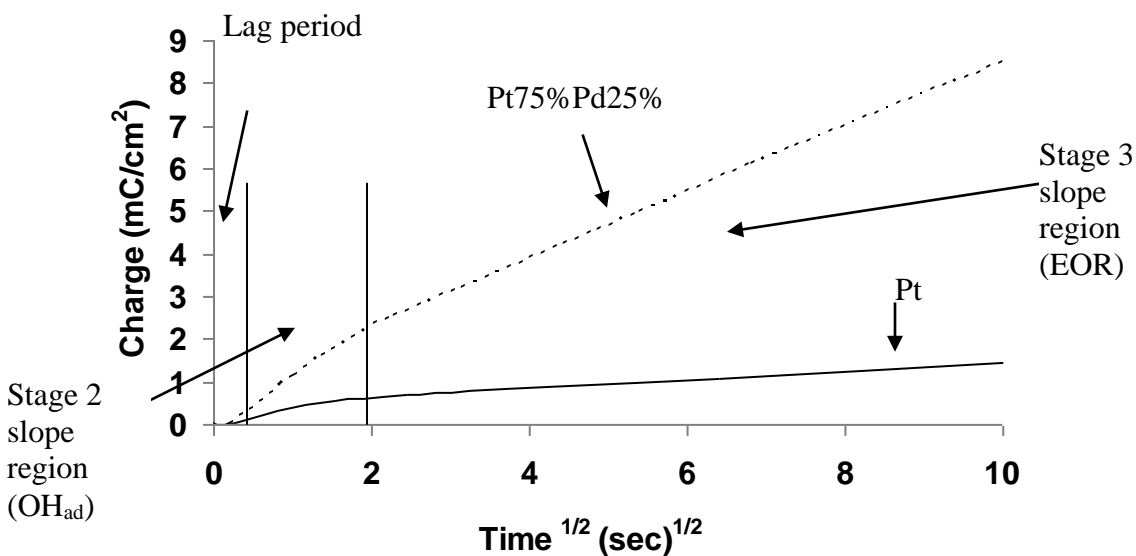


Figure 3.8(a): Chronocoulometric data for a Pt75%Pd25% deposition solution, (120 mC/cm<sup>2</sup> in deaerated 0.1 M KNO<sub>3</sub>), dashed line and Pt100%, solid line, 0.5 M ethanol and deaerated 0.1 M KNO<sub>3</sub> from OCP to 0.4 V vs. MMS.

As the rate of the reaction increases, a decreasing intercept on the  $t^{1/2}$  axis should be observed. These separate regions in 0.1 M KNO<sub>3</sub> could be determined and will be outlined in further detail in section 4.5. This hypothesis agrees with the data previously

observed in this work that the electrocatalysis is a relatively slow and complex process with several stages.

After this initial 'lag' or induction period in near neutral media, two separate slopes are observed, reported as two different processes taking place. Figure 3.8(b) shows the potential step collected at a Pt75%Pd25% electrode applied from 0.4 V to 0.45 V. By starting at a potential where PdOH<sub>ads</sub> formation has already started, a different profile to the charge vs. time plot was recorded. There were not the same features present compared to the potential step from 0 V vs. MMS to 0.4 V vs. MMS. This may be due to the now readily available OH species for ethanol oxidation progresses. The lag period was still evident from the carbon electrode.

Initially the dissociative adsorption of water has to take place to facilitate oxidation on the metal surface. The second slope observed at longer periods of time may be the initial oxidation step of ethanol. The Pt/Pd bimetallic electrode shows increased charge, however both electrodes undergo identical induction periods. Figure 3.8(c) shows the same potential step in basic media.

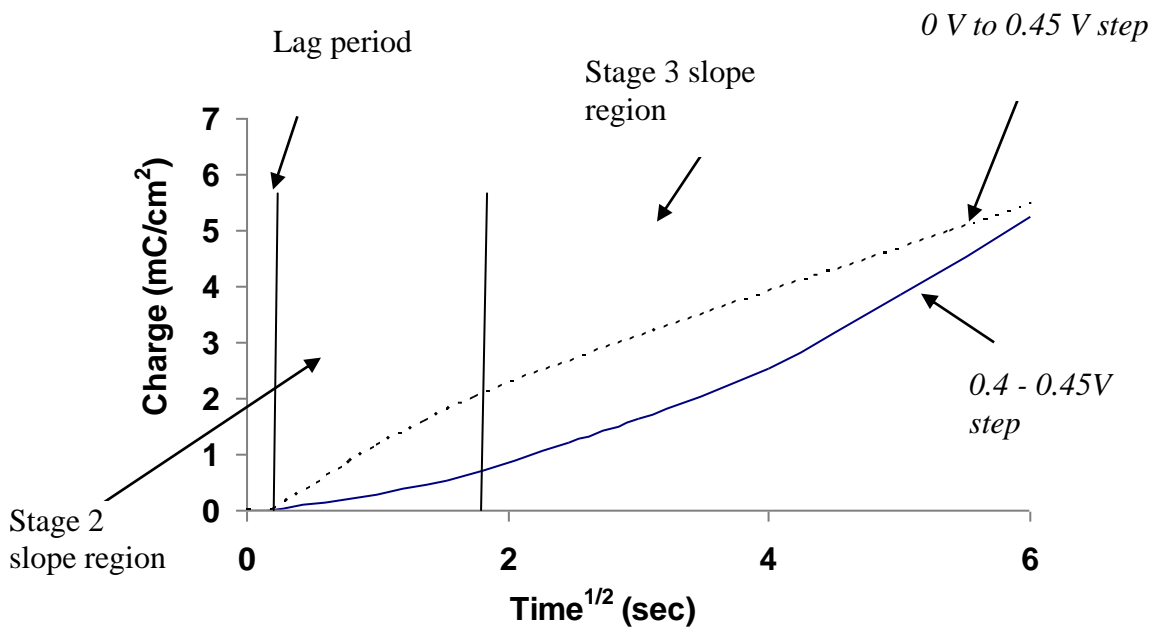


Figure 3.8(b): Chronocoulometric data for a Pt75%Pd25% deposition solution, (120 mC/cm<sup>2</sup> in deaerated 0.1 M KNO<sub>3</sub>), from OCP to 0.4 V vs. MMS (dashed line), from 0.4 V to 0.45 V (solid line), 0.5 M ethanol and deaerated 0.1 M KNO<sub>3</sub>.

The 'lag' period at short timeframes is again observed, but it is shorter by a factor of 2. Furthermore, there is a rapid increase in charge collected over the same time period compared to near neutral media, though the palladium electrode still collects the highest charge. This may be due to the ready availability of OH<sup>-</sup> in comparison to that water dissociation required in KNO<sub>3</sub> or lower pH.

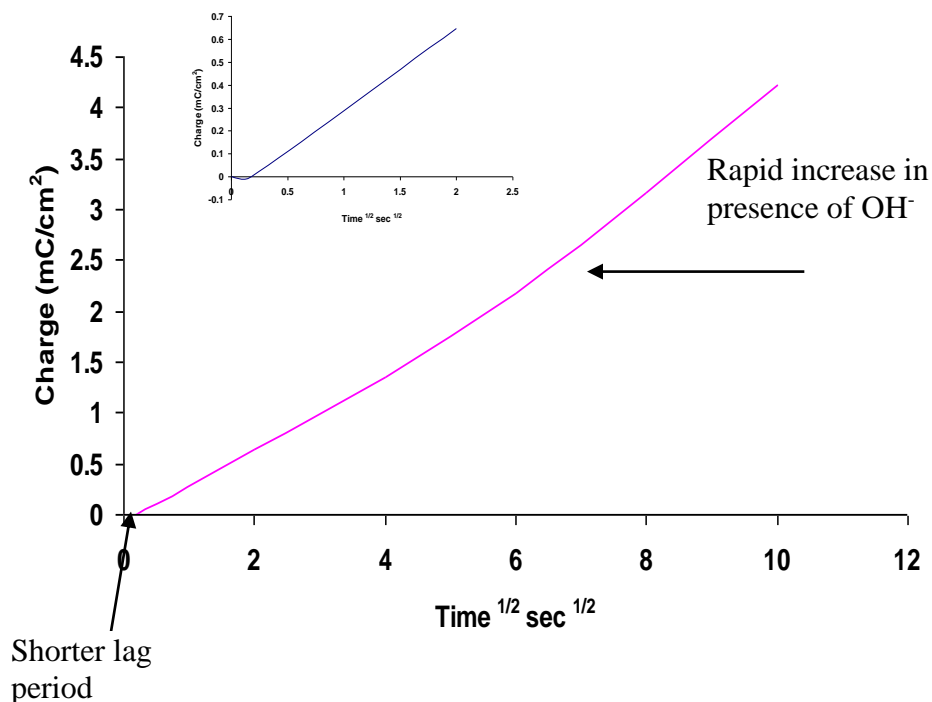


Figure 3.8(c): Chronocoulometric data for a Pt:Pd electrode 75%:25% deposition solution, (120 mC/cm<sup>2</sup> in deaerated 0.1 M KNO<sub>3</sub>), (solid line) in 0.5 M C<sub>2</sub>H<sub>5</sub>OH and deaerated 1 M NaOH, from OCP to 0.4 V vs. MMS. (inset – induction period at 0-0.2 s<sup>1/2</sup> of the main data plot).

The availability of OH<sup>-</sup> in solution in basic media may be the cause of this immediate and exponential increase as well as the second potential step in neutral electrolyte, as the reaction is more immediate without the water dissociation step. Figure 3.8(d) shows the direct comparison in charge between near neutral and high pH for the potential step.

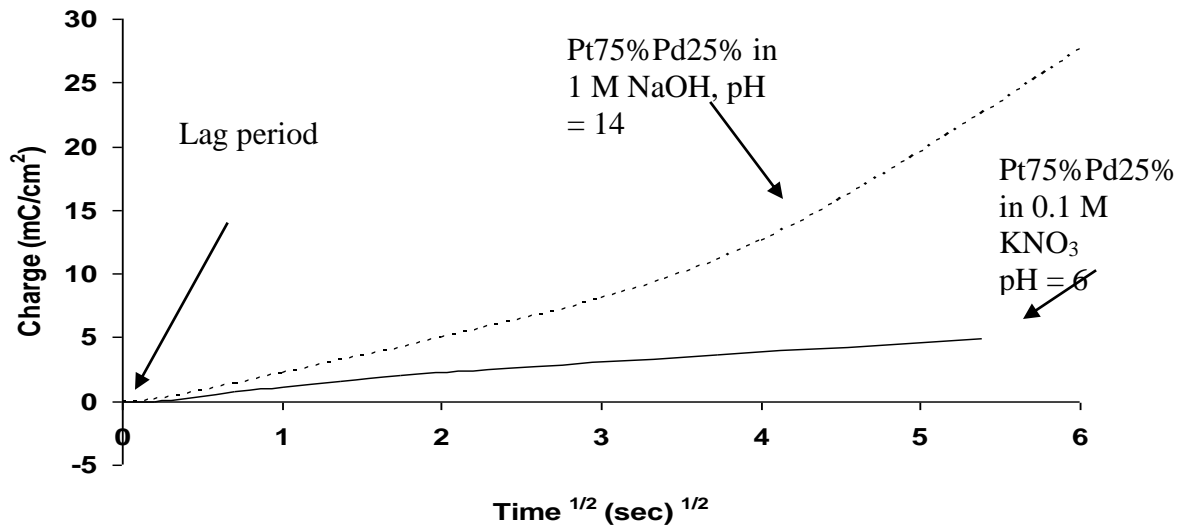


Figure 3.8(d): Chronocoulometric data for a Pt:Pd electrode 75%:25% deposition solution (deaerated 0.1 M  $\text{KNO}_3$ ), in deaerated 1 M NaOH and 0.5 M  $\text{C}_2\text{H}_5\text{OH}$  (dashed line) and 0.1 M  $\text{KNO}_3$  and 0.5 M  $\text{C}_2\text{H}_5\text{OH}$  (solid line), in from OCP to 0.4 V vs. MMS.

The Pt75%:Pd25% electrode in 1 M NaOH shows considerably greater charge than all three other electrodes and environment combinations. Furthermore, when the potential step was increased from OCP to further data points, the charge was found to increase or decrease in line with the distance from 0.4 V vs. MMS.

When the initial potential was taken from the potential associated with peak A or peak B rather than OCP, similar interesting results were found in  $\text{KNO}_3$ . With the potential stepped from 0.40 V to 0.45 V, the appearance of the data appeared to be similar to that in basic media which has been stepped from OCP – a rapid increase instead of the two different slopes and the lag period had been halved from 0.04 s to 0.02 s compared to current time plot in figure 3.8(a).

### 3.9 Effect of scan rate on Ethanol Oxidation Reaction at palladium catalysts

Figure 3.9(a) below illustrates overlaid CVs taken from a variety of different scan rates.

The best performing electrode, Pt75%Pd25% was selected to examine the impact of scan rate on a palladium electrode.

As observed with platinum in section 2.15, the features evident at 10 mV/s are less clear as the scan rate increases. However, the current is notably increased from approximately 0.8 mA/cm<sup>2</sup> to 1.82 mA/cm<sup>2</sup>, a twofold increase for peak A. Peak B is unclear in the same potential window, but the peak was present at 1.2 V vs. MMS with a wider upper potential limit. Furthermore, a similarity is observed to that at a platinum electrode in the shift in potential between the maximum current for peak A and peak B, whereas peak C remains consistent, taking off at 0 V vs. MMS. This positive shift in potential indicates that the reaction requires more energy as the EOR progresses, though the current produced is increasing. For this reason, 10 mV/s was determined to be a suitable scan rate for bimetallic catalysts in later sections. As mentioned previously, the range of scan rates published ranges from 10 mV/s to 100 mV/s, typically being the midpoint, 50 mV/s.

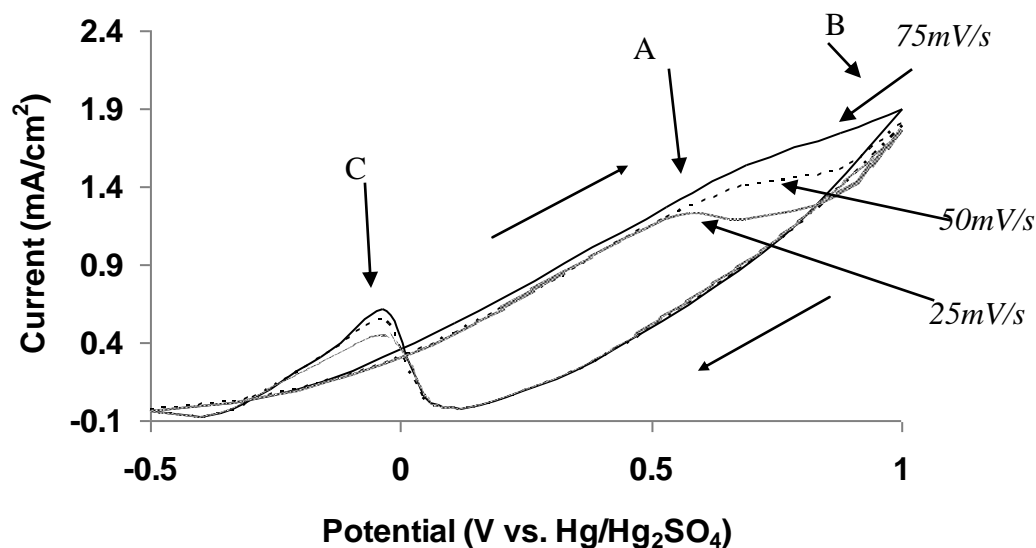


Figure 3.9(a): Cyclic voltammogram showing different scan rate of Pt75%Pd25% ( $120 \text{ mC/cm}^2$  in  $0.1 \text{ M KNO}_3$ ) CPE, at selected scan rates:  $75 \text{ mV/s}$  (solid line),  $50 \text{ mV/s}$  (dashed line),  $25 \text{ mV/s}$  (shaded line). Ethanol oxidation with  $0.5 \text{ M C}_2\text{H}_5\text{OH}$  in deaerated  $0.1 \text{ M KNO}_3$  ( $10^{\text{th}}$  sweep), with an MMS reference electrode,  $\text{pH} = 6$ .

As with results obtained with the carbon ink and carbon paper electrodes, it was found that the slower the scan rate applied, the more detailed in voltammetry observed, allowing the reaction to be illustrated. At higher scan rates, above  $100 \text{ mV/s}$ , very little detail could be established by voltammetry more than the appearance of a broad peak assigned to peak C on the returning cathodic sweep. To help determine whether peak C is an adsorption process or the re-oxidation of the fuel, the peak current was plotted against the scan rate from  $10 \text{ mV/s}$  to  $75 \text{ mV/s}$  and a linear increase was obtained. The linear decrease can be seen from figure 3.9(a) that larger currents for peak C are obtained at lower scan rates as this allows the EOR to occur with such slow kinetics. A linear plot indicates an adsorption process.

Figure 3.9(b) shows the EOR for a fresh Pt75%Pd25% electrode run to shorter terminal potentials. It is clear that peak A is apparent on the forward scan (dashed line) up to 0.4 V. When the terminal potential is shortened to 0.2V vs. MMS, neither peak A or C is observed.

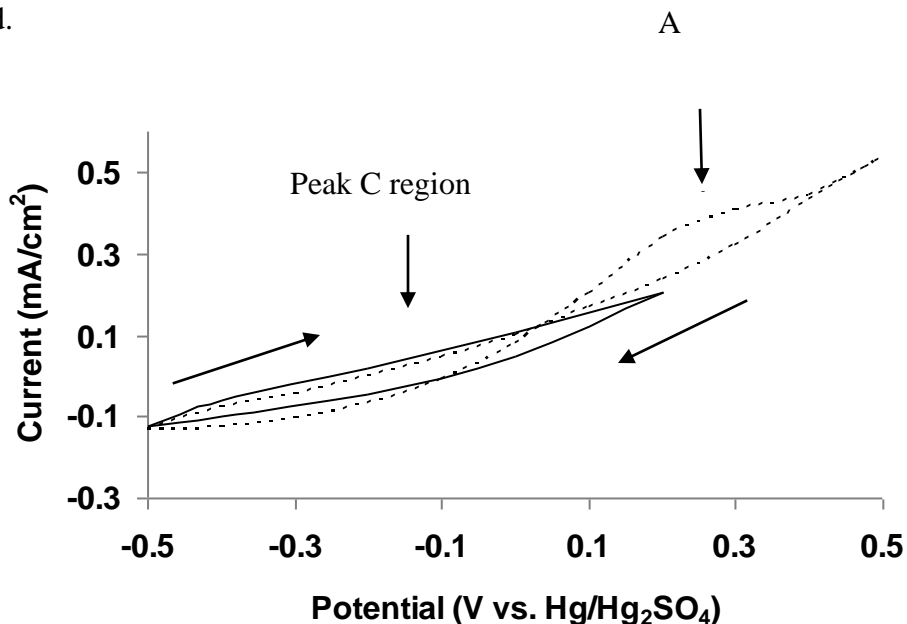


Figure 3.9(b): Cyclic voltammogram showing different terminal potentials of Pt75%Pd25% deposit/CPE (120 mC/cm<sup>2</sup> in 0.1 M KNO<sub>3</sub>), at a scan rate of 10 mV/s, 0.5 M C<sub>2</sub>H<sub>5</sub>OH in deaerated 0.1 M KNO<sub>3</sub>. Terminal potential of 0.2 V vs. MMS (solid line) on first sweep, terminal potential of 0.5 V vs. MMS (dashed line) on second sweep, pH = 6.

It is thought that peak C occurs as a direct result of an adsorbed intermediate formed by the reaction at peak B. This intermediate is most likely carbon monoxide, though multiple intermediates have been found as a product in this reaction. Peak A does not produce an adsorbed intermediate available for oxidation at 0 V vs. MMS, which is where peak C is normally observed. As a result, it can be concluded that peak A is a mix of the water

dissociation and initial ethanol adsorption, as opposed to an ethanol oxidation step (peak B).

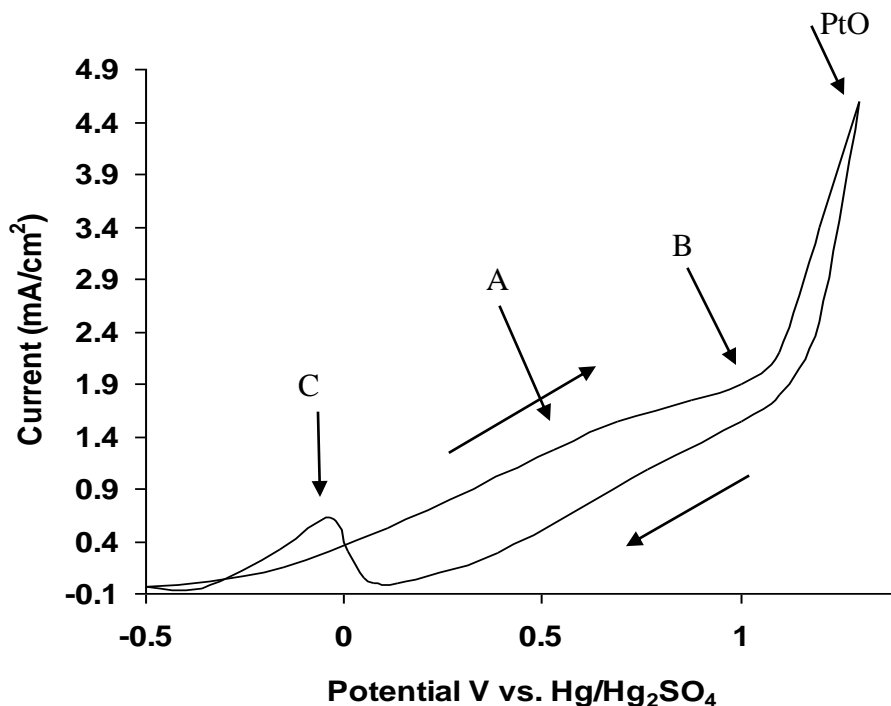


Figure 3.9(c): Cyclic voltammogram of a Pt75%Pd25% (120 mC/cm<sup>2</sup> in 0.1 M KNO<sub>3</sub>) deposit/CPE, at selected scan rates: 75 mV/s (solid line). Ethanol oxidation with 0.5 M C<sub>2</sub>H<sub>5</sub>OH in deaerated 0.1 M KNO<sub>3</sub>, (10<sup>th</sup> sweep) with an extended potential window to 1.4 V vs. MMS, pH = 6.

Figure 3.9(c) shows the extended potential window for a Pt75%Pd25% electrode at a scan rate of 75 mV/s. The current collected and features are identical to those in figure 3.9(a) on the forward and negative scans between -0.5 V and +1.0 V vs. MMS. When the window is extended in order to record the far side of peak B and, as such, prove the presence of peak B at 75 mV/s, the current associated with Pt oxidation masks any reaction underneath, similar to that observed for hydrogen evolution and electrodeposition noted in chapter 2. The rapid increase in current at 1.4 V vs. MMS is in

excess of  $4.3 \text{ mA/cm}^2$ . As a result, the maximum useful upper potential limit in this work is  $+1.0 \text{ V}$ . The presence of peak C should be an indication that ethanol oxidation is occurring at  $+1.0 \text{ V}$  as peak C does not occur without alcohol oxidation.

### 3.10 Conclusions

Palladium was chosen as a catalyst to enhance ethanol oxidation on platinum. It was found that at peak A, the initial adsorption of ethanol onto the catalyst surface, the current was higher at Pt75%Pd25% electrode compared to that of a Pt100% electrode. The composition of the electrode was determined SEM-EDX analysis. This increased current was ascribed to the first step of the bifunctional mechanism for ethanol oxidation where palladium reacts with water to form  $\text{PdOH}_{\text{ads}}$  more readily than platinum.

A measure of the enhanced oxidation is the onset potential for peak A. The onset potential was found to be slightly lower at the Pt75%Pd25% electrode than for a 100% platinum electrode. When the palladium content of the bimetallic catalyst was increased, the performance of the electrode was extensively decreased. When Pt10%Pd90% catalysts were used, the voltammetry changed where peak A, the initial oxidation step, become more prominent in relation to peak B and the opposite was recorded at a 100%Pt electrode. This indicated that while the first oxidation peak is affected by lower platinum content, but that the second peak is dependent on ethanol adsorption. Peak B was assigned to the oxidation of a  $\text{C}_2$  substance, which contains a carbon-carbon bond, one of which is acetaldehyde. A 100% palladium electrode was found to be active towards the

EOR in 1 M NaOH with one broad oxidation peak on the forward scan. There was over a threefold increase in current in 1 M NaOH when compared to the bimetallic catalysts.

A potential step was conducted at the palladium catalysts. The subsequent chronocoulometry data obtained showed a ninefold increase in charge compared to the Pt100% electrode in potassium nitrate electrolyte and a further fivefold increase in 1 M NaOH for a Pt75%Pd25% electrode. The charge collected in neutral media was distinct from that collected in high pH electrolyte. The Anson plot obtained showed a lag period of 0.2 s which resulted in an intercept on the time axis rather than the typical intercept on the charge axis associated with  $Q_{dl}$ . This was ascribed to the availability of  $OH^-$  and the resistance of the electrode. In high pH the lag period is decreased and the charge increased rapidly in comparison to neutral media.

There were two distinct slopes as charge increased in  $KNO_3$  and these were described as the initial dissociation of water to produce  $OH_{ads}$  for ethanol oxidation to progress. When the potential step was moved to a starting potential from OCP, 0 V, to where  $OH_{ads}$  had been initiated in neutral media, from 0.4 V up to 0.45 V, the charge collected exhibited the same features as 1 M NaOH where OH is readily available. This indicated that the dissociation of water is a key competing process for peak A. This process does not produce an adsorbed intermediate which contributes towards peak C. Peak C is only observed as an adsorbed intermediate from the reaction at peak B or ethanol oxidation at 0.8 V vs. MMS.

### 3.11 References:

1. Shen, P.K.; Xu, C.; (2006), *Electrochem. Comm.*, **8**, 184-188.
2. Bockris, O'M. J.; Reddy, K.N., A; Gamboa-Aldeco, M.; (2000) "Modern Electrochemistry 2A – Fundamentals of Electrodeics", Chp. 7, 1275-1277.
3. Chen, X-m.; Lin, Z-j.; Jia, T-t.; Cai, Z-m.; Huang, X-l.; Jiang, Y-q.; Chen, X.; Chen, G-n.; (2009), *Anal. Chim. Acta*, 54-58.
4. Fang, X.; Wang, L.; Shen, P.K.; Cui, Bianchini, C.; (2010), *J. Power Sources*, **15**, 1375 – 1378.
5. Xu, C.W.; Wang, H.; Shen, P.K.; Jiang, S.P.; (2007), *Adv. Mater.*, **19**, 4256.
6. Xu, C.W.; Liu, Y.L.; Yuan, D.S.; (2007), *Int. J. Electrochem. Sci.*, **2**, 674.
7. Liu, J.P.; Ye, J.Q.; Xu, C.W.; Jiang, S.P.; Tong, Y.X.; (2008), *J. Power Sources*, **177**, 67-70.
8. Chen, Y.; Zhuang, L.; Lu, J.; (2007), *Chinese J. Catal.*, **28**(10), 870-874.
9. Gupta, S.S., Datta, J., (2006), *J. Electroanal. Chem.*, **594**, 665-669.
10. [www.kitco.com/charts/rhodium](http://www.kitco.com/charts/rhodium), viewed May 2015.
11. Liu, J., Ye, J., Xu, C., Jiang, S.P.; Tong, Y., (2007), *Electrochem. Comm.*, **9**, 2334-2339.

12. Del Colle, V., Berna, A., Tremiliosi, G., Herrero, E., Feliu, J.M., (2008) *Phys. Chem. Chem. Phys.*, **10**, 3766.
13. Antolini, E. (2007), *Appl. Catal. B: Environ.*, **74**, 3-4, 337-350.
14. Hammer, B.; Norskov, J.K, (2000) *Adv. Catal.*, **45**, 71.
15. Demirci, U.B., (2007), *J. Power Sources*, **173**, 11-18.
16. He, T., Kreidler, E., Xiong, L., Ding, E., (2007), *J. Power Sources*, **165**, 87-91.
17. [www.kitco.com/historical/charts/palladium](http://www.kitco.com/historical/charts/palladium), viewed May 2015.
18. [www.kitco.com/historical/charts/platinum](http://www.kitco.com/historical/charts/platinum), viewed May 2015.
19. <http://minerals.usgs.gov/minerals/pubs/commodity/platinum/550401.pdf>, viewed May 2014.
20. Gonzalez, E.R.; Tremiliosi Filho, G.; International Electrochemistry Conference, Nice, October 2010.
21. Burke, L.D.; Healy; O'Dwyer; O'Leary; (1989), *J. Electrochem. Soc.*, **136**, 4.
22. Gupta, S.S.; Datta, J.; (2005) *J. Chem. Sci.*, **117**, 4, 337-344.
23. Liang, J.; Scott, K.; (2010), *Electrochim. Acta*, **6**, 224-241.
24. Hui, C.L.; Li, X.G.; Hsing I-M.; (2005), *Electrochim. Acta*, **51**, 711-719.
25. An, L.; Zhao, T.S.; Chen, R.; Wu, Q.X.; (2011), *J. Power Sources*, **196**, 6219-6222.

26. Li, Y.S.; Zhao, Z.X.; Liang, J.; (2009), *J. Power Sources*, **187**, 387-392.
27. Varcoe, J.R.; Slade, R.T.; (2005), *Fuel Cells*, **5**, 187-200.
28. Lai, S.C.S.; Kleijn, S.E.F.; Oeztuerk, F.T.Z.; van Rees, V.C.; Vellinga; Koning, J.; Rodriguez, P.; Koper, M.T.M.; (2010), *Catal. Today*, **154**, 92-104.
29. Kiros, Y.; Schwartz, S.; (2000), *J. Power Sources*, **87**, 101-105.
30. Kim, J.W.; Park, S.W.; (2003), *J. Electrochem. Soc.*, **150**, E560-E566.
31. Wang, L.; (2010), *J. Power Sources*, **195**, 8036-8043.
32. Yi, Q.; Niu, F.; Sun, L.; (2011), *Fuel*, **90**, 2617-2623.
33. Xu, C.; Tian, Z.; Chen, Z.; Jiang, S.P.; (2008), *Electrochem. Comm.*, **10**, 246-249.
34. Shen, S.Y. ; Zhao, Xu, J.B.; Li, Y.S.; (2010), *J. Power Sources*, **195**, 1001-1006.
35. Huang, J-J.; Hwang, W-S.; Weng, Y-C; Chou, T-C; (2009), *Mater. Trans.*, **50**, 1139-1147.
36. Bianchini, C.; Bambagioni, V.; Filippi, J.; Marchionni, A.; Vizza, F. ; Bert, P.; Tampucci, A. ; (2009), *Electrochem. Comm.*, **11**, 1077-1080.
37. Liu, J, Ye, J, Xu, C., Jiang, S.P.; Tong, Y; (2008), *J. Power Sources*, **177**, 67-70.
38. Antolini, E.; (2009), *Energ. Environ. Sci.*, **2**, 915-931.
39. Wang, H. ; Xu, C. ; Cheng, F. ; Jiang, S.; (2007), *Electrochem. Comm.*, **9**, 1212-1216.

40. Xu, C.; Shen, P.K.; Liu, Y.; (2007), *J. Power Sources*, **164**, 527-531.
41. Nguyen, S.T.; Law, H.M.; Nguyen, H.T.; Kristian, N.; Wang, S.; Chan, S.H.;  
Wang, X.; (2009), *Appl. Catal. B: Environ.*, **91**, 507-515.
42. Cheng, T.T.; Gyenge, E.L.; (2009), *J. Appl. Electrochem.*, **39**, 1925-1938.
43. Hasan, M.; Newcomb, S.B.; Rohan, J.F.; Razeeb, K.M.; (2012), *J. Power Sources*, **218**, 148-156.
44. Su, Y., Xu, C.; Liu, J.; Liu, Z. ; (2009), *J. Power Sources*, **194**, 295-297.
45. Shen, S.Y. ; Zhao, T.S. ; Wu, Q.X. ; (2012), *Int. J. Hydrogen Energ.*, **37**, 575-582.
46. Wang, D. ; Liu, J.; Wu, Z.; Zhang, J.; Su, Y.; Liu, Z.; Xu, C.; (2009), *Int. J. Electrochem. Sci.*, **4**, 1672-1678.
47. Yu, E.H. ; Krewer, U. ; Scott, K.; (2010), *Energies*, **3**, 1499-1528.
48. He, Q.; Chen, W.; Mukerjee, S.; Chen, S.; Laufek, F.; (2009), *J. Power Sources*, **187**, 298-304.
49. Xu, J.B.; Zhao, T.S.; Li, Y.S.; Yang, W.W.; (2010), *Int. J. Hydrogen Energ.*, **35**, 9693-9700.
50. Oliveira, M.C. Rego, R.; Fernandes, L.S.; Tavares, P.B.; (2011), *J. Power Sources*, **2011**, 6092-6098.
51. Liu, Z.; Zhao, B.; Guo, C.; Sun, Y.; Shi, Y.; Yang, H.; Li, Z.; (2010), *J. Colloid Interf. Sci*, **351**, 233-238.

52. Pierozynski, B.; (2013), *Int. J. Electrochem. Sci.*, **8**, 634-642.
53. Liu, J.; Ye, J.; Xu, C.; Jiang, S.P.; Tong, Y.; (2007), *Electrochem. Comm.*, **9**, 2334-2339.
54. Bianchini, C.; Shen, P.K.; (2009), *Chem. Rev.*, **109**, 4183-4206.
55. Nguyen, S.T.; Si Lang Tan, D.; Lee, J-M. ; Chan, S.H. ; Wang, J.Y. ; Wang, X. ; (2011), *Int. J. Hydrogen Energ.*, **36**, 9645-9652.
56. Dutta, A.; Mahaptra, S.S.; Datta, J.; (2011), *Int. J. Hydrogen Energ.*, 1-9.
57. Nagle, L.C. ; Burke, L.D. ; (2010), *J. Solid State Electr.*, **14**, 1465-1479.
58. Zhou, Z-Y.; Wang, Q.; Lin, J-L. Tian, N.; Sun, S-G.; (2010), *Electrochim. Acta*, **55**, 7995-7999.
59. Xie, S-W.; Chen, S.; Liu, Z-Q.; Xu, C-W.; (2011), *Int. J. Electrochem. Sci.*, **6**, 882-888.
60. Lai, S.C.S.; Koper, M.T.M., (2009) *Phys. Chem. Chem. Phys.*, **11**, 10446.
61. Xu, C.; Tian, Z.; Shen, P.;Jiang, S.P.; (2008), *Electrochim. Acta*, **53**, 2610-2618.
62. She, P.L.; Yao, S.B.; Zhou, S.M.; (1999), *Chinese Chem. Lett.*, **10** (5), 407-410.
63. Wang, Y.; Nguyen, T.S.; Liu, X.; Wang, X.; (2010), *J. Power Sources*, **195**, 2619-2622.
64. Yan, Z.; Meng, H.; Shi, L.; Li, Z.; Shen, P.K.; (2010), *Electrochem. Comm.*, doi:10.1016/j.elecom.2010.03.007.

65. Zhu, L.D.; Zhao, Xu, J.B.; Liang, Z.X.; (2009), *J. Power Sources*, **187**, 80-84.
66. Yu, E.H.; Scott, K.; (2014), *J. Power Sources*, **137**, 248-256.
67. Datta, J.; Dutta, A.; Mukherjee, S.; (2011), *J. Phys. Chem. C*, **115**, 15324-15334.
68. Zhao, T.S. Li, Y.S.; Shen, S.Y.; (2010), *Energ. Power Eng. China*, **4** (4), 443-458.
69. Bott, AW; Heineman, WR; (2004), *Curr. Sep.*, **20**, 4.
70. Pletcher, D; “Southampton Group: Instrumental Methods in Electrochemistry”, (2001), Horwood Publishing, P.55-58.

#### **Chapter Four: Nickel electrocatalysts and Tafel analysis**

## 4.1 Introduction

In this chapter, the role and contribution of nickel (Ni) within electrodeposits as working electrodes is explored in order to determine its suitability as a catalyst. In addition, Tafel analysis was carried out on various electrodes at selected potential ranges. Tafel plots are taken from very slow scan rates, below 5 mV/s and it can be used to analyse kinetic data for a catalyst in various operating conditions and to determine exchange current density values,  $j^0$ .

Transition metals such as Ru, Sn, Mo, Os, Pd and Bi as well as Fe, Co and Ni have been used as alternative non-PGM based catalysts.<sup>1-3</sup> Furthermore, considerable work has been conducted on transition metals with respect to platinum free ORR.<sup>4-6</sup> As the recent trend for DEFC operation in basic media becomes more feasible, such transition metals have come into focus for the ethanol oxidation reaction<sup>1,7-9</sup> and nickel has shown interesting prospects for promoting the overall rate of the EOR<sup>10</sup> depending on the surface.<sup>3</sup> When Ni is used as a bimetallic electrode, Ni is oxophilic<sup>10</sup>, generating nickel oxides, NiO<sub>2</sub>, and nickel oxyhydroxides, NiOOH.<sup>11</sup> In addition, there are multiple proposed EOR mechanisms in different media and how nickel acts upon the EOR. Recent work by Su<sup>10</sup> reported that nickel modifies the d-band centre of palladium, facilitating ethanol adsorption, and then nickel oxides refresh the surface sites of palladium<sup>12</sup>, the morphology of nickel spheres<sup>13</sup> and through nickel alloys.<sup>11</sup> Consequently, nickel was selected to study a non-PGM surface to study the EOR, with the ultimate goal of identification and testing of a platinum free catalyst.

Throughout the chapter, the various nickel oxides and hydroxides formed will be discussed along with their potential relationship to the contribution of nickel in a DEFC electrocatalyst. A combination of both platinum and palladium will be discussed as a comparison, developing from the work presented in earlier chapters 2 and 3. Platinum in particular, is not sufficiently oxophilic to provide enough oxygen species for further ethanol oxidation, particularly at low potential.<sup>11</sup> The oxides and hydroxides that readily form on Ni surfaces could play a large role in ethanol oxidation<sup>14</sup> and they have been previously shown to be involved in alcohol oxidation,<sup>4</sup> as well as being used as a substrate for noble metal deposition<sup>3</sup> which may be considered as a cost effective alternative to the use of gold or other precious metals. Finally, Tafel analysis was carried out with respect to the EOR in order to determine the kinetics of the ethanol reaction.<sup>15</sup> Research by Liu<sup>16</sup> has shown that the Tafel slope calculated can change depending on different reaction conditions and potential regions, providing information on both on reaction activity and the irreversibility of the ethanol oxidation reaction.

The difference between the cost of the more inexpensive metals such as Zn, Ni and Sn are orders of magnitude less than that of gold in 2015,<sup>17</sup> which is often used as a conductive support layer for electrocatalysts. This is a powerful driving force in the current development of the DEFC, particularly enhancement of the ORR and improving the EOR at non-PGM catalyst surfaces.

An example of a nickel-containing electrode currently in development is that of Hypermec AcTa.<sup>18</sup> Nickel is also used in the Alkaline Fuel Cell (AFC) as Raney nickel, a

nickel aluminium alloy. This is primarily due to its ready availability and cost which can replace PGM catalysts for other hydrogen based fuel cells.

## **4.2 Experimental**

Nickel was electrodeposited onto carbon supports which were used as nickel electrodes in a conventional three electrode system. The nickel was deposited from a prepared solution of 0.01M NiCl<sub>2</sub> in ultrapure H<sub>2</sub>O. A mercury/mercury sulphate (MMS, Hg/Hg<sub>2</sub>SO<sub>4</sub>), +640mV vs. SHE, purchased from Radiometer Analytical Instruments (ref 640) was used as the reference electrode with a Pt sheet as an auxiliary electrode. CHI 600A and CHI 620A series potentiostats were used to both perform and to collect the electrodeposition, cyclic voltammetric, chronoamperometry, chronocoulometry data and Tafel plots as required.

Carbon ink electrodes were, as before, prepared by coating a non-porous plastic sheet (Xerox) with a finely dispersed particle-based graphite inside an ink binder solvent (Acheson Industries, Electrodag 423 SS). The ink coating was then allowed to dry. The fabricated electrodes were then sectioned into 1 cm<sup>2</sup> samples used for further testing, acting as working electrodes. A solution of commercial nail polish was added to the stem of each electrode in order to guarantee its geometrical area as described in sections 2.2 and 3.2.

The temperature of the cell was maintained at room temperature, 293 K, and solutions were de-aerated with oxygen-free nitrogen (BOC gases). A range of electrolytes were used, specifically 0.5 M sulphuric acid, 0.1 M potassium nitrate and sodium hydroxide, 1 M NaOH, purchased from Sigma Aldrich. Typically the scan rate was set to 10 mV/s, however a range of scan rates were also employed for some studies ranging between

1 mV/s to 10 mV/s. Pure ethanol was purchased from Sigma Aldrich. The concentration of ethanol was maintained at 0.5 M. The temperature was monitored using an iKa® C-MAG HP7 heating plate.

Tafel plots were obtained at 1 mV/s from a potential step applied from the open circuit potential to 0.4 V vs. MMS in deaerated ethanol and 0.1 M KNO<sub>3</sub> or 1 M NaOH. A variety of catalyst surfaces electrodeposited (120 mC/cm<sup>2</sup>) onto carbon ink electrodes (CIE) and Toray® carbon paper electrodes were employed.

#### **4.3 Ni/C Electrode Appearance:**

Figure 4.3(a) shows an SEM image of a 100% nickel electrodeposit on a carbon ink electrode backbone (Ni/CIE). With 120 mC/cm<sup>2</sup> charge collected, the size of the particles is considerably less than that shown previously of platinum or palladium. The smaller size clusters may aid activity for EOR with a larger surface area and a typical particle size of 12 nm. This particle size is at least three times smaller than both the platinum and palladium particles observed at the same charge in chapter two and three.

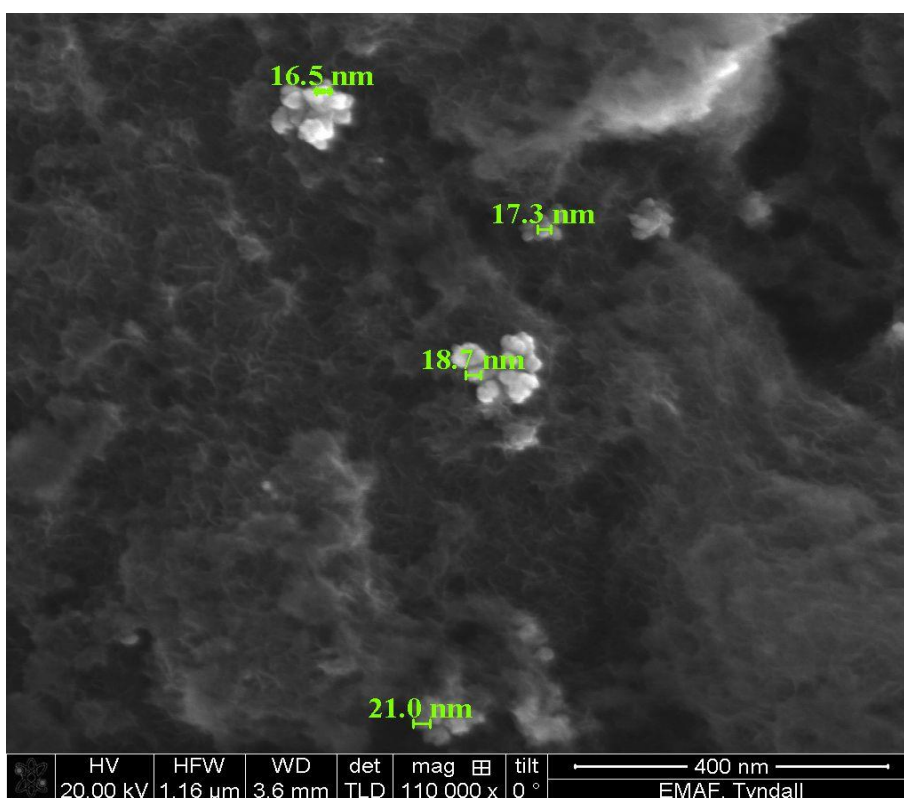


Figure 4.3(a) SEM-EDX image of a nickel electrodeposit/CIE, 120 mC/cm<sup>2</sup>, from an electrodeposition solution containing 0.01 M NiCl<sub>2</sub> and 0.1 M KNO<sub>3</sub>.

Figure 4.3(b) shows an image corresponding to element mapping of a carbon ink electrode with a nickel electrodeposit, where red reflects the presence of nickel. The mapping revealed that a greater quantity of nickel closely packed at the surface instead of

comparatively individual clusters as in figure 4.3(a). When an element map is conducted for carbon in the same area of the electrode, the presence of carbon is not clear at the sections of the electrode covered by the deposit.

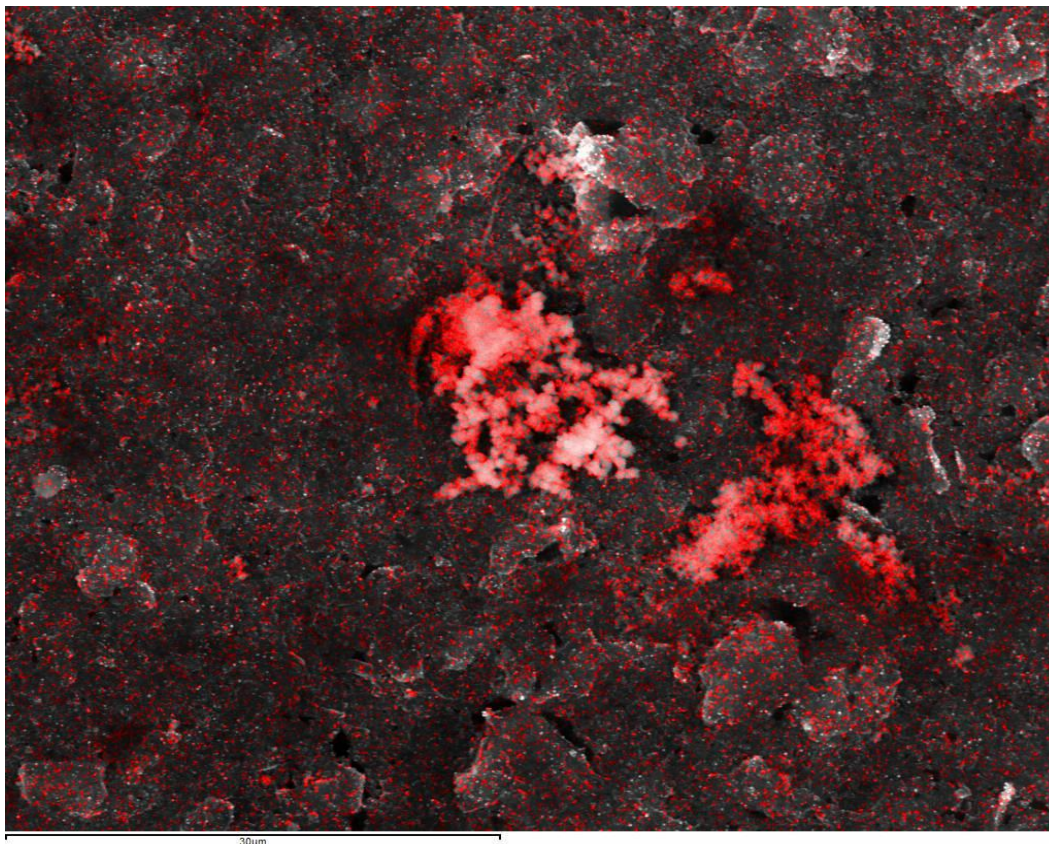


Figure 4.3(b) SEM-EDX and overlaid elemental mapping image of nickel (red) present across a CIE when larger deposits are allowed to develop from an electrodeposition solution containing 0.01 M  $\text{NiCl}_2$  and 0.1 M  $\text{KNO}_3$ .

To characterise the electrode, a CV from open circuit potential (0.5 V vs. MMS) of an electrode with nickel electrodeposit in background electrolyte was conducted (figure 4.3(c)). The current increases slowly from 0 V vs. MMS to 0.4 V vs. MMS before increasing to 0.5  $\text{mA}/\text{cm}^2$  at +1.0 V vs. MMS as a metal oxide, NiO, forms before the

oxygen is reduced in a broad peak, A, at -0.2 V vs. MMS. The presence of this reduction peak was used as an indicator as to the presence of nickel on the carbon ink or carbon paper electrode.

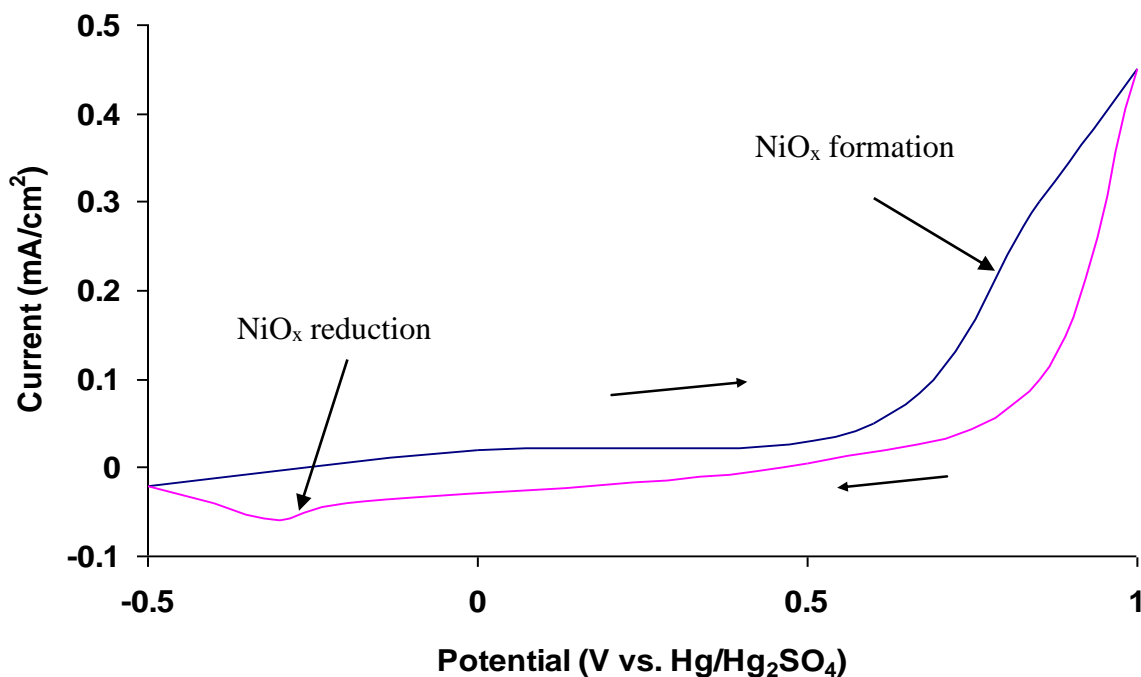


Figure 4.3(c): CV from a 100% nickel electrodeposit/CIE in background electrolyte, 120 mC/cm<sup>2</sup> charge passed at -1.0 V vs MMS in deaerated 0.1 M KNO<sub>3</sub> with an MMS reference electrode at a scan rate of 10 mV/s.

#### 4.4 Electrooxidation of ethanol at nickel electrodes.

One postulated mechanism for the EOR on nickel is shown in equations 1-4 below.<sup>19</sup>

Early work by Motheo<sup>20</sup> suggests that Ni oxidation is limited to NiO<sub>2</sub>, forming acetic

acid and Ni(OH)<sub>2</sub>, based on NiO<sub>2</sub> being stable at pH 14. Riyanto<sup>19</sup> and Tarasevich *et al.*<sup>21</sup> extrapolated that NiOOH was the key species capable of reacting with a number of functional groups<sup>19</sup> from ethanol to form Ni(OH)<sub>2</sub>. Byproducts such as acetaldehyde and acetic acid were determined, concluding that acetic acid is readily formed from acetaldehyde, though the intermediates predicted in equations 1-4 were not identified.



Figure 4.4(a) shows a CV for the ethanol oxidation reaction in near neutral pH obtained from an electrodeposit containing 10% platinum and 90% nickel (by deposition solution) with a total charge of 120 mC/cm<sup>2</sup>. By comparison, figure 4.4(b) shows the CV for the same reaction at a 90% platinum and 10% nickel electrode (by deposition solution). The current observed at the platinum 90% electrode is considerably higher for peak A, the initial ethanol oxidation and water dissociation peak, where the current observed is greater after the initial positive sweep than after four runs of the lower platinum content electrode, returning 0.2 mA/cm<sup>2</sup> compared to 0.17 mA/cm<sup>2</sup> for the higher platinum electrode. However, in figure 4.4(a), the current is observed to increase by a multiple of three to 0.6 mA/cm<sup>2</sup> at pH 6, to the region containing peak B (above 0.4 V vs. MMS) whereas there is a relatively slight increase in figure 4.4(b) from peak A to peak B. The second peak observed on the forward sweep, peak B – assigned to the oxidation of

acetaldehyde in chapter two and three – is aided by the presence of increased formation of oxygen-containing species.

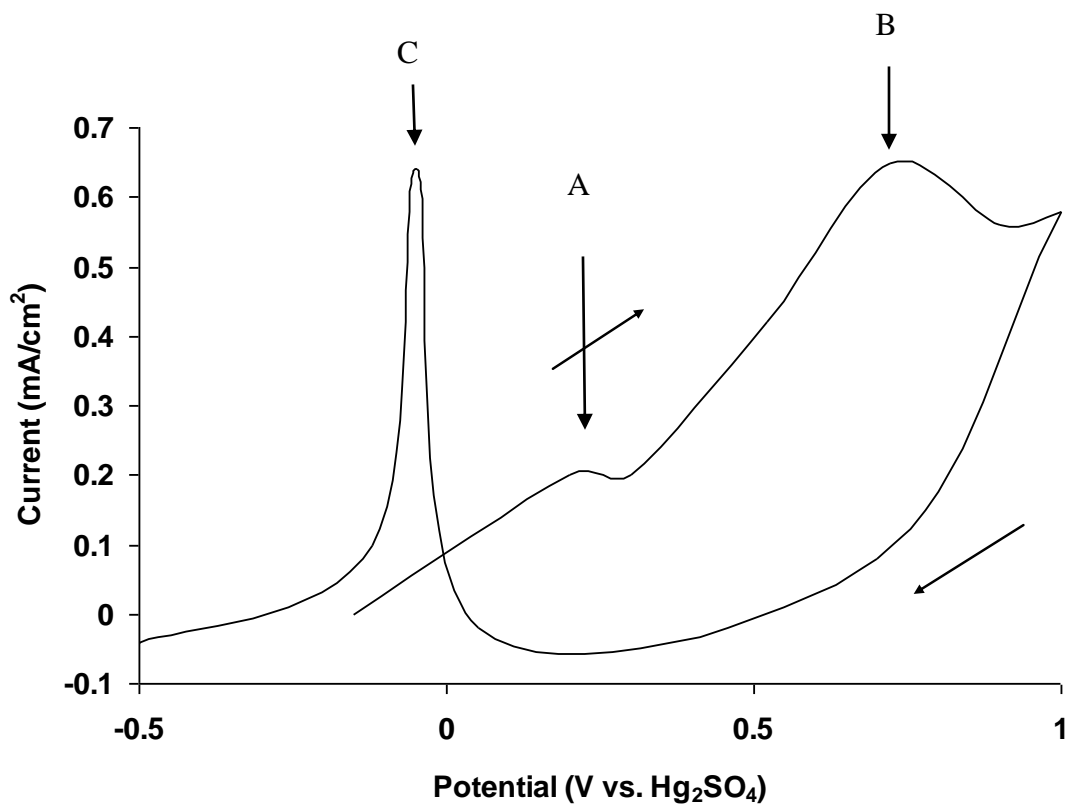


Figure 4.4(a): Cyclic Voltammogram from a Pt10Ni90 on a carbon ink electrode (120 mC/cm<sup>2</sup> in 0.1 M KNO<sub>3</sub>) charge passed at -1.0 V vs. MMS with 0.5 M ethanol and deaerated 0.1 M KNO<sub>3</sub> with an MMS reference electrode at a scan rate of 10 mV/s, pH = 6.

A feature of figure 4.4(b) echoes that of figure 3.9(c), where the full extent of peak B is not observed at pH 6 using the best performing catalyst of Pt90%Ni10%. When the potential window is increased further beyond +1.0 V, the result is similar to that at an increased scan rate. As a result, the peak may be masked under the oxidation current. The

ethanol oxidation associated with peak B is thought to have taken place as peak C, the adsorbed intermediate product of ethanol oxidation directly associated with peak B.

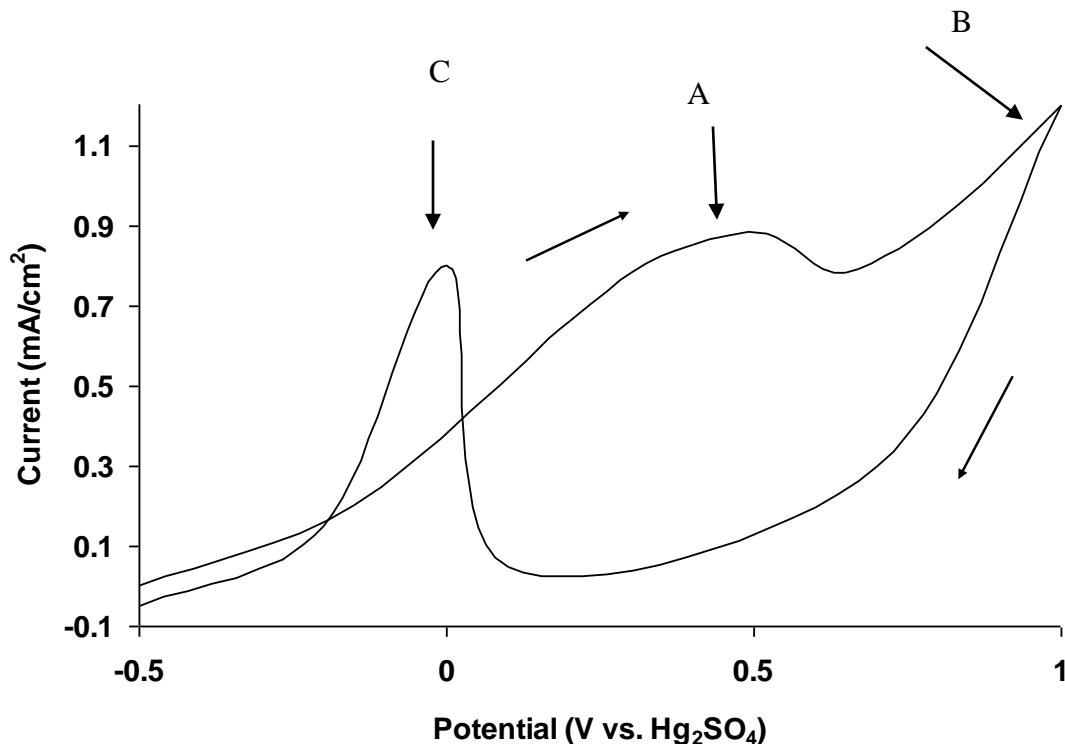


Figure 4.4(b): Cyclic Voltammogram from a Pt90%Ni10%/CIE (120 mC/cm<sup>2</sup> in deaerated 0.1 M KNO<sub>3</sub>) for the EOR, 0.5 M ethanol and 0.1 M KNO<sub>3</sub>, with an MMS reference electrode at a scan rate of 10 mV/s, 1<sup>st</sup> scan.

The oxygen containing species for nickel has been described as predominantly being Ni(OH)<sub>2</sub> and some NiOOH formed from NiOH<sub>aq</sub><sup>22</sup> and that these compounds are the main component of nickel species which promote the EOR in non-acidic conditions. They can both exist according to the reactions shown in equations 5 and 6 below<sup>22</sup>:





When performing the EOR with nickel, the various nickel hydroxides that exist makes it difficult to determine which form is present at a particular moment. The schematic Bode diagram in figure 4.4(c) highlights the various forms of  $\beta$ -NiOOH,  $\gamma$ -NiOOH,  $\alpha$ -Ni(OH)<sub>2</sub> and  $\beta$ -Ni(OH)<sub>2</sub> adapted from Van der Van *et al.*<sup>23</sup> Lyons suggests that Ni(OH)<sub>2</sub> is most readily formed by electrodeposition, however in every case the hydroxyl ion is created forming the  $\alpha$  or  $\beta$  hydroxides and which subsequently form NiOOH.<sup>22</sup>

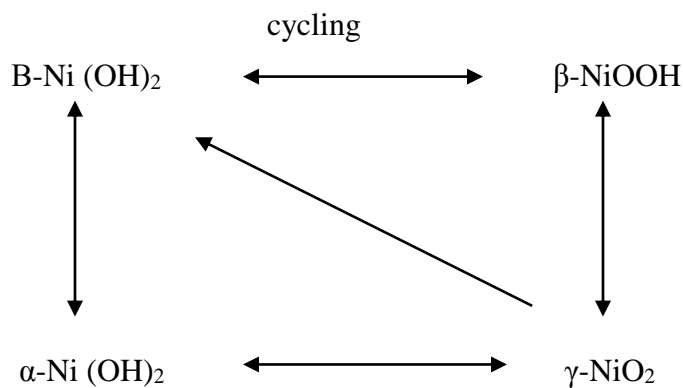


Figure 4.4(c): Bode Diagram showing the various forms of nickel hydroxide, nickel oxide and nickel oxyhydroxides.<sup>23</sup>

As with bimetallic electrodes studied previously in chapter two and three in platinum and palladium, the EOR proved most clear for electrodes with both high and low amounts of the secondary metal – in this case, nickel. At an intermediate catalyst composition, such as Pt50%Ni50% prepared by electrodeposition, the composition of the resultant electrode is unpredictable and when examined by SEM-EDX analysis, bears little relation to that expected from the deposition solution. Similarly, the EOR shows unreliable activity from one electrode to another. However, at either extreme differences are noticed as in figure

4.4(a) and figure 4.4(b). As a comparison to ethanol oxidation at a bimetallic electrode, Pt10%Ni90% [figure 4.4(a)], voltammograms were run at the same electrolyte, pH 6, for an electrode with comparative mass of platinum. The result is shown in figure 4.4(d), for a corresponding platinum loading of 12 mC/cm<sup>2</sup>. It is noticeable that the current obtained at 12 mC/cm<sup>2</sup> Pt is lower than that of the 120 mC/cm<sup>2</sup> Pt10%Ni90% electrode, particularly for the relationship between peak A and peak B as with the comparison between figure 4.4(a) and figure 4.4(b). For these reasons, both the highest performing bimetallic catalyst, Pt90%Ni10% was selected in this work as the best performing catalyst in pH 6 and pH 14. Pt10%Ni90% was selected to judge the effect of the highest current in the presence of nickel and the effect of the nickel oxyhydroxides and hydroxides – particularly for Tafel analysis in section 4.6. As nickel content increases, the balance between CH<sub>3</sub>CO<sub>ads</sub> and OH<sub>ads</sub> alters and the current<sup>12</sup> and power decreases when compared to a platinum group metal surface.

By increasing nickel content, it will also lead to the blockage of platinum sites in NaOH<sup>12</sup> which is not desired as nickel itself has no activity toward ethanol oxidation.<sup>12</sup> Similarly to palladium in neutral to high pH, the Ni(OH)<sub>2</sub>, and consequently the OH<sup>-</sup> ions present, are very readily adsorbed and saturate the platinum sites, retarding the ethanol reaction through the by lack of CH<sub>3</sub>CO<sub>ads</sub>.<sup>12</sup> This process, leading to high concentrations of OH<sub>ads</sub> formed at high potentials, causes the current to rapidly decrease through blockage of the active sites and consequently decreases EOR catalytic activity. Ultimately, the influence of nickel on the EOR can be observed by the current recorded at an equivalent loading of platinum, The equivalent loading of platinum to a 10% platinum, 90% nickel electrode,

12 mC/cm<sup>2</sup> is shown in figure 4.4(d) .The current measured at a platinum electrode is higher (0.4 mA/cm<sup>2</sup>) at lower potentials than the equivalent Pt10%Ni90% electrode (0.2 mA/cm<sup>2</sup>) at low potentials in pH 6 electrolyte, where the presence of large quantities of nickel may be inhibiting the ethanol adsorption, in agreement with the results found by Zhang.<sup>12</sup> However at higher potentials, the current for peak B is increased in the presence of nickel, aiding the EOR. This is different to the results found for palladium, which worked best at lower potentials as described in section 3.5. In figure 4.4(d), an extra feature is recorded, peak D, where the reduction of platinum oxides begin before the oxidation peak, peak C appears as the scan approached 0 V vs. MMS. This re-oxidation is consistent with previous results where the surface Pt-O needs to be removed to make the Pt sites active to the EOR once again.

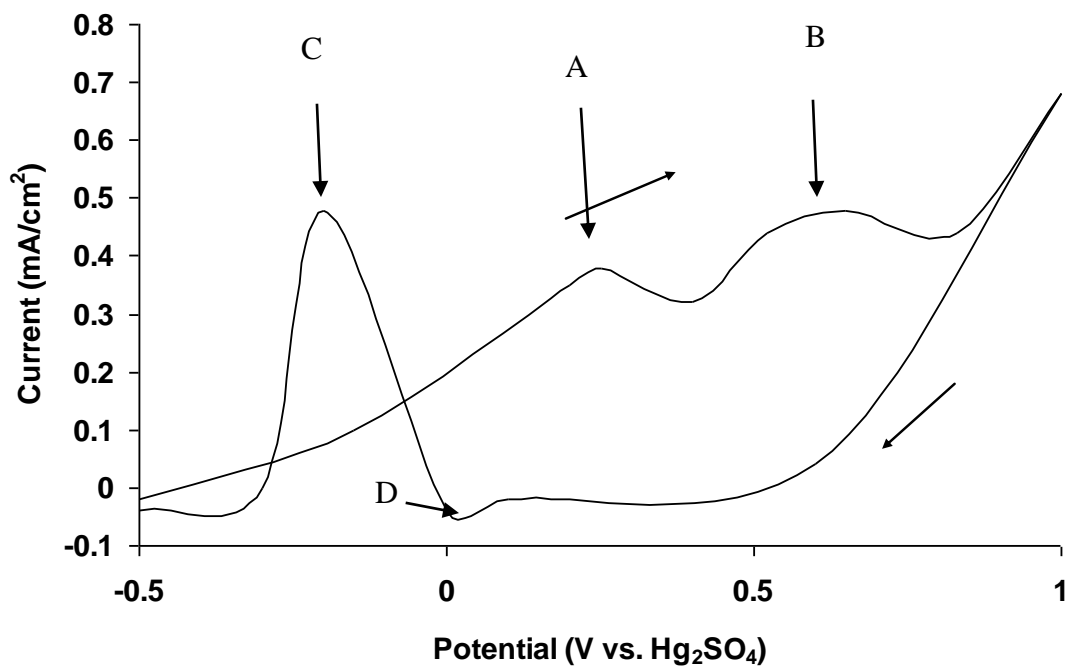


Figure 4.4(d): CV from a Pt100% carbon ink electrode (deposition solution) – 12mC/cm<sup>2</sup> charge passed at -1.0 V vs. MMS for the ethanol oxidation reaction, 0.5 M C<sub>2</sub>H<sub>5</sub>OH and 0.1 M KNO<sub>3</sub> with an MMS reference electrode at a scan rate of 10 mV/s.

Figure 4.4(e) shows the oxidation of ethanol at a Pt10%Ni90% electrode in pH 14, 1 M NaOH. There is one broad shoulder peak on the positive sweep, peak X. After a substantial drop in current as the potential drops to 0.8 V vs. MMS on the negative sweep, there is one clear, broad peak, peak Y, is shown at 0.55 V vs. MMS. This peak is due to the EOR and agrees with the voltammetry observed by Qiu *et al.*<sup>24</sup> Upon repeated cycling, the high availability of OH<sup>-</sup> and consequently, OH<sub>ads</sub> is facilitating the EOR and intermediate product formation, particularly CH<sub>3</sub>CO<sub>ads</sub>. However the current is considerably above that in near-neutral pH. In high pH, the readily availability of OH<sup>-</sup> ions is commonly reported as a consequence of the presence of Ni(OH)<sub>2</sub>.<sup>1, 22</sup> As shown in equation 6, Ni(OH)<sub>2</sub> can frequently form NiOOH as shown in figure 4.4(c).

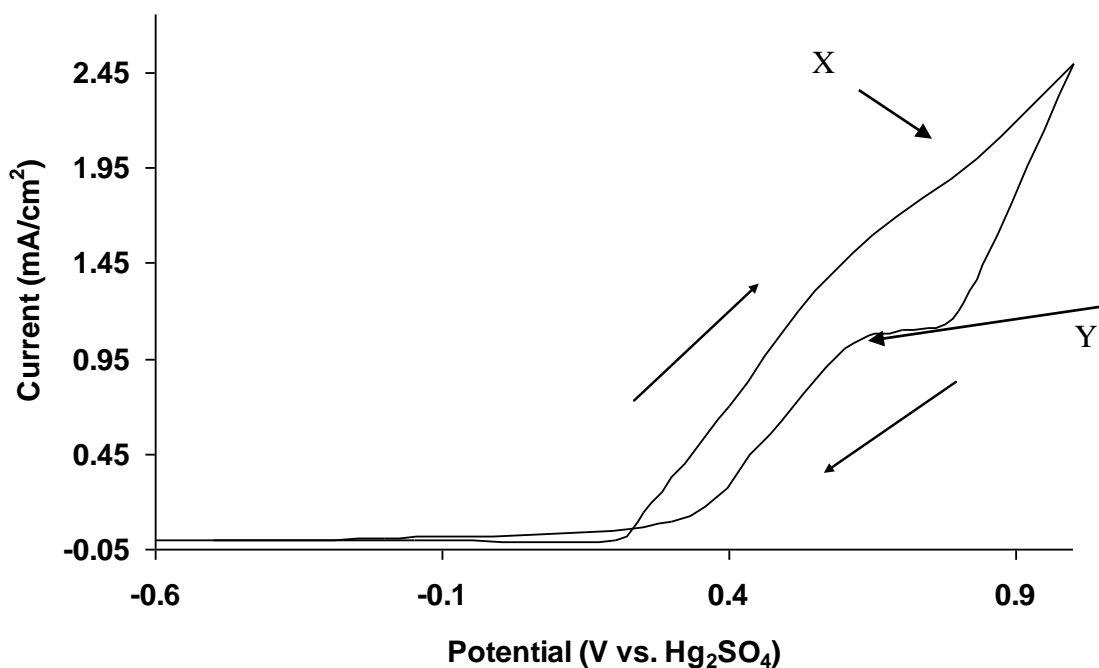


Figure 4.4(e): CV from a Pt10%Ni90%/CIE ( $120 \text{ mC/cm}^2$  in deaerated  $0.1 \text{ M KNO}_3$ ),  $0.5 \text{ M C}_2\text{H}_5\text{OH}$  and  $1 \text{ M NaOH}$  with an MMS reference electrode and at a scan rate of  $10 \text{ mV/s}$ ,  $\text{pH} = 14$ .

Meanwhile, PdNi has been used in literature as an exploration into platinum free catalysts and ethanol oxidation.<sup>12-13, 25-26</sup> Figure 4.4(f) shows a CV obtained from a Pd70%Ni30%, a platinum-free electrodeposited catalyst in ethanol and potassium nitrate ( $\text{pH} 6$ ).

Notably, two broad peaks, labelled A and B, collected through the voltammetry are similar to those observed at catalysts containing platinum. However, there is no evidence of peak C, assigned as a characteristic of alcohol oxidation in the presence of platinum (in section 2.8 and 2.9) on the cathodic sweep. This may be due to the lack of re-oxidation of the fuel, peak C, as the metal oxide is reduced, ascribed to peak D, in figure 4.4(f). Peak D is assigned to be the metal oxide being reduced in a similar fashion to  $\text{NiO}_x$  reduction

in figure 4.3 (c) and for palladium in section 3.4. The peak associated with CO oxidation at platinum catalysts, typically sits at the same potential as this reduction peak, below 0 V vs. MMS at pH 6. Conversely, it could be the lack of  $\text{CO}_{\text{ads}}$  formed by the platinum free catalyst. The current is gradually increasing on the forward sweep for all peaks, reaching a maximum of  $0.15 \text{ mA/cm}^2$  for peak A and  $0.35 \text{ mA/cm}^2$  for peak B. This is similar behaviour found at platinum electrodes recorded to this point in pH 6 electrolyte. Similarly, current observed at a platinum electrode for the first sweep is similar to that of the PdNi electrode. This may indicate that the nickel is facilitating the reaction to take place at the palladium surface, where the palladium electrode substitutes for the platinum surface in the mechanism outlined previously in sections 1.2, 2.9, 2.15 and 3.5. The nickel proceeds to provide sufficient oxygen species at higher potentials for peak B to be recorded to aid oxidation as observed in figure 4.4(a) and adsorption of ethanol to the palladium surface. The Pd-C bond does facilitate oxidation in the presence of  $\text{OH}^-$  ions as shown in section 3.5 with the EOR at high pH (1 M NaOH). From figure 4.4(f), it can be concluded that the dissociation of water at pH 6 provides enough  $\text{OH}^-$  to enables this ethanol oxidation, for peaks A and B.

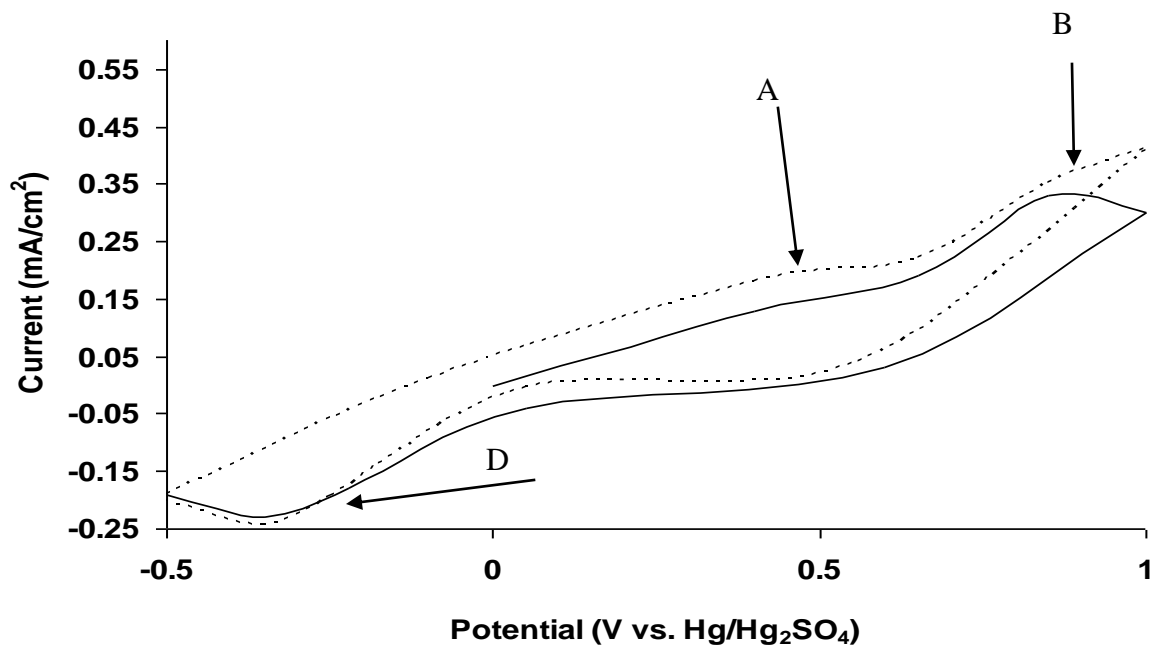


Figure 4.4(f): CV from a Pd70%Ni30% electrodeposit/CIE ( $120 \text{ mC/cm}^2$  in deaerated  $0.1 \text{ M KNO}_3$ ) in  $0.5 \text{ M C}_2\text{H}_5\text{OH}$  and deaerated  $0.1 \text{ M KNO}_3$ , with an MMS reference electrode and a scan rate of  $10 \text{ mV/s}$ , from 1<sup>st</sup> sweep (solid line) and 5<sup>th</sup> sweep (dashed line),  $\text{pH} = 6$ .

The lack of peak C may indicate that the product is not an adsorbed species – such as  $\text{CO}_{\text{ads}}$  - at a platinum free catalyst compared to a platinum electrode. This indicates that the electrode may not be poisoned on a platinum free catalyst or give reduced performance over each cycle, perhaps from the renewed catalyst surface. Consequently this removes any adsorbed poison that represents peak C observed on PtNi electrodes. The electrode is therefore able to act on the EOR in this limited potential window, registering current of  $0.10 \text{ mA/cm}^2$  to  $0.15 \text{ mA/cm}^2$  for Peak A and  $0.25 \text{ mA/cm}^2$  to  $0.35 \text{ mA/cm}^2$  for peak B - over a longer period of time.

Figure 4.4(f) further reinforces the notion that the crucial role of nickel is to supply the necessary hydroxides so consequently palladium can act as the substitute for platinum in producing a platinum free catalyst for the EOR.

#### 4.5 Potential step and Chronocoulometry

Figure 4.5(a) shows the current/time curve obtained from the imposition of a potential step, associated with the best performing Pt90%Ni10% electrode, from OCP at 0 V to 0.4 V vs. MMS. Beyond 20 s, the current drop is negligible up to 100 s. At short times, an electrode can be characterised for borohydride oxidation and ethanol oxidation,<sup>27-29</sup> in conflict with some papers which run the potential step in excess of 100 seconds<sup>25-27</sup> The double layer building out at offering less information for interpretation at such long timeframes.

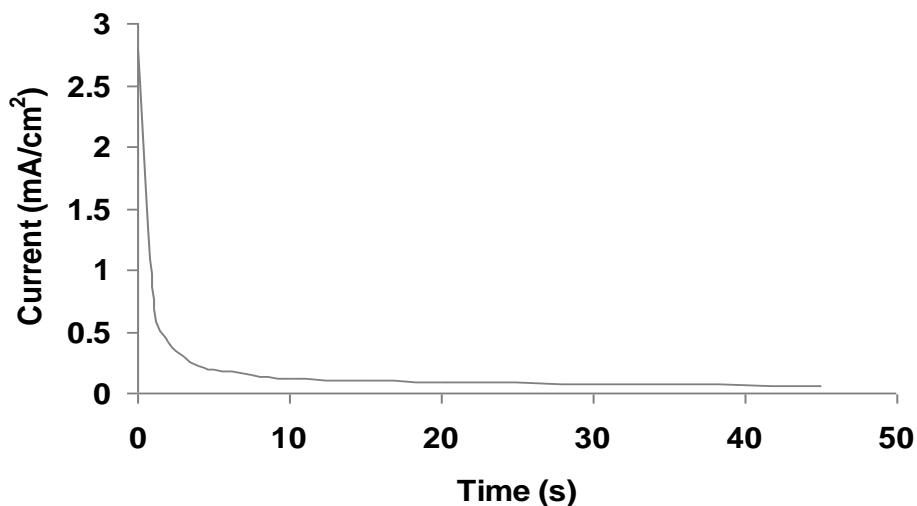


Figure 4.5(a): Potential step for a Pt90%Ni10% electrode ( $120 \text{ mC/cm}^2$  in deaerated  $0.1 \text{ M KNO}_3$ ),  $0.5 \text{ M C}_2\text{H}_5\text{OH}$  and deaerated  $0.1 \text{ M KNO}_3$  from open circuit potential (0 V to 0.4 V vs. MMS).

Figure 4.5(b) shows the integrated data from the potential step for a Pt90%Ni10% electrode compared to that of the best performing platinum palladium electrode (by deposition solution). Typically, a charge axis intercept provides information such as the charge associated with the double layer,  $Q_{dl}$ . The platinum nickel electrode outperforms the platinum palladium electrode with higher charge at comparable times. Furthermore, the 'delay' or induction period from 0-0.4 s is similar to that experienced at platinum and palladium electrodes and close to that shown by Santos and Siqueira for the oxidation of borohydride.<sup>29</sup> The technique has been typically used in electroanalytical work for reduction reactions where mass transport is the only mode of transport<sup>29</sup> but has also been used in oxidation processes to determine kinetic values.<sup>29</sup> In terms of ethanol oxidation, the current densities observed can further confirm EOR catalyst performance.<sup>25</sup>

The Pt90%Ni10% electrode recorded a higher charge on the Pt75%Pd25% electrode – from 6.05 mC/cm<sup>2</sup> for the nickel electrode to 5.84 mC/cm<sup>2</sup> – particularly for the second slope observed which is observed beyond 2 s ( $t^{1/2}$ ). This indicates that the EOR takes place more readily at the nickel electrode, suggesting that as soon as the water is split at near neutral pH providing the  $OH_{ads}$ , nickel is better at facilitating the EOR, producing more  $OH_{ads}$  consistently than platinum or palladium.

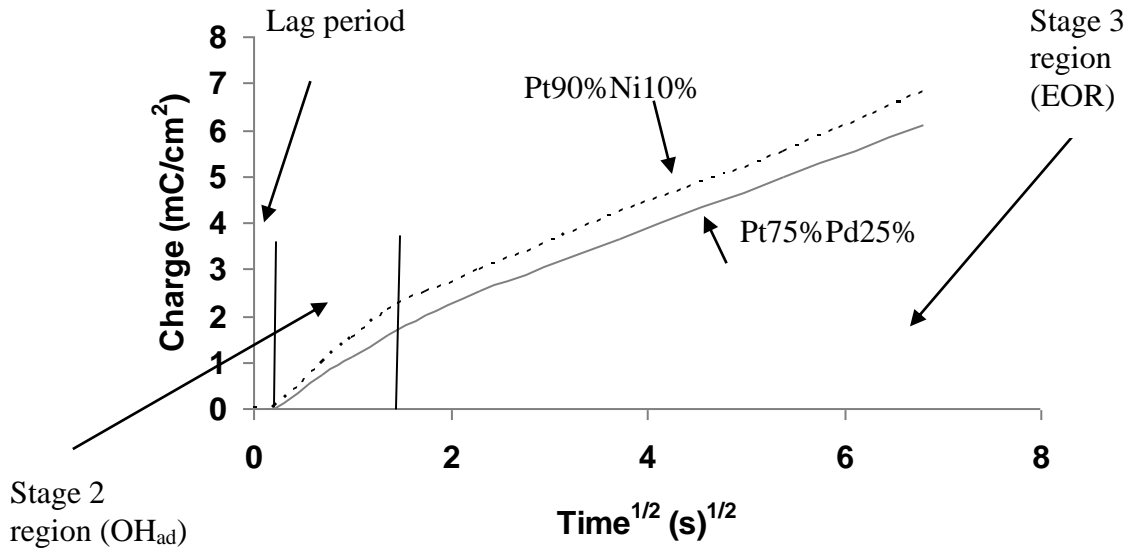


Figure 4.5(b): Charge,  $Q$ , vs.  $\text{time}^{1/2}$ ,  $\text{s}^{1/2}$ , for a Pt90%Ni10% (dashed line) to that of Pt75%Pd25% electrode (solid line) in 0.1 M  $\text{KNO}_3$ , 0.5 M  $\text{C}_2\text{H}_5\text{OH}$ , from a potential step from 0 V to 0.45 V vs. MMS, showing the three regions of reaction in neutral media.

Figure 4.5(c) highlights the first two seconds of the data presented above in the Anson plot shown in figure 4.5(b), divided into three regions or stages in  $\text{KNO}_3$ ; the lag period, the water dissociation step, and ethanol adsorption and oxidation. This identical behaviour has also been observed at a platinum and bimetallic electrodes previously in section 3.6. The negative intercept on the y-axis has been recorded by the Southampton Electrochemistry Group<sup>30</sup> and Santos<sup>29</sup> for various solutions, with a flat response at very short times at  $0.2\text{s}^{1/2}$ . This is perhaps further indication that in  $\text{KNO}_3$ , the carbon ink causes an initial delay or induction period which is responsible for stage 1. This delay appears the reason why there is a lack of positive y-axis intercept, which would

correspond to the double layer charge,  $Q_{\text{intercept}}$ , where is composed of a sum of  $Q_{\text{dl}}$ , and the charge associated with adsorption,  $Q_{\text{ad}}$ .

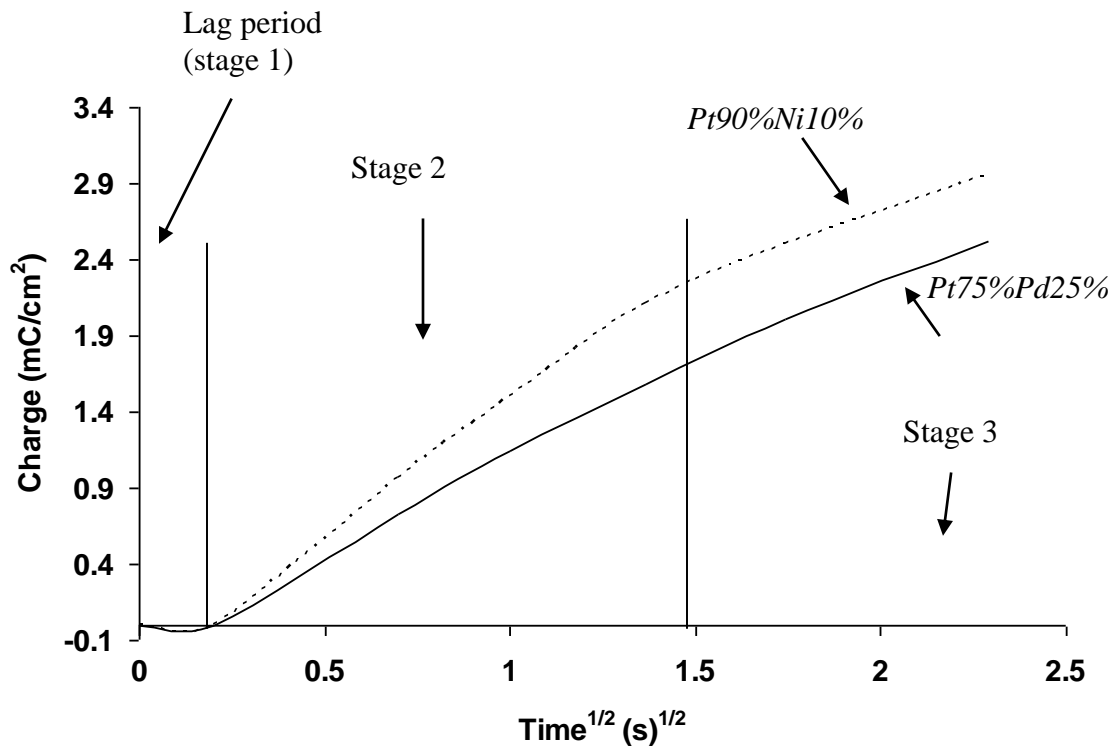


Figure 4.5(c): Charge,  $Q$ , vs.  $\text{time}^{1/2} \text{ s}^{1/2}$  for a Pt90%Ni10% (dashed line) compared to that of Pt75%Pd25% electrode (solid line) [ $120 \text{ mC/cm}^2$  in  $0.1 \text{ M}$  deaerated  $\text{KNO}_3$ ],  $0.5 \text{ M}$   $\text{C}_2\text{H}_5\text{OH}$  in deaerated  $0.1 \text{ M}$   $\text{KNO}_3$ , from a potential step from  $0 \text{ V}$  to  $0.45 \text{ V}$  vs. MMS at short times.

Beyond  $0.2 \text{ s}^{1/2}$ , the increase in charge commences in stage 2. This can be attributed to the  $\text{OH}_{\text{ads}}$  being formed at low potentials to provide the necessary oxygen species to promote the EOR. Beyond stage 3, the rate of increase of charge over time remains constant and notably slower than in stage 2 which can be explained by ethanol oxidation

being facilitated by both  $\text{OH}_{\text{ads}}$  and ethanol adsorption at 0.4 V vs. MMS. These observations are based on data obtained in previous voltammetry, through chapters two, three and four.

#### 4.6 Tafel Analysis

Tafel analysis is a common method of determining electrode kinetics across electroanalytical chemistry. This includes analysing the best catalyst for the EOR at a variety of scan rates ranging from 0.2 mV/s up to 10 mV/s<sup>31-35</sup> The Tafel slope can be used to show the kinetics of the EOR.<sup>15</sup> Subsequently the best performing catalyst has the numerically lowest Tafel slope. Tafel analysis was applied to the initial ethanol adsorption and oxidation step, peak A in pH 6 and initial ethanol oxidation in pH 14, in this work. The Butler-Volmer Equation is represented in equation 7 and 8<sup>16</sup>, where  $\alpha$  = anodic transfer co-efficient,  $E^{\circ}$  is the standard potential, R is the gas constant, 8.314 J/K/mol, T is the temperature, (K), j is the current,  $j^0$  is the exchange current density, F is Faraday's number, 96,485 C/mol and n is the number of electrons,  $\eta$  or  $E-E^{\circ}$  is the overpotential.

$$j = j^0 \cdot e^{[\alpha n F / RT \times (E - E^{\circ})]} \quad \text{Equation (7)}$$

$$\log j = \log j^0 + (\alpha n F / 2.303 RT) \cdot \eta \quad \text{Equation (8)}$$

The Butler-Volmer equation describes the relationship between current and potential under certain conditions. From this, the Tafel equation can be used when the

overpotential is sufficiently far from  $E^0$ , typically in excess of 100 mV. The Tafel equation is below in equation 9, where  $\eta$  = overpotential,  $j$  is the current,  $j^0$  is the exchange current density, and  $a$  is a constant according to the equation 10.

$$\eta = 2.303RT/\alpha F (\log j - \log j^0) \quad \text{Equation (9)}$$

$$a = -2.303RT/\alpha F \cdot \log (nFAk^0C) \quad \text{Equation (10)}$$

For equation 10,  $A$  is the area of the electrode,  $k^0$  is the heterogenous rate constant (cm/s),  $C$  is the concentration,  $n$  is the number of electrons transferred,  $F$  is Faraday's constant (96,485 C/mol),  $R$  is the universal gas constant (8.314 J/K/mol),  $\alpha$  is the anodic transfer co-efficient and  $T$  is temperature. A major problem with Tafel data is the difference in concentration at the surface of the electrode to the bulk solution in this case caused by the adsorbance of ethanol to the surface at peak A. Liang *et al.*<sup>15</sup> found slopes of 120 mV/dec and 250 mV/dec for a palladium electrode in 1 M KOH at 3 mV/s in 1 M ethanol. Gupta reported a Tafel slope of 129 mV/decade for a CuNi alloy in 1 M ethanol at 1 mV/s.<sup>36</sup> It was found that the kinetics of the EOR is affected by multiple surface reactions. One reason why elements such as surface coverage must be taken into account is mentioned by Velazquez-Palenzuela *et al.*<sup>37-38</sup> when quoting the Tafel law for the Tafel slope,  $b$ , in equation 11:

$$b = 2.303(RT)/\alpha F \quad \text{Equation (11)}$$

Where  $R$ = gas constant, 8.314 J/K/mol,  $T$  = temperature,  $n$  is the number of electrons and  $F$  is Faraday's Constant: 96,485 C/mol. In equation 11, there is no consideration given to

concentration and Velazquez-Palenzuela<sup>37-38</sup> reported that the Tafel slope was strongly affected by the electrochemical environment of the catalyst particles. Liang and Liu cover the impact of different Tafel slopes at different potentials for palladium in KOH.<sup>15-16</sup> Liang found a range of 120 mV/decade to 240 mV/decade and Liu measured a Tafel slope of up to 315 mV/decade rather than the theoretical value of 60 mV/decade which corresponds to a one electron transfer with no surface concentration effects. It was found that the EOR mechanism is complicated by oxide formation at higher potentials. Figure 4.6(a) below shows a representative Tafel plot obtained for a variety of nickel/CIE electrodes, with particular comparison to nickel electrodes. The scan rate was 0.5 mV/s as a slow scan returns more stable results. The lower scan rate is an attempt to try to keep the surface concentration of ethanol constant

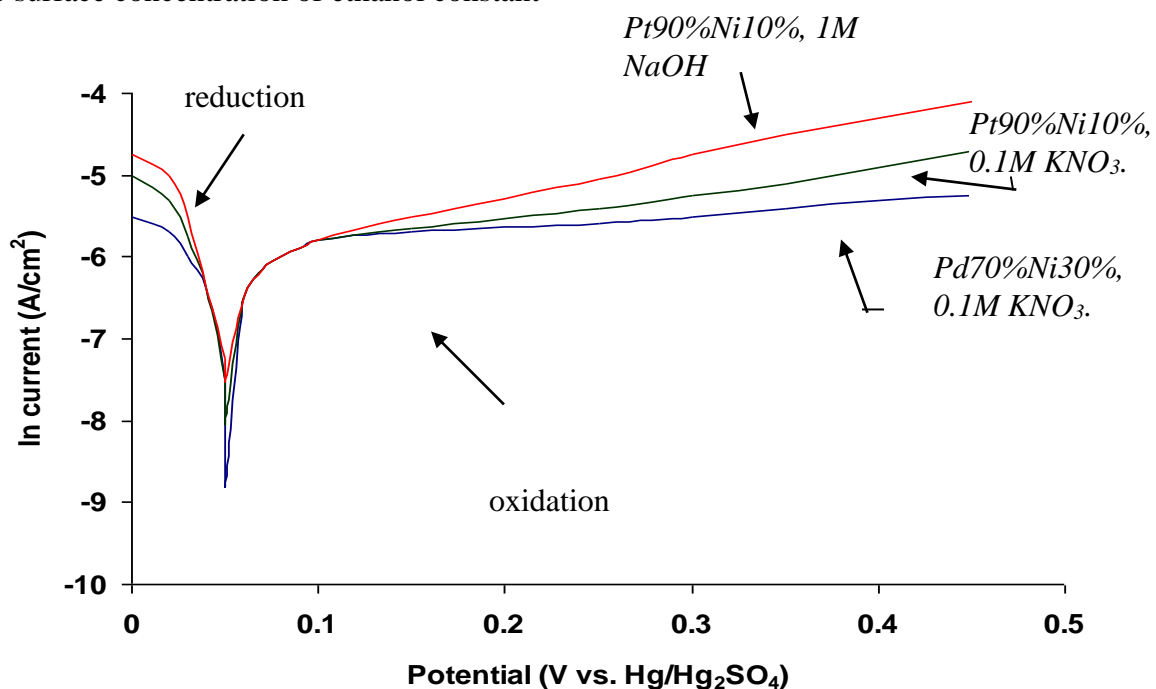


Figure 4.6(a): Tafel plots for a selection of nickel/CIE electrodes (120 mC/cm<sup>2</sup> in deaerated 0.1 M KNO<sub>3</sub>) in deaerated 0.5 M C<sub>2</sub>H<sub>5</sub>OH at 1 mV/s. Blue: Pd70%Ni30% in

0.1 M KNO<sub>3</sub>. Green (dashed): Pt90%Ni10% in 0.1 M KNO<sub>3</sub>. Red: Pt90%Ni10% in 1 M NaOH.

Two important Tafel criteria are a linear increase over one decade of current and that the overpotential is in excess of 100 mV. Figure 4.6(a) does not show the possibility of  $iR$  correction or the effect of a potential drop. Accounting for potential drop increased the linearity of the oxidation or in other terms, decrease the Tafel slope slightly. It was calculated that there is the potential drop effect at  $10^{-5}$  A to  $10^{-6}$  A of between 0.1 mV to 8.6 mV based on the resistances obtained by EIS. As the resistance of the electrode increases, the potential and current measured are negatively, impacting the Tafel slopes according to equation twelve, where  $E$  = potential,  $E_{\text{measured}}$  potential,  $I$  = current and  $R$  is the resistance. This can cause non-linearities in Tafel plots. The carbon ink and carbon paper electrodes contribute a resistance as seen in section 2.7 and in chapter five.

$$E = E_{\text{measured}} - iR \quad \text{Equation (12)}$$

Table 4.6(a) categorises a broader collection of Tafel slopes, primarily concerning nickel electrodes in near neutral and high pH, relating to peak A in near neutral pH voltammetry in section 4.4. In comparison to that of nickel co-deposit electrodes, the 100% platinum, palladium and platinum-palladium co-deposit electrodes possess high Tafel slopes. High Tafel slopes equate to low propensity towards the EOR and low Tafel slopes are matched to high activity for the EOR. This may be, in part, due to the relatively poor conductivity of the carbon substrate and island configuration of the electrode surface mentioned before in chapter 2.5, but is also reported to be consistent with very high Tafel slopes, observed

for other electrodes.<sup>16</sup> The values range from 242 mV/dec for a Pt75%Pd25% in 1 M NaOH electrode up to 519 mV/dec for a Pt10%Pd90% electrode in near neutral pH. Using this table, the best catalyst for the EOR is Pt75%Pd25% in high pH.

As a general rule, the Tafel slopes were calculated to be lower in 1 M NaOH for all electrodes than when placed in near neutral pH, furthermore reinforcing the suggestion that high pH conditions are the best environment for the EOR. At higher potentials – such as for peak B in the CV data in section 4.4 – the Tafel data is substantially complicated<sup>15</sup> by the formation of a metal oxide rather than a metal hydroxide. Consequently, the Ni(OH)<sub>2</sub> and especially<sup>19</sup> NiOOH formed at a nickel electrode may be advantageous when compared to the strongly adsorbed PdO found at higher potentials – especially in NaOH as shown in section 3.5. The PdO formed causes the oxidation current to dramatically decrease at higher potentials by blocking the active sites for ethanol adsorption or any intermediate. The overall high slopes are indicative of the low reactivity of the electrodes as the ideal slope should be a low multiple of 60 mV/dec. Values for 360 mV/dec slopes result in the  $\alpha n$  value of 0.166. As mentioned, the nature of the carbon surface and low reversibility of the Fe<sup>3+</sup>/Fe<sup>2+</sup> couple in section 2.7 may be a significant factor in this slope, although high slopes are a feature of many electrodes to date and the trend is as expected.

At higher potentials – relating to peak B in near neutral voltammetry - the Tafel slopes calculated are in agreement with Liang<sup>15</sup> and indicate there is a balance between adsorbed ethoxi and surface coverage of OH<sub>ads</sub>. The complexity of the oxide layer on all electrodes

at higher potentials becomes more difficult to interpret.<sup>15</sup> As mentioned earlier in this chapter, platinum free catalysts have been selected for methanol oxidation and ethanol oxidation<sup>12-13, 25-26, 39-43</sup> and the Tafel slope for nickel electrodes in alkaline solution.<sup>41</sup> The results from Table 4.6a show that the PdNi electrode displays the poor activity towards the EOR, however by comparison to the platinum content, it is slightly improved upon the bimetallic catalyst with 90% nickel content and 90% palladium.

<b>Electrode Composition</b>	<b>0.1 M KNO<sub>3</sub> (mV/dec)</b>	<b>1 M NaOH (mV/dec)</b>
Pt90Ni10	385	280
Pt10Ni90	514	320
Pt75Pd25	390	242
Pt10Pd90	519	386
Pd70Ni30	500	399
Pt120 mC/cm <sup>2</sup>	398	299

Table 4.6(a): Tafel Slopes for various electrodes deposited in KNO<sub>3</sub> (120 mC/cm<sup>2</sup>) in different pH environments at 0.4 V (range +/-20 mV) without potential drop compensation, pH = 6 and pH 14 respectively.

This is a promising sign for a non-platinum catalyst in the future, but further investigation is required in terms of elucidating performance and the mechanism, such as EIS and fuel cell power curves, which will be covered in chapters five and six. Liu<sup>16</sup> found the slope to

be 210 mV/dec in 1 M KOH for a Pd electrode on titanium increasing to 315 mV/decade in decreasing pH indicating the less activity for the EOR in 0.01 M KOH. Liu<sup>16</sup> calculated  $\alpha$  to be 0.28 for a 4 electron process in 0.01 M KOH with a large Tafel slope of 315 mV/decade. The number of electrons component,  $n$ , has been recently updated in the latest edition of Bard and Faulkner and it is suggested to be removed from consideration by its authors. This is due to the fact that only one electron can be transfer at any instant moment of time. It is not possible to transfer more than one electron instantaneously and for this reason,  $n$  has been removed from equation 11. Such low values of  $\alpha$  are connected with very irreversible reactions where oxidation is favoured, where  $\alpha$  is 0.5 for a single electron reversible process. This level of irreversibility agrees with the CV data collected previously. The catalyst that possesses the lowest Tafel slope is considered the best catalyst for the EOR.

The Tafel plots obtained indicate slow kinetics for peak A is consistent throughout DEFC electrocatalysts. Typically the values of Tafel slopes are in excess of 100 mV/dec and regularly they are reported as in excess of 300 mV/dec and this is the case for the catalysts in table 4.6(a) and figure 4.6(a). As the Tafel slope increases, the catalyst becomes increasingly inactive.

#### **4.7 Conclusions**

Nickel was deposited and used in conjunction with platinum and palladium to enhance ethanol oxidation. Nickel deposits did not show activity for ethanol oxidation in neutral

or alkaline electrolytes, but when used with platinum, they showed a beneficial effect. A catalyst comprising Pt10%Ni90% was compared to the equivalent loading of platinum and the current was enhanced at the nickel electrode. When a bimetallic catalyst was prepared with Pt90Ni10%, the ethanol oxidation at the nickel catalyst was improved compared to 100% platinum. The best performing catalyst, Pt90%Ni10% was then used as comparison to the Pt75%Pd25% electrode. The same potential step was performed at nickel as the palladium electrode and it was found that the nickel catalyst showed improved performance.

Tafel Analysis was carried out on a variety of the catalysts. It was found that the Tafel slopes were high, but in accordance with the literature as Tafel slopes have been regularly reported between 100 mV/decade and 350 mV/decade at pH 14. The data collected from the deposits falls into this range with the best performing catalysts at 250 mV/dec and the worst performing catalyst at over 519 mV/decade in neutral electrolyte, pH 6. Values for  $\alpha_n$  were approximately 0.166, similar to that of Liu<sup>16</sup> indicating a highly irreversible reaction.

#### 4.8 References:

1. Shen, S.Y. ; Zhao, Xu, J.B.; Li, Y.S.; (2010), *J. Power Sources*, **195**, 1001-1006.
2. Gupta, S.S, Mahaptra, S.S.; Datta, J, (2004), *J. Power Sources*, **131**, 169-174.
3. Casella, I.G.; (2009), *Electrochim. Acta*, **54**, 3866-3671.
4. Antolini, E.; (2007), *J. Power Sources*, **170**, 1-12.
5. Serov, A.; Kwak, C.; (2009), *Appl. Catal. B: Environ.*, **10**, 1-8.
6. Serov, A.; Cho, S-Y.; Han, S.; Min, M.; Chai, G.; Nam, K.H.; Kwak, C.; (2007) *Electrochem. Comm.*; **9**, 2041-2044.
7. Yu, E.H.; Scott, K.; (2004), *J. Power Sources*, **137**, 248-256.
8. Burchardt, T.; Gouérec, P.; Sanchez-Cortezon, E. ; Karicchev, Z. ; Miners, J.H., (2002), *Fuel*, **81**, 2151-2155.
9. Matsuoka, K., Iriyama, Y. ; Abe, T. ; Matsuoka, M.; Ogumi, Z.; (2005), *J. Power Sources*, **150**, 27-31.
10. Huang, J-J.; Hwang, W-S.; Weng, Y-C; Chou, T-C; (2009), *Mater. Trans.*, **50**, 1139-1147.
- 11 Su, P-C. ; Chen, H-S. ; Chen, T-Y. ; Liu, C-W.; Lee, C-H.; Lee, J-F.; Chan, T-S.; Wang, K-W.; (2013), *Int. J. Hydrogen Energ.*, **38**, 4474-4482.

12. Zhang, Z. ; Xin, L. ; Sun, K. ; Li, W. ; (2011), *Int. J. Hydrogen Energ.*, **36**, 12686-12697.
13. Maiyalagan, T.; Scott, K.; (2010), *J. Power Sources*, **195**, 5246-5251.
14. Roy, P.S.; Bagchi, J.; Bhattacharya, S.K.; (2012), *Catal. Sci. Technol.*, **2**, 2302-2310.
- 15 Liang, Z.X.; Zhao, T.S.; Xu, J.B.; Zu, L.D.; (2009), *Electrochim. Acta*, **54**, 2203-2208.
16. Liu, J.; Ye, J.; Xu, C.; Jiang, S.P. ; Tong, Y. ; (2007), *Electrochem. Comm.*, **9**, 2334-2339.
17. <http://www.kitcometals.com/charts>, viewed May 2015.
18. <http://www.sciencedirect.com/science/article/pii/S146428590770295X>, viewed May 2015.
19. Riyanto; Othman, M.R.; Salimon, J.; (2011), *Indo. J. Chem.*, **11**, 75-84.
20. Motheo, A.J.; Machado, S.A.S.; Rabelo, F.J.B.; Santos Jr., J.R.; (1994), *J. Brazilian Chem. Soc.*, **5**, 161-165.
21. Tarasevich, M.R.; Karichev, Z.R.; Bogdanovskaya, V.A.; Lubnin, E.N.; Kapustin, A.V.; (2005), *Electrochem. Comm.*, **7**, 2, 141-146.
22. Doyle, R.L.; Godwin, I.J.; Brandon, M.P.; Lyons, M.E.G.; (2013), *Phys. Chem. Chem. Phys.*, **15**, 13737-13783.

23. Van der Ven, A.; Morgan, D.; Meng, Y.S.; Ceder, C.; (2006), *J. Electrochem. Soc.*, **153** (2), A210-A215.
24. Qiu, C.; Shang, R.; Xie, Y.; Bu, Y.; Li, C; Ma, H.; (2010), *Mater. Chem. Phys.*, **120**, 323-330.
25. Wei, Y-C.; Liu, C-W.; Kang, W-D.; Lai, C-M.; Tsai, L-D.; Wang, K-W.(2011), *J. Electroanal. Chem.*, **64**, 660-667.
26. Shao, M.; (2013), *Electrocatalysis in Fuel Cells, A non and low platinum approach*, Springer.
27. Gupta, S.S, Singh, S.; Datta, J; (2009), *Mater. Chem. Phys.*, **116**, 223-228.
28. Wang, Z-B.; Yin, G-P.; Lin, Y-G.; (2007), *J. Power Sources*, **170**, 242-250.
29. Santos, D.M.F.; Sequeira, C.A.C.; (2009), *J. Electrochem. Soc.*, **156** (5), F67-F74.
30. Pletcher, D. ; *Steady, State and potential Step Techniques, Instrumental Methods in Electrochemistry*, Horwood Publishing, 57, ISBN:1-898563-80-2.
31. Tripkovic, A.V.; Popovic, Lovic, J.D.; (2001), *Electrochim. Acta*, **46**, 3163-3173.
32. Zhu, M.; Sun, G.; Xin, Q.; (2009), *Electrochim. Acta*, **54**, 1511-1518.
33. Singh, R.N.; Singh, A.; Anindita; (2009), *Carbon*, **47**, 271-278.
34. Zhang, X.L.; Jiang, Zh. H.; Yao, Zh.P.; Song, Y.; Wu, Zh.D; (2009), *Corros. Sci.*, **51**, 581-587.

35. Qin, Y.H.; Yang, H-H; Zhang, X-S.; Li, P.; Ma, C-A.; (2010), *Int. J. Hydrogen Energ.*, **35**, 7667-7674.
36. Gupta, S. Gupta, S.S.; Datta, J.; (2005), *J. Power Sources*, 124-132.
37. Velazquez-Palenzuela, A. ; Centellas, F. ; Garrido, J.A. ; Arias, C. ; Rodríguez, R.M., Brillas, E. ; Cabot, P-L. ; (2011), *J. Power Sources*, **196**, 3503-3512.
38. Velazquez-Palenzuela, A. ; Centellas, F. ; Garrido, J.A. ; Arias, C. ; Rodríguez, R.M., Brillas, E. ; Cabot, P-L. ; (2013), *J. Power Sources*, **225**, 163-171.
39. Kumar, K.S.; Haridoss, P.; Seshadri, S.K.; (2008), *Surf. Coat. Technol.*, **202**, 1764-1770.
40. Gonzalez Pereira, M.; Davila Jimenez, M.; Elizalde, M.P. ; Manzo-Robledo, A.; Alonso-Vante, N.; (2004), *Electrochim. Acta*, **49**, 3917-3925.
41. Lyons, M.E.G.; Brandon, M.P.; (2008), *Int. J. Electrochem. Soc.*, **3**, 1386-1424.
42. Nakamura, A.; Takahashi, H.; Takeguchi, T.; Yamanaka, Wang, Q.; Uchimoto, Y.; Ueda, W.; (2011), *ECS Trans.*, **41** (1), 2205-2209.
43. Ma, Y.; Du, Y.; Ye, W.; Su, B.; Yang, M. ; Wang, C. ; (2012), *Int. J. Electrochem. Sci.*, **7**, 2654-2679.

## Chapter Five: Electrochemical Impedance Spectroscopy (EIS)

### 5.1 Introduction

In this chapter, the presence of adsorbed species at the surface of the working electrode will be examined along with the EOR on the catalyst at a variety of selected potentials using EIS. An important component of the bifunctional mechanism mentioned previously is the presence of adsorbed hydroxides and adsorbed carbon intermediates. These adsorbates are present at the surface at the chosen potentials and impedance spectroscopy will be used to probe these using through signature plots at a given potential and electrode surface.

Electrochemical impedance,  $Z$ , of an ohmic circuit element is equal to the resistance  $R$  in the relationship originating from Ohm's Law below where  $R$  can be calculated using current,  $I$  and the potential,  $E$ , in equation 1:

$$R = E/I \quad \text{Equation (1)}$$

Impedance is represented by a vector, characterized by its modulus and phase shift,  $\Phi$ , shown in figure 5.1(a).<sup>1</sup> The total impedance  $z$  is the sum of its real (x-axis) and imaginary (y-axis) parts.<sup>2</sup> This representation can also be expressed as shown in equation

2

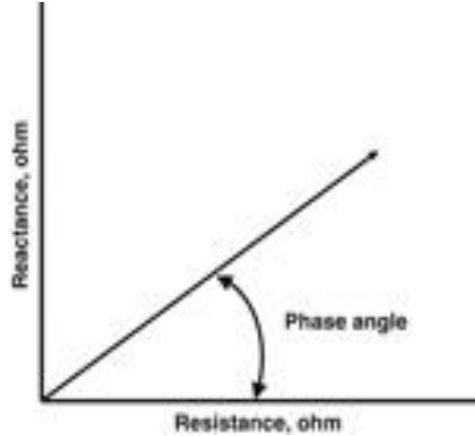


Figure 5.1(a) Vector representation of impedance in terms of real (x-axis) and imaginary (y-axis) impedance with its phase angle, adapted from Lasia.<sup>1</sup>

$$Z = Z' + jZ'' \quad \text{Equation (2)}$$

Where  $j$  is  $(-1)^{1/2}$ ,  $Z'$  is in phase and  $Z''$  is out of phase or 'imaginary' impedance. Plotting imaginary impedance against real impedance will be discussed later in this section. When a sine wave is applied as in figure 5.1(b), the phase shift,  $\Phi$ , is the difference in the crest of the peak between potential,  $E$  and current,  $i$ , can be expressed in equation 3 for potential and 4 for the current below. The phase shift for a polarisable electrode with no solution resistance should be  $-90^\circ$ .

$$E = \Delta E \sin(\omega t) \quad \text{Equation (3)}$$

$$i = \Delta i \sin(\omega t + \Phi) \quad \text{Equation (4)}$$

Where  $\omega = 2\pi f$ ,  $\omega$  is the radial frequency (rad/s) and  $f$  is the frequency in Hz.

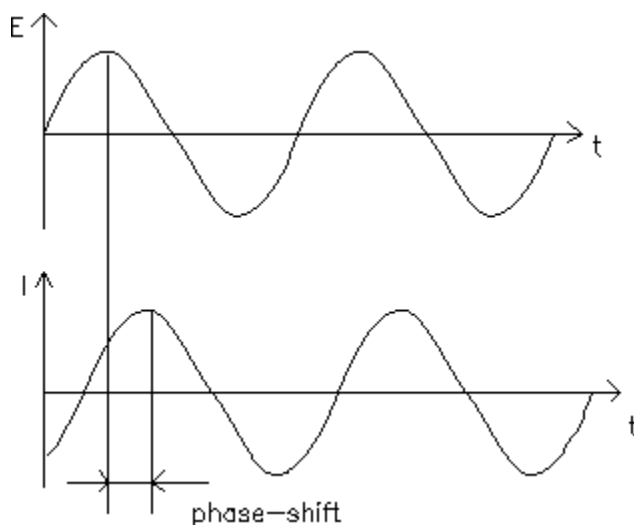


Figure 5.1(b): Image representing a sin wave for potential (top) and current (bottom) with an associated shift in the crest of the wave, adapted from Lvovich.<sup>3</sup>

An example of a simple circuit is the Randles circuit, shown in figure 5.1(c). EIS is technique known for decades<sup>4</sup> yet has only recently seen a boost in its use for electrochemical research<sup>5-7</sup> as it has the ability to determine an array of parameters.<sup>8</sup> In terms of electroanalysis, relationships can be made through the  $R_{CT}$  based on concentration or potential.<sup>4</sup> In addition, modelling of common electrical components has been described as the most important aspect of EIS when compared to other electrochemical techniques<sup>9-10</sup> and as such, the technique has become widespread, particularly in corrosion science and can be useful in the investigation of electron transfer, of mechanistics,<sup>9-12</sup> and electron transfer in electrochemical reactions.<sup>13</sup>

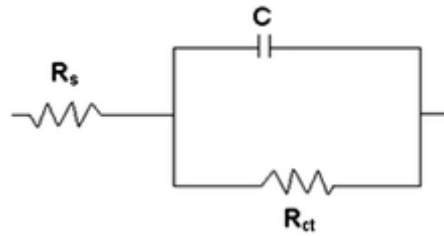


Figure 5.1(c): A circuit diagram (equivalent circuit) displaying a Randles Circuit.

There are a number of elements in the circuit and these are commonly encountered in many practical cell configurations to different degrees.<sup>14</sup>  $R_s$  is the solution resistance which is normally low in electrolytes of the order of  $5 \Omega$ . The capacitor most often represents the double layer capacitance,  $C_{dl}$  which is typically  $20\text{-}60 \mu\text{F}/\text{cm}^2$ , while the third element is the charge transfer resistance,  $R_{CT}$  which is in parallel to  $C_{dl}$ . When an adsorbed intermediate is present at an applied potential, an inductive component is necessary in series, for example, with the  $R_{CT}$  resistance shown in figure 5.1(c). An example of this is for methanol oxidation by Seland *et al.*<sup>10</sup>

Charge transfer resistance is derived from the Butler-Volmer Equation in equation 5 when the concentration at the surface is the same as the concentration of the bulk solution. At low overpotentials, the charge transfer resistance can be used to calculate the exchange current density when at equilibrium, as shown in equation 6 below.

$$i = i_0 [e^{(\alpha F\eta/RT)} - e^{-(1-\beta F\eta/RT)}] \quad \text{Equation (5)}$$

$$R_{CT} = 1/i_0 \times (RT/F) \quad \text{Equation (6)}$$

A Cole-Cole or Nyquist plot for a dummy cell is shown in figure 5.1(d), highlighting  $R_s$  as the solution resistance,  $R_{CT}$  from the beginning of the plotted arc to the final data point along the x-axis. This latter plot is composed of the imaginary impedance  $Z''$  on the y-axis plotted against the real impedance on the x-axis. The applied frequency,  $f$ , decreases as the arc moves from low values of  $Z'$  to high  $Z'$ .

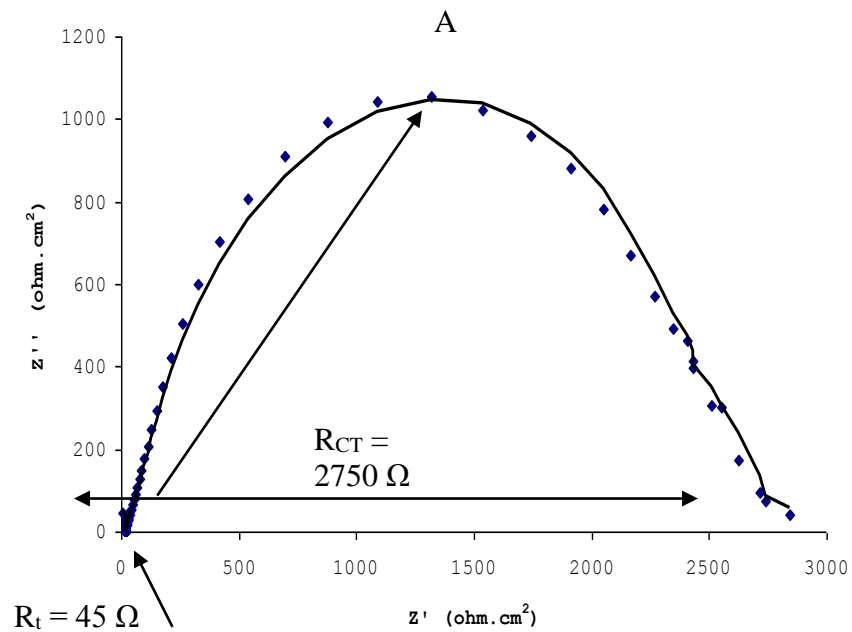


Figure 5.1(d): Nyquist plot for a dummy cell with circuit in figure 5.1(f).

At point A on a Nyquist plot, the following is true:

$$R_{CT} \times C_{dl} \times \omega_{max} = 1 \quad \text{Equation (7)}$$

There are two types of plots typically used in EIS work<sup>14</sup>: A) Nyquist Plot, and B) Bode plots. The Nyquist plot should consist of a characteristic semicircle or arc as the frequency decreases, as shown in figure 5.1(d), becomes more useful at low frequency

and high impedance facilitating a quick overview of the data. The Nyquist plot does not show frequency implicitly on its axes,<sup>15</sup> therefore it does not exhibit the complete data set. It plots imaginary impedance against real impedance. The Bode plot, however, plots the phase angle versus the logarithm of frequency or logarithm of impedance magnitude and the log frequency.<sup>14</sup> This will give frequency information and this is popular in certain fields such as corrosion. The same data from a Nyquist plot can be represented as a Bode plot shown in figure 5.1(e) and figure 5.1(f) below. When a small amplitude is applied around the reversible potential, the exchange current density can be found from  $R_{CT}$  from the equation 6 previously. As such, as  $R_{CT}$  is inversely proportional to the exchange current density when at equilibrium. As shown earlier in chapter 2.4, as the exchange current density increases, the surface is more reactive - for example, platinum has a larger current density than lead and, thus, is deemed more suitable for use in the hydrogen fuel cell.

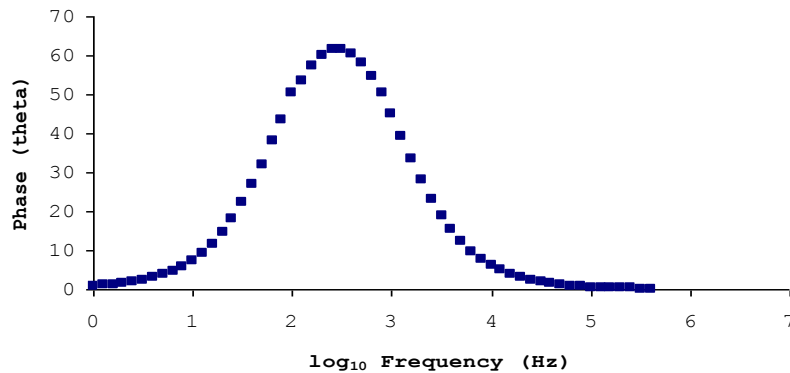


Figure 5.1(e): Phase vs. log. Frequency (Bode plot) for Nyquist plot obtained from a Dummy Cell in figure 5.1(d).  $C_{dl} = 0.8 \times 10^{-6} \text{ F}$ , Working Electrode-Reference Electrode resistance of  $2660 \Omega + 215 \Omega$  and Reference Electrode-Auxiliary Electrode resistance =  $60 \Omega$ .

EIS is increasingly being used as a practical method of investigating electrochemical kinetics by perturbing the electrode surface with decreasing frequency (from high frequency to low frequency). At lower frequencies, great detail can be collected with respect to surface reactions. The technique is a normally potentiostatic test with potentials selected from the voltammetry observed for a reaction.

Bode plots are useful to find out the impedance and phase angle associated with an individual frequency point. The Nyquist plot does not provide this information and each point on both forms of the Bode plot gives detailed information at the particular frequency. The Bode plot moves from high frequency to low frequency or from right to left on the diagram.

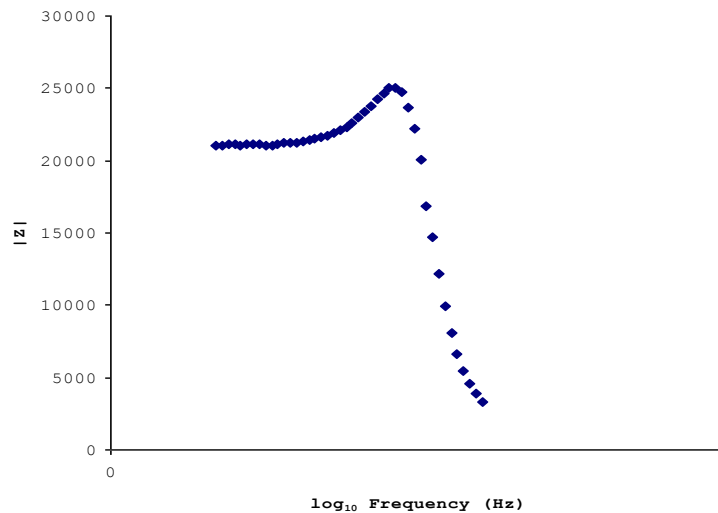


Figure 5.1(f): Impedance vs. log. Frequency (Bode plot) for the Nyquist plot in figure 5.1(d) obtained from a Dummy Cell in fig 5.1(d).  $C_{dl} = 0.8 \times 10^{-6}$  F, Working Electrode-Reference Electrode resistance of  $2660 \Omega + 215 \Omega$  and Reference Electrode-Auxiliary Electrode resistance =  $60 \Omega$ .

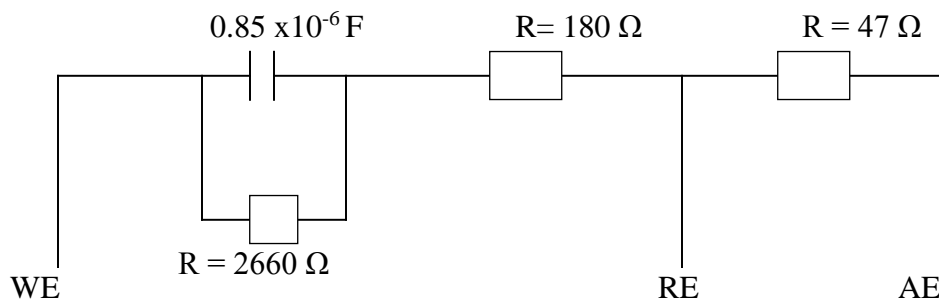


Figure 5.1(g): Circuit diagram for the dummy cell used in figure 5.1(d).

Moreover, a model circuit diagram or equivalent circuit can be applied to results obtained experimentally. The best fit model for the dummy cell is illustrated by figure 5.1(g). A model can simulate different elements of a reaction, which can include solution resistance which is typically small, resistors, capacitors – for example, to represent the double layer capacitance element, inductors to account for the presence of surface adsorbed species, and constant phase elements that represent Warburg impedance for diffusion control. Warburg impedance is indicated on a Nyquist plot by a linear increase in imaginary impedance at low frequencies. At high frequencies, the diffusing reactants do not move far. At lower frequencies, this diffusion distance distance increases, increasing the impedance.<sup>2</sup> This appears typically as a diagonal line on a Nyquist plot and has a phase shift of  $45^\circ$ . For adsorbed species, it is often found that at low frequencies the arc in a Nyquist plot begins to curve back inwards and below the x-axis.

The challenge for the technique is that EIS is in its relative infancy as a means of studying the heterogenous electrode surface<sup>4, 16</sup>, despite it being used for some electrodes

as far back as the 1920s.<sup>16</sup> It has however been used to examine electro-oxidation of small organic molecules, such as methanol, ethanol and propanol as well as electrodeposition.<sup>16</sup> It is useful to study the reaction activity of the EOR. The shorter the arc is in the Nyquist plot, the greater the rate of a reaction. Consequently, the smaller the value for  $R_{CT}$  obtained from a catalyst, the better its performance towards the EOR, as it is inversely proportional to the current density,  $i_0$ .<sup>17</sup> Furthermore, data is possible below the x-axis due to the adsorption around the voltammetric regions where current is changing quickly due to surface coverage by adsorbed species.<sup>17</sup> Results are often reported as a function of increasing potential with several arcs in one plot. Greater reaction activity is associated with improved kinetics at the surface. Ethanol oxidation on platinum, palladium or nickel has been recently studied by EIS by Dutta<sup>18-19</sup>, Han<sup>20</sup> and others<sup>17, 21-23</sup> with varying results, models and conclusions specific to the electrodes tested.

## 5.2 Experimental:

Electrodeposited metals on carbon supports were used as electrodes in a conventional three electrode system. A mercury/mercury sulphate (MMS), +640 mV vs. SHE, purchased from Radiometer Analytical Instruments (ref 640) was used as a reference electrode. A Solartron 1287 potentiostat and 1255B Frequency Response Analyser model instrument was used to collect cyclic voltammetric, potentiostatic, Nyquist and both Bode plots. CorrWare (Scribner and Associates) software was employed to programme the impedance parameters to collect the Nyquist and Bode plots. Z-View software (Scribner and Associates) was used to simulate and model the plots obtained. Z-plot software (Scribner and Associates) was used to control the amplitude and frequency applied.

The carbon ink electrodes used were prepared by coating a non-porous plastic sheet (Xerox) with a finely dispersed graphite-based particles inside an ink binder solvent (Acheson Industries, Electrodag 423 SS) as previously described. The ink coating was then allowed to dry overnight. The fabricated electrodes were then sectioned into 1 cm<sup>2</sup> used for further testing, acting as working electrodes for catalyst electrodeposition as described earlier. Nail lacquer was added to the stem of each electrode in order to guarantee its geometrical area. The best performing catalyst combinations of platinum, palladium, nickel and their co-deposits were then deposited as described previously and tested for comparison by EIS.

The temperature of the cell was kept at room temperature between 15-20° C, and the cell was de-aerated with oxygen-free nitrogen (BOC gases). A range of electrolytes was used, specifically 0.1 M potassium nitrate and sodium hydroxide, NaOH, purchased from Sigma Aldrich. To study the effect of pH, the concentration of aqueous solution of sodium hydroxide was set to pH 14 (1 M NaOH) and 0.1 M KNO<sub>3</sub> at pH 6. Typically the scan rate was set to 10 mV/s for cyclic voltammetry. Pure ethanol was purchased from Sigma Aldrich. The concentration of ethanol was kept constant to 0.5 M in electrolyte. A 5 cm<sup>2</sup> platinum sheet was used as a counter electrode for all experiments in all solutions. A Luggin Capillary was used to minimise the distance between the reference electrode and working electrode.

The frequency range used was between 10<sup>5</sup> Hz and 10<sup>-2</sup> Hz. The timeframe for each experiment was 20 minutes at each potential. The perturbation amplitude was 10 mV. The chosen potential points were selected by cyclic voltammetry, typically 0.1 V, 0.4 V, 0.5 V, 0.65 V, 0.75 V, 0.85 V, 0.95 V vs. MMS. Between each set of impedance plots, an added cyclic voltammogram was used to between each potentiostatic and impedance test for a given potential as it was found to obtain the most stable potentiostatic run from one potential to another. Therefore three runs were performed to collect data for one voltage value. The potentiostatic run is used to obtain a steady state current at the voltage required. The order – for three applied potentials: A, B and C - is outlined as follows:

1. CV from -0.5 V to +1.0 V (vs. MMS)
2. Potentiostatic test at applied potential A (vs. MMS)

3. Impedance data collected at the potential A.
4. CV from -0.5 V to +1.0 V (vs. MMS)
5. Potentiostatic test at applied potential B (vs. MMS)
6. Impedance data collected at the potential B (vs. MMS).
7. CV from -0.5 V to +1.0 V (vs. MMS)
8. Potentiostatic test at applied potential C (vs. MMS)
9. Impedance data collected at the potential C (vs. MMS)

A sample of the CV undertaken is shown in figure 5.2(a) below and the potentiostatic run operated before the impedance test is shown in figure 5.2(b). The potentiostatic run was used to show the stable time invariant current, approximately  $30 \mu\text{A}/\text{cm}^2$ .

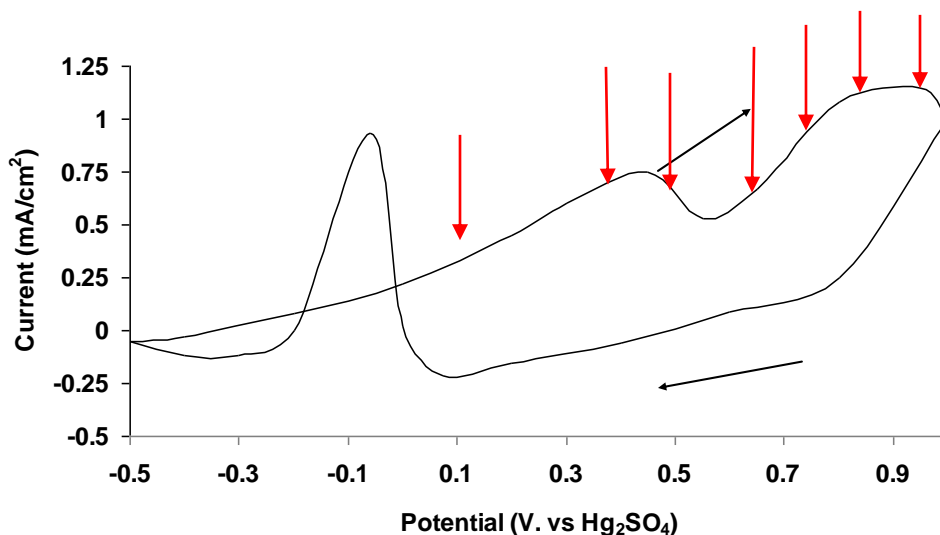


Figure 5.2(a): Typical CV used in experimental program between each impedance measurement in 0.1 M KNO<sub>3</sub>, platinum electrode ( $120 \text{ mC}/\text{cm}^2$  in 0.1 M KNO<sub>3</sub>), with MMS reference electrode, 0.5 M ethanol, at a scan rate of 10 mV/s. Arrows indicate the points on the voltammogram where impedance data was collected (red arrows).

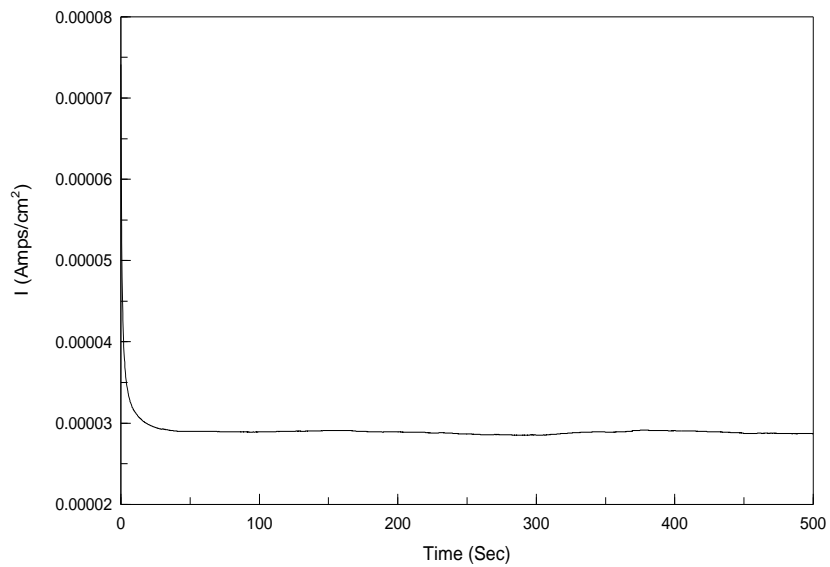


Figure 5.2(b): A typical potentiostatic run used to record the impedance at a set potential showing a stable invariant constant current over time. 0.1 V vs. MMS in 0.5 M ethanol and 0.1 M KNO<sub>3</sub> with a Luggin Capillary.

### 5.3 EIS plots – platinum sheet in ethanol

The Nyquist plot obtained for a platinum sheet working electrode in ethanol is shown in figure 5.3(a) at 0.95 V vs. MMS. A high total resistance value,  $R_t$ , made up of the resistance due to the electrode,  $R_u$ , and the solution resistance,  $R_s$ , is significant in terms of the already discussed poor conductivity of the carbon ink electrode. With a platinum sheet electrode, the total resistance,  $R_t$ , shown in figure 5.3(a) is low,  $3 \Omega$ . This is consistent with the  $R_s$  component, the solution resistance, which is present in all electrolytes and it is typically below  $10 \Omega$ . It may aid in diagnosing the induction period observed and discussed previously in sections 3.8 and 4.4, with particular attention to the chronocoulometry results recorded and section 2.7 with a large separation of peaks for a  $\text{Fe}^{3+}/\text{Fe}^{2+}$  couple and comparatively very slow kinetics at a bare carbon ink electrode.

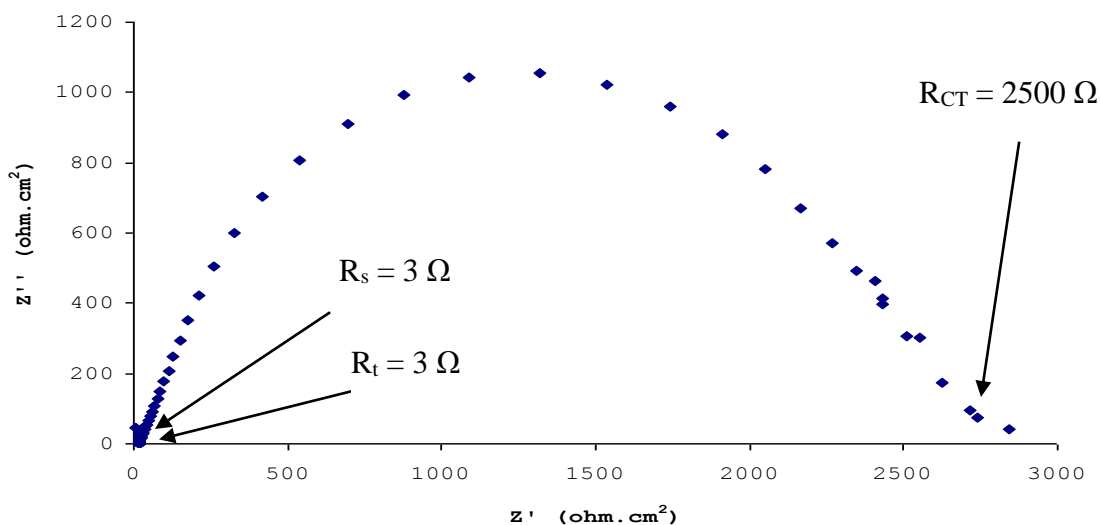


Figure 5.3(a): Nyquist plot for a  $1 \text{ cm}^2$  platinum sheet working electrode in deaerated  $0.1 \text{ M KNO}_3$  and  $0.5 \text{ M C}_2\text{H}_5\text{OH}$  with an applied potential of  $0.95 \text{ V vs. MMS}$ .

The resistance observed relating to  $R_s$ , the resistance from solution, and  $R_u$ , the uncompensated resistance from the carbon electrode, is very low at  $3 \Omega$ , in comparison to some electrodes. In particular, a carbon based electrode such as graphene,<sup>24-28</sup> where the total  $R_s$  and  $R_u$  values have been reported up to  $2000 \Omega$ , a carbon ink electrode of over  $7000 \Omega$ ,<sup>29</sup> glassy carbon and screen printed carbon electrodes.<sup>30-31</sup> The low value in figure 5.3(a) is typical of  $R_s$  for metal electrodes as the electrolyte will show a resistance, but no  $R_u$  component. Typical  $R_s$  values are from  $0-10 \Omega$  for a metallic working electrode in solution. An inductive loop was recorded at high frequencies above  $10^5 \text{ Hz}$  which is common when long cables are used for connections between the instrument and electrodes, such as crocodile clips.

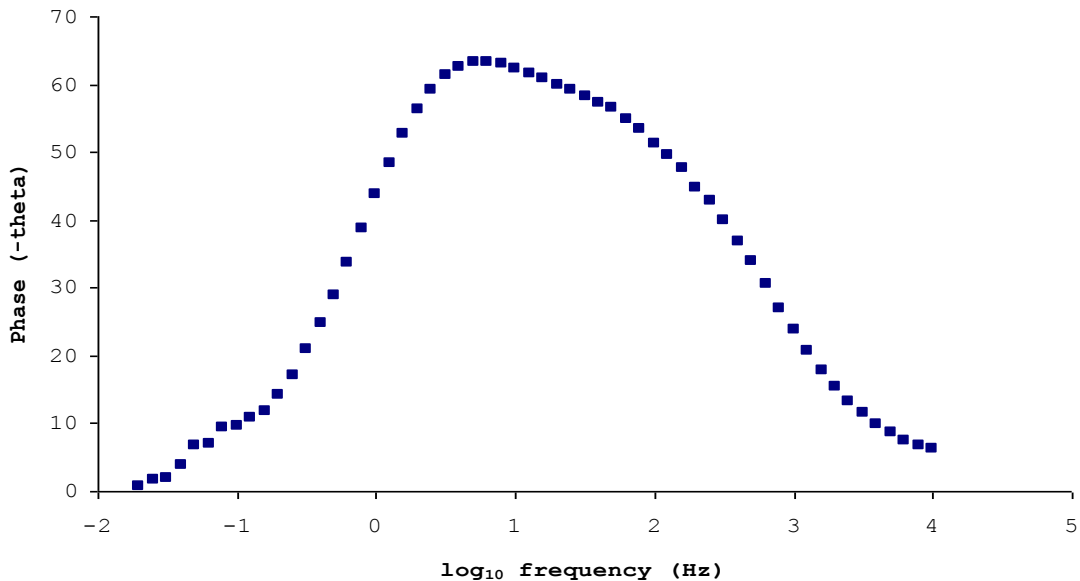


Figure 5.3(b): Phase vs. Frequency plot for a  $1 \text{ cm}^2$  platinum sheet working electrode in  $0.1 \text{ M KNO}_3$  and  $0.5 \text{ M ethanol}$  with an applied potential of  $0.95 \text{ V vs. MMS}$ , with each individual frequency data point.

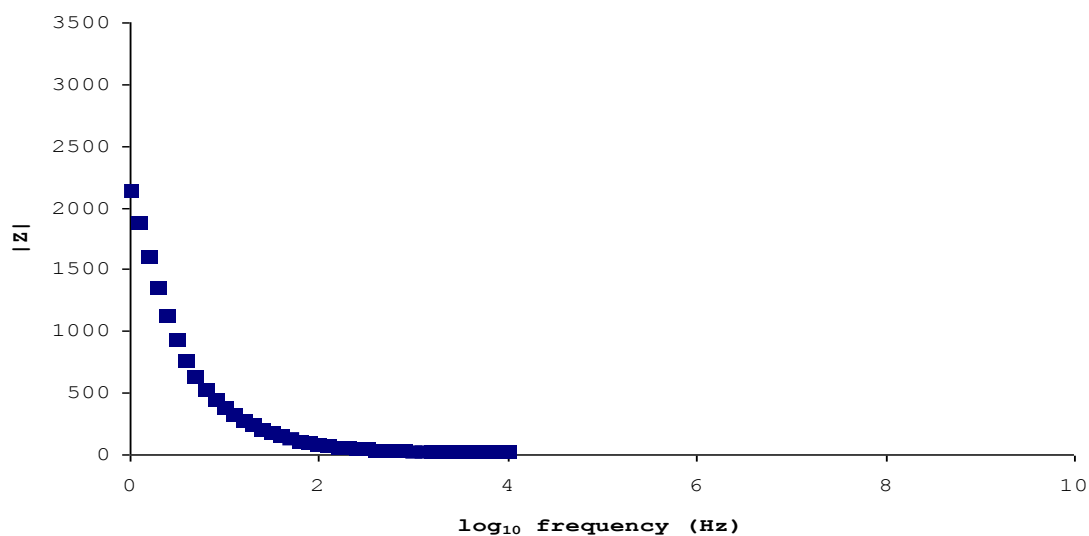


Figure 5.3(c): Impedance v Frequency plot for a 1 cm<sup>2</sup> platinum sheet working electrode in 0.1 M KNO<sub>3</sub> and 0.5 M ethanol with an applied potential of 0.95 V vs. MMS with each individual frequency point.

Between figure 5.2(a) at 0.95 V vs. MMS where the ethanol oxidation reaction is occurring readily and figure 5.3(a) where the charge transfer resistance ( $R_{CT}$ ) is 2750  $\Omega$ , values were comparable to the range found for  $R_{CT}$  by Dutta.<sup>18</sup> It can be seen that ideal EIS behaviour is recorded for the system. From a circuit perspective, the model that was found to fit the data collected best is that shown by Dutta and outlined by Rubinson<sup>14</sup> of a resistor for ethanol oxidation at platinum electrodes with a parallel RC-circuit<sup>14</sup>. The Bode plots shown in figure 5.3(b) and figure 5.3(c) are characteristic of a simple (Randles) circuit such as figure 5.1(c). As the cables are consistent through all experiment data and all experiments were conducted with auxiliary, working and reference electrodes, the inductive loop associated with the cables, above 10<sup>5</sup> Hz, was removed from all data plots.

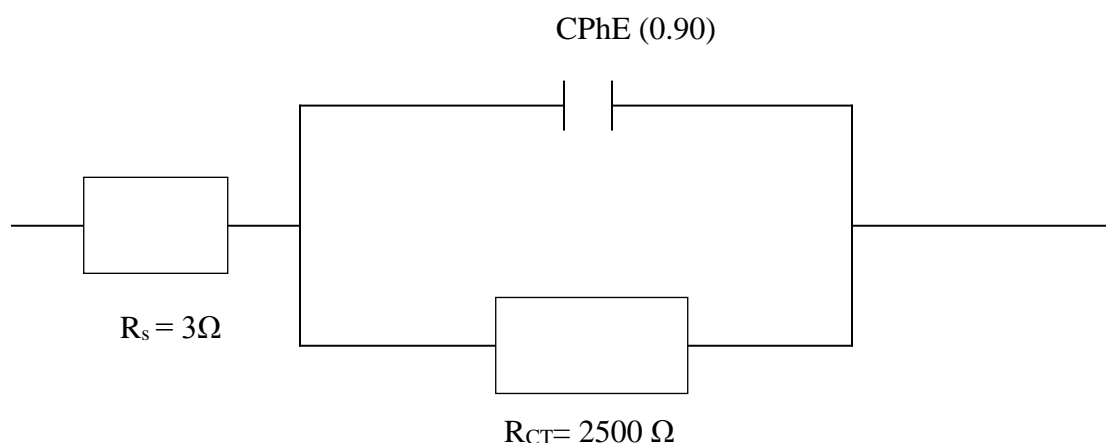


Figure 5.3(d): Circuit reported by Rubinson<sup>14</sup> for ethanol and propanol oxidation,<sup>32</sup>

$R_s$  = solution resistance,  $R_{CT}$  = charge transfer resistance, CPhE = Constant Phase Element.

#### 5.4 EIS plots – Electrodeposited Platinum

Figure 5.4(a) shows a Nyquist plot for a 120 mC/cm<sup>2</sup> platinum deposit/CIE in 0.1 M KNO<sub>3</sub> towards the EOR at 0.95 V vs. MMS. The curve obtained represents a total resistance composed of  $R_t$  (860Ω.cm<sup>2</sup>) and the resistance associated with faradaic charge transfer,  $R_{CT}$  (340Ω.cm<sup>2</sup>). It is notable that a large proportion of the total resistance ( $R_t + R_{CT}$ ) is the contribution from the solution resistance,  $R_s$ , and the uncompensated resistance,  $R_u$ . This uncompensated resistance is shown throughout the carbon electrodes tested to varying degrees at all applied potentials. It was not present for the platinum sheet electrodes indicating it is caused by the carbon electrodes (CIE or CPE). A small  $R_{CT}$  value was recorded at the highest potentials. As the potential increases, the  $R_{CT}$  decreases and the conclusion derived from this is that 0.95 V vs. MMS is the voltage where the catalyst is the most reactive. This is supported by the voltammetry observed at

pH 6 throughout chapters 2, 3 and 4. High  $R_t$  indicates low initial reactivity at the most active potential, and in addition, slow reactivity at other potentials which will be shown further in this chapter, linking the voltammetry, chronocoulometry and Tafel analysis observed throughout this work and will be presented further in application in a model fuel cell in chapter 6. The value of  $857 \Omega$ , designated  $R_u$  in this work, is attributed to the carbon ink or carbon paper electrode used. Figure 5.4(b) shows the same electrode in the same conditions with a wider scale on the x-axis. The overall resistance is significantly reduced supporting the notion of increased reactivity. From the voltammetry, there is a mix of adsorbed species and metal oxides produced at this high potential, predominantly a metal oxide being produced from 0.8 V vs. MMS up to +1.0 V vs. MMS in  $\text{KNO}_3$ .

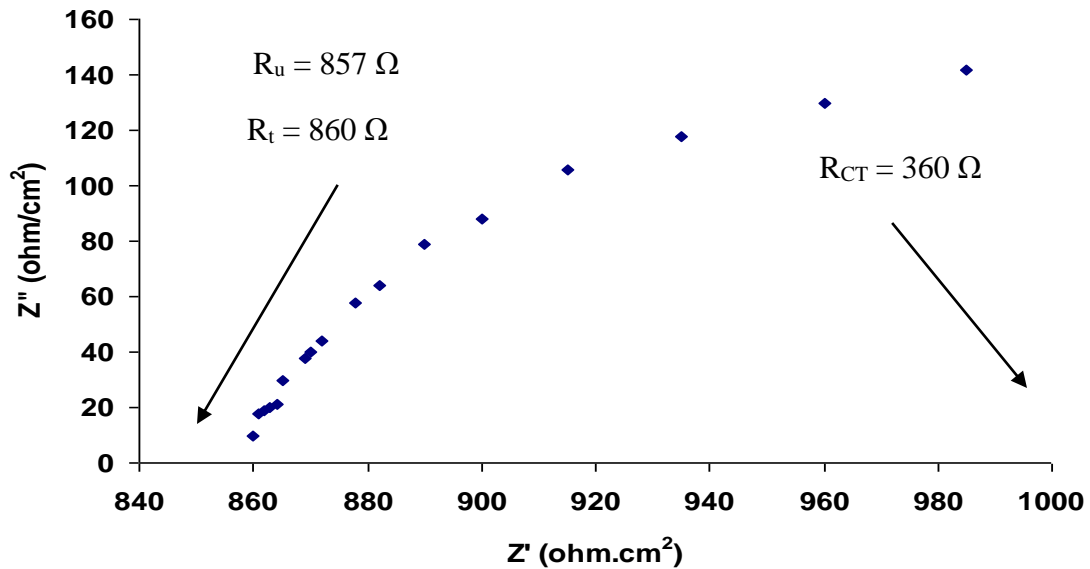


Figure 5.4(a): Nyquist plot for a platinum electrodeposit ( $120 \text{ mC/cm}^2$  in deaerated 0.1M  $\text{KNO}_3$ ) in 0.5 M ethanol and deaerated 0.1M  $\text{KNO}_3$  with an applied potential of 0.95V vs. MMS.

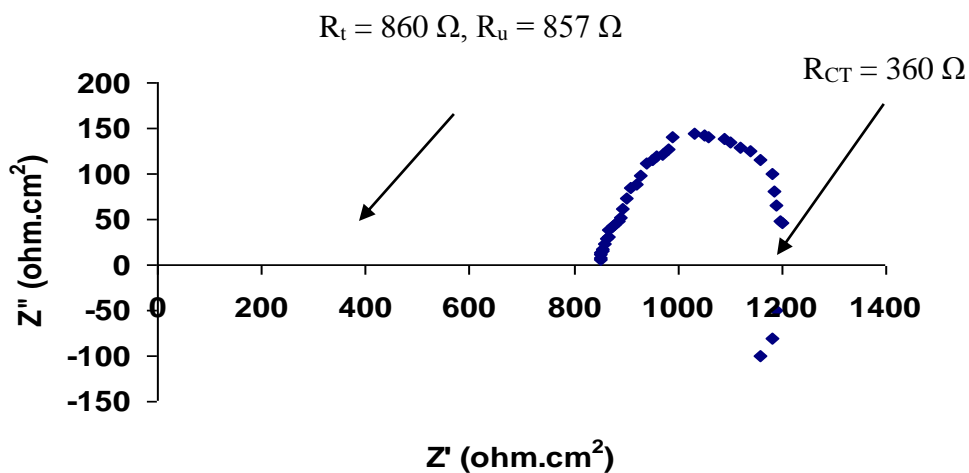


Figure 5.4(b): Expanded Nyquist plot from figure 5.4(a) for 120 mC/cm<sup>2</sup> platinum electrodeposit/CIE in 0.1 M KNO<sub>3</sub> with an applied potential of 0.95 V vs. MMS.

Overall, increasing the potential results in a decrease in the overall resistance. Figure 5.4(c) shows an identical electrode in the same conditions at 0.1 V vs. MMS, 0.4 V vs. MMS and 0.5 V vs. MMS, respectively. The predicted result from increasing potential is not observed as the trend for total resistance at 0.4 V is lower than that at 0.5 V upon repeated experiments. Figure 5.3(d) and figure 5.3(e) represent the Bode phase and Bode modulus format diagrams for the platinum electrodeposit/CIE at applied potentials of 0.4V vs. MMS and 0.5V vs. MMS in ethanol. It is notable that at the lowest potential, 0.1 V vs. MMS, total RCT is consistently at its largest. A very large RCT value at 0.1 V, ranging from 11,000 Ω.cm<sup>2</sup> to 13,000 Ω.cm<sup>2</sup> upon repeated experiments for all electrodes indicates poor reactivity. This further agrees with the voltammetry observed in previous chapters.

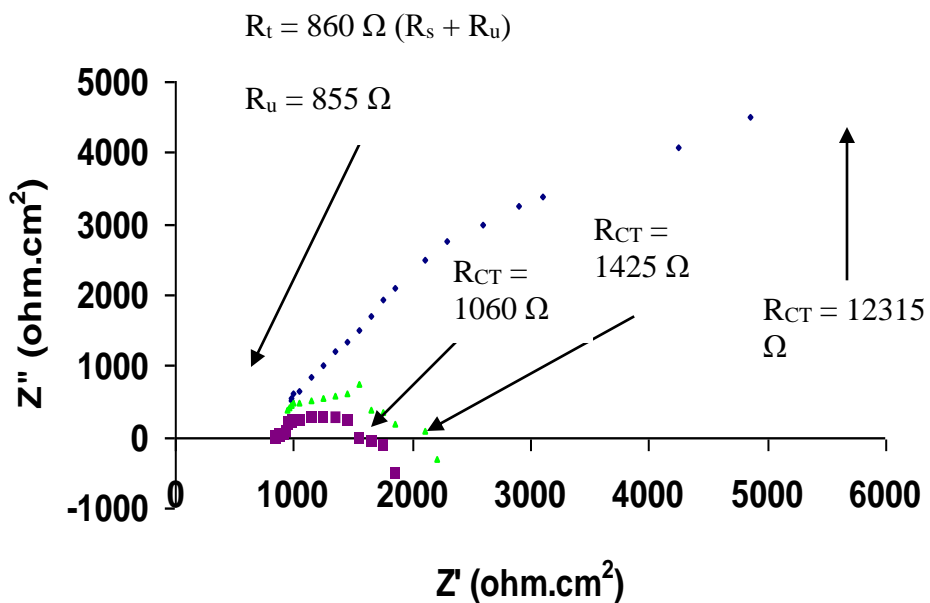


Figure 5.4(c): Overlaid Nyquist plots for a platinum electrodeposit ( $120 \text{ mC/cm}^2$  in deaerated  $0.1 \text{ M KNO}_3$ ) with applied potentials of  $0.1 \text{ V vs. MMS}$  (blue),  $0.4 \text{ V vs. MMS}$  (pink) and  $0.5 \text{ V vs. MMS}$  (green) in  $0.5 \text{ M ethanol}$  and deaerated  $0.1 \text{ M KNO}_3$ .

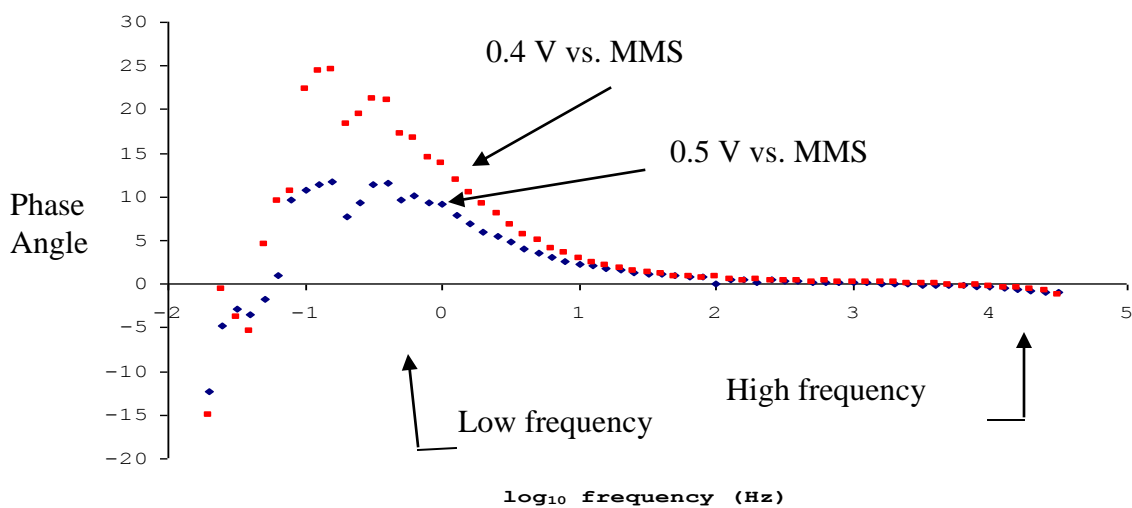


Figure 5.4(d): Overlaid Phase vs. Frequency plots for a platinum electrodeposit ( $120 \text{ mC/cm}^2$  in deaerated  $0.1 \text{ M KNO}_3$ ),  $0.5 \text{ M ethanol}$  and deaerated  $0.1 \text{ M KNO}_3$  with applied potentials of  $0.4 \text{ V vs. MMS}$  (red) and  $0.5 \text{ V vs. MMS}$  (blue).

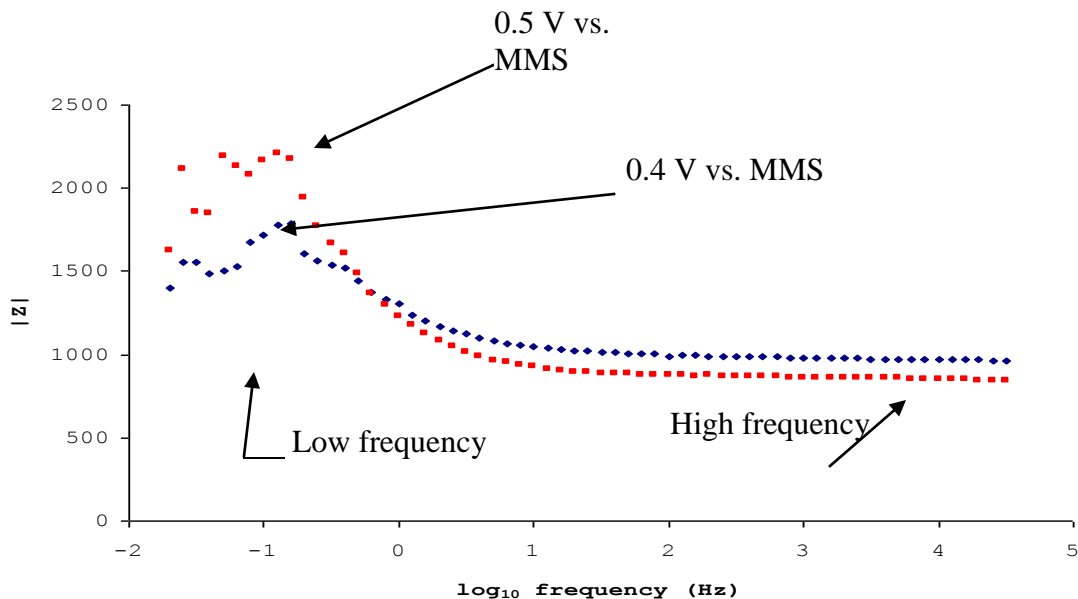


Figure 5.4(e): Overlaid impedance vs. frequency for  $120 \text{ mC/cm}^2$  platinum electrodeposit/CIE ( $120 \text{ mC/cm}^2$  in deaerated  $0.1 \text{ M KNO}_3$ ),  $0.5 \text{ M}$  ethanol and deaerated  $0.1 \text{ M KNO}_3$  with applied potentials of  $0.4 \text{ V}$  vs MMS (blue) and  $0.5 \text{ V}$  vs. MMS (red).

The decreased EOR activity at  $0.5 \text{ V}$  suggests that there is increased reactivity at the electrode at  $0.4 \text{ V}$ . From the voltammetry, it is this potential ( $0.4 \text{ V}$ ) where the first reaction occurs, peak A, which is associated with the adsorption of hydroxide from the splitting of water in near neutral electrolyte, pH 6, and the initial adsorption of ethanol onto the catalyst surface. Furthermore, at  $0.4 \text{ V}$  vs. MMS, the arc moves below the x-axis and begins to curve inwards, potentially indicating the beginning of an inductance loop. This is a characteristic impedance spectrometry for an adsorbed species at the surface of the catalyst.<sup>3</sup> This inductance with values below the x-axis have both been observed before for ethanol oxidation at a platinum electrode. This adsorption process, identified by the induction loop, may be either of the two reactions at the surface outlined in section

2.9, the simultaneous formation of  $\text{Pt}(\text{OH})_{\text{ads}}$  and  $\text{Pt}(\text{CHOHCH}_3)_{\text{ads}}$  accounting for the difference in  $R_{\text{CT}}$ .

Sample Bode plots for the platinum electrodeposit/CIE behaviour at 0.4 V vs. MMS and 0.5 V vs. MMS are shown in figure 5.4(d) and figure 5.4(e). The high frequency data points are to the right of the Bode plot and low frequency points are found on left. Very high frequency points have been shown to cause a loop at the start of Nyquist plots where the datapoints are not stable with the very long timeframes associated with these frequencies due to cable induction. At low frequencies ( $<10^{-1}$  Hz), the impedance collected at 0.4 V vs. MMS appears lower than that at 0.5 V in figure 5.4(e).

Notably, there appears to be substantial contribution caused by  $R_u$  throughout the data collected. Figure 5.4(f) shows a magnified section of the Nyquist plot associated with a platinum electrodeposit/CIE at 0.4V shown in figure 5.4(c). The  $R_u$  value is approximately 840  $\Omega$ , when expected  $R_t$  ( $R_s + R_u$ ) value is in the region of 10  $\Omega$  for a fully coated metal surface. However, this is not always the case as reported for a graphene electrode which has areas of good reactivity (edge plane) and poor reactivity (edge plane) similar to the carbon ink used in this work, returning  $R_t$  values in excess of 2000  $\Omega$ .<sup>25</sup> Furthermore, screen printed carbon ink electrodes have been reported with  $R_t$  values over 3,000  $\Omega$ .<sup>29</sup>

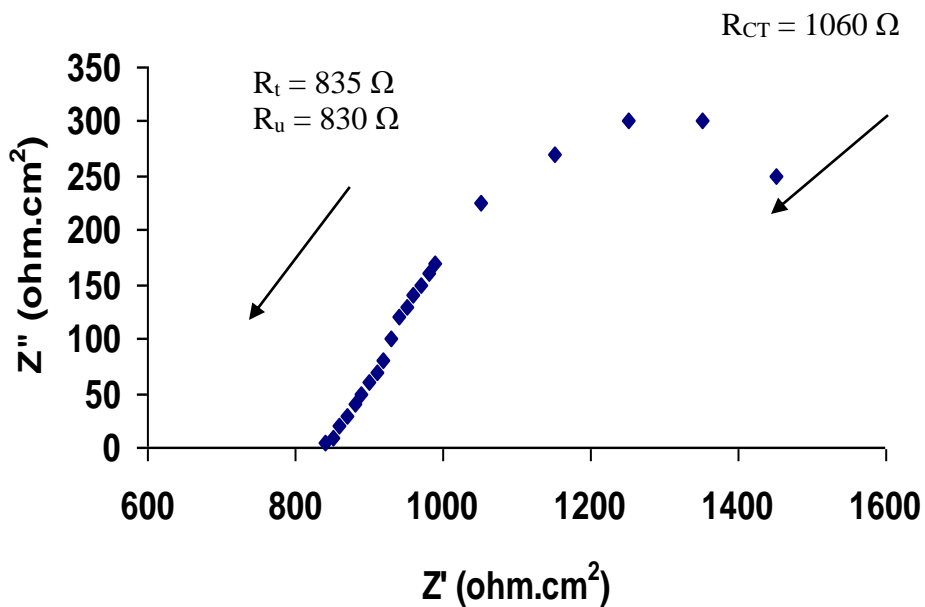


Figure 5.4(f): Magnified portion of Nyquist plot for a platinum electrodeposit/CIE (120 mC/cm<sup>2</sup> in deaerated 0.1 M KNO<sub>3</sub>), 0.5 M ethanol in deaerated 0.1 M KNO<sub>3</sub> with an applied potential of 0.4 V vs. MMS, pH = 6.

This high  $R_u$  value, 830  $\Omega$ , is significant in terms of the poor conductivity already discussed of the carbon ink electrode and helps in diagnosing the induction period observed and discussed previously. This was noted in chapters 3 and 4, paying particular attention to the chronocoulometry results, and in section 2.7 where there was a poor separation of peaks for a  $Fe^{3+}/Fe^{2+}$  couple. There was also comparatively very slow kinetics at a bare carbon ink electrode. The platinum sheet electrode in ethanol results recorded in figure 5.3(a) confirms this theory. Hence, the large  $R_u$  value was assigned solely to the carbon ink. This means that an extra resistor in series in the circuit model must be included separately in this work compared to the established model for ethanol oxidation by Gupta<sup>32</sup> and Dutta.<sup>18</sup> To test carbon ink against carbon paper, the Nyquist

plot obtained from a platinum electrodeposit ( $120 \text{ mC/cm}^2$ ) on a CPE is shown in figure 5.4(g) at 0.4 V below. The resistance observed relating to  $R_u$  is slightly reduced by approximately  $200 \Omega$  to  $620 \Omega$ , supporting the view that slower kinetics at the carbon and neutral media was responsible for the large  $R_u$  value and can be reduced via improved porosity or improved electron transfer mentioned throughout this work.

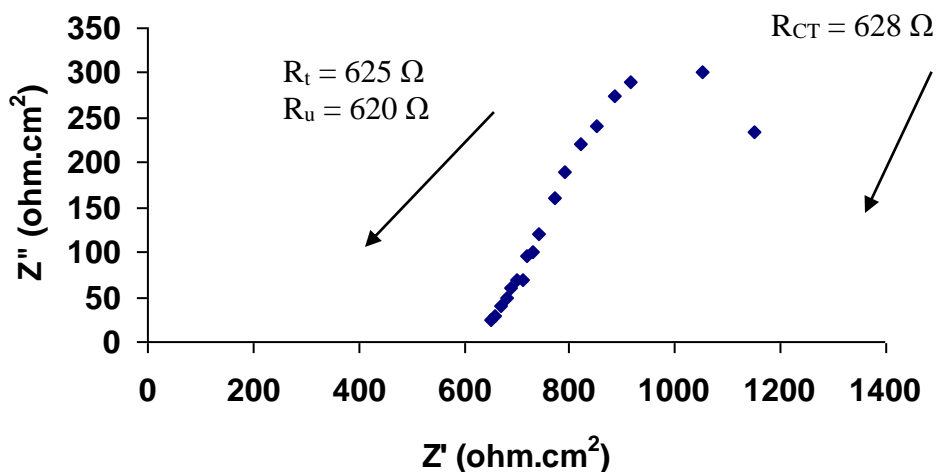


Figure 5.4(g): Full portion of Nyquist plot for a platinum electrodeposit/CPE ( $120 \text{ mC/cm}^2$  in deaerated  $0.1 \text{ M KNO}_3$ ),  $0.5 \text{ M ethanol}$  and deaerated  $0.1 \text{ M KNO}_3$  with an applied potential of  $0.4 \text{ V vs. MMS}$ ,  $\text{pH} = 6$ .

The  $R_t$  value has been reduced to approximately  $625 \Omega \cdot \text{cm}^2$  at a carbon paper electrode from  $845 \Omega \cdot \text{cm}^2$  at a carbon ink electrode. The charge transfer resistance has also decreased at the same potential to  $628 \Omega$  from  $1060 \Omega$  at a carbon ink electrode. This further indicates CPEs shows improved performance over CIEs. This suggests that the electrodeposit/CPE combination is the best performing catalyst at  $0.4 \text{ V vs. MMS}$ .

However, the uncompensated resistance is still present, inherent to a carbon surface in this work and as recorded by other groups. By comparison to some carbon surfaces, the

induction period is substantially less at the CIE and CPE than the 2000  $\Omega$  at a graphene surface. A possible reason for this may be due to the reported poor reactivity of a graphene surface outside of its edges and its sister material, carbon nanotubes reported by Banks *et al.*<sup>33-34</sup>

Consequently, using EIS can be a useful tool to perform a diagnostic assessment for such popular electrodes for quick analysis of a suitable carbon surface before taking further analysis such as voltammetry or ethanol fuel cell data collection. With respect to circuits, models should be treated with caution. A good looking fit can be obtained by adding lots of circuit elements to a model which may not have relevance to cell process studied.<sup>35-36</sup> A good fit to a data set does not necessarily represent an accurate physical model of the cell.<sup>35</sup> The full model for ethanol oxidation in this work is below:

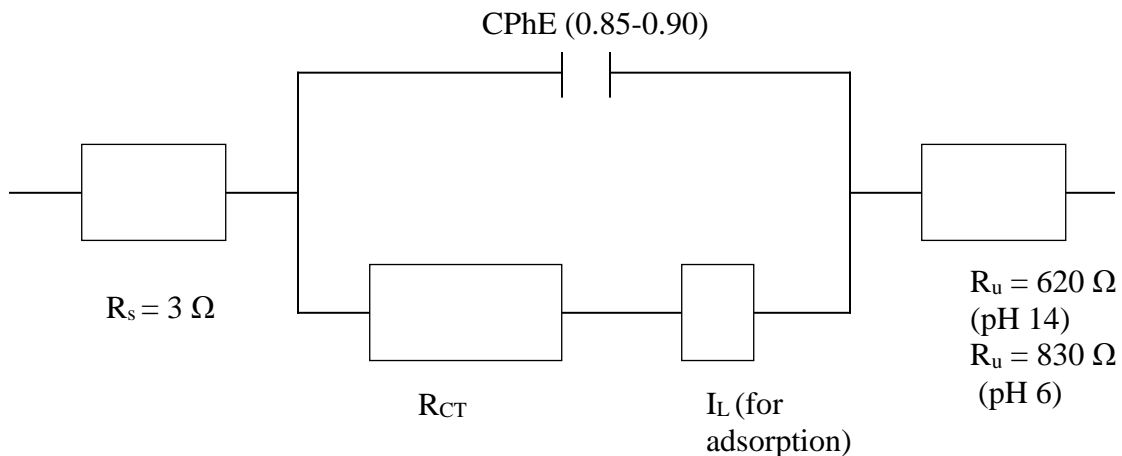


Figure 5.4(h): Circuit for ethanol oxidation (black) and which has been adapted with extra circuit elements added to account for adsorption at 0.4 V vs. MMS (inductive loop,  $I_L$ , and  $R_u$  = carbon electrode resistance) with  $R_s$  = solution resistance,  $R_{CT}$  = charge transfer resistance, CPhE = Constant Phase Element.

In addition to the circuit shown in figure 5.3(d) from Rubinson<sup>14</sup>, this work needed to include an extra resistance associated with the electrode in series and an inductive loop element ( $I_L$ ) and the resistance associated with the carbon surface,  $R_u$  where adsorbed species are present, due to the loop observed at low frequencies. The inductive loop and uncompensated resistance are added in the circuit in figure 5.4(h).

<b>Applied Potential (V vs. Hg/Hg<sub>2</sub>SO<sub>4</sub>)</b>	<b>R<sub>CT</sub> (Ω.cm<sup>2</sup>) (0.1 M KNO<sub>3</sub>)</b>	<b>R<sub>CT</sub> (Ω.cm<sup>2</sup>) (1 M NaOH)</b>
0.1	12,365	11,329
0.3	5,375	3,229
0.4	1,060	1,245
0.5	1,425	850
0.85	590	520
0.95	510	452

Table 5(a): A table of  $R_{CT}$  values for the best performing platinum electrocatalyst/CIE, (120 mC/cm<sup>2</sup> in 0.1M KNO<sub>3</sub>) in 1 M NaOH and 0.5 M ethanol or 0.1 M KNO<sub>3</sub> and 0.5 M ethanol at applied potentials, based on circuit in figure 5.4(h).

Furthermore, Gupta tabulates the  $R_{CT}$  value as a function of applied potential for their own circuit (figure 5.3(d)) and this is the approach used for data collected in this chapter. This approach categorises the main circuit element that changes across all potentials and

is still common to all potentials. The  $R_t$  measured in each electrolyte remains unchanged for all deposit/CIEs ( $830 \Omega$  at pH 6 and  $620 \Omega$  in pH 14) in this chapter. Similarly, the Constant Phase Element (CPhE) is employed to model the non-ideal capacitive behaviour, which is common as the oxide or hydroxide layer is formed such as the dissociation of water at 0.4V or the formation of PtO at higher potentials, in excess of 0.8V vs. MMS. The CPhE is common to many DEFC models for this reason. A CPhE can be characterised by the constant obtained in the model. If the model exhibited ideal capacitive behaviour, the CPhE element should approach 1, which is a true capacitor. When the CPhE element falls below 0.80, it is often termed a poor capacitor. The CPhE is used instead of the capacitor in real cells ( $C_{dl}$ ) to illustrate the double layer. It is often signified by a depressed semicircle on a Nyquist plot. The range in this work 0.85 and 0.90 for all electrodes. Table 5(a) highlights the range of  $R_{CT}$  values obtained at a platinum electrodeposit,  $120 \text{ mC/cm}^2$ , at the applied potentials shown in near neutral and base electrolyte, pH 6 and pH 14, respectively.

### **5.5 EIS data – electrodeposited Pd/CIE, Ni/CIE, Au/CIE**

Impedance testing was carried out on the best performing co-deposit/CIE catalysts. In particular those discussed previously in chapters three and four, namely a Pt75%Pd25%/CIE electrode and Pt90%Ni10%/CIE electrode as well as Pd70%Ni30%/CIE supports, and an Au/CIE were tested. This was completed to conduct a comparison in terms of surface reactivity and to aid and support the adsorption theory associated with the operation of the bifunctional mechanism.

Figure 5.5(a) presents a similar graph for an Au/CIE at 0.4 V vs. MMS in pH 6 electrolyte. Gold has been used in many DEFC electrodes as mentioned previously in sections 2.7, 2.9 and 2.16. It has been tested directly on a gold substrate and compared to carbon electrodes by Choi *et al.*<sup>37</sup> Notably, Choi found that electron transfer is further improved on HOPG surfaces than the smooth gold or glassy carbon surfaces due to the high amount of edge planes on HOPG.<sup>37</sup> The CPhE value obtained at this potential was the largest of all CIEs tested at 0.90. The  $R_t$  value is substantially larger at 6,268  $\Omega$  and postulated that this is because the particles of gold across the CIE were more dispersed across the electrode, exposing more of the carbon ink electrode and causing a greater uncompensated resistance,  $R_u$ , component. Furthermore, the  $R_{CT}$  from the model was the largest of all electrodes at 9153  $\Omega$  beyond 0.1 V vs. MMS. This suggests a very inactive surface for ethanol oxidation and as such agrees with poor activity towards the EOR on gold electrodes found throughout this work.

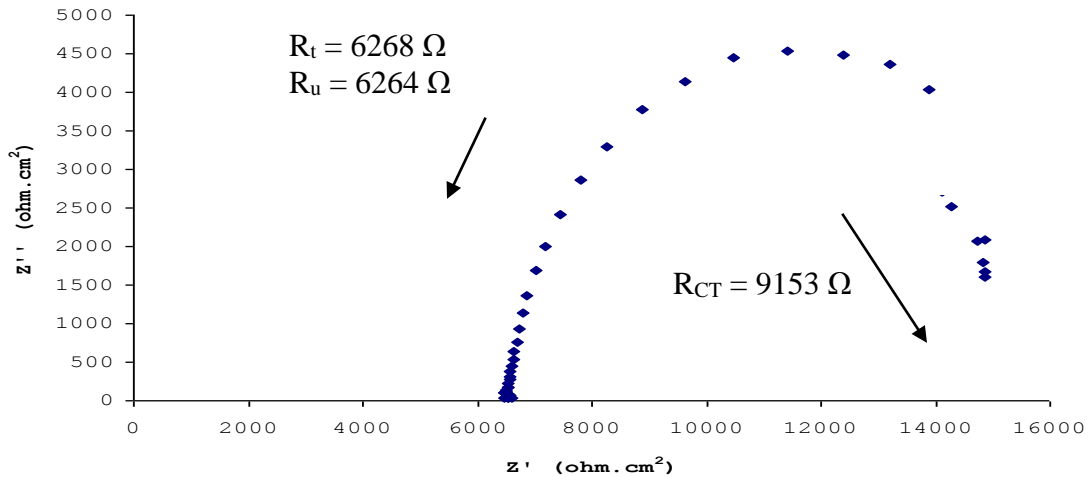


Figure 5.5(a): Nyquist plot obtained from a gold electrodeposit/CIE ( $120 \text{ mC/cm}^2$  in deaerated  $0.1 \text{ M KNO}_3$ ),  $0.5 \text{ M}$  ethanol and  $0.1 \text{ M KNO}_3$  with an applied potential of  $0.4 \text{ V}$  vs MMS,  $\text{pH} = 6$ .

Figure 5.5(b) shows a Nyquist plot for a Pt75%Pd25% electrode at multiple applied potentials in  $\text{KNO}_3$  and, further, at  $0.85 \text{ V}$  in  $1 \text{ M NaOH}$  in figure 5.5(c). The EOR at different pH is pivotal to determine the optimum conditions for the catalyst. This is a direct comparison between the first peak in the CV in previous chapters, peak A at  $\text{pH} 6$  and peak X in  $\text{pH} 14$  electrolyte. Of particular interest is the decreased total resistance in  $\text{NaOH}$  and that  $0.85 \text{ V}$  vs. MMS is where the characteristic features of adsorbed species are observed. A smaller uncompensated resistance,  $R_u$ , was associated with the electrode. As observed previously in voltammetry, one peak was recorded at approximately  $0.85 \text{ V}$  on the forward sweep in  $1 \text{ M NaOH}$  and a nearby (in terms of potential) peak on the return sweep.

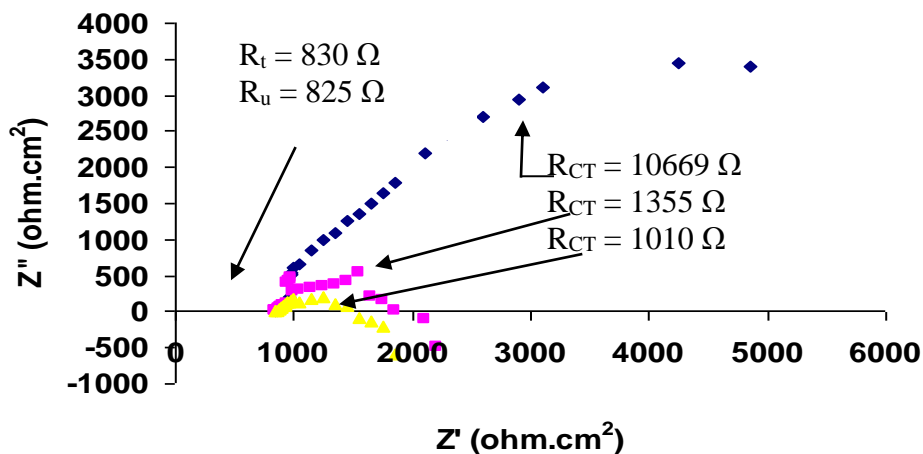


Figure 5.5(b): Nyquist plot obtained from a Pt75%Pd25% electrodeposit/CIE

(120 mC/cm<sup>2</sup> in deaerated 0.1 M KNO<sub>3</sub>) in deaerated 0.1 M KNO<sub>3</sub> and 0.5 M ethanol with an applied potential of 0.1 V vs. MMS (blue), 0.4 V vs. MMS. (pink) and 0.5 V vs. MMS (yellow), pH = 6.

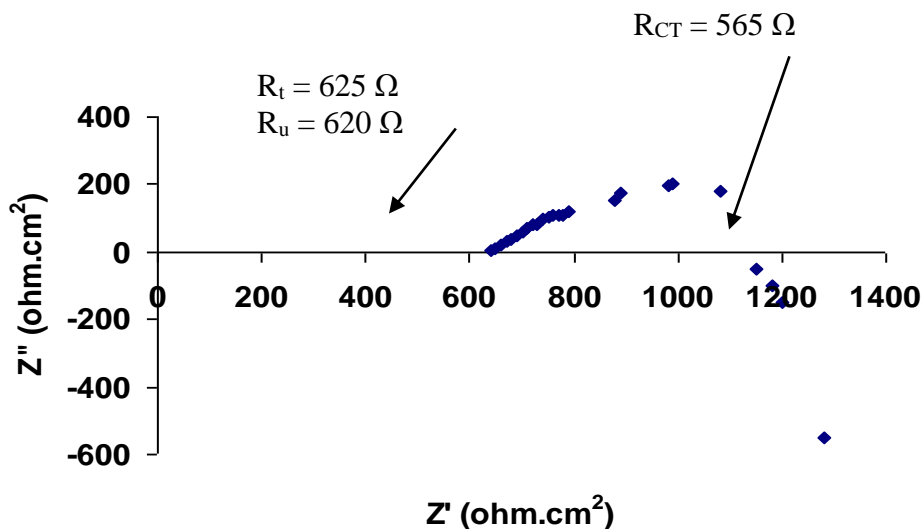


Figure 5.5(c): Nyquist plot obtained from a Pt75%Pd25% electrodeposit/CIE (120 mC/cm<sup>2</sup> in deaerated 0.1 M KNO<sub>3</sub>) in deaerated 1 M NaOH and 0.5 M ethanol with an applied potential of 0.85 V vs. MMS, pH = 14.

Table 5(b) categorises the charge transfer resistance collected from the circuit modeling of the best performing Pd electrodes in a range of pH, fitted to the circuit shown in figure 5.4(h). In 1 M NaOH, the voltammetry shows no features of adsorption below 0.7 V vs. MMS and consequently, there was no tendency for the EOR to occur. Consequently, at the potentials associated with peak A in the CVs from near neutral pH, there was increased reaction in 0.1 M KNO<sub>3</sub> around 0.4-0.5 V vs. MMS than compared to high pH conditions at the same potential. This resulted in a lower  $R_{CT}$  value.

<b>Applied Potential (V vs. Hg/Hg<sub>2</sub>SO<sub>4</sub>)</b>	<b>R<sub>CT</sub> (Ω.cm<sup>2</sup>) (0.1 M KNO<sub>3</sub>)</b>	<b>R<sub>CT</sub> (Ω.cm<sup>2</sup>) (1 M NaOH)</b>
0.1	10,669	10,117
0.4	1,010	3,085
0.5	1,355	1,165
0.75	956	826
0.85	700	565
0.95	535	328

Table 5(b): A table of R<sub>CT</sub> values for the best performing Pd bimetallic electrodeposit/CIE, Pt75%Pd25% (120 mC/cm<sup>2</sup> in deaerated 0.1 M KNO<sub>3</sub>) in 1 M NaOH and 0.5 M ethanol or 0.1 M KNO<sub>3</sub> with 0.5 M ethanol at various applied potentials, based on the fitted circuit model in figure 5.4(h).

Nickel electrodes have been tested in alkaline media for activity towards the EOR by Kim and Park,<sup>38</sup> though the experiments were conducted with nickel wire, rather than

with nickel deposits. The equivalent circuit proposed by Kim<sup>38-39</sup> agrees with that collected from the deposits in this work with an extra resistor in series to that of previous electrodes for platinum and palladium. Furthermore, the resistance of the electrode from this work has to be factored in. Figure 5.5(d) below shows the Nyquist plot for the best performing bimetallic catalyst containing nickel, Pt90%Ni10% electrodeposit/CIE at 0.4 V vs. MMS.

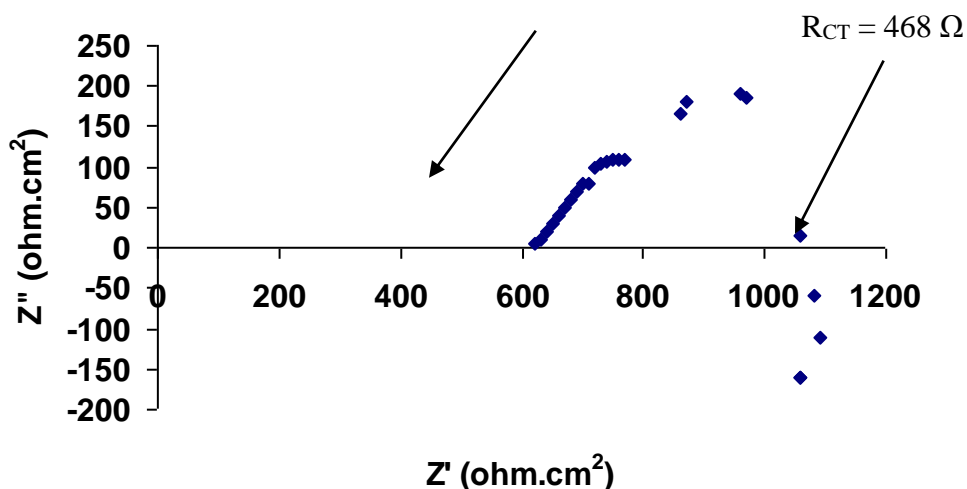


Figure 5.5(d): Nyquist plot obtained from a Pt90%Ni10% electrodeposit/CIE (120 mC/cm<sup>2</sup> in 0.1 M KNO<sub>3</sub>) in deaerated 1 M NaOH and 0.5 M ethanol with an applied potential of 0.85 V vs. MMS, pH = 14.

Table 5(c) below summarises the charge transfer resistances measured at selected applied potential conditions for a Pt90%Ni10% electrodeposit/CIE in 1 M NaOH or 0.1 M KNO<sub>3</sub> with 0.5 M ethanol. As potential decreased, the charge transfer resistance reduced as expected in high pH. All applied potentials exhibited lower  $R_{CT}$  in high pH.

<b>Applied Potential (V vs. Hg/Hg<sub>2</sub>SO<sub>4</sub>)</b>	<b>R<sub>CT</sub> (Ω.cm<sup>2</sup>) (0.1 M KNO<sub>3</sub> + 0.5 M ethanol)</b>	<b>R<sub>CT</sub> (Ω.cm<sup>2</sup>) (1 M NaOH + 0.5 M ethanol)</b>
0.1	10,665	9,925
0.4	3,618	3,151
0.5	2,646	2,296
0.75	1,252	965
0.85	928	468
0.95	782	400

Table 5(c): A table of R<sub>CT</sub> values for the best performing nickel bimetallic electrocatalyst/CIE, Pt90%Ni10% (120 mC/cm<sup>2</sup> in 0.1 M KNO<sub>3</sub>) in 1 M NaOH and 0.5 M ethanol or 0.1 M KNO<sub>3</sub> and 0.5 M ethanol at applied potentials, based on the fitted circuit model.

Figure 5.5(e) shows a Nyquist plot from a Pd70%Ni30% electrodeposit/CIE. The voltammetry (as observed in section 4.4) at 0.95 V seems to support the Nyquist plot obtained, where the difference in this  $R_t$  and  $R_{CT}$  ( $850\Omega$  and  $420\Omega$  respectively at 0.95V vs. MMS) respectively decreases in line with an increase in applied potential. By comparison, a Pd70%Ni30% electrodeposit/CIE does not display an inductance loop associated with an adsorption process. The most prominent peak in the voltammetry of the Pd70%Ni30% electrodeposit/CIE was for peak B at 0.95 V vs. MMS. The model that fits this Nyquist plot is the standard ethanol oxidation circuit model, shown in figure 5.3(d). This result infers that the peak at higher potentials in neutral electrolyte, pH 6, is primarily an oxidation step of the already adsorbed ethanol instead of a separate adsorption step.

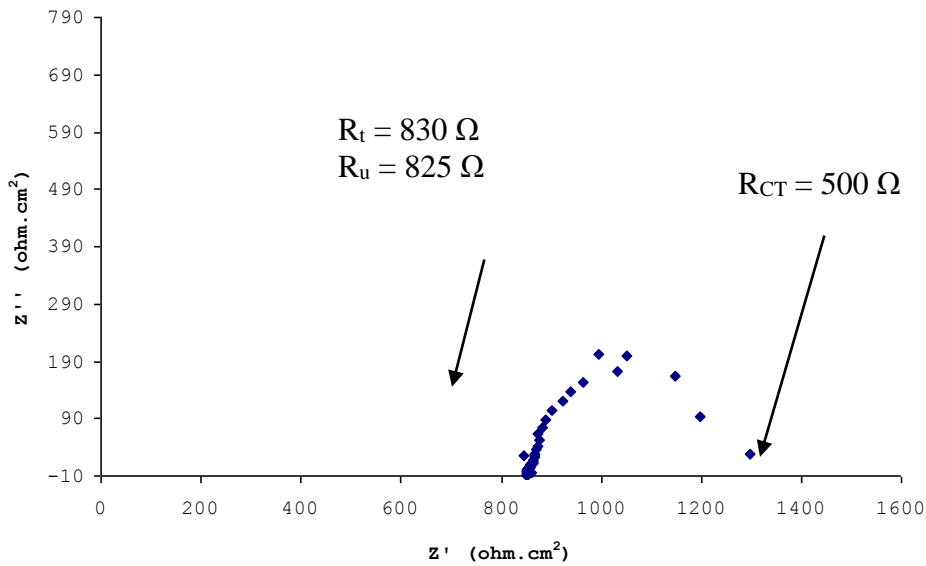


Figure 5.5(e): Nyquist plot for a Pd70%Ni30% electrodeposit/CIE ( $120 \text{ mC/cm}^2$  in deaerated  $0.1 \text{ M KNO}_3$ ),  $0.5 \text{ M ethanol}$  and  $0.1 \text{ M KNO}_3$  with an applied potential of  $0.95 \text{ V vs. MMS}$ ,  $\text{pH} = 6$ .

## 5.6 Conclusions

The Electrochemical Impedance Spectroscopy data provided detail about the electrodes at particular potentials in the presence of ethanol. The Nyquist plots were obtained at set values according to peaks A and B in the cyclic voltammogram of ethanol oxidation. At the crest of the peaks, the catalysts exhibited an inductive loop which is related to an adsorption process occurring at that potential. Seland *et al.*<sup>9</sup> have shown how applying different set potentials based on the voltammetry of methanol oxidation as well as formic acid oxidation and it has been found to apply to ethanol oxidation in this chapter. The charge transfer resistance,  $R_{CT}$ , was used to categorise the catalysts. The  $R_{CT}$  value should decrease with increasing potential according to its inverse relationship to the rate of the reaction and this was observed. However, the Nyquist plots at 0.45 V and 0.55 V vs. MMS exhibited an exception to this trend.

The fitted circuit diagram was found to be similar to the simple RC-parallel circuit reported by Gupta and Rubinson<sup>14</sup> for ethanol oxidation, but it also required with extra added elements to account for the uncompensated resistance due to the electrode and the inductive loop for adsorption. Typically, the resistance of the solution,  $R_s$ , was low at 3  $\Omega$ , but the uncompensated resistance,  $R_u$ , was very large in comparison to metal electrodes in the same solution. This uncompensated resistance for a carbon ink and paper electrodes reflects the slow kinetics at various carbon electrodes. The values of

620  $\Omega$  and 830  $\Omega$ , in pH 14 and pH 6 respectively, are low compared to some carbon electrodes in the literature such as graphene, screen printed electrodes and other carbon ink electrodes. It was found that the uncompensated resistance decreased slightly when 1 M NaOH was used as the electrolyte, which indicated that the kinetics were slightly improved with the availability of  $\text{OH}^-$ . The slow kinetics shown by the carbon electrode here reinforce the findings of previous chapters of the lag period in the chronocoulometry and high peak separation for the  $\text{Fe}^{3+}/\text{Fe}^{2+}$  couple. It is an important finding to note that the carbon surface contributes a detrimental effect to EOR kinetics, and yet it does not promote an enhancement towards ethanol oxidation.

## 5.7 References:

1. Lasia, A.; "Electrochemical Impedance Spectroscopy and its Applications, in Modern Aspects of Electrochemistry by B.E. Conway, R.E. White and J. O'M. Bockris", Kluwer Academic Plenum Publishers, New York, (1999), 32, 143-248.
2. Application Note, "Basics of Electrochemical Impedance Spectroscopy", Gamry Association Inc.
3. Lvovich, V.F.; (2012), "Impedance Spectroscopy, Applications to Electrochemical and Dielectric Phenomena", John Wiley and Sons Ltd., ISBN: 978-0-470-62778-5.
4. Randviir, E.P.; Metters, J.P., Stainton, J.; Banks C.E.; (2013), *Analyst*, **138**, 2970-2981.

5. Hlavata, L.; Benikova, K.; Vyskocil, V.; Labuda, J.; (2012), *Electrochim. Acta*, **71**, 134.
6. Mathebula, N.S. Pillay, J.; Toschi, G.; Verschoor; Ozoemena, K.I.; (2009), *Chem. Comm.*, 3345.
7. Liu, G.; Iyengar, S.G.; Gooding, J.J.; (2012), *Electroanal.*, **24**, 1509.
8. Erdem, A.; Muti, M.; Karadeniz, H.; Congur, C.; Canavar, E.; (2012), *Colloid. Surf. B*, **95**, 222.
9. Seland, F.; Tunold, R.; Harrington, D.A.; (2008), *Electrochim. Acta*, **53**, 6851-6864.
10. Seland, F.; Tunold, R.; Harrington, D.A.; (2006), *Electrochim. Acta*, **51**, 3827-3840.
11. Azevedo, D.C.; Lizcano-Valbuena, W.H.; Gonzalez, E.R.; (2004), *J. New Mater. Electrochem. Sys.*, **7**, 1.
12. Otomo, J.; Li, X.; Kobayashi, T.; Wen, C.; Nagamoto, H.; Takahashi, H.; (2004), *Electroanal. Chem.*, **573**, 99.
13. Wu, G.; Li L.; Xu, B.Q.; (2004), *Electrochim. Acta*, **50**, 1-10.
14. Rubinson, J.F.; Kayinamura, Y.P.; (2009), *Chem. Soc. Rev.*; **38**, 3339-3347.
15. Application Note 11, "Electrochemical Impedance Spectroscopy: Basic Principles", <http://www.metrohm-autolab.com>.

16. Orazem, M.E. Triballet, B.; (2008), "Electrochemical Impedance Spectroscopy", John Wiley and Sons Ltd., ISBN: 978-0-470-04140-6.
17. Désilets, C.; Lasia, A.; (2012), *Electrochim. Acta*, **78**, 286-293.
18. Dutta, A. ; Datta, J.; (2013), *Int. J. Hydrogen Energ.*, **38**, 7789-7800.
19. Dutta, A. ; Mahaptra, S.S.; Datta, J.; (2011), *Int. J. Hydrogen Energ.*, **36**, 14898-14906.
20. Han, L.; Ju, H.; Xu, Y.; (2012), *Int. J. Hydrogen Energ.*, **37**, 15156-15163.
21. Gupta, S.S.; Singh, Datta, J.; (2010), *Mater. Chem. Phys*, **120**, 682-690.
22. Mikolajczyk, T.; Turemko, M.; Pierozynski, B.; (2014), *J. Electroanal. Chem.*, **735**, 32-35.
23. Castro Luna, A.M.; Bonesi, A.R.; Moreno, M.S.; Zampieri, G.; Bengió, S.; Triaca, W.E.; (2014), *Int. J. Hydrogen Energ.*, **39**, 8690-8696.
24. Pumera, M.; (2011), *Mater. Today*; **14**, 308-315.
25. Bonanni, A.; Pumera, M.; (2012), *Electrochem. Comm.*, **16**, 19-21.
26. Bonanni, A.; Pumera, M.; (2013), *Electrochem. Comm.*, **26**, 62.
27. Loo, A.H.; Bonanni, A.; Pumera, M.; (2013), *Electrochem. Comm.*, **28**, 83-86.
28. Casero, E.; Parra-Alfambra, A.M.; Petit-Domiguez, M.D.; Pariente, F.; Lorenzo, E. ; Alonso, C. ; (2012), *Electrochem. Comm.*, **20**, 63-66.

29. Truong, L.T.N.; Chikae, M.; Ukita, Y.; Takamura, Y.; (2011), *Talanta*, **85**, 2576-2580.
30. Wen-Zhi, L.; You-Qin, L.; (2009), *Sensors and Actuators*, **141**, 147-153.
31. Yan, M.; Zang, D.; Ge, S.; Ge, L.; Yu, J.; (2012), *Biosens. Bioelectron.*, **38**, 355-361.
32. Gupta, S.S.; Datta, J.; (2005), *J. Power Sources*, **145**, 124-132.
33. Brownson, D.A.C.; Kampouris, D.K.; Banks C.E.; (2011), *J. Power Sources*, **196**, 4873-4885.
34. Randviir, E.P.; Brownson, D.A.C.; Banks, C.E.; (2014), *Mater. Today*, **17**, 426-432.
35. <http://www.pirg.ch.pw.edu.pl/instrukcje/eis-introduction.doc>, viewed May 2015.
36. Mansfield, F.; (1990), *Electrochim. Acta*, **35**, 1533.
37. Choi, S.; Seo, B.; Kim, J.; (2010), *Bullet. Kor. Chem. Soc.*, **31**, 104-111.
38. Kim, J-W.; Park, S-M; (2005), *J. Kor. Electrochem. Soc.*, **8**, 3, 117-124.
39. Park, S-M.; Yoo, J-S.; (2003), *American Chem. Soc.*, 455A.

## Chapter 6: Fuel Cell Power Curves

### 6.1 Introduction:

The basic principle of fuel cell operation is that the potential difference between the catalytic oxidation of a fuel at one surface, the anode, and oxygen reduction at another, the cathode, generates current flow.<sup>1, 2</sup> Typically, a membrane is used across these catalytic surfaces to complete the current through either proton exchange or anion exchange created at the anode or cathode. An example of this set up is shown in figure 6.1(a).

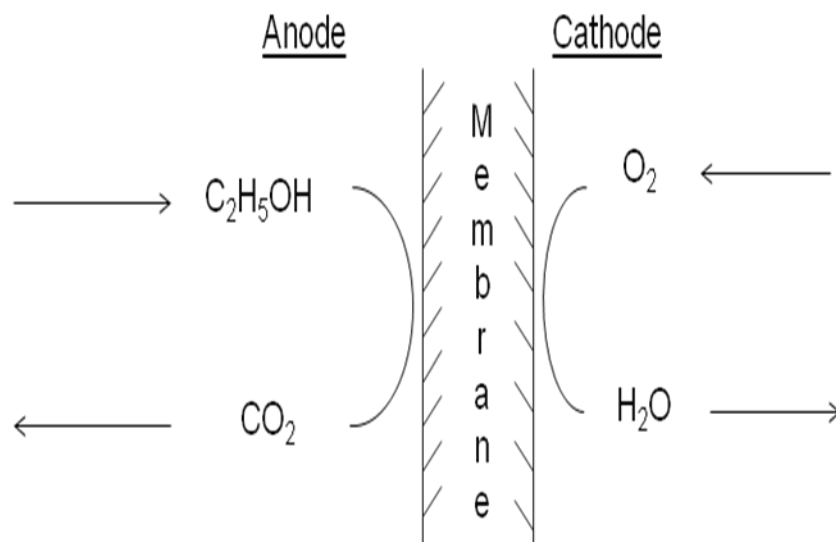


Figure 6.1 (a): Diagram of a Membrane Fuel Cell with an inflow of ethanol (fuel) at anode and inflow of oxygen gas at the cathode. Ions travel from anode to cathode or cathode to anode across the central membrane.

Liquid fuels at room temperature can be used in this experimental configuration which is a major advantage over gaseous fuels such as hydrogen.<sup>2</sup> They are far easier to transport, store and handle than hydrogen.<sup>1,2</sup> It has been reported that the thermodynamic efficiency of liquid fuel cells at low temperature can be close to 100%.<sup>3</sup> Low molecular weight alcohols are therefore thought to be potential fuels for this reason. The reactions at the anode and cathode for ethanol are shown in figure 6.1(b) as shown previously.

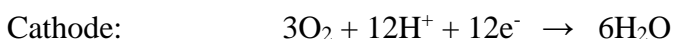
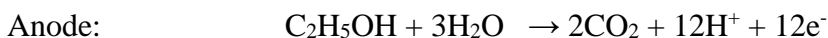


Figure 6.1(b): Full equations at the anode and cathode surface of a typical direct ethanol fuel cell (DEFC).

The open circuit potential of a fuel cell is reported as 1.14 V for ethanol, but is less due to losses including the slow kinetics of platinum towards the oxygen reduction reaction and fuel crossover across the membrane. Indeed the selectivity of the exchange membrane is of critical importance and it was found to have a substantial effect on the methanol fuel cell.<sup>3</sup> The potential drop at open circuit can be as much as 0.4 V at 50 °C.<sup>1</sup>

DEFCs can be grouped by the electrolyte for the specific membrane used. In acidic conditions, Nafion<sup>®</sup> has been used as the membrane – a perfluorosulphonated polymer with its principle of ion exchange as described in section 1.2 - which is commercially available. The bulk of published papers previously use this proton exchange membrane (PEM) due to its chemical stability and availability. The cost can be prohibitive with the quantity of platinum required at such acidic conditions. At high pH, less work has been conducted in fuel cells due to their poor chemical stability in harsh conditions, typically using either sodium hydroxide or potassium hydroxide as an electrolyte. However, increasingly, such Anion Exchange Membranes (AEM) – have been reported to be stable and used in fuel cells. As a result, research at high pH electrolyte is growing dramatically in the past seven years.<sup>4</sup> In conjunction with this, less platinum may be required due to the availability of hydroxide anions in the electrolyte and improved kinetics for the oxygen reduction reaction at surfaces other than platinum. The first step in operating a

fuel cell is to configure the most appropriate membrane electrode assembly (MEA). An example of a disassembled polymer membrane fuel cell is shown in both figure 6.1 (c) and figure 6.1(d).

The inflow of fuel passes through the bipolar plates, flowing across the electrode surface in a serpentine configuration and the resultant products formed are collected. The anode and cathode is typically mechanically pressed onto the membrane, where, for an AEM, hydroxide ions produced at the cathode cross to the anode.

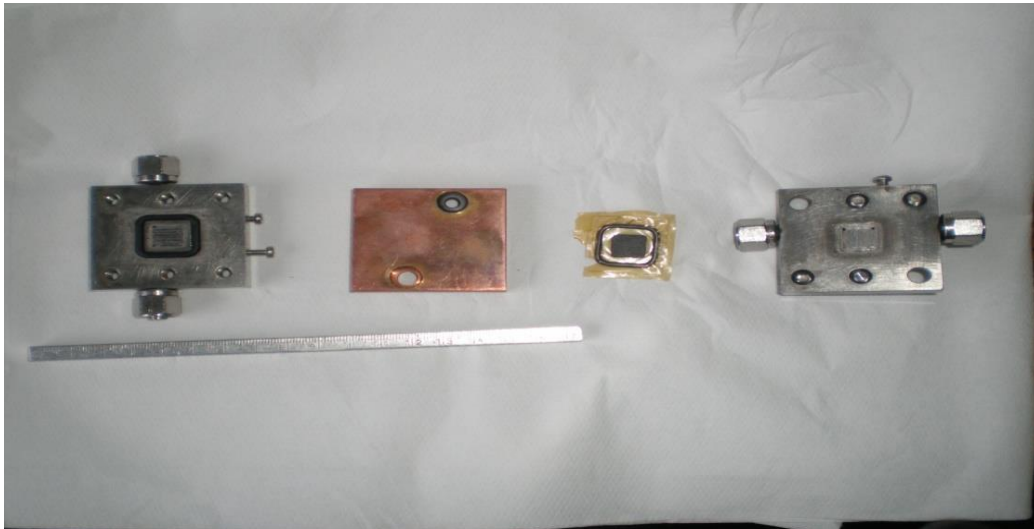


Figure 6.1(c): A sample fuel cell operating with a Proton Exchange Membrane or Anion Exchange Membrane. From left to right: Bipolar plate with central serpentine flow unit; outer heating plate; membrane electrode assembly with an embedded electrode and gas diffusion electrode; identical bipolar plate.

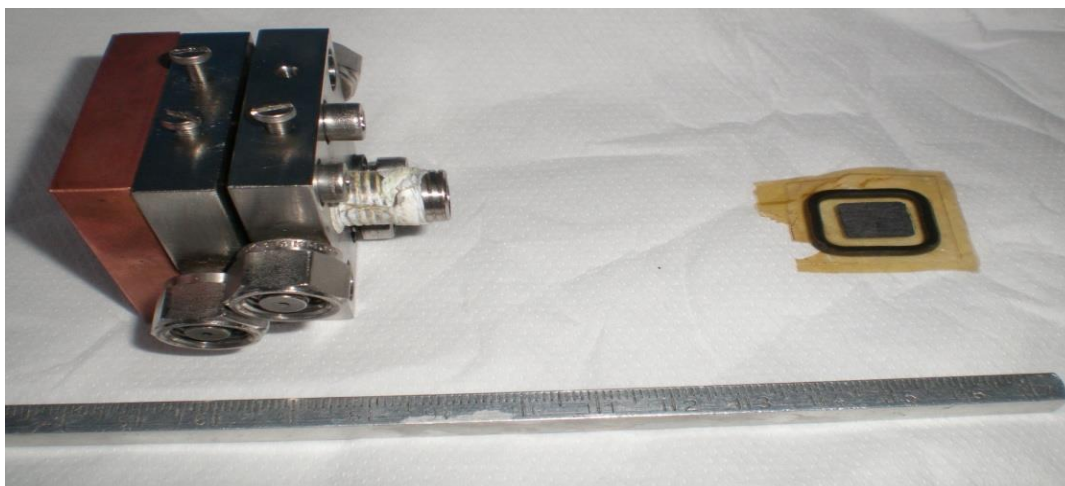


Figure 6.1(d): Sample set up of outer heating plate and bipolar plates. The membrane electrode assembly (right) is placed between the two bipolar plates.

A major issue with this fuel cell set up is the Membrane Electrode Assembly (MEA) and membrane performance. Recent research has been focused on the stability of the membrane rather than system design.<sup>1</sup> Membraneless fuel cells are increasingly being looked at to solve the problem of fuel crossover, as discussed in section 1.2. because the fuel permeates across the membrane and it is oxidised on both sides causing a performance drop - in particular that of a microfluidic membraneless fuel cell such as Lam *et al.*<sup>6-11</sup> are increasingly popular. Other limitations of the membrane design include cost, availability, membrane degradation (high pH) and ohmic losses.<sup>5</sup> An example of an experimental membrane fuel cell arrangement including fuel tanks, gas supply and electronics is shown in figure 6.1(e). By comparison simple membraneless devices are an attractive practical alternative for relatively low power devices such as mobile phones and laptops<sup>5</sup> by replacement of a fuel cartridge.



Figure 6.1(e): Example Fuel Cell Apparatus at the Physik Department E19, Technical University of Munich (TUM).

Ethanol tank

Typically, the characteristic performance curve of a fuel cell can be described as in figure 6.1(f). The ideal or theoretical maximum potential is higher than the value observed in practice when no current is flowing, the thermodynamic limit. The lower this Open Circuit Voltage (OCV) value is, the poorer a catalyst is for the oxidation reaction. As the current increases, the power decreases with the peak power being observed during the ohmic losses portion of the curve.

Mass Transport losses signifies the inactivity of the catalyst surface, where at the point where most current is observed, the concentration of the reactant(s) at the surface is zero or decreasing rapidly. A perfect fuel cell would exhibit as constant potential over time, independent of current.

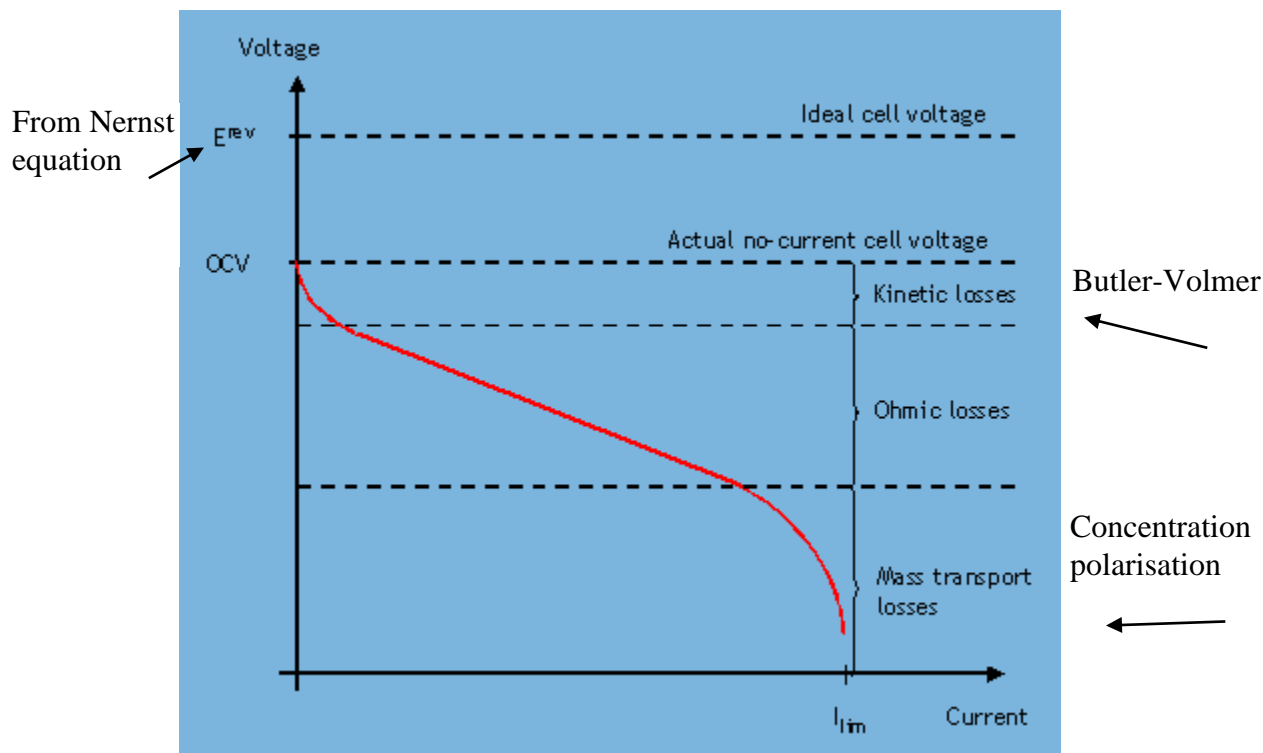


Figure 6.1(f): A Typical Fuel Cell performance over time, potential drop from Open Circuit Potential adapted from fuelcell.no. <sup>6</sup>

## 6.2 Experimental:

Carbon ink electrodes were prepared by coating a non-porous plastic sheet (Xerox) with a finely dispersed particle-based graphite inside an ink binder solvent (Acheson Industries, Electrodag 423 SS). The ink coating was then allowed to dry. The fabricated electrodes were then sectioned into  $1 \text{ cm}^2$  samples used for further testing, acting as working electrodes. A solution of commercial nail polish was added to the stem of each electrode in order to guarantee its geometrical area.

Vulcan XC72-R electrodes were prepared using 10 mg and 50 mg of a high surface area carbon powder with 57.5 % pre-loaded platinum (DeNora Chemicals, USA), supplied by

the Technical University of Munich, TUM. The powder sample was added to a solution of ethanol and de-ionised water. The resultant solution was allowed to evaporate slowly where a pre-defined weight of carbon ink (Acheson Industries, Electrodag 423 SS) was added. This process incorporated the carbon powder into an ink mixture and was then spread onto a plastic non-porous support and when dry, subsequently cut into 1 cm<sup>2</sup> electrodes. Where required, the ink/powder mix was prepared identically, painted onto a carbon paper electrode and allowed to dry. The electrodes were allowed to dry and subsequently manufactured by forming 1 cm<sup>2</sup> samples.

The Membraneless Fuel Cell experimental set up used to collect power curve data in this chapter is shown in figure 6.2(a). A close-up image of the air cathodes (Carbon/MnO<sub>2</sub> composite) used is shown in figure 6.2(b). The resistor box was initially set at very high resistance, and decreased in a stepped fashion, within a range from 10 M Ω to 10 Ω. The air cathode used was a commercially available MnO<sub>2</sub>/carbon supported in Ni mesh. This was electrically connected to a crocodile clip and fixed to the resistor box.

The air cathode was placed as high as practically possible in the solution and kept in place using a retort stand. This enables air to access through to the solution and react at the cathode. The cell containing the fuel and electrolyte used was typically a petri-dish style container or beaker. The anode or carbon ink electrodes were placed as far away from the air cathode as possible. The current, *I*, was calculated using Ohm's Law through measuring the potential, *E*, and varying the resistance, *R*. The power was subsequently calculated using the potential and current (*E* x *I*).



Figure 6.2(a): Diagram showing typical experimental set-up including resistor box, air cathode, anode and voltmeter.

The temperature of the cell was kept between 293 K and 333 K. The temperature study was carried out using an iKa<sup>®</sup> C-MAG HP7 heating plate. A range of electrolytes were used, specifically 0.1M potassium nitrate (pH 6) and sodium hydroxide, NaOH, purchased from Sigma Aldrich. To study pH, the concentration of aqueous sodium hydroxide was set to pH 14 (1 M NaOH). Solutions of ethanol, methanol and glucose were purchased from Sigma Aldrich. The concentration of ethanol set at 0.5 M ethanol.



Figure 6.2(b): Close up image of air cathode ( $\text{MnO}_2$ /carbon composite) used in sample fuel cell.

### 6.3 Commercial Anode Test

As a proof of concept test for the carbon supported electrodeposits later in the chapter, figure 6.3(a) shows power curve data obtained from a plastic fuel cell container with a pre-loaded platinum mesh as the anode. This platinum mesh had a comparatively high loading of platinum compared to the chosen electrocatalysts. The open circuit potential in

ethanol was 663 mV, by comparison to that in the blank solution which was found to be 165 mV. Over time, as the resistance drops, the current increased to a maximum of 20 mA. The maximum power measured was 2.82 mW. This level of power and current is still low compared to the demand of mobile applications such as laptops which require up to 3 W.<sup>7</sup>

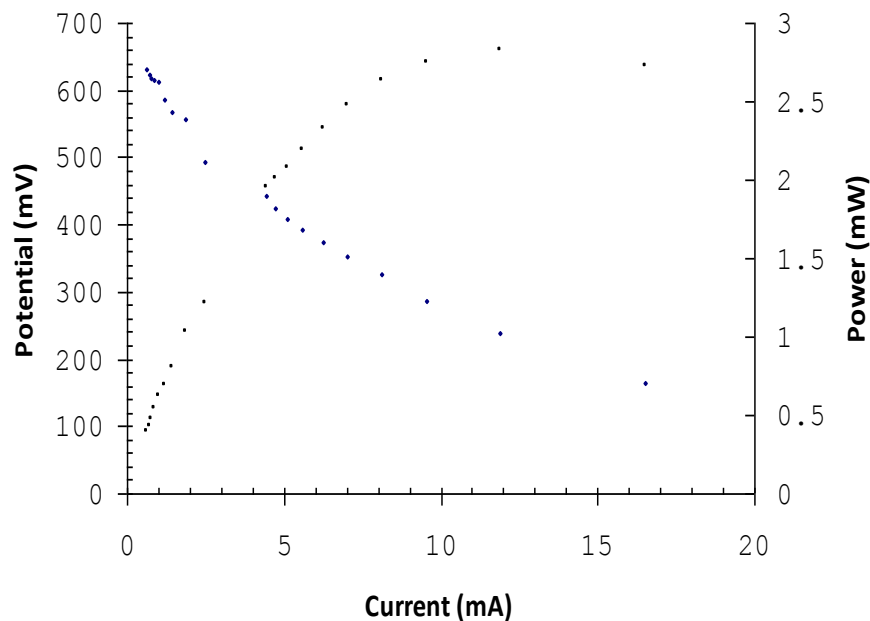


Figure 6.3(a): Power curve data obtained from a commercial platinum mesh electrode (anode) in 0.5 M C<sub>2</sub>H<sub>5</sub>OH, 1 M NaOH, with an air electrode as cathode.

In the blank solution the current observed was considerably lower in comparison and below the mid-range resistance, the current does not increase. Figure 6.3(b) shows this identical experimental arrangement without ethanol present, containing background electrolyte, NaOH, with respect to potential and current. When ethanol is added, the drop in potential from 663 mV to 170 mV remains greater than the blank solution owing to the catalysis of ethanol.

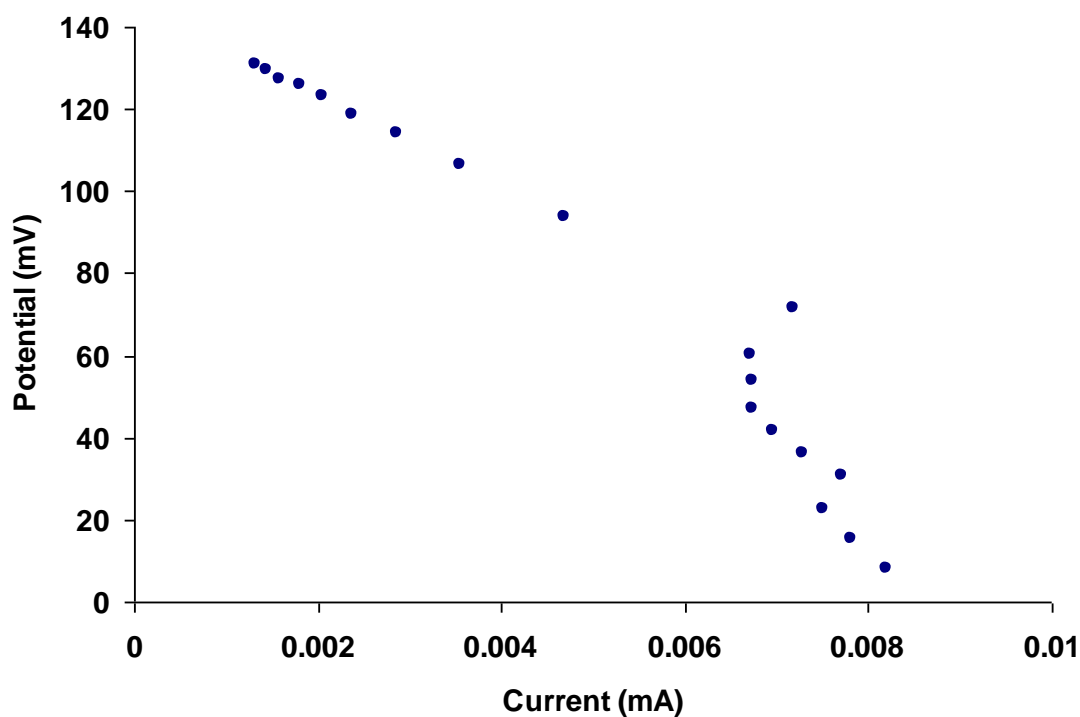


Figure 6.3(b): Power curve data obtained from a commercial platinum mesh electrode in 1 M NaOH with no C<sub>2</sub>H<sub>5</sub>OH (a ‘blank’ solution).

The stability of the data collected in ethanol indicates that the experimental set-up can give useful information about the performance of the anode and suitability of the air electrode as cathode. The set-up allows analysis the current and power attainable for practical applications easily and quickly.

#### 6.4 Platinum Deposits on Carbon Ink and Carbon Paper

Carbon Ink Electrodes (CIE) were used as the anode with initially 120 mC/cm<sup>2</sup> loading of noble metal in neutral and high pH media. Figure 6.4(a) shows a 100% platinum

electrodeposit in 0.5 M ethanol and 1 M NaOH. The open circuit potential (OCP) observed is 500 mV. The theoretical potential is 1.145 V from the Nernst equation<sup>3</sup>, but a drop is observed in any conditions with every electrode as outlined previously (section 6.1). As an example, work conducted by Antolini<sup>2</sup> with commercially available platinum on carbon (E-Tek) possessed an OCP of 480 mV for a direct ethanol fuel cell at elevated temperature.

The hysteresis on the platinum electrode is observed over time as the potential and power drops. This may be indicative of the gradual poisoning of the electrode with running time. Unlike other characterisation methods for electrocatalysts, any poisoning intermediates at the surface of the electrode will not be removed unlike, for example, in cyclic voltammetry, where the re-oxidation peak describes metal oxide removal. In a 'realistic' fuel cell, the potential will settle at a potential based on the voltage difference between the anode and cathode. From cyclic voltammetry at potentials below 400 mV, ethanol oxidation intermediates formed may not be oxidised from the catalyst surface, resulting in a steady drop in performance. The power observed, 30  $\mu\text{W}$ , is low compared to that found published to date for automotive applications. This drop is pronounced over time, and is approximately halved upon a successive second run to 15  $\mu\text{W}$  as shown in figure 6.4(a). However in comparison to that in microbial fuel cells, the power is similar for a low loading of platinum.

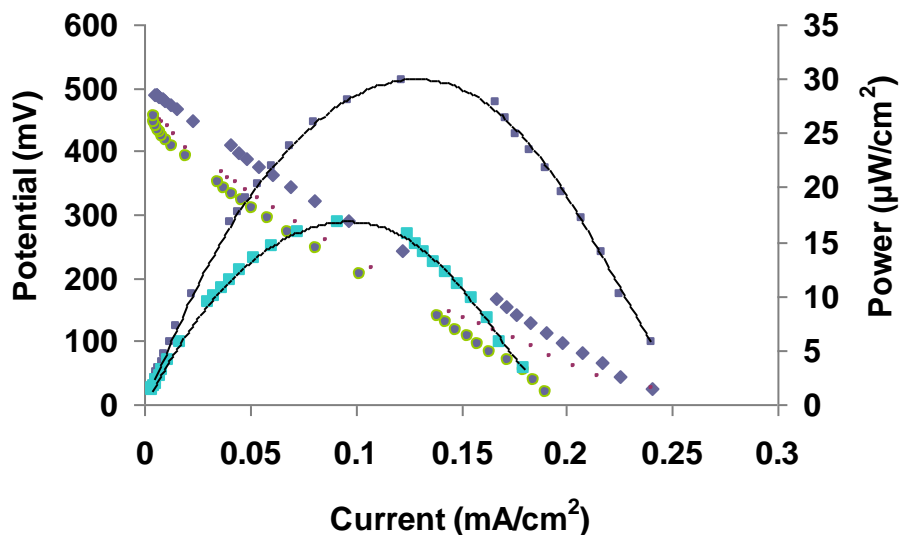


Figure 6.4(a): Power curve data from the first second and third runs plotted from a  $1 \text{ cm}^2$  carbon ink electrode containing platinum electrodeposit ( $120 \text{ mC/cm}^2$  in deaerated  $0.1 \text{ M KNO}_3$ ) in  $0.5 \text{ M}$  ethanol and deaerated  $1 \text{ M NaOH}$  at room temperature.

By comparison, figure 6.4(b) shows a platinum electrode ( $120 \text{ mC/cm}^2$ ) in pH 6,  $0.1 \text{ M KNO}_3$  and  $0.5 \text{ M}$  ethanol. The OCP and power were reduced compared to the high pH electrolyte (pH 14) while the drop in potential is increased over that in NaOH. The drop in power however has decreased by less in  $\text{KNO}_3$  than that measured in NaOH. The maximum power at pH 14 is approximately  $30 \text{ } \mu\text{W}$  to  $15 \text{ } \mu\text{W}$  compared to a drop from  $6 \text{ } \mu\text{W}$  to  $4 \text{ } \mu\text{W}$  in neutral electrolyte. This may highlight the importance of hysteresis and fouling of the electrode, despite the low power and the extended poisoning of the electrode over time in NaOH at high pH. With longer run times, the electrodes in  $\text{KNO}_3$  electrolyte decrease in power in increasingly smaller proportion to the original power of the fresh electrode. With the increased power observed at the fresh electrode in NaOH, the subsequent experiments were conducted in NaOH to maximise the power from the

electrode. It should be noted however that on occasion the solution in NaOH turned to a yellow colour from a colourless sample over the period of the experiment. This colour change in high pH has been attributed to aldol condensation reactions forming unwanted side products outlined by Panagiotopoulou *et al.*<sup>8</sup> This, as outlined in section 2.9 and 2.16, affects the possible reaction pathway with high pH, and reinforces the need to consider a delicate balance in pH for the EOR.

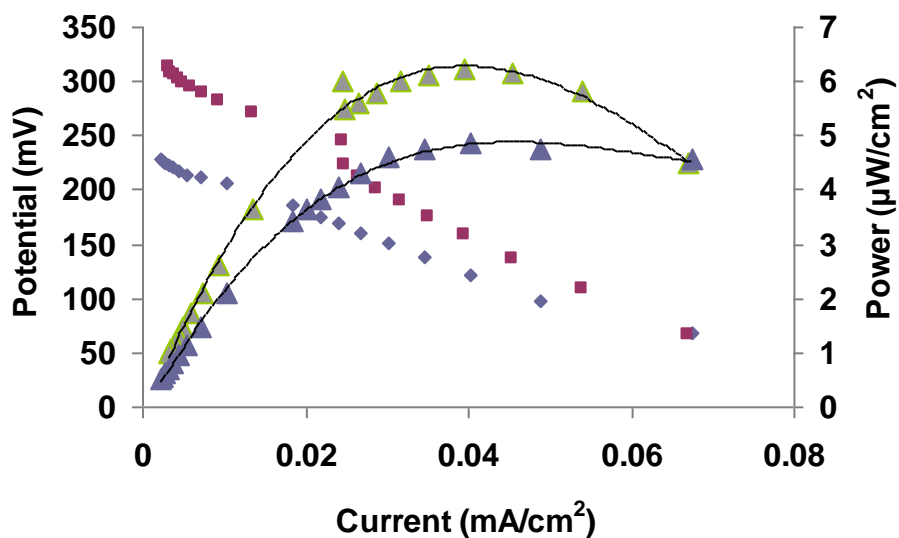


Figure 6.4(b): Power curve data plotted from the first two runs of a 1 cm<sup>2</sup> carbon ink electrode containing platinum electrodeposit (120 mC/cm<sup>2</sup> in deaerated 0.1 M KNO<sub>3</sub>), 0.5 M ethanol and deaerated 0.1 M KNO<sub>3</sub>.

Figure 6.4(c) shows the overlaid power curves obtained from a selection of electrodes for the EOR in 1 M NaOH. The fresh platinum electrodeposit in high pH remains at a maximum output of approximately 30 μW of power from the cell and 150 μA of current and the power observed from the blank carbon electrodes are practically negligible and do not influence the power observed from the catalyst electrodes. The gold catalyst gives

a power output of 5  $\mu\text{W}$ , a low current in NaOH similar to that observed from Pt in  $\text{KNO}_3$ . However, this is further confirmation that Au deposits are not active towards the EOR, even in high pH, reinforcing the electrochemistry observed in chapter 2.6. This also hints that gold can play a bystander role in the active catalyst surface to prevent poisoning.

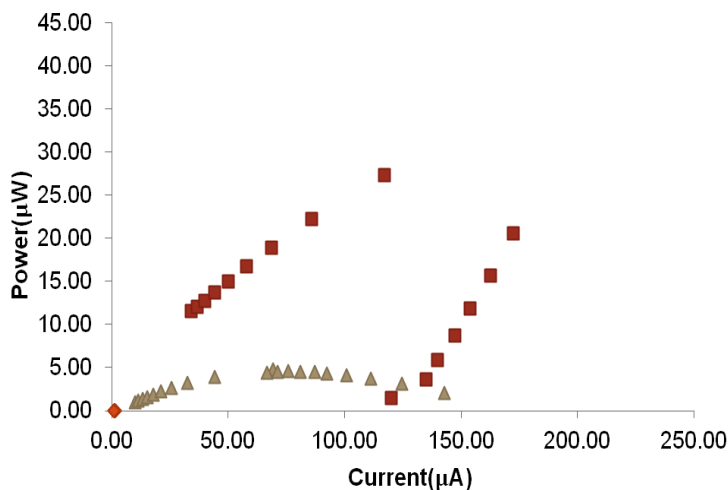


Figure 6.4(c): Power curve data obtained from a  $1\text{cm}^2$  carbon ink electrode; square = platinum electrodeposit/CIE ( $120\text{ mC}/\text{cm}^2$  in deaerated  $0.1\text{M KNO}_3$ ),  $0.5\text{ M}$  ethanol and deaerated  $1\text{M NaOH}$ ; triangle = gold electrodeposit/CIE ( $120\text{ mC}/\text{cm}^2$  in deaerated  $0.1\text{ M KNO}_3$ ),  $0.5\text{ M}$  ethanol and deaerated  $1\text{ M NaOH}$  and diamond = blank CIE in  $0.5\text{ M C}_2\text{H}_5\text{OH}$  and deaerated  $1\text{ M NaOH}$  and a blank CPE in  $1\text{ M NaOH}$  and  $0.5\text{ M C}_2\text{H}_5\text{OH}$  (overlaid diamond).

When the loading of platinum was increased, there was a gradual increase of power up to  $55\text{ }\mu\text{W}$  for a  $240\text{ mC}/\text{cm}^2$  Pt electrodeposit in a high pH environment as shown in figure 6.4(d). The blank carbon paper electrode showed negligible current and power once more, while power of  $20\text{ }\mu\text{W}$  was measured from a  $60\text{ mC}/\text{cm}^2$  Pt deposit. From a ‘best fit’ line added to the data points there is an increase in power as the Pt loading increases

showing the stability of the electrode. There is an increase of approximately 110  $\mu\text{A}$  for each doubling of Pt loading. However, the lowest loading of platinum showed a larger increase from 0  $\mu\text{A}$  to 175  $\mu\text{A}$ .

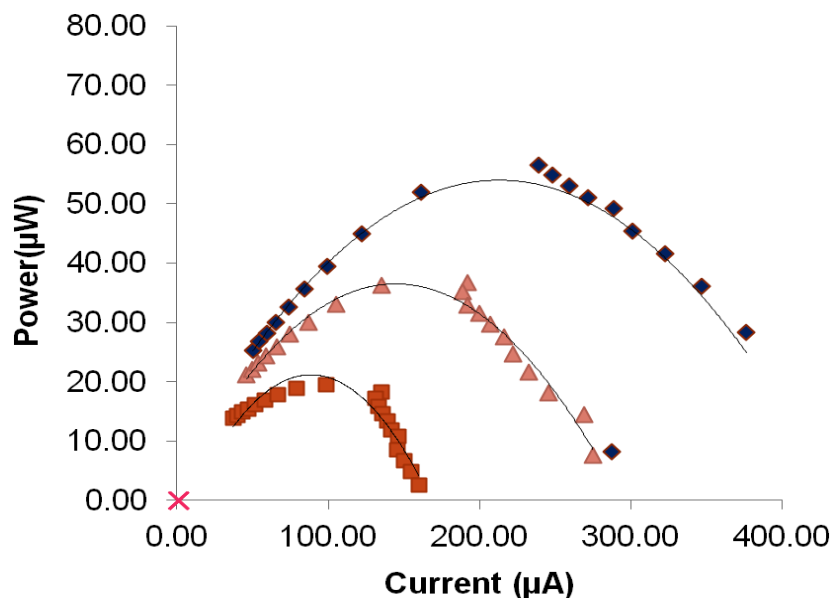


Figure 6.4(d): Power curve data obtained from a  $1 \text{ cm}^2$  CIE containing an increasing loading of a platinum electrodeposits/CIE (deaerated  $0.1 \text{ M KNO}_3$ ), x = blank CPE (0% platinum), square = ( $60 \text{ mC/cm}^2$  in  $0.5 \text{ M ethanol}$  and deaerated  $1 \text{ M NaOH}$ ), triangle = ( $120 \text{ mC/cm}^2$  in  $0.5 \text{ M ethanol}$  and deaerated  $1 \text{ M NaOH}$ ), diamond = ( $240 \text{ mC/cm}^2$  in  $0.5 \text{ M ethanol}$  and deaerated  $1 \text{ M NaOH}$ ).

This may be due to the lower loading controlling the size of the agglomerated particles and restricting nucleation to a small size as indicated by SEM in section 2.6, 3.3 and 4.3. Furthermore, these results reinforce the results in chapter two where increasing the loading of platinum does not show a linear increase in current, or power in this case. If the  $240 \text{ mC/cm}^2$  showed a linear increase in current and power, the power observed would be approximately  $80 \mu\text{A}$ . Figure 6.4(e) shows the effect to temperature on a

platinum electrocatalyst/CIE up to 60 °C at pH 6. At room temperature, the power recorded is approximately 5 μW, however, as temperature was increased, there was up to a ninefold increase in power in near-neutral pH to 45 μA.

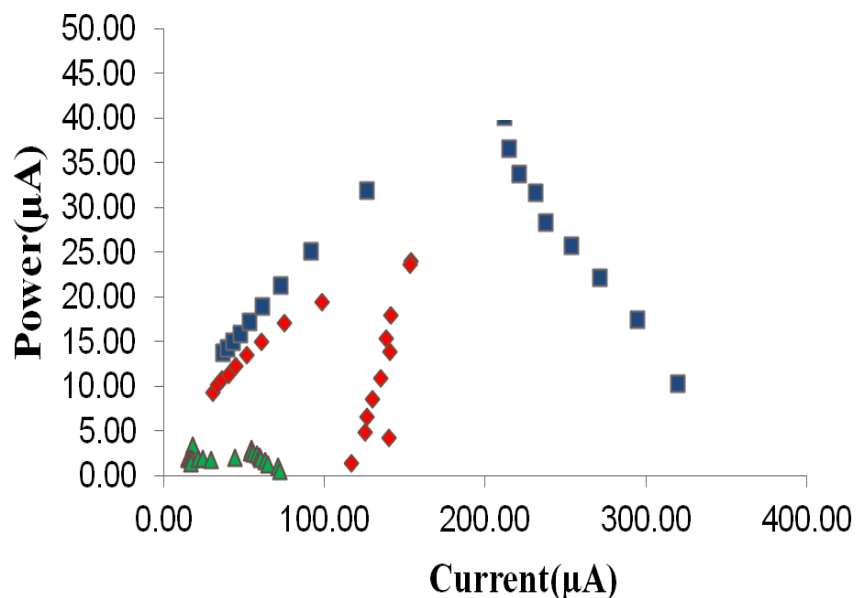


Figure 6.4(e): Power curve data obtained from a 1 cm<sup>2</sup> carbon ink electrode of a platinum electrodeposit (120 mC/cm<sup>2</sup> in deaerated 0.1 M KNO<sub>3</sub>), 0.5 M ethanol and deaerated 0.1 M KNO<sub>3</sub> with increasing temperature, triangle = room temperature, 20 °C; diamond = 40 °C; square = 60 °C.

This performance is improved on the reaction at room temperature in NaOH, showing that increased temperature at near-neutral pH can compete with NaOH at room temperature. Above 75 °C, the solution in the petri-dish began to bubble and evaporate as expected and the collected data was too unstable for any conclusion to be deduced at that temperature.

## 6.5 Power curves for selected bimetallic electrodes

When testing bimetallic electrodes, the best performing PtPd electrode was selected, based on previous voltammetry in section 3.5. The 25% palladium electrode was selected as the best performing catalyst and the results are shown in figure 6.5(a) for the catalyst in 1 M NaOH and compared to that of platinum in 1 M NaOH overlaid.

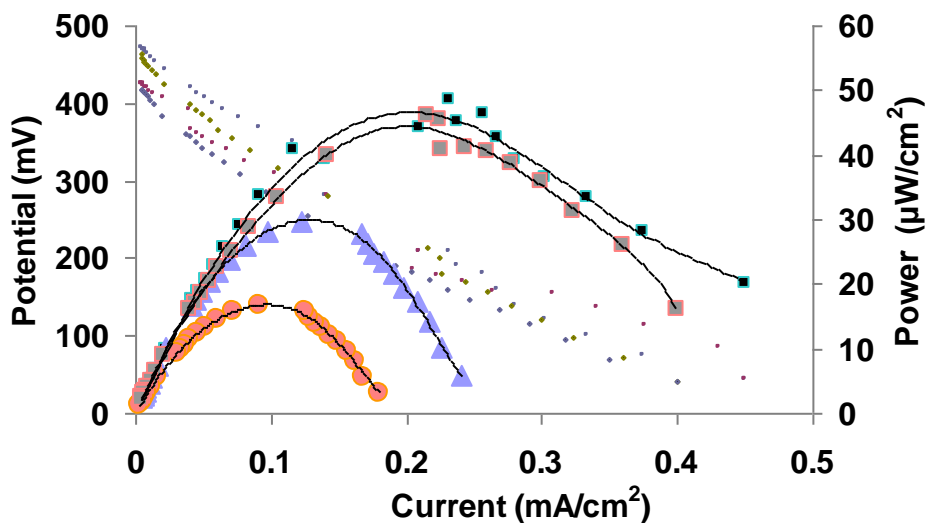


Figure 6.5(a): Power curve data and hysteresis effect obtained from a  $1 \text{ cm}^2$  electrodeposits/CIE ( $120 \text{ mC/cm}^2$  in deaerated  $0.1 \text{ M KNO}_3$ ), square = PtPd/CIE, triangle and circle = platinum/CIE,  $0.5 \text{ M ethanol}$  and deaerated  $1 \text{ M NaOH}$ .

The performance of the Pt75%Pd25% electrode was improved upon the platinum catalyst with recorded power of  $48 \text{ } \mu\text{W}$  and increased current at maximum power of up to  $450 \text{ } \mu\text{A}$ . The hysteresis effect was also notably decreased for the palladium catalyst, though the decrease is still visible. This is an indicator of improved performance over longer running times. The drop from  $48 \text{ } \mu\text{W}$  to  $44 \text{ } \mu\text{W}$  is sharply improved on the 50% decrease for a platinum electrode on repeated runs.

When nickel was selected as a catalyst for the fuel cell arrangement, the 90% platinum electrode was chosen for the greatest activity as shown in section 4.4. By comparison, another nickel electrode was selected with lower platinum content. Figure 6.5 (b) shows the power curve data recorded for the 10% nickel electrode in 1 M NaOH. The power has increased to over 100  $\mu\text{W}$  for a fresh electrode and dropped to 69  $\mu\text{W}$  when the hysteresis effect is taken into account. This is the highest current, power and potential observed for all electrodeposited catalysts in this chapter. The OCP also increased to 603 mV on a fresh electrode, dropping to 518 mV, a value higher than both palladium electrodes and platinum electrocatalysts previously. The current has increased to 600  $\mu\text{A}$ . As shown in chapter four, nickel is very active in terms of producing the necessary hydroxyl species, NiOOH or NiOH to aid further completion of the EOR in high pH and these results agree with the theory that nickel and other common transition metals are much more valuable in high pH. The ability of transition metals to be stable at high pH, while more unstable in low pH, is the key factor behind development of platinum free catalysts in the future. PdNi or RuNi may provide the necessary ethanol adsorption and oxygen species at the nickel surface to complete oxidation.

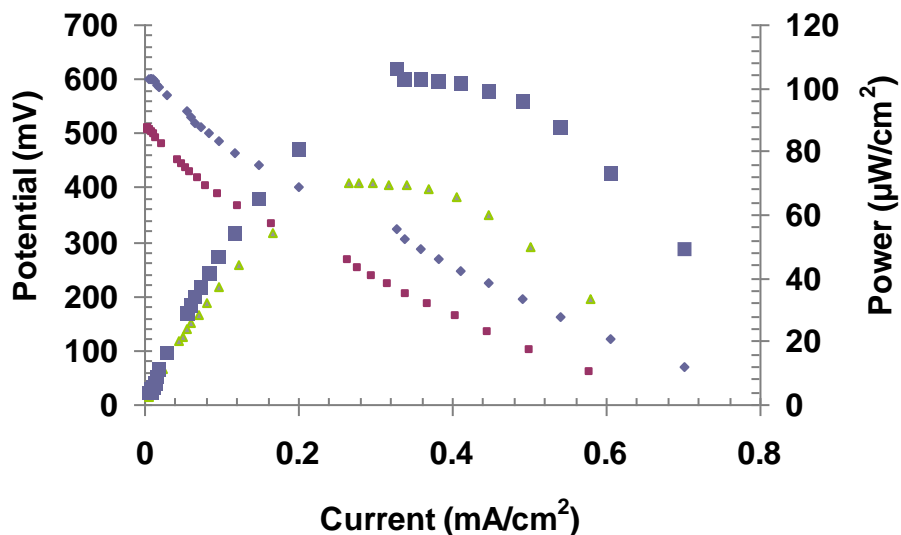


Figure 6.5(b): Power curve data and hysteresis effect obtained from a 1 cm<sup>2</sup> carbon ink electrode containing Pt90%Ni10% electrodeposit/CIE (120 mC/cm<sup>2</sup> in 0.1 M KNO<sub>3</sub>), 0.5 M ethanol and deaerated 1 M NaOH, pH = 14.

Figure 6.5(c) illustrates the power curves recorded with a increased nickel content. As shown previously in chapter four, as the proportion of nickel is increased beyond 10%, the power dropped steeply from 100 μW to 46 μW. The fresh electrode, Pt75%/Ni25%, was then measured at 460 μA dropping to 360 μA as the run time continued. The OCP recorded was slightly lower than that of Pt, however the power recorded remains higher than that measured at a fresh platinum electrode, again reinforcing the benefit of nickel providing the extra oxygen required for the EOR.

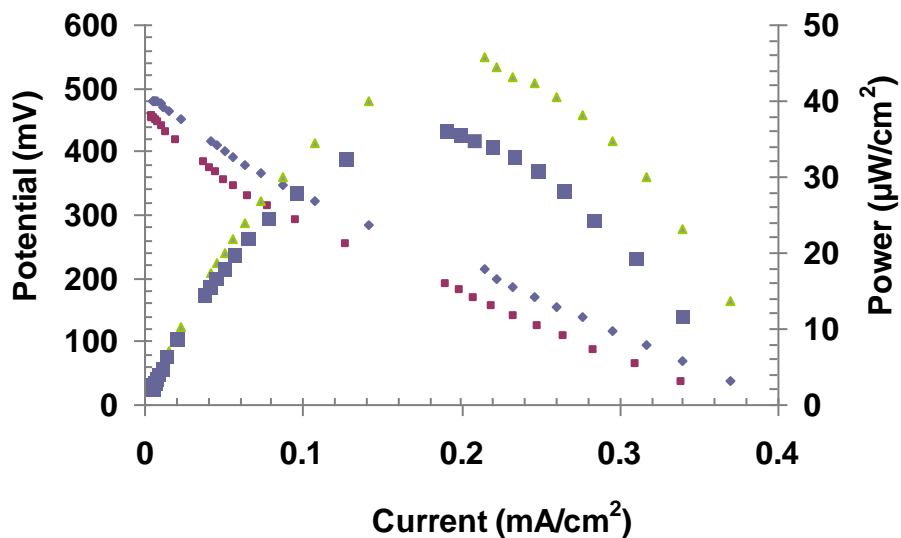


Figure 6.5(c): Power curve data obtained from a  $1 \text{ cm}^2$  carbon ink electrode containing Pt75%Ni25% electrodeposit/CIE ( $120 \text{ mC/cm}^2$  in  $0.1 \text{ M KNO}_3$ ),  $0.5 \text{ M}$  ethanol and deaerated  $1 \text{ M NaOH}$ ,  $\text{pH} = 14$ .

Finally, a 25% platinum and 75% nickel electrode was run in  $1 \text{ M NaOH}$  and the result is shown in figure 6.5(d). While the power had only decreased slightly compared to that of the previous nickel electrode, the current is halved from  $0.4 \text{ mA/cm}^2$  to  $0.15 \text{ mA/cm}^2$ , though this is substantially increased from that of palladium (in  $\mu\text{A}$ ). The data collection was a lot less stable and the limiting current was reached much more quickly exhibited by the ‘collapse’ in potential for the later voltage readings. These final potential versus current data points are very similar to the typical fuel cell curve shown in figure 6.1(f), where mass transport losses account for this drop.

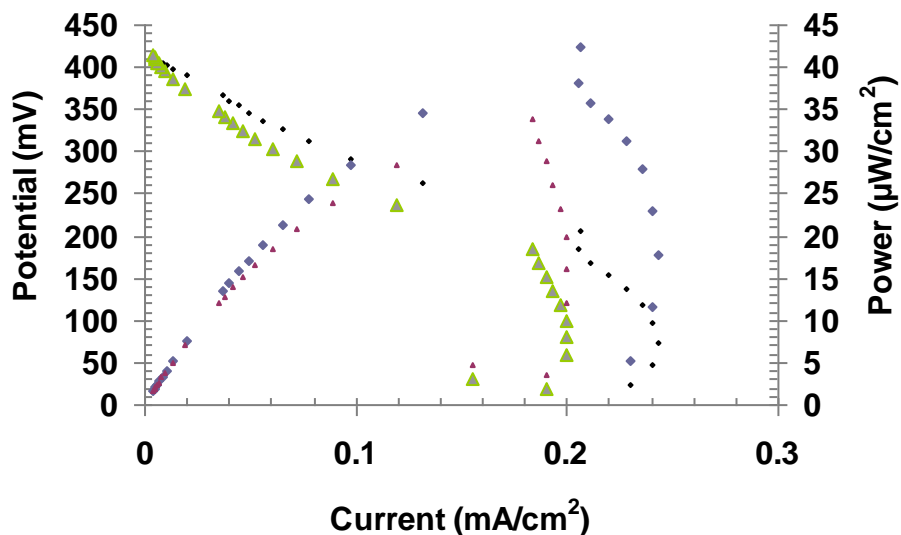


Figure 6.5(d): Power curve data obtained from a  $1\text{cm}^2$  carbon ink electrode containing Pt25%Ni75% electrodeposit/CIE ( $120\text{ mC/cm}^2$  in  $0.1\text{ M KNO}_3$ ),  $0.5\text{ M}$  ethanol and deaerated  $1\text{ M NaOH}$ , first two runs,  $\text{pH} = 14$ .

Table 6(a) categorises a selection of electrodeposits, catalysts and electrodes by the measured potential difference (or OCP) in mV. This is the potential present with no current flowing and the greater the value, the better the catalyst towards the EOR. In addition to the power curves observed in this chapter, the value measured at both a carbon ink and carbon paper electrode is zero, showing no catalytic contribution towards the EOR from carbon. This agrees with the theory, previously discussed in sections 2.9, sections 3.8, 4.5 and 5.4, that the impact of the carbon surface upon the EOR is restricted only to the inhibition of the early steps of the catalysis, in particular the formation of  $\text{MOH}_{\text{ad}}$  at lower potentials, where M represents the metal catalyst such as palladium or nickel. The best performing catalysts determined by cyclic voltammetry, potential step and Tafel analysis in previous chapters show higher potential to that of platinum, but also

the individual catalyst itself in the case of nickel and palladium (600 mV for 10% nickel to 274 mV at a nickel electrode). Furthermore, metals such as cobalt show very low activity towards the EOR when compared to other inactive metals such as gold with 23 mV measured at very high resistance. As a result, the current is very small when the resistance is reduced.

<b>Selected Electrode</b>	<b>Measured Potential Difference (mV)</b>
Pt	500
Ni	274
Pd	48
Pt90%Ni10%	600
Pt75%Pd25%	575
Au	125
Co	23
C	0

Table 6(a): Measured Potentials at selected electrodeposits/CIE (120 mC/cm<sup>2</sup> in 0.1 M KNO<sub>3</sub>), 0.5 M ethanol and deaerated 1 M NaOH with an air cathode at high resistance – the ‘open circuit potential’.

### 6.6 Power curve data obtained from Vulcan XC72 electrodes

Figure 6.6(a) shows the power curves recorded with a carbon ink electrode and Vulcan XC72R powder mix. This type of electrode had no electrodeposited catalyst added. The activity and power measured is due to the 57.5% platinum preloaded into the Vulcan powder with a high surface area carbon sourced from the Technische Universität München. It can be seen that power was twice the magnitude of all other electrodeposited catalysts tested previously. 200  $\mu\text{W}$  was observed on a fresh Vulcan electrode and the hysteresis effect can still be noticed in the drop in power to 150  $\mu\text{W}$ . This hysteresis can also be seen in the drop in potential from 580 mV to 548 mV and continues to drop upon further running time.

However this power was still in the magnitude of microwatts suggesting a potential limiting current from the experimental setup, aside from the activity of the catalyst. The process of electrodeposition itself has been removed in the Vulcan powder electrodes and there was no large increase in power to watts and milliwatts for alcohol fuel cells seen in many publications at various catalysts and numerous electrodes and conditions.<sup>9-23</sup> The carbon ink may be again the inhibiting influence in order to mobilise the Vulcan powder onto the electrode framework; the mobilisation of the powder – including carbon black is a common problem to overcome in manufacturing catalysts from commercial powders or standards.

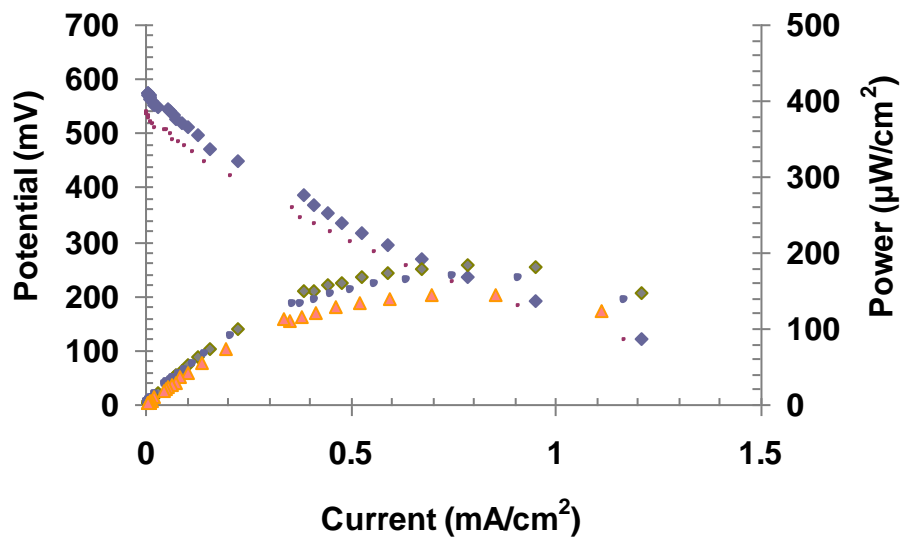


Figure 6.6(a): Power curve data obtained from a 1 cm<sup>2</sup> carbon ink electrode containing a paste incorporated with Vulcan XC72 powder, 0.5 M ethanol and deaerated 1 M NaOH, first two runs, pH = 14.

To investigate the effect of immobilising the Vulcan powder, the ink/powder mix was then painted onto a pre-prepared carbon paper electrode. Figure 6.6(b) shows the Vulcan powder immersed in the carbon ink, however the mix is spread upon a carbon paper electrode and the electrolyte is 1 M NaOH. The power has dropped on a fresh carbon paper electrode to 146 μW compared to 200 μW from the all-in-one ink/powder CIE.

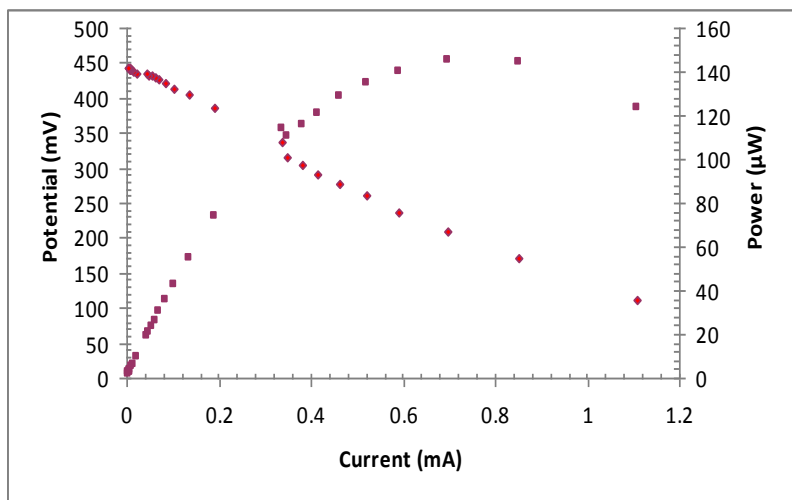


Figure 6.6(b): Power curve data obtained from a 1 cm<sup>2</sup> carbon paper electrode containing a carbon ink paste incorporated with Vulcan XC72 powder, 0.5 M ethanol and deaerated 1 M NaOH, first run, pH = 14.

The potential was dropped from 580 mV to 450 mV on a fresh electrode, but the current has only slightly decreased to 1.5 mA on the painted electrode. Consequently, the optimum condition, based on this work, was to manufacture the immobilised powders intrinsically to the structure of the electrode itself with higher power observed in figure 6.6(a).

## 6.7 Conclusions

An analogue fuel cell was set up to collect power curves for a variety of electrocatalysts. This was a simple, repeatable apparatus which employed Ohm's Law to collect potential, resistance and current data. A fault of this set up is that there was no membrane to

separate the two reactions. Both reactions, anode and cathode, could occur at both electrodes and this impaired the potential value collected. A platinum mesh electrode was used to show the proof of concept and the power obtained for a large mass of platinum was between 2 and 3 mW. This is a high value compared to the geometric area of the electrodeposits, but when normalised for area, this gap would be reduced. The electrodeposits behaved very well in the fuel cell arrangement and reproducible with a clear hysteresis effect over time.

The loading of platinum electrodes were tested and produced a gradual increase for double the loading. The power obtained would be suitable for small applications such as microbial fuel cells ranging from 20-300  $\mu\text{W}/\text{cm}^2$ . The highest power was recorded for the Vulcan XC72 coated electrode. The highest performing electrocatalyst was for Pt90%Ni10% at 100  $\mu\text{W}/\text{cm}^2$ . The Open Circuit Potential recorded at maximum resistance was indicative of the performance of the catalysts from all the previous voltammetric data, potential step, Tafel analysis and EIS. The electrode closest to the theoretical voltage of 1.14 V was the better catalyst. It was shown that the best performing bimetallic catalysts had a higher potential than that of a 100% platinum deposit (500 mV) and the Pt90%Ni10% (600 mV) and Pt75%Pd25% (575 mV) electrodes showed slightly improved power than that of platinum in agreement with the previous voltammetry.

The power obtained in neutral media was considerably lower than the power recorded at pH 14. High pH was the best performing electrolyte throughout in terms of current and power for all electrodes.

## 6.8 References

1. Chia, Z.W.; Lee, J.Y.; (2010), “Direct Ethanol Fuel Cells”, *Energy Production and Storage*, John Wiley and Sons Ltd, 229-252.
2. Antolini, E.; (2009), *Energ. Environ. Sci.*, **2**, 915-931.
3. Krewer, U.; Vidakovich-Koch, T.; Rihko-Struckmann, L.; (2011), *Chem. Phys. Chem.*, **12**, 2518, 2544.
4. Li, Y.S.; Zhao, T.S.; Liang, Z.X.; (2009), *J. Power Sources*, **187**, 387-392.
5. Varcoe, J.S.; Slade, R.T.; (2010), Anion Exchange Membranes, 60<sup>th</sup> International Society of Electrochemistry Meeting, Nice, France.
6. [http://www.fuelcell.no/principle\\_fctheory\\_eng.htm](http://www.fuelcell.no/principle_fctheory_eng.htm), viewed May 2015.
7. Lam, A.; Wilkinson, D.P.; Zhang, J.; (2008), *Electrochim. Acta*, **53**, 6890 – 6898.
8. Panagiotapoulou, P.; Antoniadou, M.; Kondarides, D.I.; Lianos, P. ; (2010), *Appl. Catal. B: Environ.*, **100**, 124-132.

9. Matsuoka, K., Iriyama, Y.; Abe, T.; Matsuoka, M.; Ogumi, Z.; (2005), *J. Power Sources*, **150**, 27-31.
10. Chen, R.; Zhao, T.S.; (2007) *Electrochem. Comm.*, **9**, 718-724.
11. Yu, E.H.; Scott, K.; (2004), *J. Power Sources*, **137**, 248-256.
12. Bambagioni, V.; Bianchini, C.; Marchionni, A.; Filippi, J. ; Vizza, F. ; Teddy, J. ; Serp, P.; Zhiani, M.; (2009), *J. Power Sources*, **190**, 241-251.
13. Chetty, R.; Scott, K.; (2007), *Electrochim. Acta*, **52**, 4073-4081.
14. Coutanceau, C.; Rakotondrainibé, A.F.; Lima, A.; Garnier, E. ; Pronier, S. ; Léger, J-M. ; Lamy, C. ; (2004), *J. Appl. Electrochem.*, **34**, 61-66.
15. Coutanceau, C. ; Demarconnay, L. ; Lamy, C. ; Léger, J-M. ; *J. Power Sources*, (2006) 156, 14-19.
16. Bianchini, C. ; Shen, P.K.; (2009), *Chem. Rev.*, **109**, 4183-4206.
17. Lamy, C.; Lima, A.; LeRhun, V.; Delime, F.; Coutanceau, C.; Léger, J-M. ; (2002), *J. Power Sources*, **105**, 283-296.

18. Simoes, F.C.; dos Anjos, D.M. ; Vigier, F. ; Léger J-M. ; Hahn, F. ; Coutanceau, C.; Gonzalez, E.R. ; Tremiliosi-Filho, G. ; de Andrade, A.R.; Olivi, P.; Kokoh,K.B.; (2007), *J. Power Sources*, **167**, 1-10.
19. Wendt, H.; Spinace, E.V.; Neto, A.O.; Linardi, M.; (2005), *Quim. Nova*, **28**, 1066-1075.
20. Shen, S.Y., Zhao, T.S., Xu, J.B.; Li, Y.S.; (2010), *J. Power Sources*, **195**, 1001-1006.
21. Li, H.; Sun, G.; Cao, L.; Jiang, L. ; Xin, Q ; (2007), *Electrochim. Acta*, **52**, 6622-6629.
22. Colmati, F.; Antolini, E.; Gonzalez, E.R.; (2006), *J. Power Sources*, **157**, 98-103.
23. Lamy, C.; Rousseau, S.; Belgsir, E.M. ; Coutanceau, C. ; Léger, J-M. ; (2004), *Electrochim. Acta*, **49**, 3901-3908.

## **Chapter 7: Achievements, Conclusions and Future Work**

### **7.1 Achievements and Conclusions**

To conclude the project, the aims of the work should be assessed. In addition, the future work that could be conducted to develop the research further will be discussed. The details of publications currently being edited and submitted along with details of a poster and presentations of results will be given at the end of this chapter. The aims of the project were set out in section 1.5.

A quick and simple method to manufacture electrodes for the study of the EOR was achieved in comparison to the Bönemann method where no expensive materials or complex procedures were required. The CIE and Toray carbon paper electrodes (CPE) were found to be sufficiently conductive to use as electrode surfaces onto which islands of noble metals were deposited. The electrodes were manufactured with common materials and were found to be robust and reproducible.

Selected metals suitable for the EOR were successfully deposited by a quick and simple electrodeposition method. The particle size was successfully controlled by the charge deposited. The deposits ranged from 10-200 nm dependent on the length of time passed for their deposition. Nickel deposits were found to be the smallest particles around 10-20 nm and in addition, Ni electrodes showed a notable increase in activity from the equivalent platinum electrode when used in a bimetallic configuration. At high levels of

Ni, the EOR was enhanced in comparison to the similar Pt and Pd electrodes. Consequently, the smaller particles appeared to enhance performance. It was found that the metals of interest deposited in 2D nucleation 'islands' equally across the face of the carbon electrodes used and successful deposition was heavily dependent upon the fine tuning of electrolyte, deposition method, pH, and the choice of reference electrode. Ideally, deposition from chloride salts should be avoided where possible. Once fine tuned, behaviour towards the EOR from the deposited metals was found to be consistent and repeatable.

The platinum content of a given multimetallic electrocatalyst was reduced to the lowest quantity possible whilst not affecting the performance found from the equivalent loading of platinum electrode. With respect to palladium, the lowest quantity of platinum was found to be a reduction from 100% to 75%. When the composition comprised of more than 25% palladium, the activity found in the EOR is considerably decreased to make the electrode a poor catalyst. Therefore, the focus moved to introduce more inexpensive transition metals to further decrease the platinum content and examine the behaviour from such electrocatalysts, ideally producing a platinum-free catalyst as an ultimate goal. This is in contrast with Pt90%Ni10% giving the best performance. Gold deposits/CIE were found to be inactive towards the EOR; however it has been used by other groups as an electrode material, particularly as a conductive layer and in a 'bystander' role to facilitate ethanol oxidation at platinum. The proportionate amounts on the electrode were based upon the composition of the deposition solution and quantified by SEM-EDX analysis.

All electrocatalysts were tested in neutral electrolytes, moderately alkaline pH and strongly basic conditions. Neutral electrolytes allow for the continued use of Nafion<sup>®</sup> exchange membranes and performed similar to acidic conditions without the added problems of the corrosive materials and environments associated with low pH. At strongly basic pH, the current observed and power observed from all electrodes was substantially increased. Notably different and distinctive voltammetry and chronocoulometry data was recorded in neutral and basic pH. It was found that the EOR neutral media obtained showed similar current to that in acidic electrolytes of approximately 1 mA/cm<sup>2</sup>.

Voltammetric data, potential step and coulometric data were used to analyse the EOR at different electrocatalytic surfaces alongside fuel cell data and EIS results. The major issue found throughout each technique was with the carbon electrode performance. The immediate 'lag' period for the chronocoulometric data was assigned to the conductivity of the electrode surface where the electron needs to move through the ink to the surface of the ink and this difficulty with the carbon electrodes was also evident in the EIS data. The very high initial resistance,  $R_u$ , was observed up to 620  $\Omega$  at pH 14 and 830  $\Omega$  at pH 6 at a carbon electrode subjected to ethanol oxidation, separate from the typical solution resistance,  $R_s$ , which remained consistent at 3  $\Omega$ . When a metal sheet was used instead in the same conditions, the  $R_u$  value was almost completely removed, indicating the presence of the two separate resistances,  $R_s$  and  $R_u$ , for the carbon electrodes tested. This did not affect the subsequent reaction taking place, aside from the EIS data assigned to the EOR semicircle or features in the data collected by potential step testing. It will

reduce the current and power observed through other techniques and is crucial information in the overall picture.

Despite this issue, three carbon supports were analysed as a cross comparison for the electrocatalysts used. The Vulcan XC-72R carbon support has been commonly used previously, but it is no longer commercially available from De Nora Technologies. A sample obtained by this author was incorporated with some carbon ink with a platinum loading. No electrodeposit was added to the Vulcan XC72-R, but similar features were observed by voltammetry. The observed CV peaks with the metal catalysts could then be assigned as to the EOR with no interaction from any other material deposited. As briefly mentioned above, the surface morphology of the electrocatalysts was observed and the impact of size and shape on the EOR was evaluated. When deposited in acid conditions, metals formed different structures entirely in valleys and edges of the carbon surface to that of a neutral deposition solution.

The optimum operating conditions of the catalysts tested initially were based on the acid environment that has been well studied previously. Consequently, increasing the pH to neutral and especially high concentrations of  $\text{OH}^-$  at pH 14 is of great interest. However at pH 7, the current recorded was greater than that at pH 11 and at pH 7, it is still possible to use Nafion<sup>®</sup> membranes if required. The current observed and catalyst performance in all conditions and tests carried out at pH 14 has been superior to that of all other conditions and this reflects the current trend to move towards such high pH. The

development of Anion Exchange Membranes from a situation of low power and interest in 2004 further facilitates high pH as the main consideration in future.

Carbon supports are popular as a means by which to test catalysts and it was found that carbon paper was the most suitable electrode surface for deposition and the EOR throughout this work. The porosity of the electrode may play a part as seen by SEM images with individual fibres of carbon providing a better surface for metal reduction than the carbon ink. The CIEs used allowed for quick analysis of the EOR, however, there was an inherent resistance in the ink that slowed the process of ethanol oxidation; shown particularly by the EIS data collected compared to a platinum disc electrode. A porous yet simple carbon electrode is preferential for ethanol oxidation. The CIE also showed a slow reaction with ferrocyanide compared to the platinum and gold deposits on carbon.

Using EIS – Nyquist plots in particular – the presence of adsorbed species can be seen at particular potentials (vs. MMS) with a characteristic inductive loop. Furthermore, EIS has clearly shown the impact of the carbon ink electrode supports with a large resistance associated with the electrode itself. This does agree with Seland in terms of characteristic plots at defined voltages. At 0.1 V (vs. MMS) with no reaction appearing to take place by any other technique and no peak by Cyclic Voltammetry, the total resistance observed with a large semi-circle indicates no or little reaction associated with ethanol oxidation. As the voltage is increased, the charge transfer resistance dropped, associated with increasing reactivity as expected. However, at certain potentials, where peaks were

observed by CV, the reactivity increased where adsorbed reactants may be the cause. The loop of the Nyquist plots further reinforces this suggestion. The re-oxidation peak, labelled peak C throughout, have been suggested as due to further ethanol oxidation as well as adsorbed CO to the catalyst surface as soon as the Pt-O, peak D, is reduced. The potential at which this peak occurs is very similar to that of CO oxidation, with its current increasing with elevated scan number indicating increased production of CO<sub>ad</sub>. In addition, the two peaks on the forward sweep could be considered similarly reactions associated with adsorbed species. For these reasons, EIS has proven most valuable in determining surface reactions at potentials of particular interest in a fuel cell which operate frequently around 0.3 V-0.5 V.

The membraneless model used in chapter six proved the most useful fuel cell apparatus in collecting relative power curves for the catalysts and the most suitable environments in which they operate. It was easily manipulated with an air electrode and by monitoring the current over time. There is interest in developing membraneless fuel cell cells particularly for microbiological use. A membrane remains a specialist material that needs further improvement – with respect to both the anion exchange membranes currently available and commonly used Nafion<sup>®</sup> proton exchange membranes. The results collected from the fuel cell arrangement in chapter six reinforce findings in earlier chapters over the benefit of both other platinum group metals than Pt and transition metals for ethanol oxidation. Transition metals in high pH are stable enough and they provide sufficient OH<sub>ad</sub> to enhance the current and power observed to that of equivalent platinum in the case of nickel or 100% platinum in the case of palladium. It has also been shown that decreased

power and current has been recorded for ethanol oxidation in platinum free catalysts. The power curves obtained are useful as a direct comparison of performance, but it offers no information on the kinetic impact of the carbon surface. The power curves obtained for a carbon electrode showed no influence on the power. However through the other techniques used in this work, there is a clear effect in terms of carbon slowing EOR kinetics and this needs to be evaluated for other electrodes such as graphene.

In terms of mechanistic information, information could be taken from the chronocoulometric and voltammetric data. The platinum and palladium bimetallic catalysts used indicated a symbiotic relationship to enhance oxidation. When platinum was in low proportions to palladium, measured by SEM-EDX, peak A was more prominent than peak B in neutral electrolytes compared to catalysts with high proportions of platinum to palladium. Peak A is associated with the initial ethanol adsorption and formation of a metal hydroxide from the dissociation of water. The subsequent drop in current for peak B indicates that platinum is still required to maximise the current for this oxidation and that this step is predominantly associated with the oxidation of ethanol.

In addition, the chronocoulometric data collected in neutral electrolyte showed interesting features depending upon the starting potential. When the potential was stepped from 0.4 V to 0.45 V, there may be a dynamic system in place at the starting potential (0.4 V), whereby the metal hydroxides are already formed before the potential step is applied. The contribution from the oxidation that takes place between 0.1 V to 0.4 V is not recorded. However, the charge vs. time plot recorded from the step from 0.4 V to 0.45 V shows

very similar features to that where  $\text{OH}^-$  is readily available, in high pH. This is a further indicator that peak A is linked with the formation of MOH. The increased current and earlier onset potentials, observed at peak A by voltammetry can be ascribed to the increased or decreased formation of PdOH or NiOH<sub>2</sub>. This may be used as a part of a screening test for potential EOR catalysts as well as use of SEM-EDX to determine particle size, EIS to determine the role of the supporting carbon layer as well as power curves which are a direct comparison.

## **7.2 Future Work**

There are a few areas and topics that require future work resulting from this body of research. Platinum free catalysts can be investigated comprehensively with selected metals such as ruthenium or nickel. Palladium can also be used. Of particular interest may be gold electrodes based on the complete inactivity for gold towards ethanol oxidation. Gold is a very good conductor, however it will not be poisoned by ethanol intermediates unlike platinum group metals as found in section 2.9. It may be an ideal co-catalyst for experimental work, but may prove expensive on an industrial scale. The advantage to electrodepositing a thin uniform gold layer on a carbon surface may result in carbon ink becoming more reactive, reducing the delay experienced at a bare carbon ink electrode throughout this work. From this layer, active catalyst can then undergo nucleation on the gold surface and become more active to the EOR, based on recent work on gold indicating 100% production of CO<sub>2</sub> from an ethanol fuel cell. Gold, as outlined in sections 2.9 and 2.16, may act to aid reactivity with regard to the bifunctional

mechanism, as mentioned throughout this work, through separating neighbouring islands of the active catalyst. Carbon paper can be selected as an easily available substrate over carbon ink. Techniques such as Differential Electrochemical Mass Spectrometry, Raman Spectroscopy and High Performance Liquid Chromatography (HPLC) may prove useful to clearly identify the products from ethanol oxidation.

A major area of future work is to use reliable anion exchange membranes, as they are more readily available than previously and are in continual development. By testing electrodeposited catalysts in a full membrane electrode assembly in high pH, the cost can be decreased and current increased. Using a complete fuel cell on a larger electrode surface, the carbon paper should produce greater performance based on the findings of this work, whereas the carbon ink can be taken out of consideration further due to the lack of porosity. The weave structure of the carbon paper fibres as shown in section 2.7 facilitates the ethanol to move through the surface and therefore being immediately available to react without any delay that has been determined to be associated with the carbon ink surface. Furthermore, within an MEA arrangement, such a path is critical for electrons to pass through the membrane and complete the circuit through the catalyst surface. These conductive fibres are also ideal for electrodepositing as well as for various electrochemical techniques examined throughout chapters two, three and four. Future work should concentrate on simple porous electrodes manufactured using simple robust materials than the use of HOPG, or requiring expensive reagents, such as Argon gas such as that in the Bönemann method described in section 2.6. Electrodepositing is preferred for quick analysis through reduction of a metal salt onto the electrode surface. Other

common techniques typically require mobilisation through emulsions such as carbon black and Vulcan XC72 powder as discussed in section 2.7. Differential Electrochemical Mass Spectrometry can be added to the waste flow from the full fuel cell which can instantly identify, in-situ, the products formed by the MEA, in particular the fraction of  $\text{CO}_2$ ,  $\text{CH}_3\text{COOH}$  or other substances outlined in the EOR pathway in sections 2.9 and 2.15, 3.5 and 4.4.

Furthermore, such a set up will deduce the operating potential when in conjunction with a suitable transition metal cathode. This particular value (for example, 0.4 V vs. MMS), will assign the products with a particular potential from the electrochemical analysis in this work. Should the fuel cell operate at a higher or lower potential, different products and different current would be expected.

### **Presentations carried out from this work**

*“Low Temperature Direct Ethanol Fuel Cell Electrocatalysts”*, May 2008, COST 543

Action: Workshop, St. Andrews University, St. Andrews, Scotland.

*“Preliminary Experiments on Direct Ethanol Electrocatalysts in Acid Electrolytes”*, May

2009, COST 543: Workshop Groups 4 and 5, TKK (Aalto) University, Espoo, Helsinki,

Finland.

*“COST 543 Action: Bioethanol Processing STSM; Between the DIT and the Technische*

*Universität München”*, November 2010, Dublin Institute of Technology Graduate

Research, Upper Mount Street, Dublin 2, Ireland.

*“Electrocatalysts in high pH media for the DEFC”*, May 2011, COST 543 Action:

Concluding Meeting, Faculty of Science Building, (TTK), Eötvös Loránd University,

Budapest, Hungary.

*“Electrocatalysts in Neutral Media for the DEFC”*, May 2011, Eirelec 2011;

Electrochemistry - the future?, Adare, Co. Limerick, Ireland.

*“Domestic Fuel Cells: Glucose and Ethanol”*, July 2011, Dublin Institute of Technology,

School of Chemical and Pharmaceutical Sciences, Kevin St Lower, Dublin 8, Ireland.

*“Electrocatalysts for the ethanol oxidation reaction under neutral and alkaline conditions”*, 28<sup>th</sup> June 2013, 65<sup>th</sup> Irish Universities Chemistry Research Colloquium, Trinity College, Dublin.

### **Poster Presentations**

*“Ethanol oxidation in neutral media for the DEFC”*, D.A. Fox; A.J. Betts; J.F. Cassidy, October 2010, Symposium 7 (s-07-P-017): Electrodeposition for Material Synthesis and Nanostructure Fabrication, 61<sup>st</sup> meeting of the International Society of Electrochemistry, Electrochemistry from Biology to Physics, Nice, France.

“Ethanol oxidation, catalyst deposition”

3<sup>rd</sup> Annual Materials Ireland Conference, December 14<sup>th</sup> 2010, CREST, Dublin Institute of Technology, Kevin St. Dublin 8.

### **Publications submitted through this research**

1. *Enhanced activity for ethanol oxidation at platinum oxidation at platinum and palladium deposits on a carbon ink support*, DA Fox, AJ Betts, JF Cassidy, *Electrochem. Comm.*, (in review).

2. *Electrochemical Impedance Spectroscopy on various carbon supports towards the*